

# **Dynamic protein-chromatin interactions in heterochromatin and during the DNA damage response on the single molecule level**

THÈSE N° 8706 (2018)

PRÉSENTÉE LE 28 SEPTEMBRE 2018

À LA FACULTÉ DES SCIENCES DE BASE

LABORATOIRE DE CHIMIE BIOPHYSIQUE DES MACROMOLÉCULES

PROGRAMME DOCTORAL EN CHIMIE ET GÉNIE CHIMIQUE

ÉCOLE POLYTECHNIQUE FÉDÉRALE DE LAUSANNE

POUR L'OBTENTION DU GRADE DE DOCTEUR ÈS SCIENCES

PAR

**Andreas Linus BACHMANN**

acceptée sur proposition du jury:

Prof. C. Heinis, président du jury

Prof. B. Fierz, directeur de thèse

Dr J. Müller, rapporteur

Prof. C. Eggeling, rapporteur

Prof. A. Boghossian, rapporteuse



ÉCOLE POLYTECHNIQUE  
FÉDÉRALE DE LAUSANNE

Suisse  
2018



## Acknowledgements

Special thanks I dedicate to Beat Fierz for supporting and leading the project, for his tutoring and critical reading of various manuscripts. I further thank all the jury members of the thesis and I thank all current and previous members of LCBM for their support and for providing expertise. In particular I thank Karthik Maddi and Iuliia Boichenko, who were working with me on different aspects of the RNF168-project. I also thank Caroline Lechner and Nora Guidotti for providing reagents. For collaboration I thank Louise Bryan, Sinan Kilic, Jeongyoon Choi, Katharina Tauscher, Christian Benda, Joachim Lutz, Andreas Marx and Jürg Müller. For administrative management I thank Marie Munoz, Jacky Gremaud, Marie Jirousek and Anne Lene Odegaard. I further would like to give thanks to my friends and family for always supporting me. I thank Nature Structural and Molecular Biology to publish our work and to give me permission to re-use content from the published article.





## Abstract (Deutsch)

Dynamische Regulierung von Chromatin, einen Gefüge aus DNS und Histone-Proteinen, erfolgt durch posttranslationale Modifikationen (PTMs) und Effektorproteine. HP1 $\alpha$  und PRC2 werden durch repressive PTMs (H3K9me3, H3K27me3) dirigiert und ermöglichen Heterochromatinbildung, welche zu Genabschaltungen führt. In der DNS Schadens-Antwort, klar definierte räumliche und zeitliche Kontrolle des Chromatin Kompaktionslevels ist essentiell und weitere PTMs werden laufend installiert um Proteine durch dynamische Zellsignalwege zu leiten. Chromatin Ubiquitylierung (H2AK15ub) in der RNF168-geleiteten Signalkaskade ist von erheblicher Bedeutung, um den passenden DNS Reparaturvorgang auszuwählen. Deregulierung der genannten Prozesse führt oft zu Krebs und neurodegenerativen Krankheiten. In dieser Studie präsentieren wir eine Methode, um Chromatin-Protein Interaktionen mit Totalreflexionsmikroskopie (TIRFM) und *in vitro* Chromatin-Herstellung chemisch-definierter, modifizierter Histone. Koloalisierungsexperimente mit Fluoreszenz-markierten Chromatinfasern und Proteinen ermöglichten uns dynamische Chromatin-Protein Interaktionen auf dem Einzelmoleküllevel zu untersuchen. Wir untersuchten verschiedene Bindungsmodelle des HP1 $\alpha$ -Proteins und beobachteten hochdynamisches Verhalten von HP1 $\alpha$  in Abhängigkeit der Verfügbaren Bindungsstellen und der HP1 $\alpha$ -Konzentration. HP1 $\alpha$ -Dimerisierung, welches multivalente Bindungen ermöglicht, erhöhte die Assoziation im Bezug auf Chromatin und verlangsamte die Dissoziation und führte folglich zu verstärkter Chromatinbindung. Ausserdem führten wir Experimente durch, um Chromatin- und DNS-Interaktionen mit PRC2 in Abhängigkeit des Zusatzfaktors PHF1 zu studieren. Wir erhielten erhöhte Residenzzeiten für PRC2, wenn PHF1 in den Messungen eingebunden war. Strukturvorhersagung und Mutagenesestudien identifizierten ein neues winged-helix (WH) Motif in PHF1, welches verantwortlich war für den erhöhten Bindingeffekt in Messungen mit PRC2-PHF1. Zusätzlich, beobachteten wir zeitlich verlängerte Chromatin-PRC2 Interaktionen, wenn H3K27me3-, H3K27M oder H3K36me3-Modifikationen vorhanden waren. Des weiteren charakterisierten wir den Chromatinschreibefaktor RNF168. Wir konnten veränderte Ubiquitylierungsaktivitäten, in Abhängigkeit von der Verfügbarkeit des Nukleosom-sauren-Flecks, welche durch Zuführung des Kompetitors RAPTA-C oder durch H4K16 Acetylierung, eine PTM charakteristisch für Euchromatin, verändert wurde, feststellen. RNF168 ist ein multivalenter Lesefaktor für Ubiquitin-Markierungen und dementsprechend zeigten wir spezifische Bindungen des Ubiquitin-Bindungsmoduls 1 (UDM1) zu nativen oder synthetisch hergestellten K63-gelinkten Ubiquitinketten, während K48-gelinkte Ubiquitinketten keine Interaktion herbeiführten. Im Gegensatz konnten wir keine klare Beteiligung des zweiten Ubiquitin-Bindungsmoduls (UDM2), welches H2A.XK15ub erkennen kann, nachweisen. Zusammenfassend konnten wir einen tieferen Einblick in die Bindungsarten von HP1 $\alpha$ , PRC2 und RNF168 gewinnen. Es ist von grosser Bedeutung grundsätzliche Bindungsmechanismen von Proteinen und Chromatin-Regulationsmechanismen zu verstehen, um neue Ziele für Medikamente zu finden.

## Schlüsselwörter

Chromatin, DNS-Schadens-Antwort, Einzelmolekül Totalreflexionsmikroskopie, exprimierte Proteinligation, Heterochromatinbildung, HP1 $\alpha$ , PHF1, PRC2, posttranslationale Modifikation, RNF168, Ubiquitylierungstest

## Abstract

Dynamic regulation of chromatin, a structure consisting of DNA and histone proteins, is mediated through histone post-translational modifications (PTMs) and effector proteins. HP1 $\alpha$  and PRC2 are recruited to repressive PTMs (H3K9me3, H3K27me3) and enable heterochromatin formation, which leads to gene silencing. During the DNA damage response, tight spatial and temporal control of the chromatin compaction state is required and novel PTMs are installed to guide proteins through dynamic signalling pathways. In the RNF168-mediated signalling cascade, appropriate DNA repair mechanisms are selected through ubiquitination (H2AK15ub) of chromatin. Improper regulation of these processes leads to cancer and neurodegenerative diseases. Here, we present a method to study chromatin-protein interactions employing total internal reflection fluorescence microscopy (TIRFM) and *in vitro* chromatin assembly of chemically defined, modified histones. Colocalization experiments of fluorescently labelled chromatin fibres and proteins allowed us to observe dynamic chromatin-protein interactions on the single-molecule level. We tested different binding models of HP1 $\alpha$ , and we measured a highly dynamic behaviour of HP1 $\alpha$  towards chromatin in dependence of the available binding sites or HP1 $\alpha$  concentration. HP1 $\alpha$  dimerization allows multivalent binding, increased chromatin association and decreased dissociation and thus leads to a more stable mode of chromatin binding. Further, we studied PRC2 recruitment to chromatin and DNA in dependence of the accessory factor PHF1. We measured increased residence times of PRC2 when PHF1 was included. Structure prediction and mutagenesis studies identified a novel winged-helix (WH) motif of PHF1, which was responsible for the enhanced binding effect in PRC2-PHF1 measurements. Moreover, binding of PRC2 towards chromatin was prolonged in the presence of H3K27me3, H3K27M or H3K36me3 histone PTMs. Next, we characterized the chromatin writer RNF168. We show altered ubiquitination activities dependent on accessibility of the nucleosome acidic patch, which was tested by addition of a competitor (RAPTA-C) or by introducing H4K16 acetylation, which leads to an open chromatin conformation. RNF168 is a multivalent reader of ubiquitin marks and we show binding specificity of ubiquitin binding module 1 (UDM1) towards native and synthetic K63-linked ubiquitin chains, while no interaction with K48-linked ubiquitin chains was detected. In contrast, we could not determine a clear contribution of the second binding module (UDM2), which recognizes H2A.XK15ub. In summary, we gained insight into different binding modes of HP1 $\alpha$ , PRC2 and RNF168. Understanding basal protein binding mechanisms and chromatin regulation is essential to find new drug targets.

## Keywords

Chromatin, DNA damage response, expressed protein ligation, heterochromatin formation, HP1 $\alpha$ , PHF1, post-translational modification, PRC2, RNF168, single-molecule total internal reflection fluorescence microscopy, ubiquitination assay

# CONTENTS

ACKNOWLEDGEMENTS.....	I
ABSTRACT (DEUTSCH).....	III
ABSTRACT .....	V
LIST OF FIGURES.....	XI
LIST OF TABLES.....	XV
LIST OF FORMULAS.....	XVII
I INTRODUCTION.....	1
1. Investigating a dynamic chromatin landscape	1
1.1. Chromatin packaging	1
1.2. Interpreting the histone code based on multivalent chromatin	4
2. Heterochromatin protein 1	9
3. Polycomb repressive complex 2	11
4. RNF168-dependent ubiquitination during the DNA damage response	13
4.1. The ubiquitination system	13
4.2. The DNA damage response cascade	15
5. Applied chemistry to functionalize proteins	19
6. Single-molecule studies of chromatin dynamics	25
6.1. Relevance of dynamic single-molecule analysis	25
6.2. TIRFM principles	26
7. Aims of the project	29
II RESULTS.....	33
1. Single-molecule dissection of dynamic heterochromatin establishment by HP1 $\alpha$	33
1.1. Introduction	33
1.2. Prerequisites for TIRF microscopy	36
1.2.1. HP1 $\alpha$ purification and labelling	37
1.2.2. Designing semi-synthetic chromatin fibres	42
1.2.3. Measuring protein dynamics on the single molecule level	45
1.3. HP1 $\alpha$ binds specifically to H3K9me3	48
1.4. HP1 $\alpha$ binds chromatin in a highly dynamic and competitive manner	53

1.5. Dimerization of HP1 $\alpha$ prolongs residence time on modified chromatin	54
1.6. Peptide-mediated dimerization of HP1 $\alpha$ prolongs binding on modified chromatin	60
1.7. Conclusion	65
2. Dynamics of the chromatin silencer complex PRC2	67
2.1. Introduction	67
2.2. PHF1 prolongs binding of PRC2 to chromatin and DNA	68
2.2.1. Expression, purification and labelling of PRC2	68
2.2.2. Determining PRC2-chromatin interactions on the single-molecule scale	70
2.3. A winged-helix domain of PHF1 is essential for PRC2-chromatin Interactions	75
2.4. Defined chromatin modifications prolong PRC2 binding events	81
2.5. Conclusion	83
3. RNF168 in the DNA damage response	85
3.1. Introduction	85
3.2. Generation of the ubiquitination machinery	86
3.3. Ubiquitination kinetics of chromatin fibres by RNF168	100
3.3.1. Activity of RNF168 towards chromatin arrays	100
3.3.2. RNF168-mediated ubiquitination depends on accessibility of the nucleosome acidic patch	103
3.3.3. Testing UDM2 of RNF168 with semi-synthetic H2A.XK15ub	105
3.4. UDM1 of RNF168 is able to bind K63-linked ubiquitin chains	110
3.5. Conclusion	111
<b>III CONCLUSIONS AND DISCUSSIONS.....</b>	<b>113</b>
1. HP1 $\alpha$ is a highly dynamic, multivalent chromatin reader	115
2. A winged-helix motif of PHF1 facilitates prolonged residence time of PRC2 on chromatin and DNA	117
3. K63-linked ubiquitin chains recruit RNF168 to chromatin via UDM1 and allow ubiquitination of H2A/H2A.X dependent on the nucleosome acidic patch	119
4. Concluding remarks	121
<b>IV MATERIAL AND METHODS.....</b>	<b>123</b>
1. MATERIALS	123

2. METHODS	125
2.1. SDS-polyacrylamide gel electrophoresis	125
2.2. Western blotting	125
2.3. Agarose gel electrophoresis	126
2.4. Cloning	126
2.4.1. CPEC	126
2.4.2. Gibson cloning	129
2.4.3. Bacmid production	131
2.5. Cell cultures and baculovirus production	132
2.6. Peptide synthesis	133
2.7. HP1 $\alpha$ purification and labelling	134
2.8. TEV protease expression and purification	136
2.9. Expression and purification of ubiquitin machinery proteins	137
2.9.1. UBE1 purification	137
2.9.2. UBE2D3 purification	137
2.9.3. Ubiquitin purification	138
2.9.4. RNF168 purification from bacterial expression	139
2.9.5. RNF168 purification from insect cell expression	140
2.10. CoA labelling	141
2.11. Ybbr labelling	141
2.12. Nucleosome core particle assembly	142
2.12.1. 177bp 601 DNA recovery	142
2.12.2. Histone octamer assembly	144
2.12.3. Mononucleosome assembly	145
2.12.4. Chromatin assembly	145
2.13. Agarose polyacrylamide composite gel electrophoresis	146
2.14. Preparation of flow channels for TIRF microscopy	146
2.15. TIRF imaging	147
2.15.1. HP1 $\alpha$ TIRF imaging	148
2.15.2. PRC2 TIRF imaging	148
2.15.3. TIRF data analysis	149
2.16. Thermophoresis assays	150
2.17. Ubiquitination assays	150
2.18. Pull-down of ubiquitin chains by RNF168	151

2.19. FRAP measurements	152
V ABBREVIATIONS.....	153
VI APPENDIX.....	159
VII REFERENCES.....	169
VIII CURRICULUM VITAE.....	181



## List of Figures

Figure 1 Nucleosome X-ray structure (human)	1
Figure 2 Two-start helix model of the chromatin 30 nm-fibre	3
Figure 3 Histone post-translational modifications	5
Figure 4 Writers, readers and erasers of the histone code	6
Figure 5 Conserved structure of the HP1 protein family	9
Figure 6 Core components of the PRC2 complex including PHF1	12
Figure 7 Attachment of ubiquitin to a substrate lysine by a native peptide bond using E1, E2 and E3 enzymes	13
Figure 8 Crystal structure of ubiquitin and the seven lysine residues	14
Figure 9 DNA damage response cascade illustrating ubiquitination by RNF8 and RNF168	16
Figure 10 Reaction scheme of native chemical ligation	19
Figure 11 Intein splicing	21
Figure 12 Intein <i>trans</i> -splicing	22
Figure 13 Expressed protein ligation	23
Figure 14 Total internal reflection illumination	27
Figure 15 Possible binding modes for HP1 $\alpha$	34
Figure 16 Experimental setup of TIRF measurements	35
Figure 17 HP1 $\alpha$ final fraction (15 % SDS-PAGE gel)	37
Figure 18 Synthesis and purification of peptide P1	38
Figure 19 Reaction scheme of EPL for HP1 $\alpha$ labelling	40
Figure 20 Labelling and analysis of HP1 $\alpha$	41
Figure 21 Traceless semi-synthesis of H3K9me3	42
Figure 22 Histone octamer integrity and chromatin formation	44
Figure 23 Verification of the H3K9me3 histone mark and chromatin integrity of full-length arrays	45
Figure 24 Photobleaching of HP1 $\alpha$ -Atto532, laser penetration and chromatin integrity during single molecule conditions	47
Figure 25 Experimental setup to monitor HP1 $\alpha$ dynamics on chromatin and generation of cumulative histograms	50
Figure 26 HP1 $\alpha$ binds specifically H3K9me3-modified chromatin, which mediates rapid rebinding	53
Figure 27 HP1 $\alpha$ binds in a competitive manner to H3K9me3-modified chromatin	54

Figure 28 Strategy to covalently link HP1 $\alpha$ in its dimeric form containing a fluorescent label	55
Figure 29 Peptide synthesis of P2	56
Figure 30 Analysis of covalently linked dimeric HP1 $\alpha$ after expressed protein ligation with the labelled peptide P2	58
Figure 31 Kinetics of HP1 $\alpha_{\text{cdm}}$	59
Figure 32 Two-dimensional histogram to compare dissociation and association behaviour of HP1 $\alpha$ and HP1 $\alpha_{\text{cdm}}$	60
Figure 33 Foci formation of mEOS3.2-HP1 $\alpha$ (wt, I163E and W174A) and enhanced FRAP of mEOS3.2-HP1 $\alpha$ mutants compared to wt mEOS3.2-HP1 $\alpha$	61
Figure 34 Analysis of peptide P3 and P4 after synthesis	62
Figure 35 Thermophoresis unveils interactions between P3 and HP1 $\alpha$	63
Figure 36 Dissociation- and association kinetics of HP1 $\alpha$ without and with peptides P3 and P4	64
Figure 37 Possible binding modes for PRC2 in dependence of PHF1	68
Figure 38 Ybbr-labelling of a protein	69
Figure 39 Purified and fluorescently labelled PRC2 (SDS-PAGE, 13 %)	70
Figure 40 Monitoring PRC2 binding towards chromatin on the single molecule level	71
Figure 41 Chromatin and DNA TIRF measurements unveil binding of PRC2 or prolonged binding of PHF1-PRC2	73
Figure 42 High-affinity binding of PRC2 to mononucleosomes and DNA is enhanced by PHF1	75
Figure 43 Crystal structure of Pcl <sub>PHD2-WH</sub>	76
Figure 44 Testing mutants of Pcl <sub>PHD2-WH</sub>	77
Figure 45 The Pcl and PHF1 domains bind dsDNA	78
Figure 46 Generation of DY-547 labelled PHF1 <sup>WH&gt;E</sup> -PRC2	78
Figure 47 Dissociation and association kinetics of PRC2, PHF1-PRC2, PHF1 <sub>C</sub> -PRC2 and PHF1 <sup>WH&gt;E</sup> -PRC2 towards chromatin and naked DNA	79
Figure 48 DNA binding of PRC2 by PHF1 permits more efficient H3K27 methylation	81
Figure 49 H3K27me3-, H3K27M- and H3K36me3-modified chromatin fibres prolong PRC2 residency time	82
Figure 50 Possible binding modes for RNF168	85
Figure 51 UBE1 purification relies on protein expression in Rosetta cells (15 % SDS-PAGE gels)	87
Figure 52 UBE2D3 re-cloning, expression and purification (15 % SDS-PAGE gels)	89
Figure 53 Activity assay to monitor ubiquitination of H2A in histone octamers dependent on UBE2D3 (15 % SDS-PAGE gel)	90

Figure 54 Tag-less ubiquitin purification and analysis by RP-HPLC and ESI-MS	91
Figure 55 C-ubiquitin labelling and analysis by SDS-PAGE, RP-HPLC and ESI-MS	92
Figure 56 Maps of RNF168 constructs indicate ubiquitin binding modules (UDM1 and UDM2) and the catalytic RING domain	94
Figure 57 RNF168 expression and purification	96
Figure 58 Activity assay to monitor ubiquitination of H2A in histone octamers based on RNF168(196) (15 % SDS-PAGE gel)	97
Figure 59 Sfp labelling of RNF168(196)	98
Figure 60 S200 10/300 GL size exclusion of RNF168(196)-Alexa568 using buffer W (5 mM BME)	98
Figure 61 Activity assay to monitor ubiquitination of H2A in histone octamers based on RNF168(196) labelling (15 % SDS-PAGE gel)	99
Figure 62 Ubiquitination assay to monitor ubiquitination of H2A in histone octamers at 60 min by excluding different components (15 % SDS-PAGE gel)	101
Figure 63 Ubiquitination assay towards chromatin	102
Figure 64 Ubiquitination kinetics towards chromatin	102
Figure 65 Structure of RAPTA-C and the non-specific compound RAED-C	103
Figure 66 Ubiquitination kinetics towards chromatin (wt and H4K16ac) and impact of RAPTA-C (wt chromatin)	104
Figure 67 Quantification of ubiquitination kinetics (unmodified and H4K16ac chromatin, RAPTA-C)	105
Figure 68 Insect cell expression of full-length RNF168 for 4 days in Sf900 II medium	106
Figure 69 Purification of full-length RNF168 (RNF168F)	107
Figure 70 Activity assay of RNF168F	108
Figure 71 Ubiquitination kinetics towards chromatin (100nM) containing H2A.X and H2A.XK15ub	109
Figure 72 Specific K63-linked-ubiquitin chain pull-down by GST-RNF168(196)	110
Figure 73 Specific K63-linked-ubiquitin chain (native and synthetic) pull-down by GST-RNF168(196)	111



## List of Tables

Table 1 Kinetic parameters of HP1 $\alpha$ – chromatin interaction dynamics	65
Table 2 Kinetic parameters of PRC2 from TIRF measurements	83
Table M1 PCR reaction for vector of interest (CPEC)	127
Table M2 PCR reaction for insert of interest (CPEC)	127
Table M3 PCR program for vector/insert of interest (CPEC)	128
Table M4 CPEC PCR reaction: 2x25 $\mu$ l	128
Table M5 CPEC PCR program	128
Table M6 PCR reaction for vector of interest (Gibson)	129
Table M7 PCR reaction for insert of interest (Gibson)	130
Table M8 PCR program for vector/insert of interest (Gibson)	130
Table M9 PCR program for bacmid verification	132
Table M10 PCR reaction to create 1x177 bp 601 DNA	144
Table M11 PCR program to create 1x177bp 601 DNA	144
Table A1	159
Table A2	160
Table A3	163
Table A4	165
Table A5	166



## List of formulas

1 Snell's law	27
2 Critical angle (TIRF)	27
3 Penetration depth (evanescent field)	28
4 Dissociation kinetics	51
5 Association kinetics	51
6 Dissociation rate constant (of the short phase)	51
7 Microscopic association rate constant	51
8 Dissociation rate constant per nucleosome	51
9 Bleaching correction	72
10 Microscopic association rate constant (PRC2)	83
M1 Viral amplification	133
M2 Ubiquitination success	151
M3 Ubiquitination normalization factor	151
M4 Normalized band intensity	151
M5 Histone H2A normalization factor	151
M6 Normalized band intensity (H2A)	151





# I Introduction

## 1. Investigating a dynamic chromatin landscape

### 1.1. Chromatin packaging

Since the discovery of the involvement of deoxyribonucleic acid (DNA) in hereditary processes in 1944 and its double-helical structure in 1953, we interpret DNA as the macromolecular basis of inheritance in prokaryotes and eukaryotes<sup>1, 2</sup>. Compaction of DNA into chromatin, a highly ordered structure of DNA, histones, and a selection of non-histone proteins, is crucial to store the eukaryotic genome in the limited volume of a single cell, while maintaining DNA accessible and receptive to dynamic regulation processes such as replication, transcription and DNA damage repair<sup>3</sup>.

Eukaryotic DNA is assembled into a basic subunit called nucleosome, which is formed between ~147 bp DNA and four pairs of the core histones (H2A, H2B, H3 and H4)<sup>4-6</sup>. Already in 1997 the nucleosome crystal structure has been solved at high resolution (2.8 Å) and gave detailed insight into structural details of the nucleosome unit<sup>5</sup>. Histone octamers are formed from H3-H4 tetramers and two H2A-H2B heterodimers and electrostatically interact with DNA, which is typically wrapped 1.65 times around the histone octamers (Fig.1)<sup>5, 7-9</sup>. The core nucleosome, as we described it above, is normally linked to further nucleosomes through ~10-80 bp linker sequences, which can be occupied by linker histones (H1 or H5)<sup>10, 11</sup>. Such nucleosome particles that include ~165 bp DNA, the core histones and the linker histone are called chromatosomes. However, despite the outlined differences, these nucleosomal core particles are often referred to as “nucleosomes” in the literature.

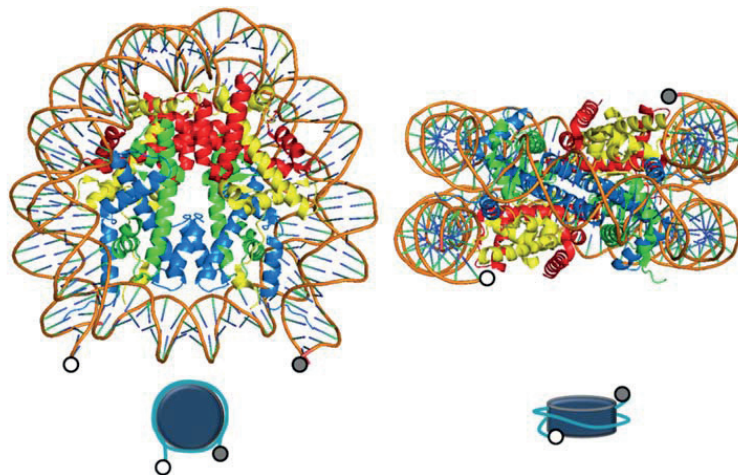


**Fig.1 Nucleosome X-ray structure (human)**

Crystal structure of the nucleosome at 2.5 Å resolution. Histone H2A (yellow), histone H2B (red), histone H3 (blue), histone H4 (green). White-grey circles serve as reference position of the DNA ends. The blue disc indicates the spatial orientation of the nucleosome. PDB: 3AFA (Tachiwana et al., 2010).

While the central  $\alpha$ -helical region of histone octamers is covered by the two-folded turns of DNA, histones possess unstructured tails at the N-/C-terminus, which protrude out of the nucleosome core and can be chemically modified at distinct positions<sup>12</sup>. This leads to various functional and structural outputs as discussed later.

Nucleosomes possess a variety of interesting features, which gives them distinct roles in chromatin architecture<sup>6</sup>. Essentially, electrostatic wrapping of DNA around highly positively charged histone octamers leads to organized compaction of DNA material inside the nucleus of a cell. The disc-like shape of nucleosomes provides a platform for regulatory proteins to interact with the DNA sequence. In particular, a negatively charged surface area in the groove of the H2A/H2B dimer, called the nucleosome acidic patch, has been shown to act as an interaction platform for certain proteins<sup>13</sup>. However, accessibility of the acidic patch can be altered by different post-translational modifications (PTMs) of histone tails. If, for example, the H4 N-terminal tail is modified as such that its positive charge at lysine 16 is removed, the histone tail will lose its usually tight electrostatic interaction with the nucleosome acidic patch<sup>14</sup>. It is a general paradigm that histone modifications serve as regulatory switches to regulate accessibility of DNA in chromatin. Regulation by histone modifications can directly affect nucleosome stability and may further lead to higher-ordered chromatin structures, a modulation which enables even tighter compaction of chromatin.

Traditionally, it was thought that nucleosomes were wrapped like beads on a string, also known as 10 nm-fibre and further compacted into higher ordered structures such as 30 nm fibres, chromatids and mitotic chromosomes<sup>11</sup>.

Several models of chromatin folding at the “30 nm-fibre”-level have been found. The one-start solenoid model, where nucleosomes interact with each other and follow a helical trajectory, was developed based on a study using cryoEM<sup>15</sup>. Alternatively, the two-start helix with two intertwined stacks of nucleosomes and compact tetranucleosomes as a basic unit was postulated based on high resolution studies of cryoEM and X-ray crystallography (Fig.2)<sup>15-19</sup>. Importantly, the two-start model with tetranucleosomes explains the interactions between the nucleosome acidic patch and the contacting H4 tail, and inter-nucleosomal interactions between the C-terminal helices of H2A and H2B are enabled<sup>17-19</sup>. A recent study from our own lab has investigated the dynamic behaviour of chromatin, which indicated the existence of the two-start model and underlined the importance of dynamic regulation of chromatin fibres<sup>19</sup>. Changes in nucleosome stacking in the micro- to millisecond timescale were observed, which over time might render different accessible chromatin structures and thus enable different proteins to interact.

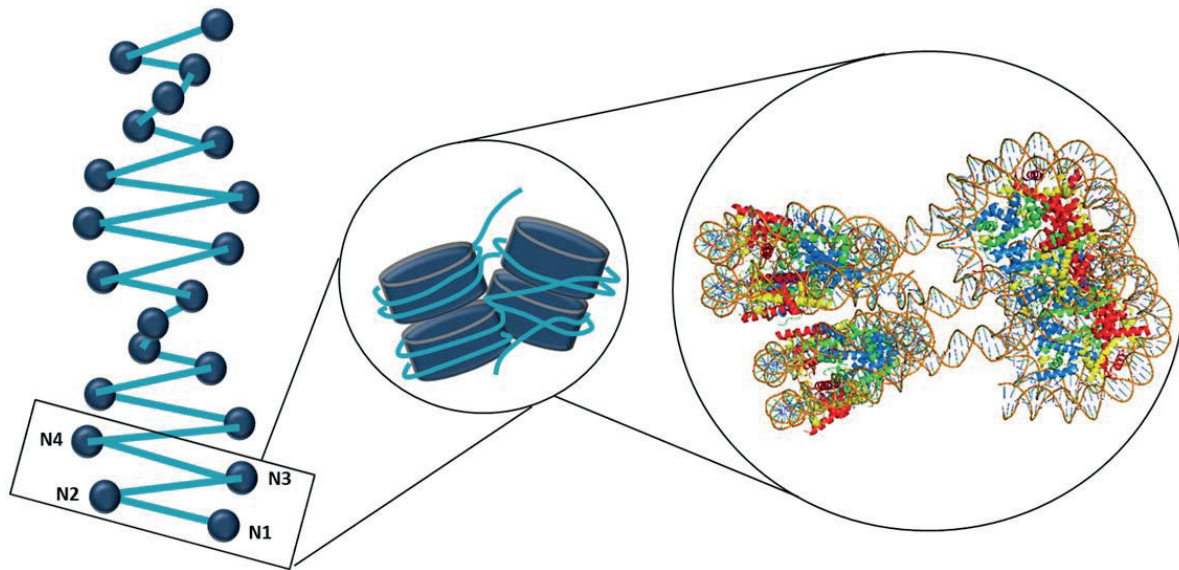


**Fig.2 Two-start helix model of the chromatin 30 nm-fibre**

A possible model of the 30 nm-fibre showing intertwined stacks of nucleosomes. The zoomed view shows a tetranucleosome unit, which is further enlarged to the tetranucleosome crystal structure. Blue spheres/cylinders denote nucleosomes, cyan treads denote DNA, N1-4 denotes the nucleosome number. PDB: 5OY7 (Ekundayo et al., 2017). Figure was adapted from Robinson et al., 2006.

However, chromatin higher order structures have been a topic of various discussions recently. A study, which combines electron microscopy tomography (EMT) with a labelling method (ChromEMT) that selectively enhances the contrast of DNA, was able to reproduce the 30 nm fibre structure *in vitro*, but not from human interphase or mitotic cells *in situ*<sup>20</sup>. Based on these findings, the authors argue against 30 nm fibres and 300-700 nm structures and conclude that chromatin is a flexible and disordered 5-24 nm diameter granular chain that folds into different concentration densities dependent on the cell cycle. Consistently, heterogeneous populations of chromatin have been observed and argue against a simple overall structure of chromatin<sup>21</sup>. Very likely chromatin organization depends on the surrounding environment including  $Mg^{2+}$  concentrations, the presence of linker histones and the linker length and thus may be able to rapidly adapt a diversity of structures<sup>19</sup>. This is compatible with the recent findings from our laboratory, showing that two-start contacts are preferred, but that chromatin fibres are dynamic and heterogeneous, thus unlikely to be observed over long length-scales in interphase chromatin<sup>19</sup>.

Together, these studies indicate that chromatin is a highly dynamic system and not merely a rigid structure. Despite the intrinsic ability of chromatin to undergo structural changes *in vitro*, remodelling *in vivo* is often mediated by chromatin remodelling proteins or by chromatin effectors, which are able to install or remove PTMs (“writers” and “erasers”) or interpret them (“readers”) to fulfil regulatory functions<sup>22</sup>. In addition, chromatin structure can also be directly influenced by histone modifications through the presence of a steric bulk

<sup>23</sup>.

## 1.2. Interpreting the histone code based on multivalent chromatin

The DNA sequence encodes for genes, which are transcribed into ribonucleic acid (RNA) and then translated into proteins. Regulation of gene expression is often mediated by chemical modifications of DNA as e.g. DNA methylation and by PTMs of histone proteins.

In the recent past, numerous different histone modifications with various functional outputs have been discovered. For example methylation of lysine and arginine residues has been shown to lead to transcriptional activation (H3K4me3, H3K36me3 or H3K79me3) or repression (H3K27me3, H3K9me3 or H3K56me3), depending on its position on the different histones<sup>24-30</sup>. Other modifications like histone acetylation are obligatory activating histone marks<sup>28</sup>. Known histone modifications also include ADP ribosylation, sumoylation, neddylation, citrullination of arginines, crotonylation of lysines, phosphorylation of serine, tyrosine and threonine residues and ubiquitination of lysines (Fig.3a and 3b)<sup>31</sup>. Since the early days of chromatin research, chromatin has been separated in two groups: Heterochromatin and euchromatin. While euchromatin is considered to be transcriptionally active and accessible chromatin being decorated with activating histone marks, heterochromatin describes a state of chromatin where nucleosomes are tightly packed and transcription of genes is generally suppressed. However, histone modifications exert functions beyond transcription and regulate cell signalling, DNA damage repair and DNA replication. Namely, phosphorylation and ubiquitination are modifications that are crucial for initiation of DNA damage repair.

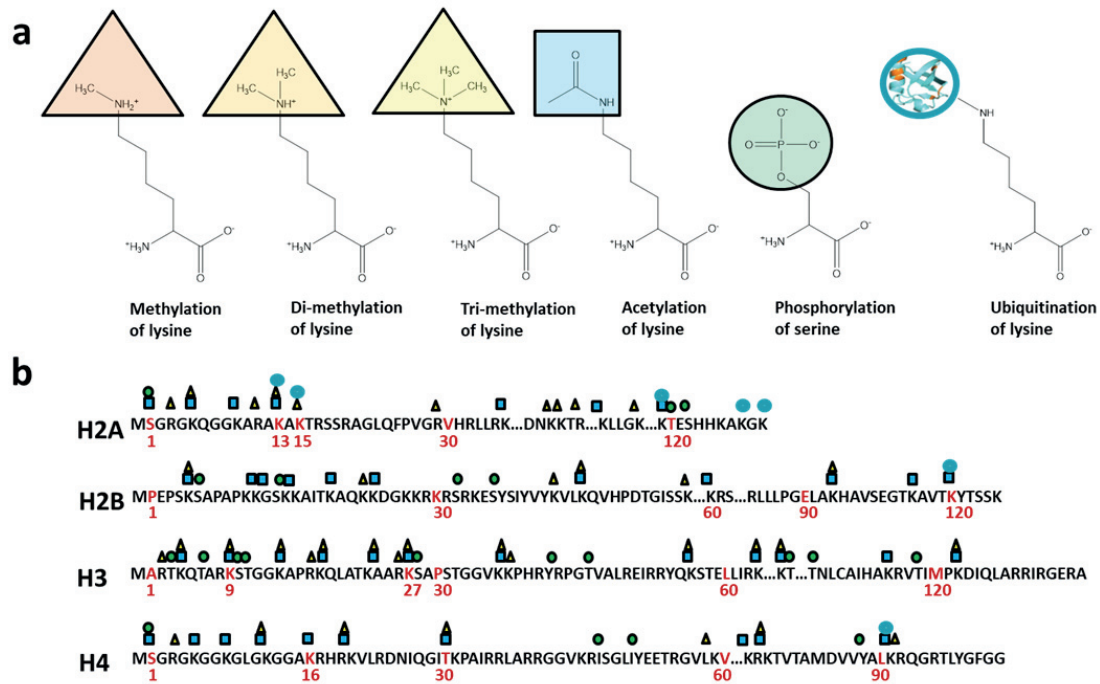


**Fig.3 Histone post-translational modifications**

**a)** Post-translational modifications of histones include mono-, di-, tri-methylation (triangles), acetylation (blue square), phosphorylation (green circle) and ubiquitination (cyan circle). The structures inside the different shapes indicate the attached chemical modification to the indicated amino acid. **b)** Shown are the amino acid sequences of human histones H2A, H2B, H3 and H4 with the known histone modifications including H2AK13/15ub, H3K9me3, H3K27me3 and H4K16ac, which are relevant for this study. The histone modification map was adapted from [www.activemotif.com](http://www.activemotif.com), «Histone modifications guide», 2018.05.01.

Nowadays, we know that histone modifications can influence chromatin condensation in a direct manner. For example acetylation of histone 4 at lysine 16 (H4K16ac) has been shown to lead to de-compaction and is associated with the transcriptionally active state of chromatin, as the typically basic tail of histone H4 is neutralized through acetylation and prevents interactions with the nucleosome acidic patch on H2A/H2B<sup>14, 32-35</sup>. Further it has been shown that ubiquitination of H2B at its C-terminus (H2BK120) also directly prevents chromatin condensation<sup>23</sup>. Thus, chromatin compaction can be altered through histone modifying complexes, as for ubiquitination on H2BK120, which is “written” through the dimeric “writer protein” RNF20/40<sup>36</sup>. More broadly, the term writer protein is used to describe the proteins, which are able to chemically modify the histone tails selectively at certain residues. They can be recruited through different modes of interactions such as binding to histones, adaptor proteins, pre-installed histone modifications or directly through DNA interactions.

Alternatively, chromatin structure can be altered by ATP-dependent remodelling complexes (e.g. SWI2/SNF2 or ISWI type complexes), which use the energy of ATP hydrolysis



to actively change chromatin structure during replication, transcription and DNA damage repair<sup>37, 38</sup>.

Histone marks are not always affecting chromatin regulation in an obvious manner. Often PTMs regulate chromatin indirectly, by recruiting effector proteins, which can bind to the respective histone mark and exert their function. Such proteins, called “reader” proteins, are able to recognize the modification of interest through a binding pocket. Well known examples of reader domains are the bromo domain of Bromodomain-containing protein 4 (BRD4), which recognizes acetyl-lysines or the chromo domain of heterochromatin protein 1 alpha (HP1 $\alpha$ ), which binds H3K9me3<sup>39-41</sup>. Binding of HP1 $\alpha$  to H3K9me3-decorated chromatin leads to formation of heterochromatin, which renders chromatin rather inaccessible. In such a condition, replication of DNA is hindered, which indicates that there is a necessity to revert the condensed chromatin state. A member of the demethylase KDM4 protein family (KDM4d), originally implicated in the DNA damage response, has been shown to play a role in demethylation of H3K9me3, which subsequently allows DNA replication<sup>42, 43</sup>. Proteins like KDM4d, which are able to remove PTMs in chromatin, are called “erasers”. They are separated into distinct families, as for example, demethylases, deubiquitinating enzymes (DUBs), phosphatases or deacetylases (HDACs), depending on which PTM they are capable of converting (Fig.4)<sup>44</sup>.

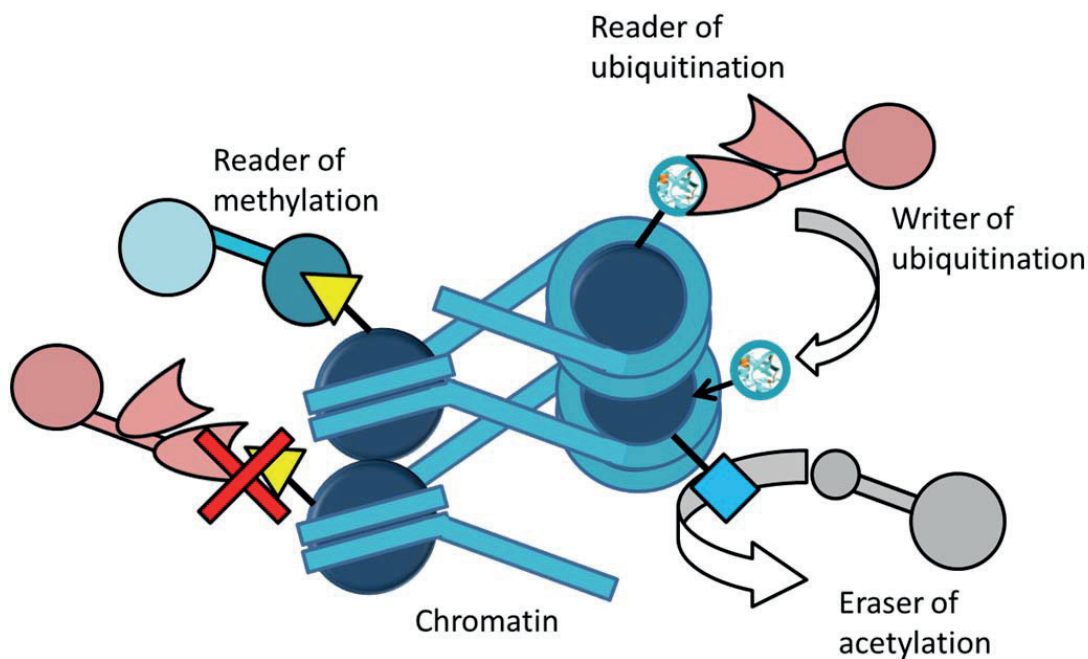


**Fig.4 Writers, readers and erasers of the histone code**

Reader proteins (red and blue) can specifically bind to histone PTMs, depending on their reader domain. Writer proteins (red) are able to install histone PTMs on chromatin. Histone PTMs can be removed by eraser proteins (grey). Yellow triangle = methylation, blue square = acetylation, cyan circle = ubiquitin, blue spheres = nucleosomes, cyan threads = DNA.

The simple picture of chromatin regulation quickly complicates by the fact that different chromatin modifications on a genomic region can be installed on different nucleosomes, different histones within nucleosomes, different histone tails within a histone and even on the same histone tail. In addition, two reader domains/proteins are able to bind in a bivalent mode to two different histone PTMs at the same time. Spatial and temporal control of chromatin writers, readers, erasers and histone PTMs is essential to regulate cell homeostasis and integration of multiple histone marks, based on their abundance on chromatin and the presence of multivalent reader proteins, leading to fine-tuning of cell regulatory pathways. This renders a programmable mechanism of selective gene regulation, which can be inherited without altering the DNA sequence itself and is known as the histone code<sup>12</sup>.

In this study we have investigated different proteins that employ different binding modes. HP1 $\alpha$  and polycomb repressive complex 2 (PRC2) are involved in the formation of different types of heterochromatin and maintenance of the chromatin silent state and are expected to exert different binding modes on chromatin, as discussed later<sup>45-47</sup>. A protein with two distinct reader domains is reflected by the DNA damage response (DDR) protein Ring finger protein 168 (RNF168) and a cooperative effect of chromatin binding is expected between these two domains<sup>48, 49</sup>.

In the following, we will introduce these chromatin effectors in more detail.





## 2. Heterochromatin protein 1

HP1 was discovered as a dominant-repressor of position-effect variegation in *Drosophila*<sup>50, 51</sup>. The highly conserved HP1 family is encoded by a class of genes called chromobox (CBX) genes<sup>52</sup>. In mammals, HP1 genes are transcribed from three different genes: The human chromosome 12 encodes for HP1 $\alpha$  (CBX5), chromosome 17 encodes for HP1 $\beta$  (CBX1) and chromosome 7 encodes for HP1 $\gamma$  (CBX3)<sup>53</sup>. Moreover, the HP1 protein family in mammals is present as several pseudogenes, which indicates multiple duplication events during evolution<sup>52</sup>. This is most likely the reason for the similarity of HP1 protein domains, because all three proteins of the HP1 protein family share a common structure of five exons, which result in a chromo domain (CD) and a chromoshadow domain (CSD), both of them being highly conserved<sup>52, 54, 55</sup>. The CD of human HP1 proteins is necessary to bind H3K9me3<sup>56, 57</sup>. The CSD is crucial for HP1 dimerization, which can be facilitated by peptides containing a PxVxl/L motif such as the human shugoshin 1 protein (hSgoL1, amino acids (AA) 448-457)<sup>58, 59</sup>. The linker region between CD and CSD, which consists of positively charged AAs, is able to bind in a non-specific manner to DNA and RNA<sup>52, 60-62</sup>. Thus, HP1 is a multivalent effector protein, which is able to bind DNA and one or several H3K9me3 marks and represents an ideal model system to investigate protein-DNA, protein-chromatin and protein-protein interactions (Fig.5)<sup>52, 59, 63</sup>.

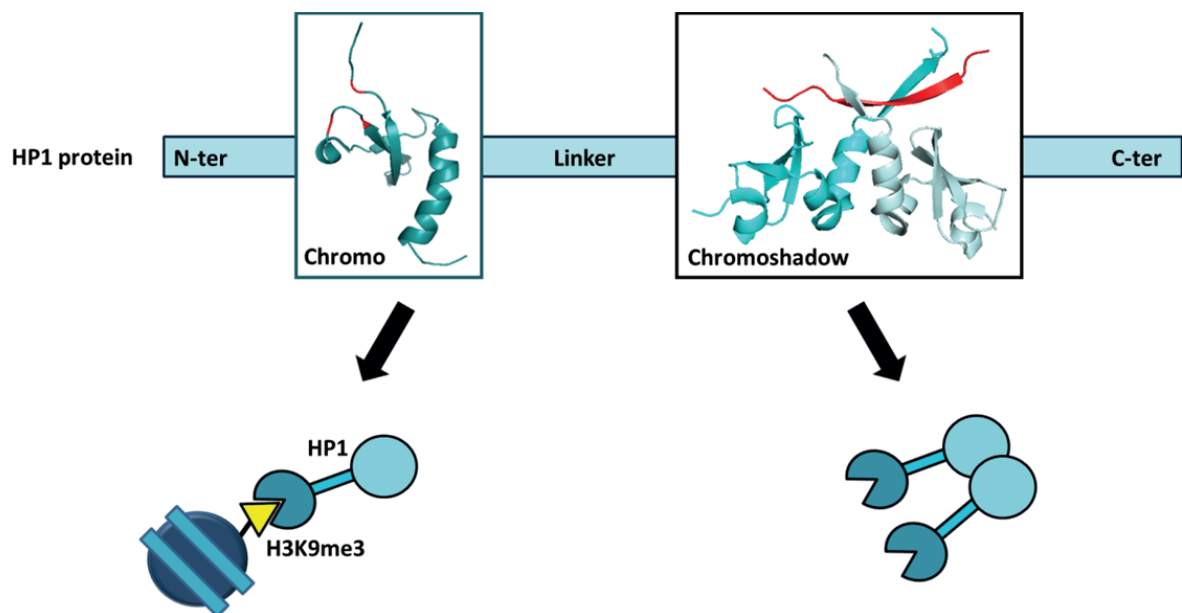


**Fig.5 Conserved structure of the HP1 protein family**

HP1 proteins translate into an H3K9me3-binding chromo domain, a hinge-region (linker) and a chromoshadow domain, which enables protein dimerization. Red residues on the chromo domain indicate the aromatic cage for binding of methylated lysine 9 (Tyr 20, Trp 41, Phe 44). The red peptide (hSgoL1) on the dimeric chromoshadow domain facilitates dimerization.

Crystal structures were retrieved from PDB: 2RVL (chromo domain, Shimojo et al., 2016) and 3Q6S (chromoshadow domain, Kang et al., 2011).

In contrast to HP1 $\beta$  and  $\gamma$ , which are able to associate with hetero- and euchromatin, HP1 $\alpha$  has been shown to bind only to heterochromatin, especially to centromeres and telomeres<sup>64</sup>. Consistently, proteins from the HP1 family play an important role in chromatin compaction<sup>65</sup>. Further, they are involved in viral latency and they control transposons via DNA methylation<sup>66, 67</sup>. Moreover, the *S.pombe* HP1 homolog (Swi6) has been shown to associate with chromatin and form oligomeric structures<sup>45</sup>. Altogether, these findings support the important role of HP1 in heterochromatin formation.

Although heterochromatin is often represented as rigid and transcriptionally inactive structure, HP1-associated heterochromatin has to remain highly dynamic. Foci of heterochromatin in the nucleus, including HP1 proteins, are visible over generations of cells. Individual HP1 molecules however are highly dynamic as shown by fluorescence recovery after photobleaching (FRAP) and fluorescence fluctuation microscopy<sup>68, 69</sup>. This observation is not surprising as in various processes, like DNA damage response or cell division, heterochromatin has to be de-condensed and HP1 has to be evicted rapidly to render chromatin easily accessible again.

During this project we aimed to study the dynamic behaviour of different proteins towards chromatin on the single molecule level using total internal reflection microscopy (TIRFM), which is a method to study fluorescently labelled molecules within a thin volume section, while reducing background fluorescence. Thus, HP1 $\alpha$  reflected an interesting binding model based on its ability as a mono- or multivalent reader of H3K9me3<sup>45, 58, 70</sup>.

### 3. Polycomb repressive complex 2

Another important factor responsible for gene repression, by formation of facultative heterochromatin is the polycomb group protein (PcG) complex PRC2, which is a reader and writer of the histone PTM H3K27me3<sup>71</sup>. Being a multi-protein complex enables PRC2 to tune its functions by addition and replacement of different subunits.

PcG proteins are implicated in chromatin silencing, the DNA damage response and contain methyl mark writer domains, as well as ubiquitin writer domains and thus serve as a highly diverse model to study protein-chromatin binding dynamics.

Members of the PcG proteins cover a set of highly conserved proteins across plants, insects and mammals and are involved in formation and maintenance of a chromatin silent state<sup>46, 72, 73</sup>. This involves homeotic gene regulation as well as human X chromosome inactivation in females, and mutants of PcG proteins are often associated with cancer<sup>74, 75</sup>.

PcG-mediated silencing is driven by at least two multi-protein complexes, namely polycomb repressor complex 1 (PRC1) and PRC2<sup>47, 76</sup>. The human PRC2-complex consists of several core proteins including embryonic ectoderm development (EED), suppressor of zeste 12 protein homolog (SUZ12), retinoblastoma-binding protein 4 (RBBP4) and the catalytic subunit enhancer of zeste homolog 2 (EZH2), which drives H3K27me3<sup>77</sup>. EZH2 is structured into several domains, including the EED-binding domain (EBD), the SANT2 domain, which mediates RNA binding and the catalytic SET domain, which depends on EED and SUZ12<sup>78-80</sup>. EED is a reader protein involved in recognition of H3K27me3, which enables PRC2-mediated heterochromatin spreading<sup>81</sup>. Consistently, mice lacking either EED, SUZ12 or EZH2 are not viable and display severe developmental and proliferative defects<sup>82</sup>. RBBP4 has been shown to be involved in nucleosome binding including histone H4<sup>83</sup>.

PRC1, is essentially formed by RING1B/BMI1, CBX4 and PH1, can bind to H3K27me3, downstream of PRC2, and acts as a RING-E3 ubiquitin ligase towards H2AK119, which further leads to gene silencing in chromatin<sup>84, 85</sup>.

Despite the conserved core subunits, the PcG family of proteins contains many members, which are interchangeable with particular subunits or can be added to one or the other polycomb repressive complex. The regulation and dynamics of these complexes is not yet well understood.

One of the earliest studied PcG genes in *D. melanogaster* was Polycomblike (Pcl)<sup>86</sup>. Knockout of the Pcl gene in the fly led to homeotic transformations and already implicated its role in PcG-regulated processes<sup>86</sup>. In mammals three paralogs of Pcl are known. All four homologs, Pcl, PHF1, MTF2 and PHF19, share a tudor domain and two plant homeodomain (PHD) finger domains. Interestingly, interaction of Pcl/PHF1 and PRC2 was required to catalyse H3K27me3 at high efficiency and Pcl/PHF1 seemed to recruit PRC2 to its target sites<sup>87-90</sup>. Moreover, direct interactions of Pcl with enhancer of zeste (E(Z)), the *Drosophila*

homolog of EZH, have been shown by the PHD fingers of Pcl<sup>91</sup>. However, the mechanism, how PHF1 enables PRC2 to perform efficient chromatin methylation, has not been elucidated in detail (Fig.6).

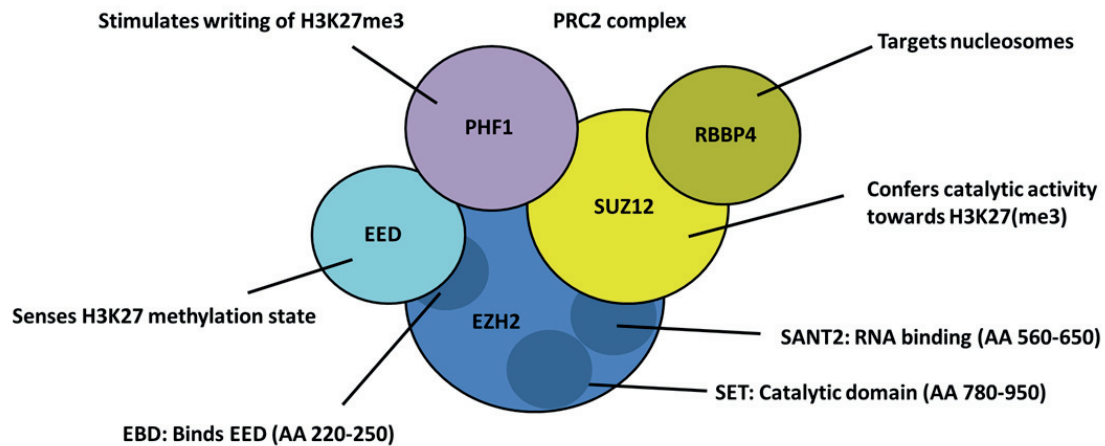


**Fig.6 Core components of the PRC2 complex including PHF1**

Shown is a schematic illustration of the PRC2 complex containing EED, SUZ12, RBBP4, EZH2 and PHF1. Indicated are the EBD-, SANT2- and SET-domains of EZH2.

## 4. RNF168-dependent ubiquitination during the DNA damage response

Coupling reader and writer functionality in effector complexes is not only observed for proteins regulating gene expression, but a common feature of most chromatin signalling pathways. A key signalling pathway is the DDR, which is triggered upon detection of DNA damage. It involves a cascade of chromatin enzymes, including kinases as well as multiple ubiquitin ligases, which read-out the chromatin state and modify histones, resulting in progressive chromatin ubiquitination<sup>92</sup>. In the following we provide a primer on the ubiquitination system in general and key factors in the DDR, in particular RNF168.

### 4.1. The ubiquitination system

Ubiquitination describes the process of installing a small protein, ubiquitin, on a suitable substrate. Ubiquitin is a highly conserved, globular protein of 8.6 kilo Dalton (kDa) and 76 AAs. It can be attached on its C-terminal glycine residue to a lysine of a suitable substrate. This process is mediated by an ubiquitin-activating enzyme (E1), which uses ATP as energy source and transfers the ubiquitin-moiety via a thioester bond to an ubiquitin-conjugating enzyme (E2). The E2 enzyme, containing ubiquitin, can be recognized by an ubiquitin ligase (E3), which ultimately transfers ubiquitin to its substrate (Fig.7)<sup>93</sup>.

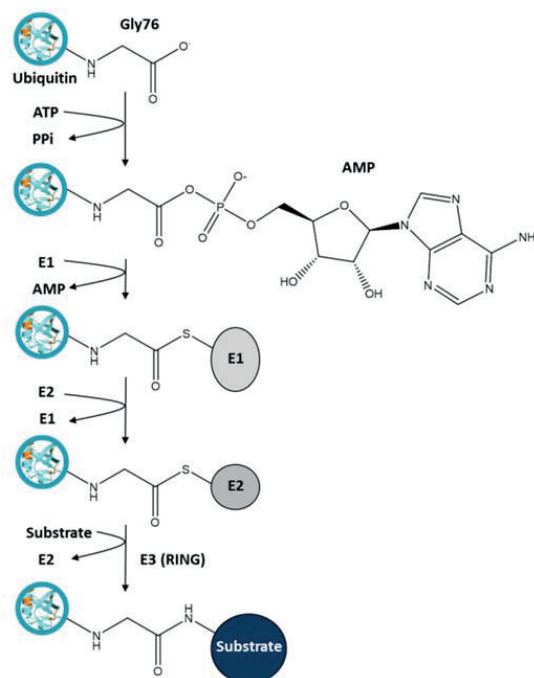


**Fig.7 Attachment of ubiquitin to a substrate lysine by a native peptide bond using E1, E2 and E3 enzymes**

Illustrated is the establishment of an ubiquitin post-translational modification on a substrate via E1, E2 and E3 (RING) enzymes by the use of ATP, mediated through thioester bonds. Figure was adapted from Kleiger et al., 2014.

Interestingly, ubiquitin itself contains seven lysine residues (K6, K11, K27, K29, K33, K48, K63), which can be ubiquitinated and which leads to ubiquitin chain formation (Fig.8)<sup>94-96</sup>. Dependent on the linkage-type ubiquitin chains can adopt a rather compacted or open conformation and different ubiquitin chains have been assigned to different cellular functions<sup>97-102</sup>. For example K11- and K48-chains are considered a mark for proteosomal degradation<sup>94, 103, 104</sup>. K63-chains on the other hand have been implicated in DNA damage repair, endocytosis and kinase activation<sup>105, 106</sup>.

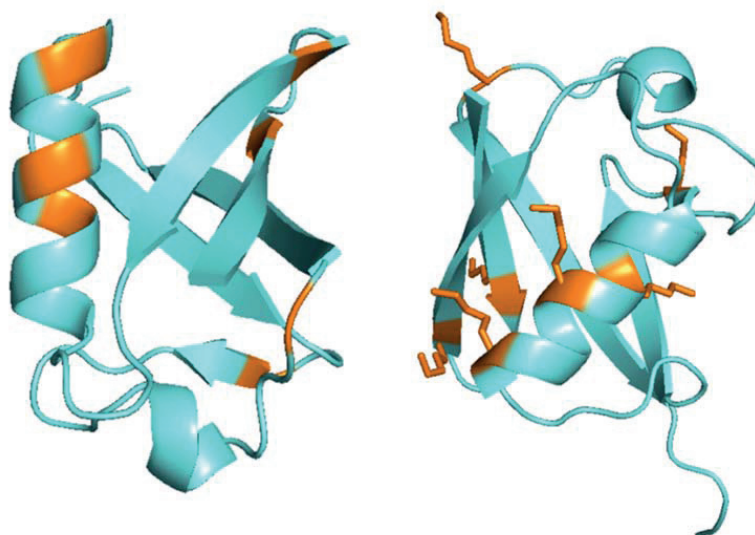


**Fig.8 Crystal structure of ubiquitin and the seven lysine residues**

Shown is the crystal structure of human ubiquitin highlighting the 7 lysine residues stained in orange (left) or as orange sticks in different orientation (right). Ubiquitin AA 1-76 (cyan), lysine residues (orange). PDB: 1UBQ (Vijay-Kumar et al., 1987).

E2 enzymes have been implicated in specific formation of K63-, K48- and K11-linked chains, however E2 enzymes involved in formation of K6-, K27-, K29- and K33-linked chains have not been reported<sup>100, 107, 108</sup>. The E3 enzyme is essential to render substrate specificity. E3 ubiquitin ligases are separated into two types. HECT-type ligases utilize ubiquitin-charged E2s to capture the ubiquitin-moiety via a thioester intermediate and only then transfer it to the substrate. Here we focus on the Really Interesting New Gene (RING)-type E3 ligases. Compared to HECT-type ligases, RING-ligases merely transfer the ubiquitin-moiety of an E2 enzyme directly to the substrate. Consistent with the general roles attributed to E1, E2 and E3 enzymes, there are only two ubiquitin-specific E1 enzymes in humans (UBE1, UBE1L2), approximately 40 different E2 enzymes and ~616 RING-E3 ubiquitin ligases<sup>105, 109, 110</sup>.

Besides ubiquitination, there are another 16 different types of modifications by ubiquitin-like proteins, including neddylation and sumoylation, which are installed by a different set of enzymes<sup>111</sup>. These types of modifications are not further discussed here.

## 4.2. The DNA damage response cascade

Ubiquitination plays a key role in the cellular pathway signalling DNA damage. The DDR is a cellular mechanism to sense DNA damage in cells as it occurs and to initiate repair mechanisms. Essentially, the role of the DDR consists of stopping the cell cycle and to decide through regulatory pathways, if the cell can be recovered by repair of the damaged DNA site, or whether it has to undergo apoptosis<sup>112, 113</sup>. Thus, DDR is crucial to avoid tumor formation and is implicated in other processes, where error-prone DNA re-arrangements can occur, as in telomere homeostasis, meiosis or to defend against viral infections<sup>114, 115</sup>.

In the early DDR, an important role is played by histone H2A.X, a histone variant of H2A with an alternated C-terminal tail. Upon DNA double-strand breaks (DSBs), H2A.X gets phosphorylated at serine 139 by phosphatidylinositol 3' kinase-related kinases (PIKK) as ataxia telangiectasia mutated (ATM) or ataxia telangiectasia mutated and Rad3-related (ATR)<sup>116-118</sup>. Although it has been shown that H2A.X phosphorylation ( $\gamma$ H2A.X) is dispensable for accumulation of DDR-signalling- and DDR-repair factors at DNA lesions, it was thought to increase their local concentration at the site of DSBs<sup>119</sup>.  $\gamma$ H2A.X can be recognized by mediator of DNA damage checkpoint 1 (MDC1) and amplifies the signal by recruiting ATM in a NBS1-dependent manner<sup>118, 120, 121</sup>. ATM subsequently leads to phosphorylation of MDC1, facilitating its oligomerization and allowing the E3 ubiquitin-ligase RNF8 to bind MDC1 through its forkhead-associated (FHA) domain<sup>118, 122-124</sup>. Thus, after the initial steps of early DDR, the phosphorylation cascade transduces to signalling through ubiquitination.

Recruitment of RNF8 allows UBC13/MMS2 dependent K63-linked polyubiquitination of a substrate. Initially, it was thought that RNF8 initiates ubiquitination on histone H2A, however this hypothesis has been tested on histone octamers and nucleosomes and RNF8 was not able to ubiquitinate H2A in nucleosomes<sup>125-128</sup>. Thus, the substrate for RNF8 remained unknown for several years until histone H1.2 and the putative PcG protein lethal(3)malignant brain tumour-like protein 2 (L3MBTL2) were suggested as targets for K63-linked ubiquitination by RNF8<sup>48, 129</sup>. L3MBTL2 is also recruited to chromatin upon phosphorylation by ATM and binds to the DDR initiator MDC1<sup>129</sup>. Noteworthy, it has been argued, if ubiquitin chain formation of histone H1 is possible at all, as only mono-ubiquitination of H1 was detected in several studies<sup>129-131</sup>. Nevertheless, in the current model RNF8 initiates ubiquitination during the DDR.

A second E3 ubiquitin ligase, RNF168, contains a motif (UDM1), which recognizes K63-linked products of RNF8. Via RNF8-mediated poly-ubiquitination of H1.2 or L3MBTL2 RNF168 is thus recruited to chromatin<sup>48</sup>. RNF168 has shown high ubiquitination activity towards H2A/H2A.X on K13/K15 and dependence of this process has been shown on accessibility of the nucleosome acidic patch<sup>35, 128, 132, 133</sup>. A second motif of RNF168 (UDM2), which allows the protein to bind to its own ubiquitination products, potentially increases the residency time of RNF168 on the nucleosome and either allow spreading of H2A/H2A.X ubiquitination to neighbouring nucleosomes or leads to ubiquitin chain elongation<sup>134</sup>.



However, it remains unclear if RNF168 catalyses chain initiation on H2A/H2A.X, chain elongation or both. Alternatively, RNF8 would be able to elongate the ubiquitin chains on H2A, which were primed by RNF168-dependent ubiquitination<sup>128</sup>. Ubiquitination of H2A/H2A.X by RNF8 and RNF168 allows down-stream factors of the DDR to localize to DNA damage sites (Fig.9).

The RAP80 protein, which recognizes K63-linked ubiquitin chains, is directed to sites of DNA lesions in complex with BRCA1 and BRCC36, which is required to drive homologous recombination (HR)<sup>135, 136</sup>. On the other hand, mono-ubiquitination of H2A at K13/15 and H4K20me2 are recognized in a bivalent mode by 53BP1, an initiator of non-homologous end joining (NHEJ)<sup>137-139</sup>. Despite 53BP1, L3MBT2 also binds to H4K20me2 and can be removed from chromatin in an RNF8-dependent manner<sup>140, 141</sup>. The exact mechanism how RNF8 and RNF168 mediate the balance to drive HR or NHEJ has not been completely understood yet<sup>142</sup>.

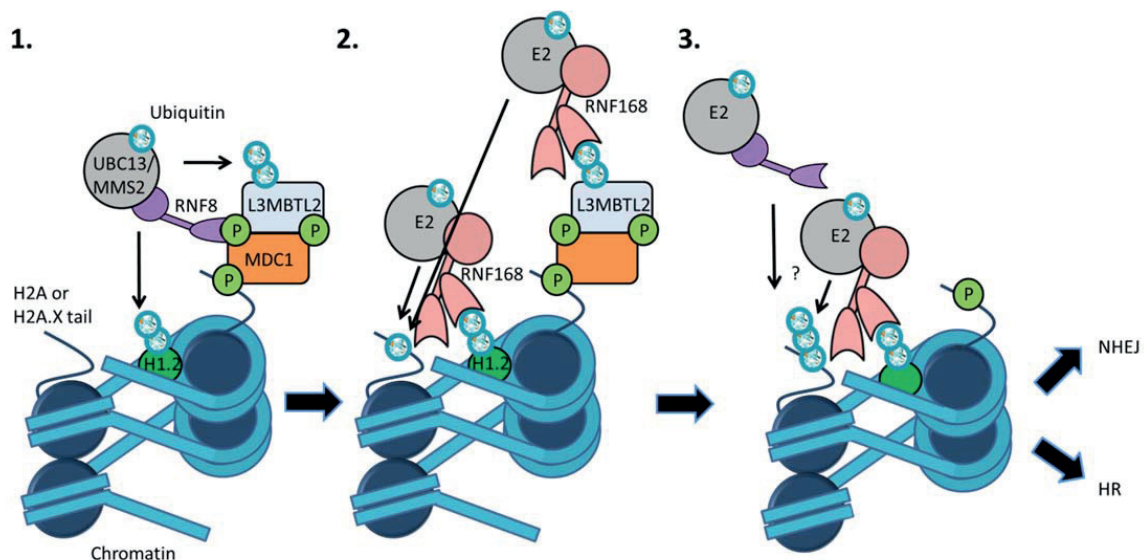


**Fig.9 DNA damage response cascade illustrating ubiquitination by RNF8 and RNF168**

**1.)** MDC1 is recruited to  $\gamma$ H2A.X and allows docking of RNF8 and L3MBTL2. RNF8 ubiquitinates (K63-linked ubiquitin chains) histone H1.2 or L3MBTL2 using UBC13/MMS2. **2.)** K63-linked ubiquitin chains recruit RNF168, which in turn ubiquitinates H2A/H2A.X on K13/15. **3.)** RNF8 or RNF168 (or both) elongate ubiquitin chains on H2A/H2A.X to recruit DDR-factors to direct the DDR repair mechanism to HR or NHEJ. P (green sphere) = phosphorylation mark

It remains unclear whether the H2A ubiquitin marks at the N-terminal histone tail (K13/K15) and the C-terminal tail (K119, K127, K129) show direct mechanistic interactions. As H2AK15ub can recruit 53BP1 or BRCA1, and the latter being a subunit of another E3 ubiquitin ligase complex, which ubiquitinates H2AK127 and K129, suggests that such interplay seems to exist<sup>143-145</sup>. The C-terminal ubiquitin mark H2AK119ub is associated with transcriptional repression, further supported by the fact that PRC1 is writing this ubiquitin mark<sup>146-148</sup>. Connections of the H2AK119ub mark and DDR have been made, but also highly questioned<sup>149-151</sup>. Further evidence was found in the putative PcG-protein L3MBTL2, which



is tightly involved in RNF8-dependent processes. Interestingly, a deubiquitinase USP3 has been able to de-ubiquitinate H2AK15ub and H2AK119ub, which also hints to an interplay between N- and C-terminal histone ubiquitin marks<sup>88</sup>.

When we started our investigations, we faced several unsolved questions concerning RNF168 regulation as how ubiquitination is propagated to neighbouring histones, how the chromatin compaction state is affected by individual ubiquitination steps, and how the dynamics of RNF168 are affected by histone PTMs in chromatin/nucleosomes. Thus, in this study we aimed to apply chemical methods and single molecule TIRFM to dissect and answer these types of questions with regard to the RNF168-DDR model system.



## 5. Applied chemistry to functionalize proteins

In this study, we aimed to elucidate how individual histone modifications can effect recruitment and binding of proteins to chromatin and how chromatin architecture affects protein binding.

To this point, various experimental strategies have been designed to dissect and understand the integrity of the histone code. However, known methods to study chromatin dynamics suffer from several drawbacks. While bulk measurements can lead to a loss of information due to averaging effects, high-resolution measurements, like cryoEM or X-ray crystallography, usually require fixation of the sample and dynamic information cannot be obtained. Cell experiments, on the other hand, are biologically meaningful, but the system is complex and control of all the different parameters is impossible. In our studies we follow a bottom-up approach by assembling different basic components and increase complexity of the system one by one.

Following this strategy, the first step was to synthesize and include post-translational modifications into proteins with native or native-like linkages. Nowadays, total chemical synthesis allows to produce elementary proteins as native histones and their analogues or di-ubiquitin chains using solid-phase peptide synthesis (SPPS)<sup>152, 153</sup>. Noteworthy, many research groups that apply SPPS make use of native chemical ligation (NCL) to create native peptide bonds<sup>154</sup>. This allows to synthesize peptides and to chemically assemble them into proteins under native conditions (Fig.10)<sup>155</sup>.

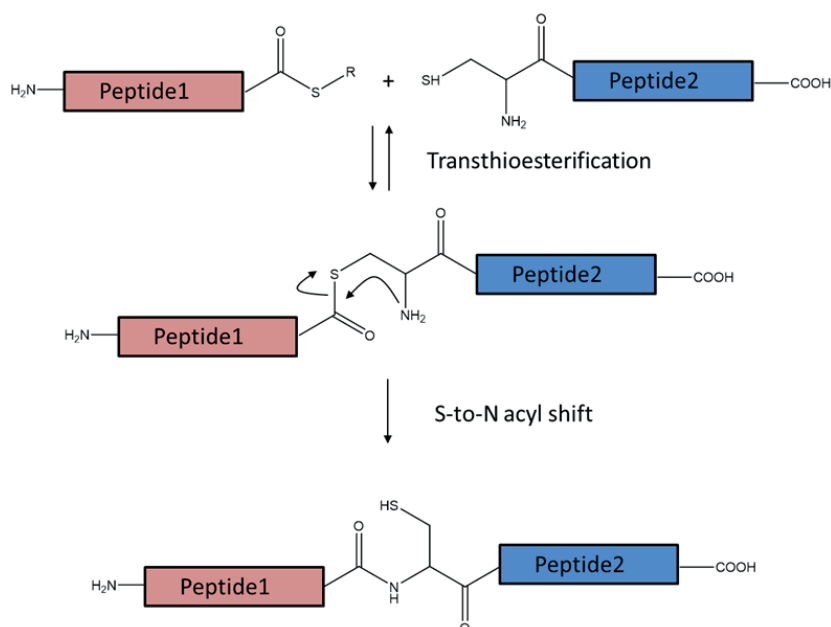


**Fig.10 Reaction scheme of native chemical ligation**

Peptide1 with a C-terminal thioester reacts with an N-terminal aminothiols (cysteine residue) of peptide2. After transthioesterification an S-to-N acyl shift leads to formation of a native peptide bond. Figure was adapted from Muir et al., 2003.

NCL enables insertion of unnatural amino acids, which are usually not accessible by using *in vitro* transcription, and incorporation of PTMs, which are not obtained in a heterogeneous manner using *in vivo* transcription<sup>155</sup>. However, development of this method opened up new questions as how to introduce  $\alpha$ -thioesters into a polypeptide, if synthetic peptides should be linked to the C-terminus or inserted into the middle of a recombinant protein<sup>155</sup>. Further, as peptides have been synthesized reliably up to ~50 residues, it remained challenging to create polypeptides of more than ~100 residues in a single ligation step.<sup>156</sup>

One solution to these problems was found in the biological system of intein splicing. Inteins are protein sequences that excise themselves from the original protein sequence, similar to introns in the DNA/RNA sequence, which are excised from protein encoding exons during mRNA splicing<sup>157</sup>. In a first step, an N-to-S (or N-to-O) acyl shift transfers the N-extein to an N-terminal Cys/Ser residue of the intein (Fig.11)<sup>155</sup>. Secondly, transthioesterification transfers the N-extein unit to a Cys/Ser at the intein C-extein boundary. The branched intermediate is further resolved through a cyclization reaction, which involves a conserved Asn residue at the C-terminus of the intein. Thus, the intein is excised as a C-terminal succinimide derivative and the two exteins are linked via an amide bond through a terminal S-to-N acyl shift<sup>155</sup>.

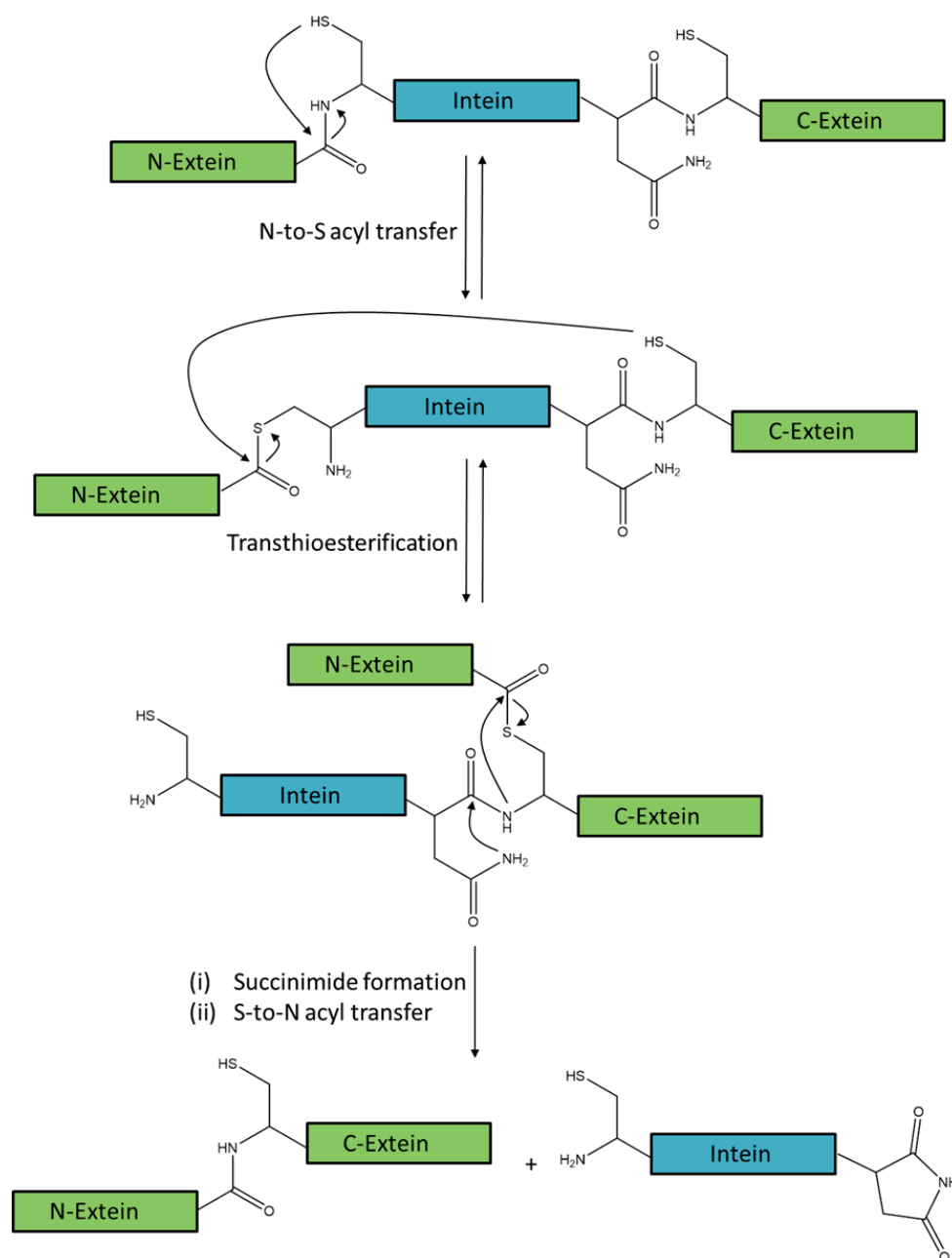


**Fig.11 Intein splicing**

Internal reactions at the intein-extein junctions are catalysed by the intein domain and mediated through a series of acyl shifts. This leads to formation of a native peptide bond between the exteins, while the intein is excised. Figure was adapted from Muir et al., 2003.

In biotechnology two categories of intein applications are widely used now. One mode of application is represented by the mutation of the conserved Asn to an Ala residue. This enables to block the intein splicing after the primary N-to-S acyl transfer. The obtained intermediate is accessible to chemical cleavage (thiolysis) by addition of small thiols (RSH). Importantly, this leads to formation of a protein  $\alpha$ -thioester, which is a suitable substrate for NCL<sup>155</sup>.

Further, it was discovered that inteins can be divided into two separate domains and be expressed individually, which renders two split-inteins without initial splicing activity<sup>155, 158, 159</sup>. However, when brought in close proximity the split-inteins can associate non-covalently and mediate normal intein splicing. This process known as intein *trans*-splicing is illustrated in Fig.12<sup>155</sup>. Among other applications, this enables to avoid premature splicing, while expressing a recombinant protein in cells.

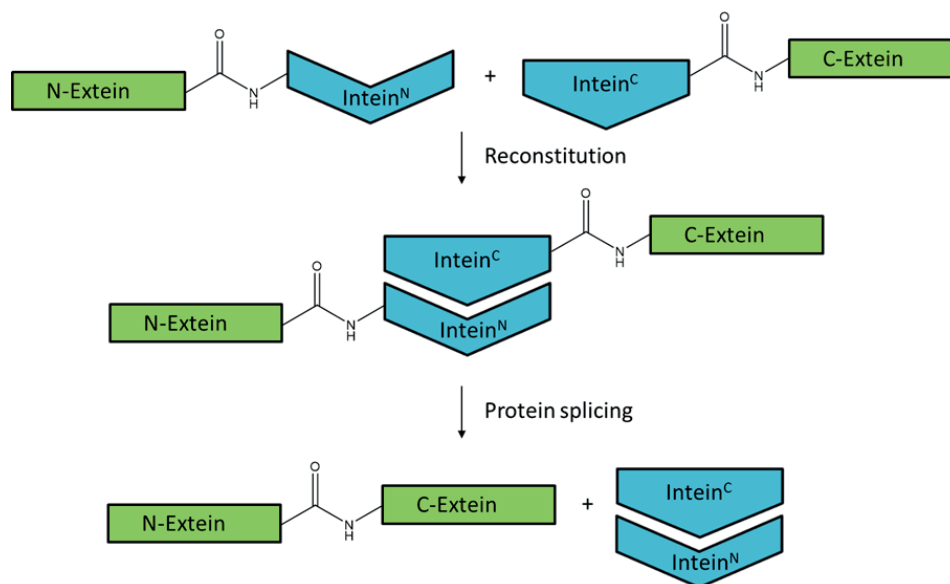


**Fig.12 Inteins *trans*-splicing**

Two polypeptides are expressed containing either an N-terminal or C-terminal segment of an intein (Intein<sup>N</sup> or Intein<sup>C</sup>). Only if the two intein domains are brought into close proximity, protein *trans*-splicing can occur normally. Figure was adapted from Muir et al., 2003.

Expressed protein ligation (EPL) was developed as a method, which combines the strength of intein-biology and NCL<sup>160, 161</sup>. In EPL, generation of the intein-mediated protein- $\alpha$ -thioester, followed by NCL, can be used to create polypeptides beyond a length of ~100 AA. This allows to chemically assemble cytotoxic proteins *in vitro*<sup>162</sup>. Importantly, the true power of EPL lies within the possibility of ligating recombinantly expressed proteins with synthetic peptides, which allows introduction of a variety of chemical modifications into proteins (Fig.13). Protein engineering by EPL enables site-specific incorporation of small modifications of amino acids into proteins, including PTMs, stable isotopes, unnatural amino acids (UAA), and EPL can be used for protein labelling with fluorophores<sup>155, 160</sup>. Opposed to nonsense suppression mutagenesis, a traditional method to introduce UAAs into proteins, EPL allows incorporating multiple UAAs into the same protein by sequential ligation and a much broader range of modifications can be applied<sup>155, 163</sup>. Thus, EPL represents a useful tool to create semi-synthetic proteins under native conditions.

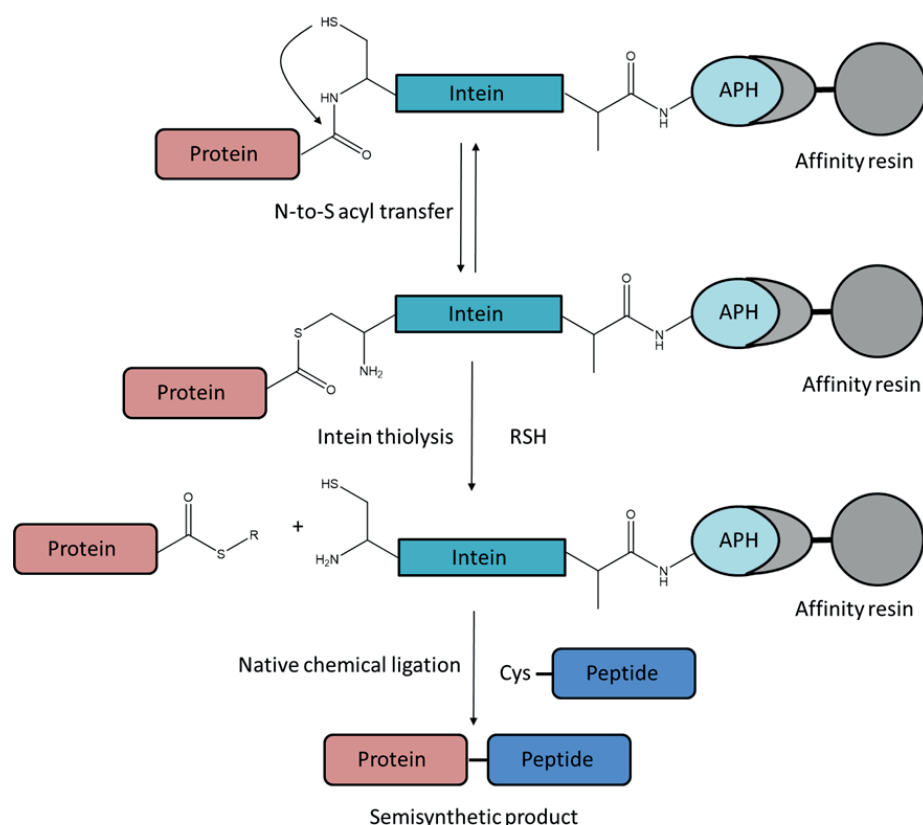


**Fig.13 Expressed protein ligation**

An expressed protein fused to an intein and an affinity purification handle (APH) is immobilized on affinity resin. An Asn to Ala mutation of the intein traps the intein splicing in an intermediate step after N-to-S acyl transfer. Thiolysis using a small thiol (RSH) produces a thioester group at the C-terminus of the protein, which can be used with a peptide, containing an N-terminal cysteine, for native chemical ligation. This renders a semi-synthetic protein product. Figure was adapted from Muir et al., 2003.

One of the numerous applications of EPL includes post-translational modification of histones. Since their discovery, histone proteins, which can be used to assemble nucleosomes *in vitro*, have always been an interesting target of investigation<sup>164</sup>. However, isolation and purification of histones often led either to heterogeneously modified populations or to low yields<sup>165, 166</sup>. A chemical approach using cysteine-reactive probes has been developed to introduce site-specific methyllysine analogues into histones<sup>167</sup>. These analogues have high similarity to the native marks, as they were captured by specific antibodies. However, they were not completely native, susceptible to oxidation and in some cases displayed different binding affinities<sup>167</sup>. In contrast, a sequential EPL strategy with desulfurization allowed to create H2BK120 containing a completely native ubiquitin mark<sup>166, 168</sup>. Availability of the H2BK120ub mark enabled to study its influence on chromatin compaction and unveiled an important role in rendering chromatin accessible<sup>23</sup>. Interestingly, this role was attributed specifically to ubiquitin, as a protein of similar size, Hub1, did not exert the same effect<sup>23</sup>. Despite EPL, also amber suppression mutagenesis was applied successfully to produce modified histones as e.g. H3K56ac<sup>169</sup>. This allowed to

identify the role of the H3K56ac mark in DNA unwrapping from the nucleosome<sup>169</sup>. These examples highlight the valuable information that was obtained using chemically modified histones.

In this study we applied EPL to modify recombinantly expressed proteins with synthetic peptides to obtain semi-synthetic proteins, which are either biologically relevant or engineered to fulfil a distinct function. For example, here, we employed EPL to modify histones for chromatin formation. As nucleosome formation and positioning on DNA can be controlled using an artificial nucleosome positioning sequence (Widom 601 nucleosome positioning sequence) and histone octamers, a protocol was established to assemble nucleosomes and chromatin fibres in a salt-dependent manner *in vitro*<sup>170, 164</sup>. Having the ability to install histone PTMs using EPL strategies and to incorporate them into nucleosomes via histone octamers, enabled us to create a controlled system of chromatin fibres (“designer chromatin”). Additionally, our expertise in purification and chemical modification of proteins and DNA provides a broad toolbox to study chromatin modification states in a highly controlled manner.



## 6. Single-molecule studies of chromatin dynamics

### 6.1. Relevance of dynamic single-molecule analysis

In chromatin research, protein recruitment and activity has been studied extensively using ensemble measurements as electromobility shift assays (EMSA), activity assays, pull-down experiments or various *in vivo* experiments<sup>35, 128, 139, 171, 172</sup>. As complementary methods, isothermal calorimetry (ITC) and thermophoresis assays have been used to study protein thermodynamics, which allows to determine kinetic parameters<sup>173, 174</sup>.

A powerful ensemble tool to investigate the histone landscape is chromatin immunoprecipitation (ChIP) and numerous variations of ChIP<sup>175, 176</sup>. Generally, ChIP unveils proteins associated with chromatin/DNA and allows detection of distinct histone modifications. A first crosslinking step of proteins and DNA allows creation of a snapshot of proteins associated with DNA. In the following step, target DNA is enriched by an antibody towards the protein/modification of interest. Crosslinking is released, proteins and RNAs are digested and the target DNA can be purified and analysed e.g. using quantitative polymerase chain reaction (PCR). A similar approach can be done to identify DNA methylation using methylated DNA immunoprecipitation (meDIP) or bisulphite sequencing.

In biology and chemistry, there is relevance to study protein binding affinity, the association and dissociation rates of a protein towards its protein-, DNA- or chromatin substrate, as it represents a basal mechanism of regulation. It is important for epigenetic researchers to unveil how protein binding is ensured to answer various questions like: How does a protein bind to chromatin and is binding facilitated by DNA or a certain histone PTM? Does a set of histone PTMs alter protein binding and do several different histone PTMs on the same chromatin interface act synergistically or do they antagonize each other? How long does a protein bind to its target? Is strong and stable protein binding a requirement for its downstream activity or is transient binding key for tight, but dynamic regulations? Ensemble measurements will never be able to detect stochastically rare events, or transient interactions, as these will be averaged out.

Thus, there is a need for complementary methods, which are able to track single molecules in a system where dynamic interactions can be resolved. Such single molecule methods are advantageous as the molecules in the experiment do not need to be synchronized in order to obtain a uniform response and thus measurements are possible at equilibrium conditions. Further, single-molecule methods allow separation of individual observations, if differently behaving subspecies of molecules are present in the experiment.

Fluorescence microscopy is a minimal invasive method to study small structures using fluorescently labelled molecules. Opposed to light microscopy, traditional fluorescence microscopy allows measurements at high contrast and thus structures down to the 200 nm can be visualized. In fluorescence microscopy the detected signal is highly specific, as the

object of investigation oftentimes is selectively labelled and the separation between excitation- and emission light allows a clear discrimination of individual fluorescence emitters. Nevertheless, tracking of single fluorophores remains challenging as the out-of-focus fluorescence introduces background signals, which makes it challenging to discriminate two labelled molecules in the imaging area <sup>177</sup>.

In order to investigate structures below 200 nm a variety of different methods has been developed. One example is given by force spectroscopic methods. Atomic force microscopy has been shown to measure deflections of individual molecules and was applied to investigate the integrity of single chromatin arrays <sup>178</sup>. On the other hand, optical tweezers allow trapping of individual molecules in a defined volume and to measure parameters of interactions. Applications were found in stretching and characterization of chromatin fibres <sup>179</sup>. Although these methods are able to measure features down to sub-nm resolution and sub-ms time scale, they suffer from non-specific interactions caused by environmental noises as mechanical vibrations, air currents, temperature and acoustic- and electrical noise <sup>180</sup>. Moreover, the applied mechanic forces can further perturb the system of investigation.

A fluorescence-based method method is Förster resonance energy transfer (FRET), which can be used as a molecular ruler to determine distances in the 0-10 nm range <sup>181</sup>. Based on energy transfer of a donor- and acceptor fluorophore, this method has been applied to assess nucleosome stability and DNA unwrapping from nucleosomes based on FRET <sup>8, 182</sup>. FRET can also be measured between fluorophores on individual molecules. Recently, a study in our own lab applied single-molecule FRET (smFRET) to monitor compaction of chromatin in dependence of magnesium ions <sup>19</sup>. In order to discriminate single molecules, the fluorescent read-out was based on TIRFM.

In TIRF illumination only a thin volume section close to the surface of the sample is excited by an electromagnetic field and distal background signals originating from labelled molecules in the solution are heavily reduced. This renders TIRFM applicable for single molecule imaging.

## 6.2. TIRFM principles

To circumvent the limitations mentioned above, we apply TIRFM to observe single molecule dynamics.

In the following we describe the principle of objective-based TIRFM in more detail to shed light on the mechanism:

A sample in aqueous solution on a glass coverslip is excited with a laser beam through the objective of the microscope. By laterally displacing the laser beam from the objective centre, the beam leaves the objective with an angle relative to the perpendicular of the glass slide and is further deflected upon reaching the solvent, due to the difference in

refractive indices ( $n$ ) of glass and solvent (water). This system is characterized by Snell's law<sup>183</sup>.

*Snell's law:*

$$n_1 \times \sin \theta_1 = n_2 \times \sin \theta_2 \quad (1)$$

As  $\sin \theta_2 = 1$ , ( $\sin 90^\circ = 1$ ) for total reflection, it follows the

*Critical angle:*

$$\theta_c = \sin^{-1} \left( \frac{n_2}{n_1} \right) \quad (2)$$

$n_2$  = lower refractive index (e.g. water)

$n_1$  = higher refractive index (e.g. glass)

$\theta_1$  = incident angle

This defines the critical angle as the incident angle  $\theta_1$  where the refractive angle  $\theta_2$  is exactly  $90^\circ$ . At an angle above the critical angle, the laser is totally reflected back and does not penetrate into the sample anymore (Fig.14). Therefore, in TIRFM only the large angles are selected by illuminating at the edge of the objective's back aperture<sup>183</sup>.

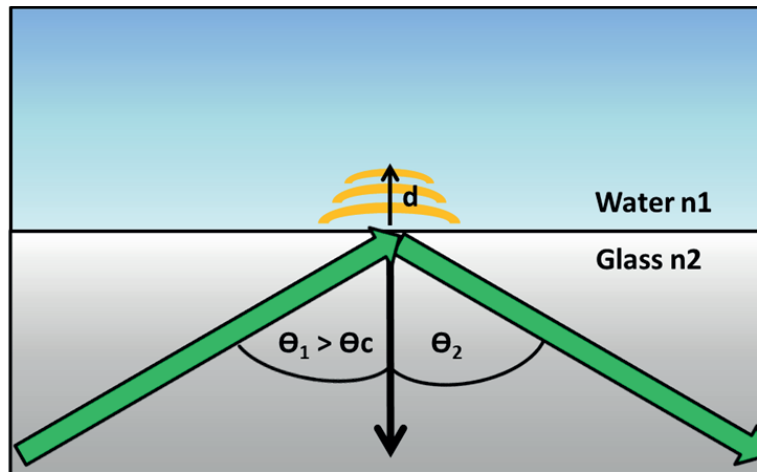


**Fig.14 Total internal reflection illumination**

An incident laser beam (green arrow) touches the interface of glass and water. When the incident angle  $\theta_1$  reaches the critical angle  $\theta_c$ ,  $\theta_2$  becomes  $90^\circ$  and the deflected laser beam is not entering the water phase anymore. When  $\theta_1 > \theta_c$ ,  $\theta_2$  is reflected back (total internal reflection) and an evanescent field (yellow) with penetration depth  $d$  is created, which can excite fluorophores.

At the site of reflection, an electromagnetic field (evanescent field) is created, the intensity of which decays exponentially with increasing distance from the glass slide. The evanescent field can reach a penetration depth of approximately 200 nm. The sample is only excited by the evanescent field, and thus the illumination volume is restricted to a small area<sup>183</sup>.

*Penetration depth:*

$$d = \frac{\lambda_i}{4\pi} \times (n_1^2 \times \sin^2 \Theta_1 - n_2^2)^{-\frac{1}{2}} \quad (3)$$

$\lambda_i$  = wavelength of the incoming light beam

Penetration depth is dependent on the wavelength ( $\lambda_i$ ) of the incoming laser beam, the refractive indices ( $n_1$  and  $n_2$ ) and the incoming angle  $\Theta_1$ .

The evanescent field can be used to only illuminate molecules close to the surface of a coverslip in contrast to common wide-field microscopy, where the background, coming from fluorescent molecules diffusing in the solution, is also illuminated. This allows observation of single molecules close to the surface up to low-nanomolar concentrations of the labelled species. By covalently attaching single molecules to the glass surface, this allows to image the attached molecules within a very small illumination volume.

In TIRFM, molecules that fluoresce, which are located close to the illumination surface, are detected. In order to limit the level of non-specific fluorescence, extremely clean glass slides are required.

## 7. Aims of the project

Histone modifications represent a fundamental system of chromatin regulation. As processes like differentiation of stem cells, cancer development and progression and many neurodegenerative diseases underlie these regulatory mechanisms, their importance cannot be ignored. A detailed understanding of the function of histone marks is crucial to understand the molecular origins of some diseases, e.g. cancer, and to identify new drug targets. In particular, many lysine methyl-marks have been associated with cancer progression<sup>184</sup>. Also, dysregulation of histone ubiquitination can result in disease, as seen in the RIDDLE syndrome, caused by improper function of the E3 ligase RNF168. The RIDDLE syndrome manifests in enhanced cellular radiosensitivity of patients, immunodeficiency and cancer predisposition<sup>125, 171, 185</sup>.

Combined efforts of chemical biology, molecular biology and cell biology have provided a large spectrum of biological and chemical tools to further study and understand the histone code. Progress has been made, but detailed molecular mechanisms are often unresolved. However, it is indispensable to characterize the individual contributions of histone marks involved in chromatin effector recruitment and regulation. Moreover, effectors are not regulated in an “all-or-nothing” fashion, but rather in a gradual and tuneable manner. To study such complex regulation requires a tightly controlled system of chromatin and associated proteins that, at this point, is not easily achieved *in vivo*.

In our research group, we work at the interface of chemistry, biology and biophysics. This allows us to develop defined chromatin systems with a high level of control towards all the components. Such a bottom-up *in vitro* approach, assembling simple protein-chromatin interaction systems, which can evolve to measuring platforms of higher complexity, can fill the lack of information given by top-down approaches.

Here, we developed a method which allows us to directly observe chromatin regulatory processes on the single molecule scale. This leads to a better understanding of fundamental regulatory processes at the chromatin level. Moreover, such an approach essentially complements classical biochemistry and cell biology methods.

The primary aim of this study was to develop and test methods to study chromatin effectors on the single molecule level in a dynamic manner using designer chromatin. We investigated dynamic HP1 $\alpha$ - and PRC2-chromatin interactions, which are involved in heterochromatin formation. We tested the impact of HP1 $\alpha$ -multivalency towards H3K9me3 and observed altered chromatin binding dynamics upon protein dimerization. Investigating the protein complex PRC2, we discovered an essential contribution of PHF1 to anchor PRC2 on chromatin through a process that is essentially driven through DNA binding and dependent on a newly identified winged-helix (WH) motif of PHF1. Further, presence of histone PTMs as H3K27me3, H3K27M and H3K36me3 stabilized PRC2-binding towards chromatin, as well. Finally, we developed a system to test ubiquitination of designer

chromatin and unravel mechanisms of RNF168-mediated ubiquitination during the DDR. We found enhanced activity of RNF168 towards H4K16ac chromatin fibres and lowered ubiquitination activity in the presence of an occluded nucleosome acidic patch using the anti-cancer agent RAPTA-C. Moreover, we identified specific interactions of RNF168 with native- and synthetic K63-linked ubiquitin chains.

In particular the aims of my studies were:

#### **Aim1: TIRFM as a tool to investigate single molecules on chromatin**

We aimed to establish a method to measure single protein binding and corresponding dynamics towards chromatin, focusing on the multivalent effector HP1 $\alpha$ . This involved establishing methods including preparation of flow channels as units for single molecule measurements, expression and labelling of proteins, assembling and labelling of chromatin arrays including desired histone marks paired with the ability for immobilization, installation and application of a TIRF microscopy system, establishment of suitable and realistic measuring conditions (buffers, flow speed, protein concentration) and finally data analysis.

#### **Aim2: Oligomerization effects of HP1 $\alpha$ on chromatin binding**

We dissected HP1 $\alpha$ -chromatin interactions dependent as a function of HP1 $\alpha$  concentration. We tested if HP1 $\alpha$  oligomerizes under measuring conditions. To unveil the kinetic dependence on HP1 $\alpha$  concentration and oligomerization we expressed and added unlabelled HP1 $\alpha$  protein to the flow cell to induce a competitive environment, which would supposedly lead to stabilization of bound HP1 $\alpha$  proteins or to competition-driven rapid rebinding events.

#### **Aim3: Multivalency of HP1 $\alpha$ on chromatin binding**

Availability of multiple histone marks (homogenic or heterogenic) leads to elongated and more rapid binding of proteins towards chromatin. To test this hypothesis, with respect to HP1 $\alpha$ , we tested if HP1 $\alpha$  dimerization (covalently or via peptide ligand) increases HP1 $\alpha$  residence time and binding rate. Notably, artificial dimerization of HP1 $\alpha$  was of high importance as, at concentrations under our TIRF measuring conditions (nanomolar range), HP1 $\alpha$  was mainly in its monomeric state.

#### **Aim4: Involvement of a novel PHF1 winged-helix domain in PRC2-chromatin binding**

Our collaborators had identified a WH motif on PHF1. We aimed to analyse PRC2 binding in single molecule measurements to understand the contribution of the PHF1 WH motif towards binding of PRC2 to chromatin and test the hypothesis that PHF1 prolongs PRC2-binding to chromatin. We performed single molecule measurements with different PHF1-mutants to unravel the contribution of the mutated residues. Additionally, we studied PRC2 binding towards modified chromatin arrays.

**Aim5: The molecular mechanisms of RNF168 chromatin ubiquitination during the DDR**

In order to dissect the mechanism of RNF168-mediated ubiquitination during the DDR, we aimed to establish a basic ubiquitination system in our laboratory. We developed ubiquitination assays with robust ubiquitination towards chromatin. This allows studying of various chromatin conditions during ubiquitination.

**Aim6: Writers of histone ubiquitin marks in dependence of the chromatin state**

We investigated the influence of the chromatin state on ubiquitination by RNF168. On one hand, we wanted to test if the accessibility of the nucleosome acidic patch would alter ubiquitination velocity by RNF168. Further, as RNF168 possesses an H2A.XK15ub binding motif, we wanted to uncover possible stimulatory effects of the ubiquitin mark on H2A.XK15, if RNF168 was indeed involved in H2A.XK15 ubiquitin chain elongation.

Based on these hypotheses, we sought to study the proteins, HP1 $\alpha$ , PRC2 and RNF168, on the single molecule level to establish and test our newly developed microscopy system and to understand different binding modes on chromatin, nucleosomes and DNA.





## II Results

### 1. Single-molecule dissection of dynamic heterochromatin establishment by HP1 $\alpha$

Essential content of this chapter has been published in Sinan Kilic, Louise Bryan, Andreas L. Bachmann and Beat Fierz, *Nature Communications*, **2015** <sup>186</sup>.

In the following chapter, I have performed protein expression and purification of HP1 $\alpha$  wild-type (wt), chromatin assembly, histone octamer and chromatin quality control, peptide synthesis of peptides **P3** and **P4**, HP1 $\alpha$  TIRF measurements on wt- and H3K9me3-modified chromatin arrays including competition assays and measurements using peptides related to dimerization. I performed thermophoresis measurements and TIRF measurements using HP1 $\alpha_{\text{cmd}}$  together with Sinan Kilic (LCBM, EPFL, CH).

Of the other experiments, HP1 $\alpha$  proteins, except the wild-type version, were expressed by Sinan Kilic. Labelling and dimerization of HP1 $\alpha$  via covalent linkage was done by Sinan Kilic, as well as measurements using HP1 $\alpha$  (W40A). Histones containing H3K9me3 were prepared by Sinan Kilic. The impact of H3K9me3 measurements was investigated by Louise Bryan (LCBM, EPFL, CH). The covalent linkage strategy of HP1 $\alpha$  was designed by Beat Fierz and performed by Beat Fierz and Sinan Kilic. FRAP experiments were carried out by Sinan Kilic. Peptides **P1** and **P2** were synthesized by Sinan Kilic.

#### 1.1. Introduction

To address whether we are able to measure protein-chromatin interaction dynamics on the single-molecule level, we sought to investigate a protein with a defined role in chromatin association. We decided to study the well described HP1 $\alpha$ -H3K9me3 modified chromatin interaction system <sup>45, 54, 65</sup>.

HP1 $\alpha$  is a key factor for heterochromatin formation <sup>65</sup>. It binds to H3K9me3 as a dimer, enabling multivalent engagement of several nucleosomes <sup>58</sup>. This indicates an important function of HP1 $\alpha$  as multivalent effector to drive chromatin compaction and thus gene repression. Although over time, heterochromatin domains are macroscopically stable, HP1 $\alpha$  in cells is highly dynamic with residency times of seconds <sup>69, 187</sup>.

Indeed, the  $K_D$  of the HP1 $\alpha$  chromo domain towards H3K9me3 is only  $\sim 25\mu\text{M}$  <sup>188, 189</sup>. This raises the question how HP1 $\alpha$  is able to fulfil its roles to engage chromatin, despite its low affinity. There are several models conceivable (Fig.15). First, on nucleosomes bearing 1-2 H3K9me3 PTMs simple association/dissociation is expected (Fig.15a). In the presence of multiple histone modifications as e.g. on neighbouring nucleosomes, upon dissociation, HP1 $\alpha$  is enabled to rapidly rebind to a neighbouring H3K9me3 mark (Fig.15b). Moreover, HP1 $\alpha$  is a multivalent chromatin reader. Thus, association is accelerated based on the

presence of two reader domains in proximity of a possible binding site. Further, if one reader domain associates with H3K9me3, the dimeric protein potentially binds to a second H3K9me3 mark before it dissociates completely from the chromatin binding site (Fig.15c). Further, HP1 $\alpha$  binding to chromatin can be stabilized by protein-protein interactions through its CSD, leading to stabilized HP1 $\alpha$ -chromatin complex formation through HP1 $\alpha$  oligomerization (Fig.15d).

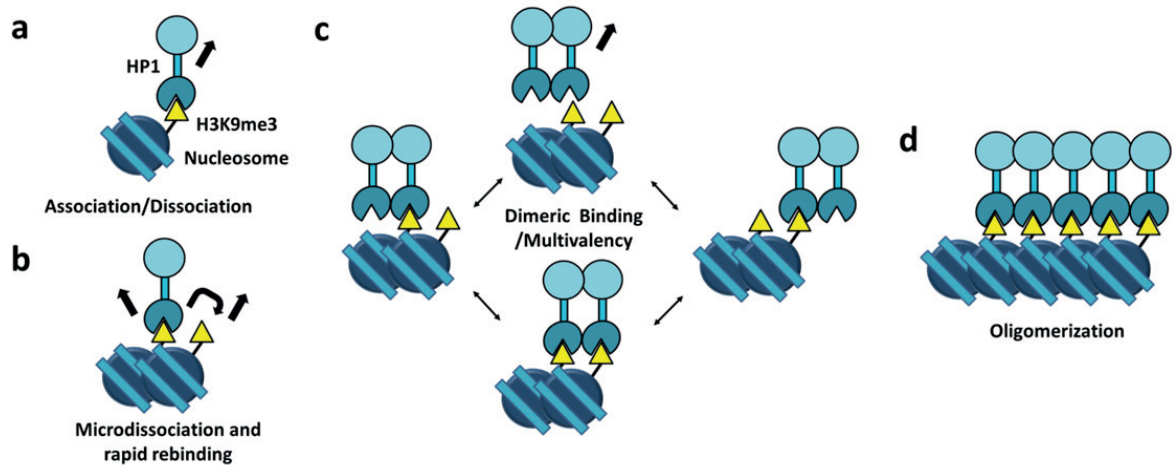


**Fig.15 Possible binding modes for HP1 $\alpha$**

**a)** In the presence of only one chemically modified nucleosome, we expected simple association and dissociation. **b)** In chromatin arrays with multiple modified nucleosomes we postulated a binding mode of microdissociations followed by rapid rebinding to a neighbouring histone mark (H3K9me3). **c)** Dimeric HP1 $\alpha$  would be able to employ one, or the other or both binding domains to bind H3K9me3, which would lead to rapid association and stabilized binding. **d)** Through the CSD of HP1 $\alpha$ , protein-protein interactions would be possible and would lead to formation of an oligomeric complex around chromatin.

To discriminate the suggested models, we envisioned to apply a single-molecule assay. This has the advantage of enabling us to monitor the individual proteins directly as they interact with chromatin. In such a system we can dissect and test all the different binding models.

In this study we applied TIRF microscopy to observe fluorophores, which are located close to the surface of a glass slide, while omitting fluorescence of the background solution. Microfluidic channels were functionalized with poly(ethylene glycol) (PEG) chains to avoid non-specific protein sticking. A subpopulation of PEG was functionalized with biotin, which can be linked to any biotin-linked molecule through neutravidin interactions. Here, we aimed to assemble designer chromatin, including a fluorescent label and a biotin-anchor for immobilization through attachment to the DNA. In an experimental setup, chromatin arrays with defined histone modifications were immobilized on the glass slide and a fluorescently labelled protein of interest (e.g. HP1 $\alpha$ ) was added to the flow channel. Colocalization of the two fluorophores (e.g. a red fluorophore on the DNA and an orange fluorophore on the protein of interest) over time allowed to measure association/dissociation times of proteins

towards individual chromatin spots on the flow channel (Fig.16)<sup>186</sup>. Overlapping binding events were identified based on increased brightness levels. Based on the distance of the DNA-attached Atto647N and the Atto532-HP1 $\alpha$  bound on the lowest nucleosome position (~17 nm), we did not expect FRET (0-10 nm) between the two dyes in these types of measurements<sup>181, 190</sup>.

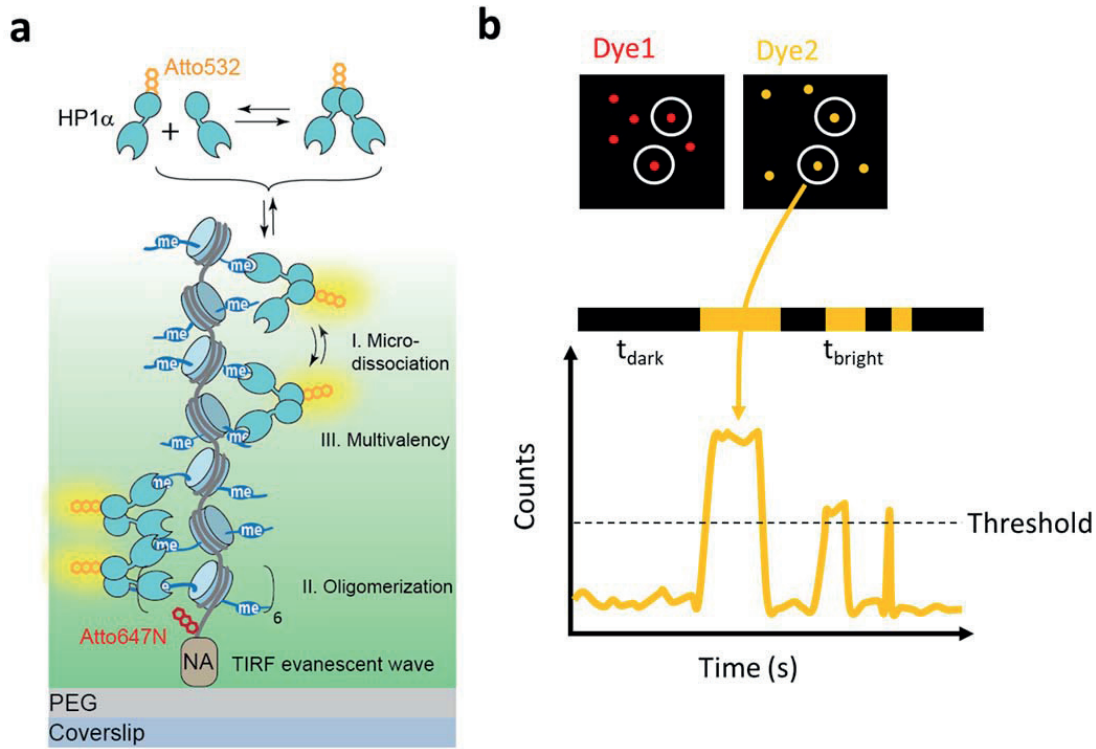


**Fig.16 Experimental setup of TIRF measurements**

**a)** Scheme of TIRFM with immobilized chromatin. Biotinylated chromatin arrays are immobilized via neutravidin (NA) interactions on the PEG surface of the glass coverslip. TIR illumination allows excitation of chromatin-bound labelled HP1-molecules (yellow halo), which are located close to the glass surface. **b)** Alternating illumination with two fluorescent dyes allows colocalization of chromatin- (dye1 on DNA, red) and protein positions (dye2 on HP1 $\alpha$ , yellow) over time (white circles). This renders a fluorescence-time trace for each chromatin spot with bound proteins (t<sub>bright</sub>) and absent protein binding (t<sub>dark</sub>). Figure was adapted from Kilic et al., 2015.

We envisioned a system where we could analyse labelled and immobilized designer chromatin chains by TIRFM. Addition of a fluorescently labelled protein, as a binding partner of chromatin that is dependent on associated histone marks, would enable us to monitor protein binding and its dynamics towards chromatin that is dependent on the histone mark landscape or the chromatin compaction state. In particular, such a system opens the paths to analyse multivalent protein binding and estimation of the relevance of histone marks. This allows distinguishing of histone PTMs responsible for primary protein binding, PTMs which are only established upon protein binding events themselves or PTMs merely helping the protein to bind.

Using TIRFM as outlined above allowed us to investigate the suggested binding models (Fig.15). HP1 $\alpha$  association/dissociation was tested using unmodified and H3K9me3-modified chromatin fibres. To test the microdissociation model, we either gradually decreased the H3K9me3-level or we performed and compared experiments between mononucleosomes and chromatin arrays. Oligomerization of HP1 $\alpha$  was assessed by titrating unlabelled HP1 $\alpha$  molecules in order to investigate reduced or increased protein dynamics. To study HP1 $\alpha$  dimerization we employed a strategy to either chemically link two HP1 $\alpha$  molecules or to facilitate CSD-dimerization by addition of a dimerization peptide.

However, development of the presented TIRF system requires a set of different prerequisites including:

1. Expression, purification and labelling of a protein of interest (e.g. HP1 $\alpha$ )
2. Chemically modified, biotinylated, fluorescently labelled chromatin arrays (e.g. H3K9me3)
3. Functional TIRF microscope including lasers (e.g. 640 nm, 532 nm) and a software for data analysis
4. Clean glassware to assemble flow channels and suitable imaging buffer conditions

In the following we discuss production of the protein of interest and designer chromatin. Detailed information describing the microscopy system, data evaluation, cleaning of glassware and utilized imaging buffer conditions can be found in chapter “IV Material and Methods”.

## 1.2. Prerequisites for TIRF microscopy

In order to monitor HP1 binding on the single-molecule scale, different components were required to perform single molecule measurements using TIRF microscopy. This included the fluorescently labelled HP1 $\alpha$  protein, 12x177 bp 601 chromatin arrays containing a histone modification (H3K9me3), a TIRF microscope with two different laser lines (red 640 nm and green 532 nm), extremely clean glass coverslips and glass slides, a homebuilt MathLab script for data analysis, which was provided by Beat Fierz (LCBM, EPFL, CH), and a suitable imaging buffer to keep the protein of interest, the chromatin arrays and the attached fluorophores in a stable condition.

The envisioned TIRF approach enables us to precisely control and modify the individual components of the biochemical system. In contrast, experiments using living cells reflect native conditions, but are highly complex with respect to individual components. Although we focused on creating completely native-, or native-like proteins and nucleosomes, a small experimental bias by artificial modifications, which cannot be omitted, remains. This includes fluorescent labelling of proteins, as the label can alter distinct characteristics of the protein of interest, as protein size or polarity, which in turn can directly

affect binding affinities and catalytic activities of the protein. To control for altered protein behaviour, we usually compared labelled and unlabelled proteins e.g. in peptide-binding assays or activity assays. Additionally, surface immobilization of chromatin fibres might introduce a bias in the mobility of the fibre in solution and thus alter protein-chromatin interactions, in particular close to the attachment site. We tried to reduce such effects by employing chromatin fibres containing 12 nucleosomes, which provide freely diffusing fibre ends on the fibre site opposed to the attachment site. In order to reduce non-specific binding of proteins to the glass surface, we utilized different passivation agents as immobilized PEG chains or BSA. In general, this is important to enable free diffusion of proteins in solution and to reduce non-specific signals of fluorescently labelled proteins that stick to the glass surface. Altogether, the applied TIRF system serves as a complementary approach to *in vivo* systems with high complexity and allows dissection of the basic interaction mechanisms.

### 1.2.1. HP1 $\alpha$ purification and labelling

A first challenge was to purify the protein of interest. HP1 $\alpha$  (CBX5) was cloned into a pET15b expression vector, which harbours an N-terminal hexahistidine-tag (6xHis) with a downstream thrombin cleavage site. The protein was expressed in *E.coli* BL21 DE3 cells during overnight expression. The cell lysate was subjected to Ni-affinity resin purification as a first purification step. Subsequently, an anion exchange chromatography (AIEX) was required to remove DNA, which was usually found in HP1 $\alpha$  elutions from the Ni-column. Pure fractions were subjected to thrombin cleavage to remove the N-terminal His-tag and the cleaved protein was further purified by gel filtration on a Superdex 200 10/300GL column. The concentrated protein elutions were complemented with 30% glycerol, flash frozen and stored at -80°C (Fig.17).

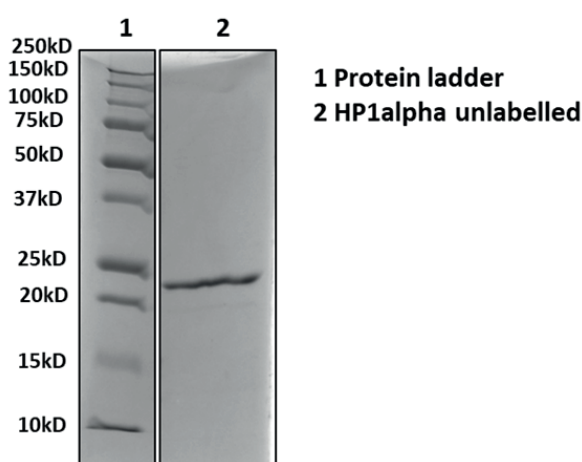


**Fig.17 HP1 $\alpha$  final fraction (15 % SDS-PAGE gel)**

HP1 $\alpha$  was obtained in high purity as visualized using Coomassie staining (expected molecular weight: 22.5 kDa, (based on ExPASy, ProtParam tool, <http://web.expasy.org/protparam/>, 2014.06.05)).

For fluorescence types of microscopy, as our TIRF system, it was required to attach a fluorescent label to HP1 $\alpha$ . To generate labelled HP1 $\alpha$ , the sequence of the *N. punctiforme* split-intein (NpuN) split intein was fused to the C-terminus after a double glycine linker, followed by a final hexahistidine tag (HP1 $\alpha$ -GG-NpuN-6xHis)<sup>191</sup>. After protein expression (expression conditions were similar to those of the unlabelled HP1 $\alpha$  protein) and purification (including thrombin cleavage of the 6xHis-tag), our strategy involved *in situ* ligation to a tripeptide containing the fluorophore Atto532 (**P1**).

The peptide **P1** was synthesized as follows:

Peptide **P1** (Thz-G<sub>2</sub>-C<sub>3</sub>-CONH<sub>2</sub>, Thz: thiazolidine) was synthesized manually on a Rink amide resin. The peptide was cleaved from the resin and purified using preparative reversed-phase HPLC (RP-HPLC). Then, the peptide was labelled with Atto532 and the reaction was quenched with  $\beta$ -mercaptoethanol (BME). The thiazolidine ring was opened using methoxylamine and the obtained EPL-reactive peptide was purified using semipreparative RP-HPLC. Final products were analysed by RP-HPLC and electrospray mass spectrometry (ESI-MS) (calculated exact mass = 1009.26 Da, observed mass = 1008.25 Da) (Fig.18)<sup>186</sup>.

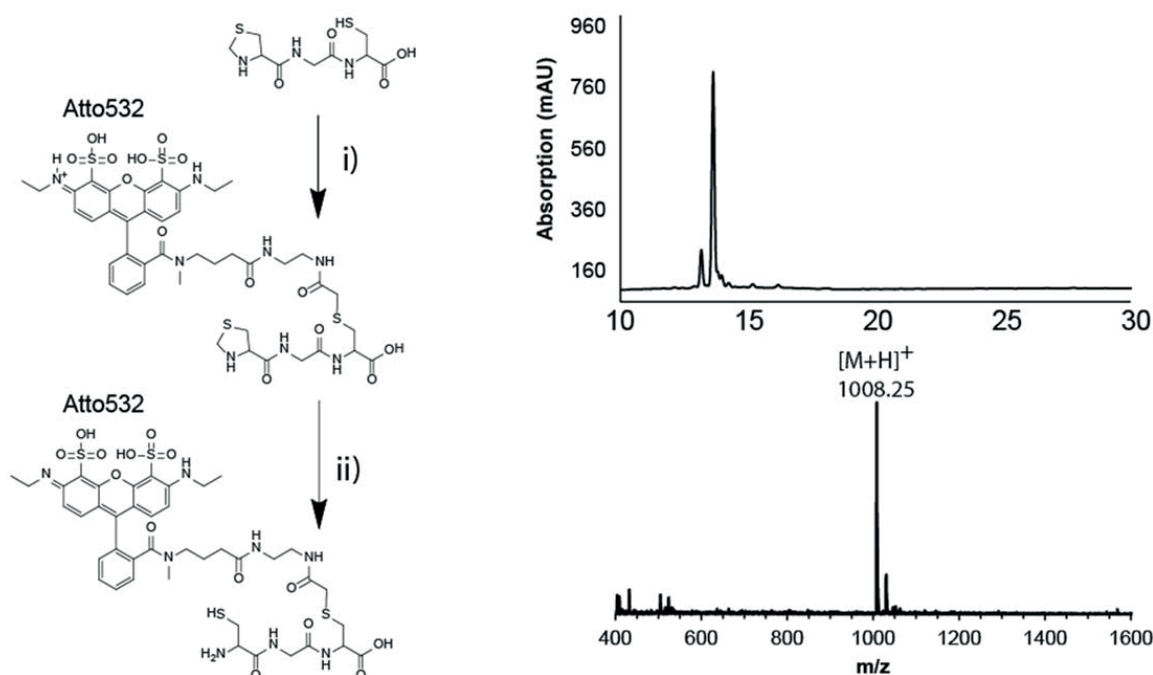


**Fig.18 Synthesis and purification of peptide P1**

Synthesis of **P1**. After manual synthesis of the solid phase, cleavage and purification, i) **P1** is coupled to Atto532-iodoacetamide in solution (20 mM Tris, pH 7.5), followed by ii) opening of the thiazolidine using 0.5 methoxylamine at pH 5. RP-HPLC and ESI-MS of the product are shown (expected mass 1009.26 Da, observed mass 1008.25 Da). Figure was adapted from Kilic et al., 2015.

Once we had created the labelling peptide **P1** and the HP1 $\alpha$  protein, containing the C-terminal split intein NpuN, the labelling reaction employing EPL was performed.

In an experimental setup, upon immobilization of the NpuN-fusion protein on a SulfoLink resin functionalized with NpuC, an N-to-S acyl shift is induced, which leads to intein splicing. Using a mutated intein version, intermediate steps of the splicing process can be intercepted by small thiols (RSH), as MESNA or MPAA, and render the protein of interest, cleaved from the mutated intein, containing a C-terminal thioester, which serves as reaction handle for EPL (Fig.19)<sup>157, 191</sup>. Further, the functionalized target molecule containing an 1,2-aminothiol group (here a peptide with an N-terminal cysteine (**P1**): CGC-Atto532) can be added, which will undergo a transthioesterification with the protein-thioester. Followed by an S-to-N acyl shift, a completely native protein (containing a cysteine) is obtained, including the selected peptide. Dependent on the composition of the target peptide, this method can be used to introduce post-translational modifications into proteins or to attach fluorophores.



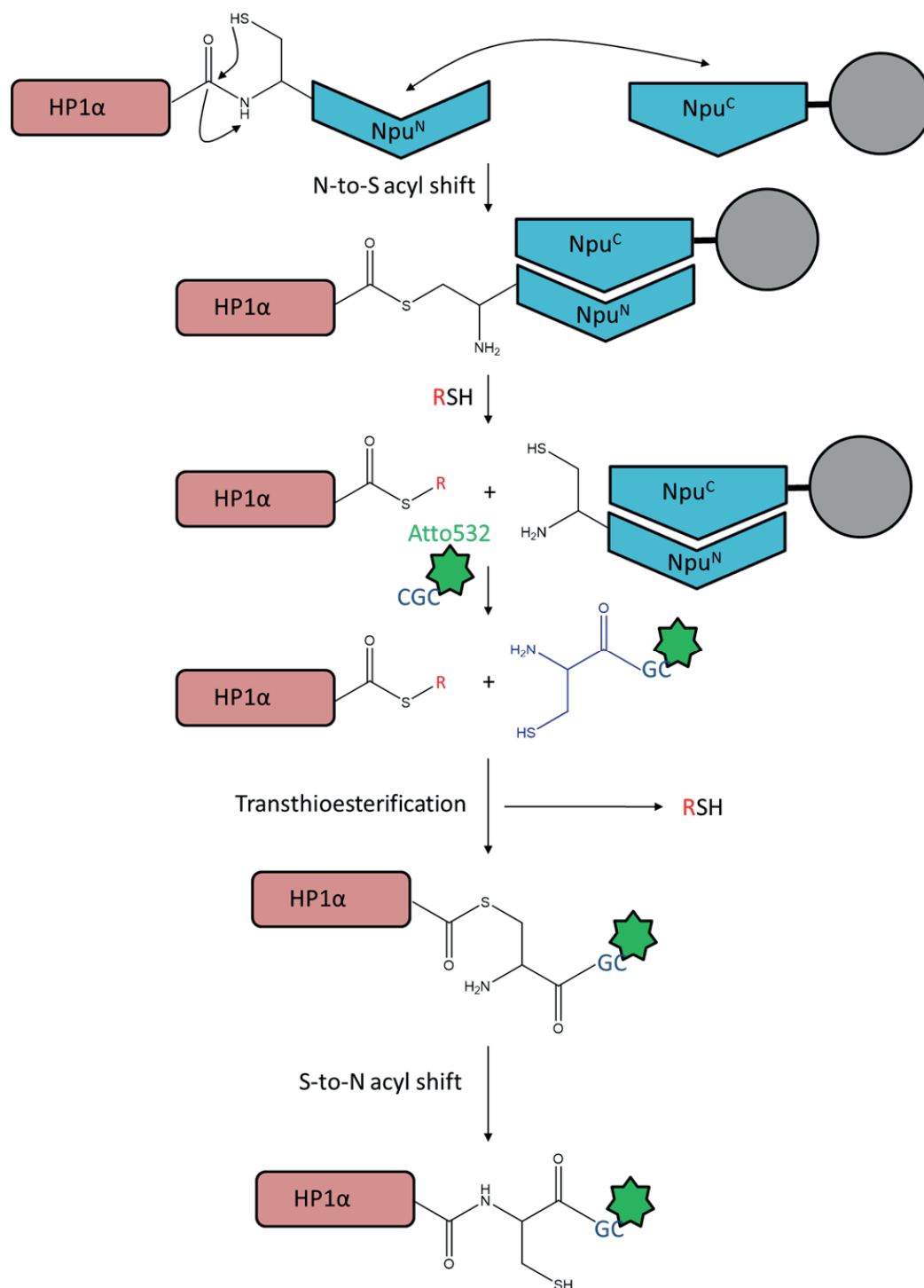


**Fig.19 Reaction scheme of EPL for HP1 $\alpha$  labelling**

Upon binding of Npu<sup>N</sup> to the immobilized Npu<sup>C</sup> an N-to-S acyl shift occurs and allows creation of a thioester coupled to the protein of interest through addition of small thiols (RSH). A functionalized peptide (CGC-Atto532) containing an N-terminal cysteine can be added to induce a transthioesterification, which couples the peptide of interest to the protein. A final S-to-N acyl shift leads to a native peptide bond between the protein of interest and the applied peptide containing a cysteine. The SulfoLink resin is indicated as grey sphere. Atto532 is indicated as green star.



We employed this strategy for HP1 $\alpha$  labelling (Fig.19). The eluate was collected and analysed by sodium dodecyl sulfate-polyacrylamide gel electrophoresis (SDS-PAGE; Fig.20a)<sup>186</sup>. Elution fractions were pooled and purified by gel filtration using a Superdex S200 10/300GL column (Fig.20b). Fractions with the labelled protein were analysed by SDS-PAGE, pooled, concentrated and 20% glycerol was added. Protein stocks were flash frozen and kept at -80°C until use. The final concentration and labelling efficiency (up to 75%) was determined by UV spectroscopy. Further the fluorescence emission spectra were analysed by fluorometry (Fig.20c). Finally, the protein was further analysed by RP-HPLC and ESI-MS (HP1 $\alpha$  (Atto532): calculated molecular weight (MW) = 23'200.0 Da, observed MW = 23'204.0 Da (Fig.20d)).

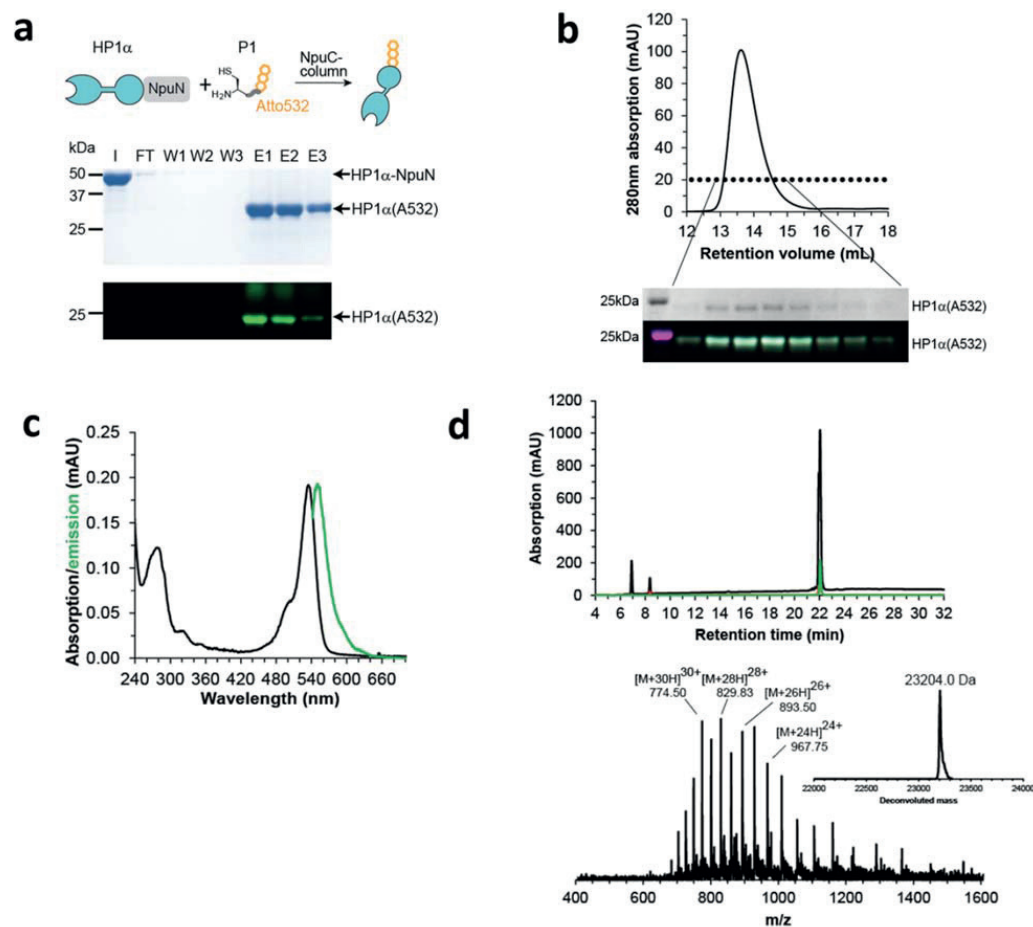


**Fig.20 Labelling and analysis of HP1 $\alpha$**

**a)** HP1 $\alpha$  fused to NpuN is expressed, bound to NpuC-beads, cleaved in ligation buffer and reacted with **P1** *in situ*, yielding labeled HP1a (HP1 $\alpha$ (A532)). (I: Input, FT: flow through, W1-3: washes, E1-3: elutions). The protein was visualized by Coomassie staining and by 532 nm illumination. **b)** Size exclusion chromatography purification of HP1 $\alpha$  after labelling. The dotted line indicates how the peak is reflected by the gel picture. The protein was visualized by Coomassie staining and by 532 nm illumination. **c)** UV absorption spectrum and normalized fluorescence emission spectrum of Atto532 labelled HP1 $\alpha$  (green). **d)** Final analysis of labelled HP1 $\alpha$  by RP-HPLC and ESI-MS (expected MW 23'200.0 Da, observed MW 23'204.0 Da). Figure was adapted from Kilic et al., 2015.

Having obtained the labelled version of HP1 $\alpha$ , we next aimed to design the applicable chromatin system for HP1 $\alpha$ .

### 1.2.2. Designing semi-synthetic chromatin fibres

To study HP1 $\alpha$  we required designer chromatin containing the H3K9me3 histone PTM. We used SPPS and EPL to create histone H3 containing the trimethyl mark at lysine 9 (H3K9me3)<sup>186, 192</sup>. To obtain H3K9me3-histones, a truncated version of the histone was recombinantly expressed (H3( $\Delta$ 1-14)A15C), while the histone PTM was synthesized as a peptide of the N-terminal tail of H3, H3(1-14)K9me3, containing a C-terminal hydrazide. The hydrazide was subsequently converted into a thioester, which allowed ligation of the peptide to the expressed protein (Fig.21)<sup>186</sup>. We decided to split the protein at residue 15 in order to reduce the length of the synthesized peptide and we selected an alanine residue to perform a traceless ligation.

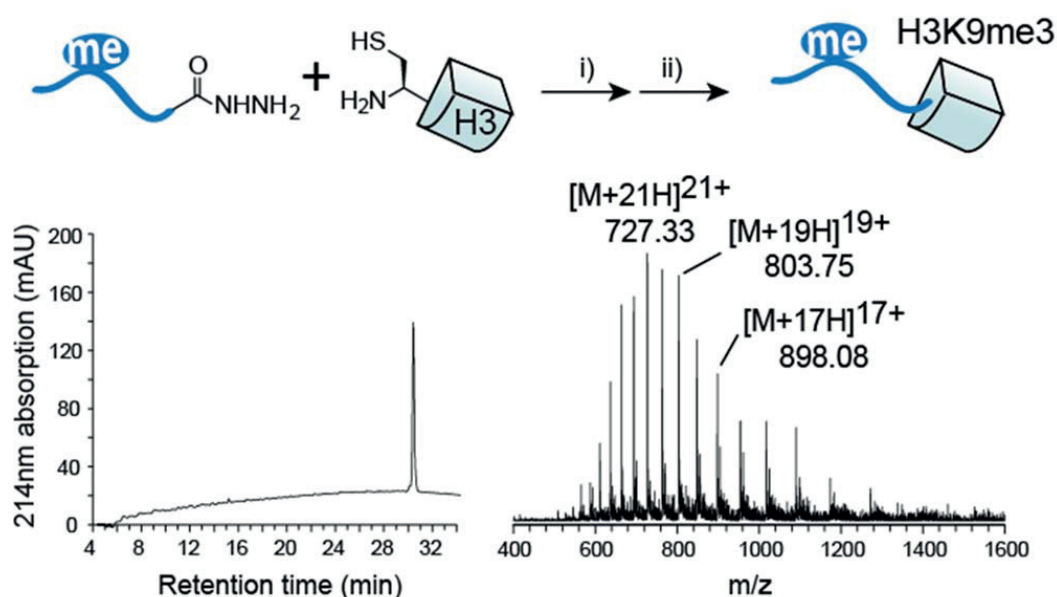


**Fig.21 Traceless semi-synthesis of H3K9me3**

Synthesis of H3K9me3 using a traceless EPL approach: (i) Oxidation of the hydrazide, *in situ* thioester formation and EPL reaction, (ii) desulfurization. Left: RP-HPLC analysis of the final protein, right: ESI-MS analysis of the final histone (MW: 15,251.8 Da calculated, 15,252 Da observed). Semi-synthesis of H3K9me3 was done by Sinan Kilic. Figure was adapted from Kilic et al., 2015.

The modified histone was incorporated into histone octamers with unmodified core histones H4, H2A and H2B as described (for details see chapter “IV, 2.12.2. Histone octamer assembly”). Unmodified histone octamers were assembled similarly.

To create defined chromatin fibres we performed a quality control of histone octamers used for chromatin assembly (Fig.22a). As the proteins were separated on SDS-PAGE as expected, we assembled chromatin arrays consisting of 601 DNA containing 12x147 bp nucleosome positioning sequences (NPS) attached to a 30 bp linker, a biotin-moiety, a fluorescent label (Atto647N), and histone octamers containing the H3K9me3 mark. The linker sequence between individual NPS contained a *ScaI* restriction enzyme digestion site to be able to easily analyse chromatin formation as single nucleosomes, as chromatin arrays would not enter 5 % TBE gels (Fig.22b). To ensure complete saturation of all the NPS with histone octamers, but avoiding oversaturation, we added a low-affinity sequence called MMTV DNA. Thus, if chromatin was oversaturated, all the MMTV DNA would be consumed and a ladder of nucleosomes would appear upon *ScaI* digestion. If chromatin was under-saturated a lot of free DNA and MMTV DNA would be visible on a 5 % TBE gel (Fig.22c).

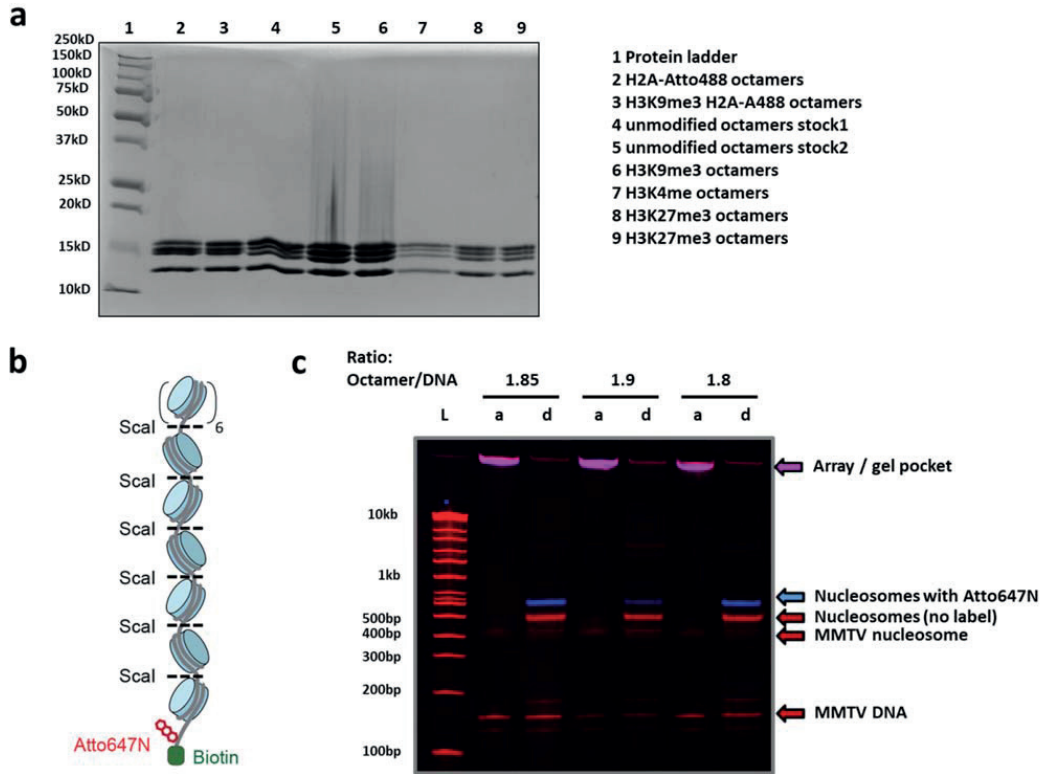


**Fig.22 Histone octamer integrity and chromatin formation**

**a)** Histone octamer integrity is shown on a 15 % SDS-PAGE gel using Coomassie staining. H4:11.367 kDa, H2B: 13.906 kDa, H2A: 14.095 kDa, H3: 15.404 kDa, (human histones, according to uniprot database, 2014.06.05). Four histones are shown in the following order (from 10 kD-15 kD): H4, H2B, H2A, H3. All the histones show defined, single bands. The amount of loaded octamers was not equalized. **b)** Illustration of labelled, biotinylated DNA (grey) used to assemble chromatin arrays containing 12 nucleosomes (blue cylinders). *Scal* digestion (restriction sites shown as dashed lines) renders mononucleosomes for gel analysis. **c)** Illustrated is analysis of chromatin formation. Red: Gelred channel, Blue: 640nm channel, Pink: Overlay of red and blue bands. Shown are three different DNA-octamer ratios (1.85 octamer / DNA, 1.9 and 1.8) that were subjected to chromatin (H3K9me3) formation by dialysis. All three 12xNPS arrays did not enter the 5 % TBE Criterion gel. *Scal*-digested arrays show mononucleosomes with and without the Atto647 label, while a faint band of MMTV nucleosomes was appearing. Importantly, the MMTV DNA was not consumed completely, indicating proper array formation. L = 2-log DNA ladder, a = non-digested array, d = *Scal*-digested array.

To confirm the presence of the H3K9me3 mark in assembled chromatin arrays, we performed an anti-H3K9me3 western blot (Fig.23a). As chromatin integrity is crucial for single molecule measurements, we analysed non-digested chromatin arrays on agarose polyacrylamide composite gel electrophoresis (APAGE), which allows analysis of native complexes of 100 kDa -3 MDa (Fig.23b). Thus, chromatin arrays were intact and saturated after chromatin assembly.

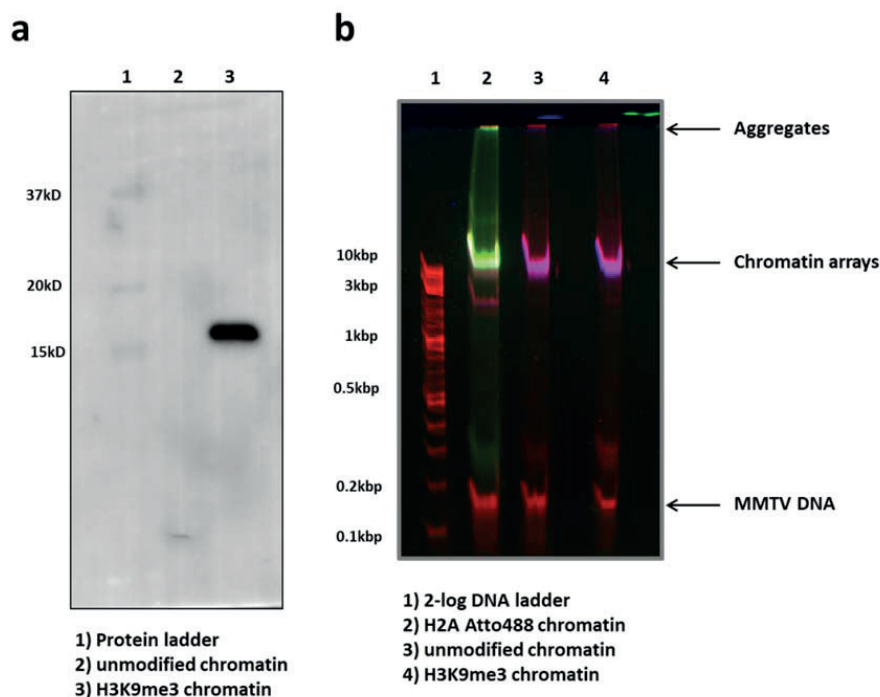


**Fig.23 Verification of the H3K9me3 histone mark and chromatin integrity of full-length arrays**

**a)** Anti-H3K9me3 western blot of the H3K9me3 mark on chromatin. Shown is specific recognition of the H3K9me3-modified chromatin array (lane3) and not the unmodified array (lane2). **b)** Chromatin integrity on an APAGE gel. Red: Gelred channel, Green: Atto488 channel, Blue: Atto647N channel. 12x177 bp 601 DNA chromatin arrays with different modifications were analysed on the APAGE gel. The Gelred channel shows chromatin arrays and MMTV DNA. The Atto488 channel shows labelled histone octamers incorporated into 601 DNA. The Atto647N channel shows labelled, biotinylated 601 DNA, which was used to form chromatin arrays.

### 1.2.3. Measuring protein dynamics on the single molecule level

Having the labelled protein and chromatin fibres with defined histone marks in hands enabled us to apply them on our TIRF microscopy system to measure single molecule dynamics between these two components.

For TIRF imaging, a fully automated Nikon Ti-E inverted fluorescence microscope, controlled by NIS-elements software, equipped with an oil immersion objective and a manually controlled TIRF illuminator arm was employed. Excitation light was provided from a home-built laser bench using 640 nm, 532 nm and 488 nm lasers. Wavelength selection and switching of the excitation light was performed using an acousto-optical tunable filter (AOTF) controlled by NIS-elements. For all HP1 $\alpha$  measurements, light intensities of 20 W/cm<sup>2</sup> were employed for 532 nm and 40 mW/cm<sup>2</sup> for 640 nm.

Microfluidic channels, which were used for microscopy, were assembled on piranha-cleaned glass slides, silanized and then passivated with PEG chains to immobilize chromatin

arrays at the PEG surface using neutravidin-biotin interactions and to avoid non-specific protein sticking to the glass. For details see chapter “IV, 2.14. Preparation of flow channels for TIRF microscopy”.

Under these conditions, using imaging buffer IB1 (see “IV, 2.15. TIRF imaging”), single Atto532 fluorophores were found to bleach with a time constant of 30 s (Fig.24a)<sup>186</sup>, while Atto647N fluorophores remained stable for > 100 s. Despite these findings, we decided to use Atto532 for HP1 $\alpha$  labelling, based on the hydrophobicity and size of Atto647N, which could potentially affect HP1 $\alpha$ -chromatin interactions. We efficiently reduced fluorophore blinking events, which were occurring rarely and of short duration, to a non-observable level by complementing the imaging buffer with trolox and a glucose oxidase/catalase enzymatic oxygen depleting system (imaging buffer IB1, see “IV, 2.15. TIRF imaging”). For imaging conditions TIRF was reached at an angle around 63 °. All measurements were performed at an angle of 64 °, resulting in a decay constant of the evanescent wave of 195 nm for 532 nm, as experimentally determined using unpublished protocols (Fig.24b)<sup>193, 194</sup>.

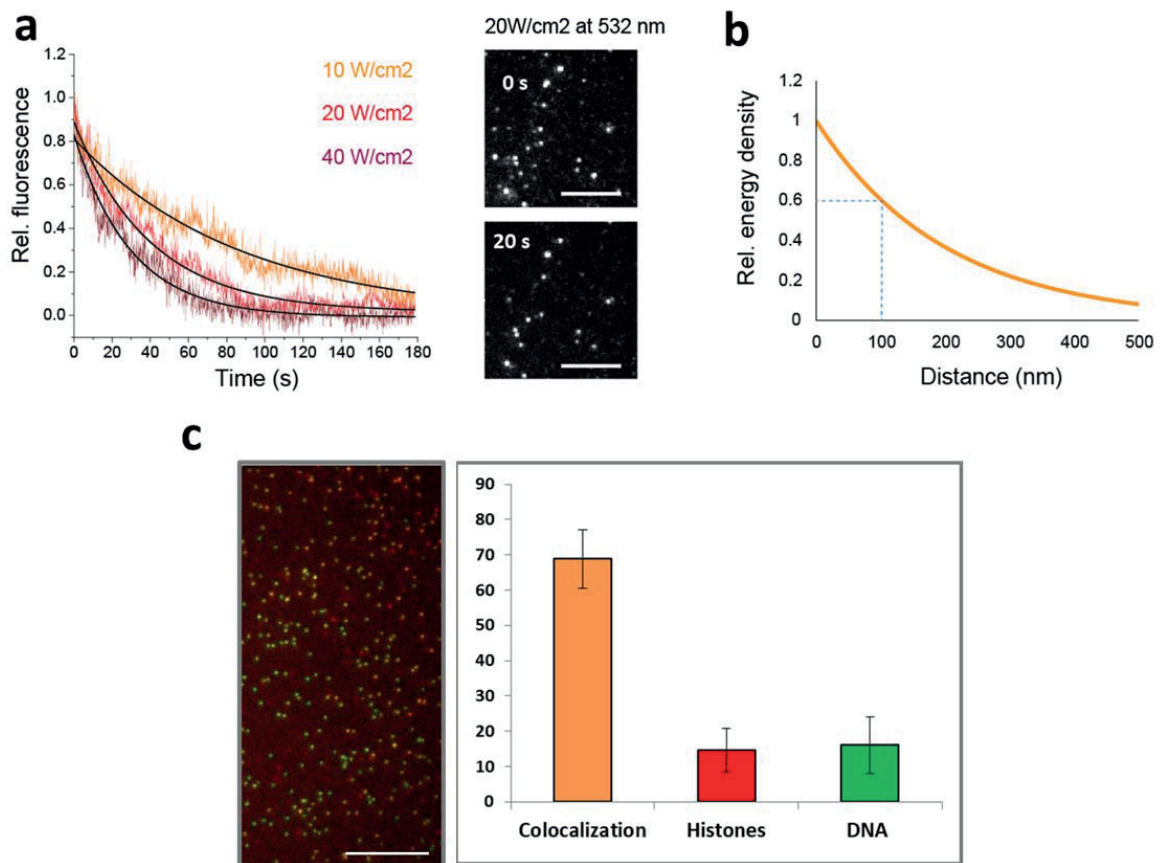


**Fig.24 Photobleaching of HP1α-Atto532, laser penetration and chromatin integrity during single molecule conditions**

**a)** HP1α was biotinylated using EZ-link biotin and immobilized on PEG-passivated coverslips using neutravidin coupling. Single HP1α molecules were imaged (inset at the right at 0 s and 20 s of irradiation) at different intensities of laser irradiation (10-40 W/cm²) and photobleaching kinetics were determined for 200-300 molecules. The accumulated kinetics were fitted to single-exponential decay, resulting in bleaching kinetics of  $\tau_{\text{bleach}} = 29.6$  s for 40 W/cm²,  $\tau_{\text{bleach}} = 40.0$  s for 20 W/cm² and  $\tau_{\text{bleach}} = 86.6$  s for 10 W/cm². Scale bars: 5 μm. **b)** Measured laser penetration at 532 nm under TIRF condition. The dashed lines indicate the approximate length of a stretched 12-mer chromatin array, demonstrating up to 40 % variation in emission intensity for HP1α bound to chromatin, depending on the binding site in the chromatin array. This indicates that the closer a fluorophore is located to the glass surface, the stronger it gets excited and thus the stronger is its emission intensity. The laser penetration was determined using multiple fluorescent microspheres (see Keyel et al., 2004). **c)** Colocalization (orange) of DNA (green, Atto647N) and histones in nucleosomes (red, Atto488). Double-labelled chromatin array integrity was proven in TIRFM, as the histone protein colocalized significantly with the DNA ( $69\% \pm 8\%$ ) based on the individual dye molecules. Scale bar: 10 μm. (individual measurements  $n=6$ ). Figure was adapted from Kilic et al., 2015.

Before we extended our studies on the HP1α binding model, chromatin integrity was further verified under single-molecule conditions: Chromatin arrays containing labelled DNA (Atto647N) and labelled histones (H2A-Atto488), were immobilized on a TIRF microscopy glass coverslip via neutravidin-biotin interactions and subsequently illuminated.



Colocalization of the H2A and DNA dye molecules was statistically significant and indicated that fully assembled chromatin arrays were immobilized on the microscopy slide (Fig.24c).

### 1.3. HP1 $\alpha$ binds specifically to H3K9me3

While investigating different proteins on designer chromatin, we were expecting different modes of protein binding. Here we describe experimental approaches to test the different protein-chromatin interaction models. Simple association/dissociation kinetics was expected for HP1 $\alpha$ , when only two H3K9me3 marks were present (on one nucleosome; Fig.15a). Extended studies on chromatin arrays, containing twelve nucleosomes with 24x H3K9me3 marks, were assessed and presence of several H3K9me3 modifications in close vicinity would enable rapid rebinding events after microdissociation of HP1 $\alpha$  (Fig.15b). As the CSD of HP1 $\alpha$  allows dimerization we further expected dimeric binding to chromatin. This should increase association times due to the presence of two binding domains and decrease dissociation, as dislocation of one H3K9me3-binding domain would not be sufficient to detach the protein from the chromatin structure completely (Fig.15c). Additionally, we were expecting multimeric protein binding for human HP1 $\alpha$ , as for the yeast homolog Swi6, which would lead to stable oligomeric structures on chromatin, that lead to heterochromatin formation (Fig.15d) <sup>45</sup>.

Our experimental setup allows immobilization of intact chromatin fibres and measuring HP1 $\alpha$  dynamics towards H3K9me3 target (Fig.16). As discussed above, protein binding can occur in various modes as for example non-specific interactions, where the protein diffuses onto chromatin and probes for a suitable binding site, but does not encounter its target. Further possibilities are monovalent-, dimeric- and multivalent-interactions with the H3K9me3 marks and presence of neighbouring H3K9me3 marks enable rapid rebinding after microdissociation. Additionally, HP1 $\alpha$  is able to dimerize and presumably forms oligomeric structures of stable chromatin binding complexes through its CSD (Fig.25a) <sup>186</sup>.

For chromatin imaging experiments with HP1 $\alpha$ , the flow channel was washed with a low salt buffer T50 (50 mM NaCl) using an automated pump. Typically, the background level of fluorescence was recorded with both 532 nm and 640 nm excitation. Neutravidin was bound to biotin-PEG chains of the channel, followed by extensive washing with T50 buffer. Subsequently, biotinylated and Atto647N labelled chromatin arrays were flowed into the channel at a concentration of 500 pM and incubated for several minutes. The immobilization step was monitored by Atto647N emission, aiming for a coverage level of 100-200 arrays in a 25 x 50  $\mu$ m imaging area. Excess chromatin in solution as well as MMTV DNA and associated nucleosomes were removed by a washing step and the buffer was replaced with imaging buffer 1 (IB1, see "IV, 2.15. TIRF imaging"), which was designed to stabilize proteins and fluorophores. HP1 $\alpha$  dilutions were freshly prepared in imaging buffer 1 and injected into the channel. Imaging of HP1 $\alpha$  binding dynamics was performed using 532 nm excitation for 10'000 frames. Every 200 frames, the excitation was switched to 640 nm for one frame to



record the positions of the chromatin arrays. These frames were used in data analysis to localize array positions and correct for stage drift. Once immobilized, chromatin arrays were used for measurements for maximal one hour, to avoid disintegration of the chromatin.

In a first attempt, it was necessary to probe the amounts of labelled protein and chromatin in the flow channels in order to obtain as many single molecule spots as possible, but being still able to separate them from each other and to obtain single binding events. It was not possible to evaluate partially overlapping binding events at different positions of a single chromatin fibre, as the individual binding times were not well defined. Thus, it was important to use low concentrations of labelled HP1 $\alpha$  to obtain single HP1 $\alpha$  molecule binding events to the chromatin fibres at a time. We examined a set of different concentrations ranging from 250-1000 pM for chromatin and 100-1000 pM of HP1 $\alpha$  and obtained useful conditions for 250 pM chromatin and 1 nM HP1 $\alpha$  (Fig.25b), where chromatin spots overlapped with HP1 $\alpha$  spots and showed temporal and spatial single dot resolution.

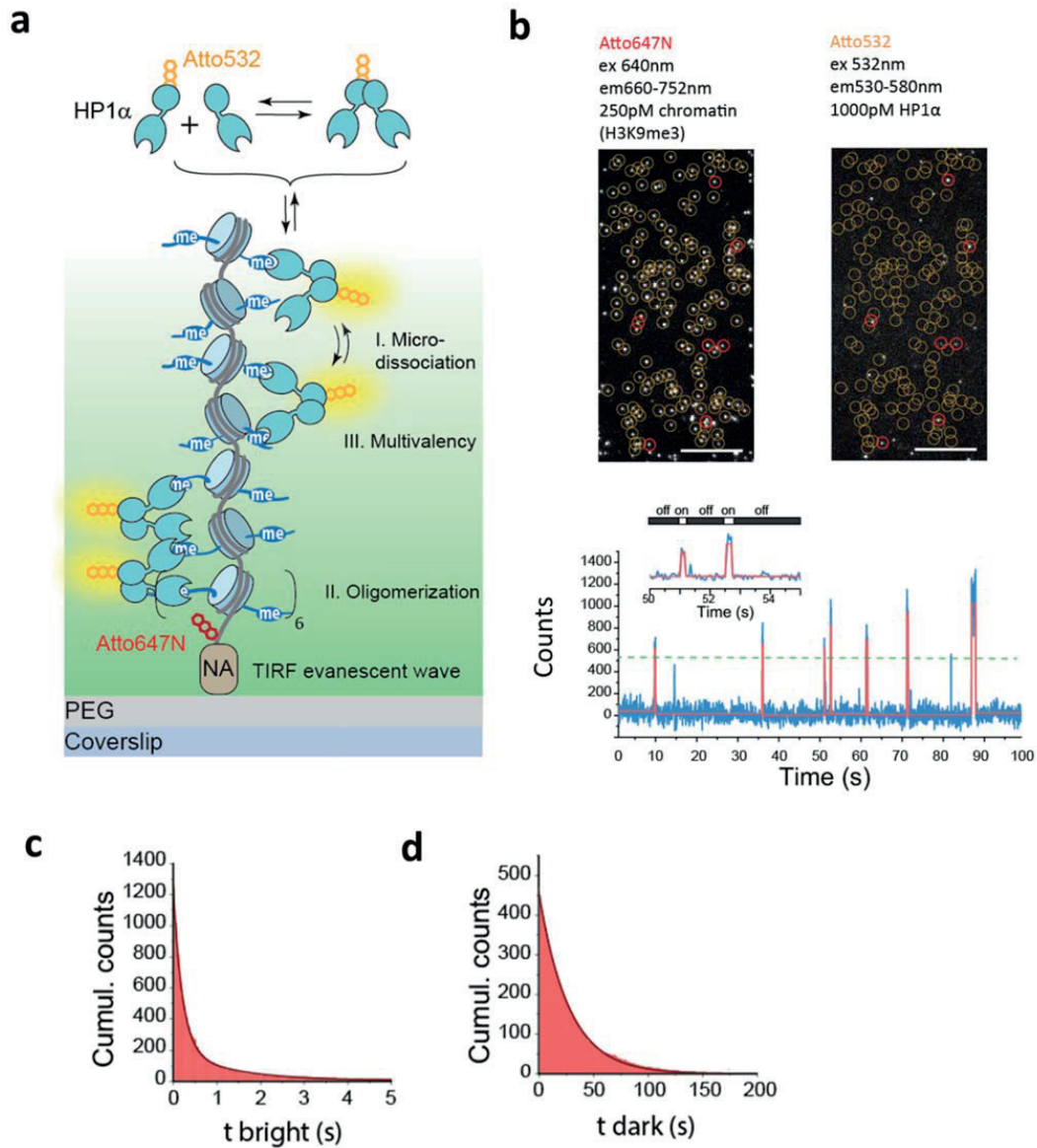


**Fig.25 Experimental setup to monitor HP1 $\alpha$  dynamics on chromatin and generation of cumulative histograms**

**a)** Scheme of the experiment: Atto532-labelled HP1 $\alpha$  interacts with immobilized H3K9me3-modified designer chromatin arrays, while the dynamic interactions are detected by TIRFM. **b)** Shown is immobilized chromatin (H3K9me3) illuminated using 640 nm excitation as single spots (left microscopy frame) and HP1 $\alpha$  using 532 nm excitation (right microscopy frame) at a single time point. Colocalization of chromatin (orange circles) and HP1 $\alpha$  is indicated for a set of chromatin spots (red circles). Scale bar: 10  $\mu$ m. The scheme on the bottom shows a time trace (blue) fitted by a step function (red) using a threshold (green dashed line) to track HP1 $\alpha$  binding events on a single chromatin position. This renders  $t_{\text{bright}}$  (ON) and  $t_{\text{dark}}$  (OFF). **c)** Dissociation kinetics: Cumulative histogram of binding intervals ( $t_{\text{bright}}$ ) for 100 chromatin arrays, fitted by a double-exponential function (fit:  $\tau_{\text{off},1} = 0.25 \text{ s} \pm 0.03 \text{ s}$ ,  $\tau_{\text{off},2} = 2.26 \text{ s} \pm 1.22 \text{ s}$ ). **d)** Association kinetics: Cumulative histogram of intervals between binding events ( $t_{\text{dark}}$ ) over 30 chromatin arrays, fitted by a single-exponential function (fit:  $\lambda_{\text{on}} = 22.9 \text{ s} \pm 9.8 \text{ s}$ ). Figure was adapted from Kilic et al., 2015.

From binding experiments using 1 nM HP1 $\alpha$  and modified chromatin (H3K9me3) we generated cumulative histograms in order to not underscore the long-phase binding events, which were more prone to noise or double binding events. Dissociation times were fitted using a double-exponential decay function to obtain two residence times ( $\tau_{off,1}$  and  $\tau_{off,2}$ ) and association kinetics were fitted using a single-exponential function (Fig.25c and 25d). While  $\tau_{off,1}$  reflects short, monovalent binding events,  $\tau_{off,2}$  reflects longer binding events, which were attributed to multivalency<sup>192</sup>. The following equations were used:

*Dissociation kinetics*<sup>195</sup>:

$$C = A_1 \times e^{-\frac{t}{\tau_{off,1}}} + A_2 \times e^{-\frac{t}{\tau_{off,2}}} \quad (4)$$

$C$  = Counts

$A_1$  = Amplitude1 (of the short phase)

$A_2$  = Amplitude2 (of the long phase)

$t$  = event time

$\tau_{off,1}$  = residence time (of the short phase)

$\tau_{off,2}$  = residence time (of the long phase)

*Association kinetics*<sup>195</sup>:

$$C = A \times e^{-\frac{t}{\lambda_{on}}} \quad (5)$$

$C$  = Counts

$t$  = event time

$\lambda_{on}$  = apparent association time constant

*Dissociation rate constant (of the short phase)*<sup>195, 196</sup>:

$$k_{off,1} = \frac{1}{\tau_{off,1}} \quad (6)$$

*Microscopic association rate constant*<sup>196</sup>:

$$k_{on} = \frac{1}{\lambda_{on} \times [protein] \times N_{array}} \quad (7)$$

$[protein]$  = protein concentration

$N_{array}$  = number of nucleosomes per DNA molecule on the array

*Dissociation rate constant per nucleosome*<sup>196</sup>:

$$K_D = \frac{k_{off}}{k_{on}} \quad (8)$$

We compared HP1 $\alpha$  binding dynamics towards modified chromatin (H3K9me3) and unmodified chromatin (H3K9me0) and we observed strongly diminished binding in the latter case (100 % H3K9me3:  $\tau_{off,1} = 0.25 \text{ s} \pm 0.03 \text{ s}$  and  $\tau_{off,2} = 2.26 \text{ s} \pm 1.22 \text{ s}$ ; unmodified:  $\tau_{off,1} = 0.08 \text{ s} \pm 0.03 \text{ s}$ ). On the other hand, association times aligned well to a single-exponential fit

and rendered an apparent association time constant ( $\lambda_{on}$ ) of  $22.9 \text{ s} \pm 9.8 \text{ s}$  (100 % H3K9me3) (Fig.25d). For the unmodified arrays the slow-phase residence time and the apparent association time constant were poorly defined, as a very low number of events were detected. Based on the fast-phase residence time ( $\tau_{off,1}$ ) and the microscopic association rate constant ( $k_{on}$ ) for the H3K9me3 condition ( $k_{on} = 3.64 \text{ M}^{-1}\text{s}^{-1} \times 10^6 \pm 1.56 \text{ M}^{-1}\text{s}^{-1} \times 10^6$ ), which takes into account the number of nucleosome positioning sequences and the HP1 $\alpha$  concentration, we were able to determine an apparent  $K_D$ -value of 1.1  $\mu\text{M}$  for HP1 $\alpha$ -chromatin (H3K9me3) interactions<sup>39, 56, 57</sup>. Additionally, a CD-mutated version of HP1 $\alpha$  (W40A) exhibited very few binding events and quick off-rates, even in fully methylated chromatin arrays (Table 1). This indicates that our measurements indeed are PTM-dependent and specific for the HP1 $\alpha$  reader domain. In summary, our data confirms that recruitment of HP1 $\alpha$  heavily depends on the presence of its corresponding histone PTM H3K9me3 on the single molecule level.

To test the contribution of the H3K9me3 mark for HP1 $\alpha$  binding, we reduced the available binding sites on chromatin by assembling chromatin arrays of varying H3K9me3 ratios: 75 % H3K9me3, 50 % H3K9me3 and 25 % H3K9me3. Indeed, we observed reduced residence times  $\tau_{off,1}$  when the methylation density was lower (Fig.26a and 26b)<sup>186</sup>. This indicates that rapid dissociation and rebinding events contribute to the measured binding dynamics in fully modified chromatin fibres. Consistently, measurements done in single nucleosomes (1x601 sequence) also resulted in faster dissociation kinetics, as H3K9me3 sites of an adjacent nucleosome were lacking (Table 1).

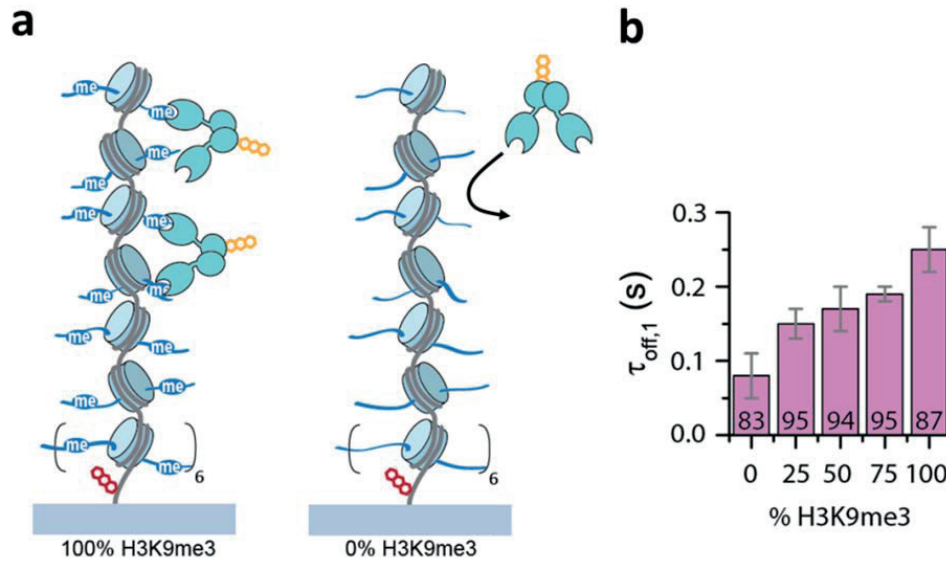


**Fig.26 HP1 $\alpha$  binds specifically H3K9me3-modified chromatin, which mediates rapid rebinding**

**a)** Scheme illustrating the increased retention of HP1 $\alpha$  on chromatin in presence of H3K9me3 modification marks. **b)** The HP1 $\alpha$  residence time ( $\tau_{off,1}$ ) depends on H3K9me3 density as numerous marks enforce microdissociation with rapid rebinding. Number indicate % amplitude of the fast phase (errors: standard error of the mean (SEM), n = 2-16 replicates). These TIRF measurements were done by Louise Bryan. Figure was adapted from Kilic et al., 2015.

## 1.4. HP1 $\alpha$ binds chromatin in a highly dynamic and competitive manner

It has been suggested that Swi6, the yeast (*Schizosaccharomyces pombe*) homolog of HP1 $\alpha$ , is crucial for heterochromatin spreading<sup>45, 70</sup>. This model proposes oligomerization of HP1 $\alpha$  on chromatin, which stabilized HP1 $\alpha$ -chromatin interactions through formation of a stable oligomeric complex. This suggests prolonged residence times of HP1 $\alpha$  onto chromatin, if the protein concentration is elevated. One of the limitations of TIRF microscopy is the relatively low measurable concentration (~10 nM) of the labelled protein species, as otherwise the protein would stick non-specifically to the glass surface and the 2x12 binding sites on the chromatin would be occupied simultaneously, which would lead to overlapping binding events. On top of that, at some point the background signal will be elevated to a disturbing level. To overcome these problems, we decided to add different amounts of non-labelled HP1 $\alpha$  protein to the flow channel (Fig.27a and 27b)<sup>186</sup>. Surprisingly, addition of unlabelled competitor HP1 $\alpha$  molecules did not lead to an increase of the fast-phase residence time  $\tau_{off,1}$ , but instead to a decrease, the more competitor was added (no competitor:  $\tau_{off,1} = 0.25 \pm 0.03$  s and  $\tau_{off,2} = 2.26 \pm 1.22$  s, 50 nM competitor:  $\tau_{off,1} = 0.19 \pm 0.05$  s and  $\tau_{off,2} = 3.97 \pm 1.31$  s, 250 nM competitor:  $\tau_{off,1} = 0.13 \pm 0.02$  s and  $\tau_{off,2} = 3.93 \pm 1.73$  s, 1000 nM competitor:  $\tau_{off,1} = 0.11 \pm 0.01$  s and  $\tau_{off,2} = 2.75 \pm 0.72$  s). This indicates

that the human version of HP1 $\alpha$  does rather compete for available binding sites, than forming a highly-oligomeric complex. Such a competition mechanism subsequently prevents rapid rebinding of dissociated HP1 $\alpha$  molecules and results in an apparent decrease in residence time, in a process termed facilitated dissociation<sup>197, 198</sup>. In fact, concentration-dependent dissociation kinetics have been recently observed for several DNA-binding proteins<sup>199, 200</sup>.

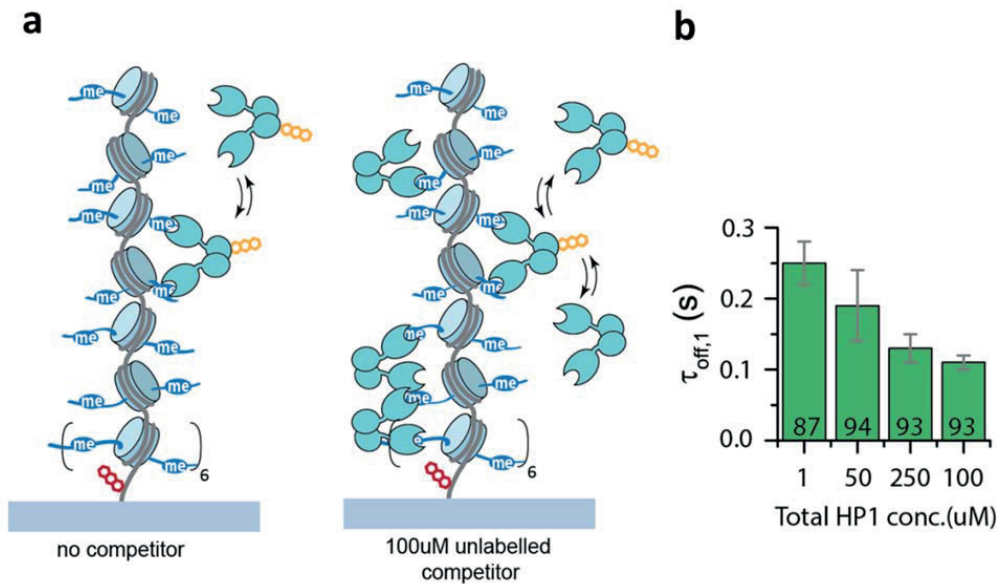


**Fig.27 HP1 $\alpha$  binds in a competitive manner to H3K9me3-modified chromatin**

**a)** Scheme illustrating the decrease in residency time of HP1 $\alpha$  in the presence of unlabelled competitor HP1 $\alpha$  molecules **b)** The HP1 $\alpha$  residence time ( $\tau_{off,1}$ ) decreases as a function of HP1 $\alpha$  concentration due to local competition. The indicated concentration of unlabelled HP1 $\alpha$  is added to 1 nM Atto532-labelled HP1 $\alpha$ . Numbers indicate % amplitude of the fast phase (errors: SEM, n = 3-16 replicates). Figure was adapted from Kilic et al., 2015.

## 1.5. Dimerization of HP1 $\alpha$ prolongs residence time on modified chromatin

We aimed to understand the contribution of multivalent chromatin interactions of HP1 $\alpha$ . In our single-molecule measurements, which were performed using 1 nM HP1 $\alpha$ , we expected a large fraction of HP1 $\alpha$  to dissociate into monomers, as  $K_D$  values for the CSD-dependent HP1 $\alpha$ -homodimerization of different subtypes have been published from 0.5-5  $\mu$ M<sup>201</sup>.

To test this hypothesis, we expressed and labelled an HP1 $\alpha$  I163E mutant, containing a disrupted CSD and thus being unable to dimerize (expression, purification and labelling was done as described for wt HP1 $\alpha$ ). To our expectation residence times on H3K9me3-modified chromatin were only slightly reduced compared to wild-type HP1 $\alpha$ , as the CD was not impeded from its proper function. Surprisingly, the apparent association time constant  $\lambda_{on}$

drastically increased ( $> 100$  s), which proves the necessity of CSD-mediated HP1 $\alpha$  interactions during chromatin binding<sup>186</sup>.

To keep HP1 $\alpha$  in a dimeric state during measurements, we developed a chemical strategy to covalently link two HP1 $\alpha$  molecules (Fig.28)<sup>59, 186</sup>. We joined two individual HP1 $\alpha$  molecules with C-terminal thioesters through a PxVxl-containing peptide containing two ligation handles. Affinity of the peptide to the CSD was ensured by the shugoshin protein sequence (hSgoL1, AA 448-457)<sup>59</sup>. hSgoL1 was chosen as it plays an important role in the protection of centromeric sister-chromatids and has been shown to interact with HP1 $\alpha$  and exerting different functions in a cell-cycle dependent manner<sup>59, 202</sup>. Thus, we synthesized a peptide, which we called **P2**. The peptide was flanked with two lysines with a cysteinyl-residue attached to their side chains and an N-terminal cysteine was used for labelling with the fluorescent dye Atto532.

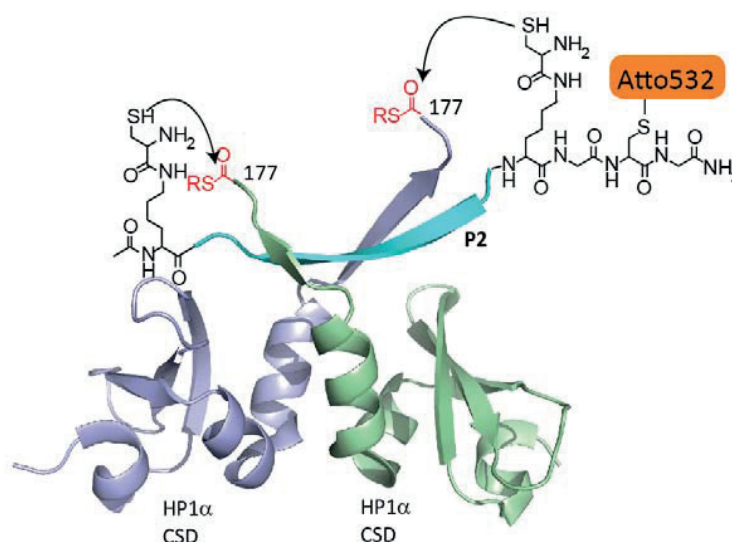


**Fig.28 Strategy to covalently link HP1 $\alpha$  in its dimeric form containing a fluorescent label**

Shown is the strategy to chemically link HP1 $\alpha_{\text{cdm}}$  (at position 177) employing the PxVxl peptide **P2** in affinity-directed dual-EPFL reaction (PDB: 3Q6S, Kang et al., 2011). Figure was adapted from Kilic et al., 2015.

Peptide **P2** (ac-K<sub>1</sub>S<sub>2</sub>L<sub>3</sub>Y<sub>4</sub>P<sub>5</sub>V<sub>6</sub>V<sub>7</sub>K<sub>8</sub>I<sub>9</sub>R<sub>10</sub>R<sub>11</sub>K<sub>12</sub>G<sub>13</sub>C<sub>14</sub>G<sub>15</sub>-CONH<sub>2</sub>) was synthesized using the following protection groups: Cys(Trt), Lys(Boc), Arg(pbf), Tyr(tBu), Ser(tBu) (Fig.29a)<sup>186</sup>. In addition, K<sub>1</sub> and K<sub>12</sub> were included containing an Alloc-protecting group. After synthesis, the N-terminus was acetylated. Then, the Alloc-groups on the two lysines were removed and the resin was subsequently washed. Next, Boc-Thz was coupled to both deprotected lysines in one step. Subsequently, the peptide was cleaved from the resin and labelled with Atto532-iodoacetamide as described for **P1**. The final product was analysed by RP-HPLC and ESI-MS (calculated MW = 2680.24 Da, observed MW= 2679.35 Da) (Fig.29b).



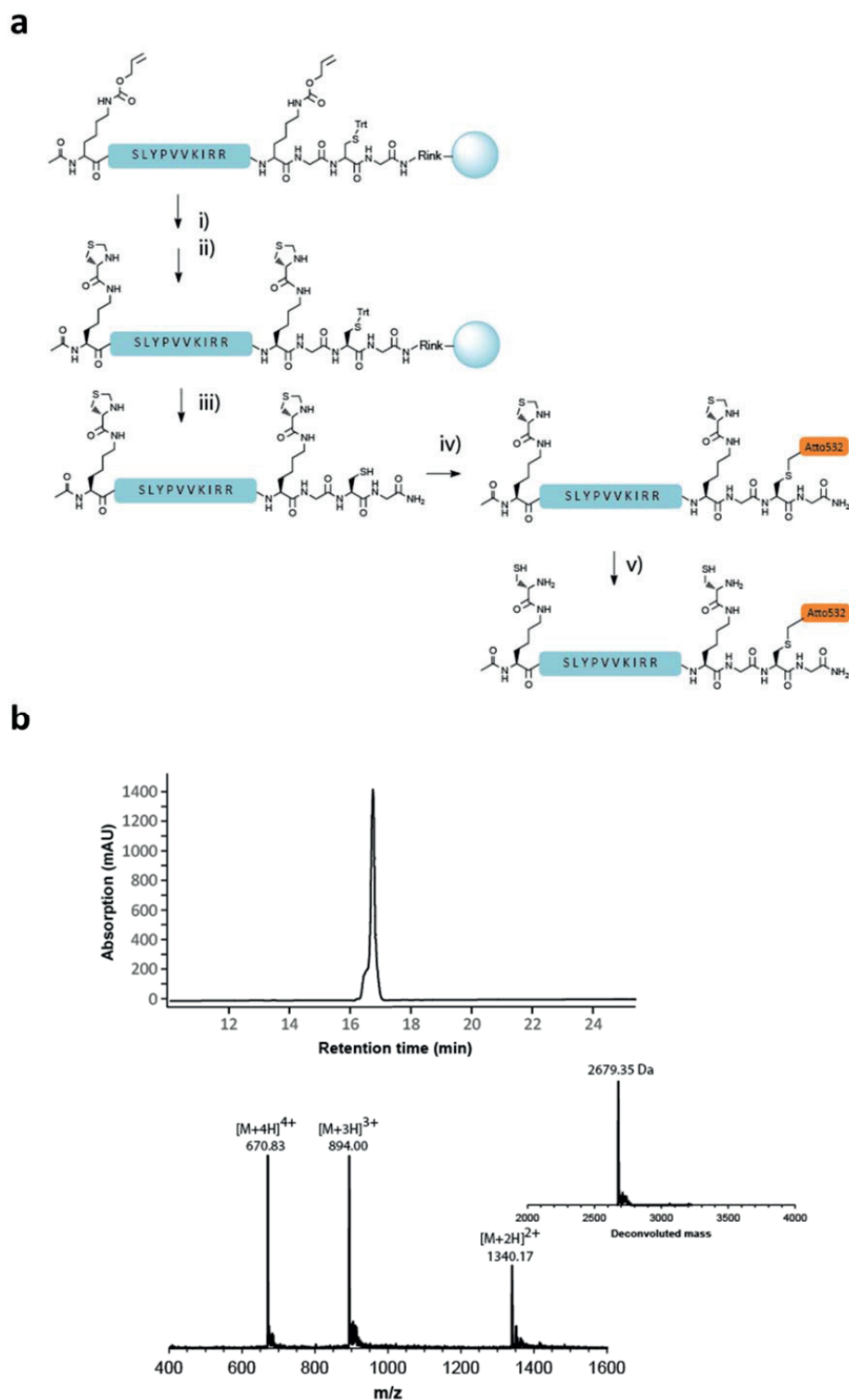


**Fig.29 Peptide synthesis of P2**

**a)** Synthesis scheme for production of **P2**. i) On-resin deprotection of Alloc-K, ii) coupling of Boc-Thz, iii) peptide cleavage, iv) labelling with Atto532-iodoacetamide, v) opening of Thz. **b)** RP-HPLC and MS analysis of **P2** (MW calculated: 2680.24 Da, measured 2679.35 Da). Figure was adapted from Kilic et al., 2015.



To link the peptide with the HP1 $\alpha$  proteins, a C-terminal thioester was introduced at position 177, as this was assessed to be optimal for reactivity, based on the protein structure. The HP1 $\alpha$ (AA 1-177)-SR was prepared via expression with a C-terminal NpuN split-intein. *In situ* dual-ligation with **P2** rendered dimeric, peptide-linked HP1 $\alpha$  dimers (HP1 $\alpha_{\text{cdm}}$ ) with a 60 % yield (this was done similarly as for HP1 $\alpha$  labelling with **P1**) (Fig.30a) <sup>186</sup>. The linked protein was successfully purified by size-exclusion chromatography and analysed by fluorometry, RP-HPLC and ESI-MS (Fig30b, 30c and 30d). To test functionality, a peptide binding assay unveiled that the HP1 $\alpha_{\text{cdm}}$  is able to bind an H3K9me3 peptide with an affinity similar to HP1 $\alpha$  ( $K_D = 12.5 \text{ uM} \pm 0.5 \text{ uM}$ ; as published in Kilic et al., 2015) <sup>186</sup>.

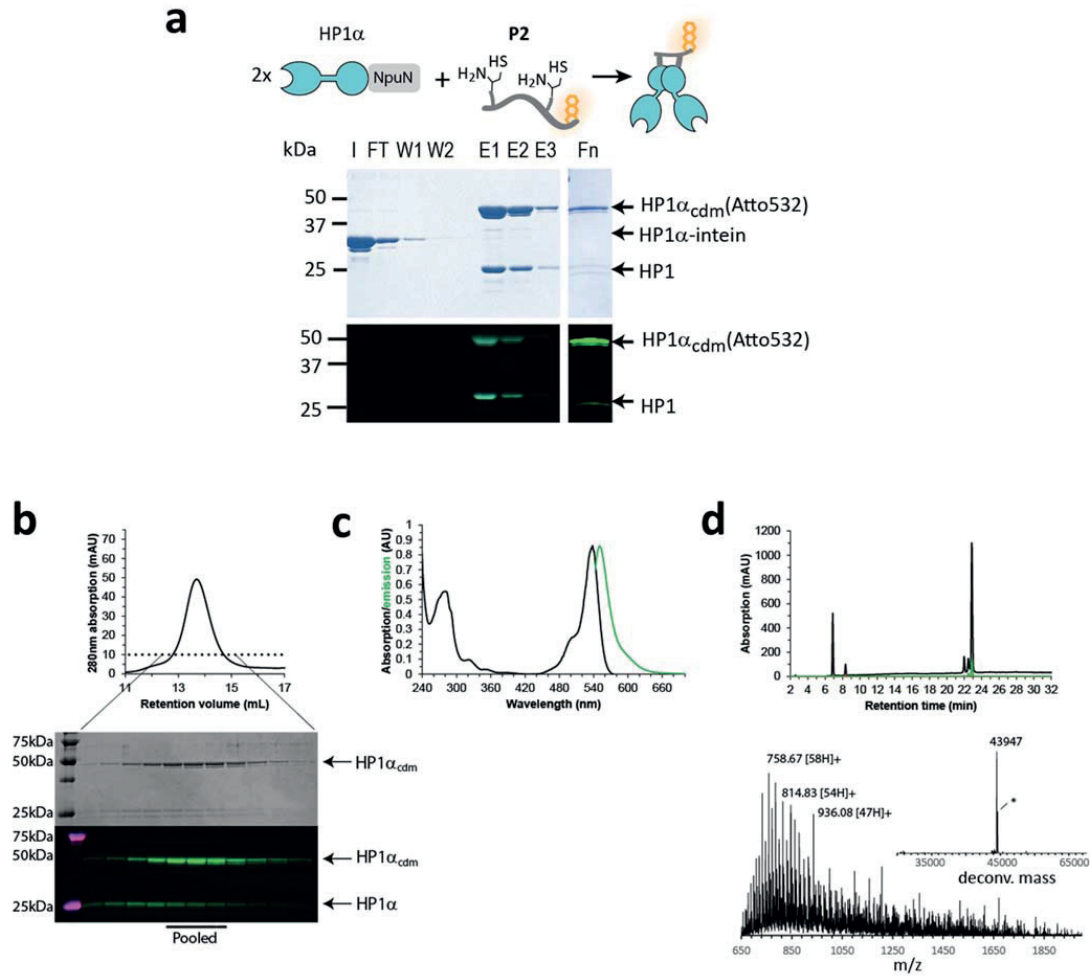


**Fig.30 Analysis of covalently linked dimeric HP1 $\alpha$  after expressed protein ligation with the labelled peptide P2**

**a)** One-pot production of Atto532-labelled HP1 $\alpha$ <sub>cdm</sub>: HP1 $\alpha$ (AA 1-177), fused to the NpuN-split intein was bound to NpuC-beads and eluted with ligation buffer containing the hSgoL1 peptide (functionalized having two cysteinyl-lysines and an Atto532 dye), yielding labelled HP1 $\alpha$ <sub>cdm</sub>. Pure HP1 $\alpha$ <sub>cdm</sub> was obtained after gel-filtration purification. Gel annotation: I = input; FT = flow through of column; W1-2 = column washes; E1-3 = elution fractions; Fn = final protein after gel filtration. The protein was visualized by Coomassie staining and by 532 nm illumination. **b)** Size exclusion chromatography purification of HP1 $\alpha$ <sub>cdm</sub>, and SDS-PAGE analysis of the fractions. The pooled fractions containing only HP1 $\alpha$ <sub>cdm</sub> are indicated. The protein was visualized by Coomassie staining and by 532 nm illumination. **c)** UV absorption spectrum and normalized fluorescence emission spectrum of HP1 $\alpha$ <sub>cdm</sub> (green). **d)** RP-HPLC and MS analysis of the final product, HP1 $\alpha$ <sub>cdm</sub> (calculated mass: 43'944.65 Da, observed mass: 43947.0 Da, \*: buffer adduct (HEPES/Na<sup>+</sup>)). Figure was adapted from Kilic et al., 2015.

We measured H3K9me3-modified chromatin binding using HP1 $\alpha$ <sub>cdm</sub> (at 0.5 nM, as this is equivalent to 1 nM monomeric HP1 $\alpha$ ) and we observed an increase in event-duration and -occurrence, when compared to HP1 $\alpha$  (Fig.31a)<sup>186</sup>. As for HP1 $\alpha$ , dissociation kinetics of HP1 $\alpha$ <sub>cdm</sub> fitted well to a double-exponential curve, which rendered  $\tau_{\text{off},1} = 0.33 \text{ s} \pm 0.01 \text{ s}$  and  $\tau_{\text{off},2} = 3.40 \text{ s} \pm 0.53 \text{ s}$ , while association kinetics were determined using a single-exponential

fit:  $\lambda_{on} = 7.45 \text{ s} \pm 1.87 \text{ s}$  (Fig.31b, 31c, 31d and 31e). This observation was further confirmed by analysing two-dimensional histograms of  $\tau_{off,1}$  and  $\lambda_{on}$  for wild-type HP1 $\alpha$  and HP1 $\alpha_{cdm}$  (Fig.32a and 32b)<sup>186</sup>. We noticed a shift of event distribution to longer residence times and shorter  $\lambda_{on}$  for the dimeric protein (Fig.31d, 31e and 32b). Together, these measurements strongly suggest that dimerization of HP1 $\alpha$  leads to prolonged chromatin binding. We explain this effect, first, by the availability of two K9me3-bearing H3-tails in the nucleosomes, second, the covalent protein dimer, which cannot dissociate into monomers and, third, an increased chance of rapid rebinding upon transient dissociation of HP1 $\alpha_{cdm}$ . Importantly, also the microscopic association rate constant increased six-fold (HP1 $\alpha_{cdm}$   $k_{on} = 22.4 \text{ M}^{-1}\text{s}^{-1} \times 10^6 \pm 0.6 \text{ M}^{-1}\text{s}^{-1} \times 10^6$ ) compared to HP1 $\alpha$  and results in an apparent  $K_D$  of 0.14  $\mu\text{M}$ , which represents about 60-fold affinity increase compared to protein binding to isolated H3K9me3 peptides<sup>186</sup>.

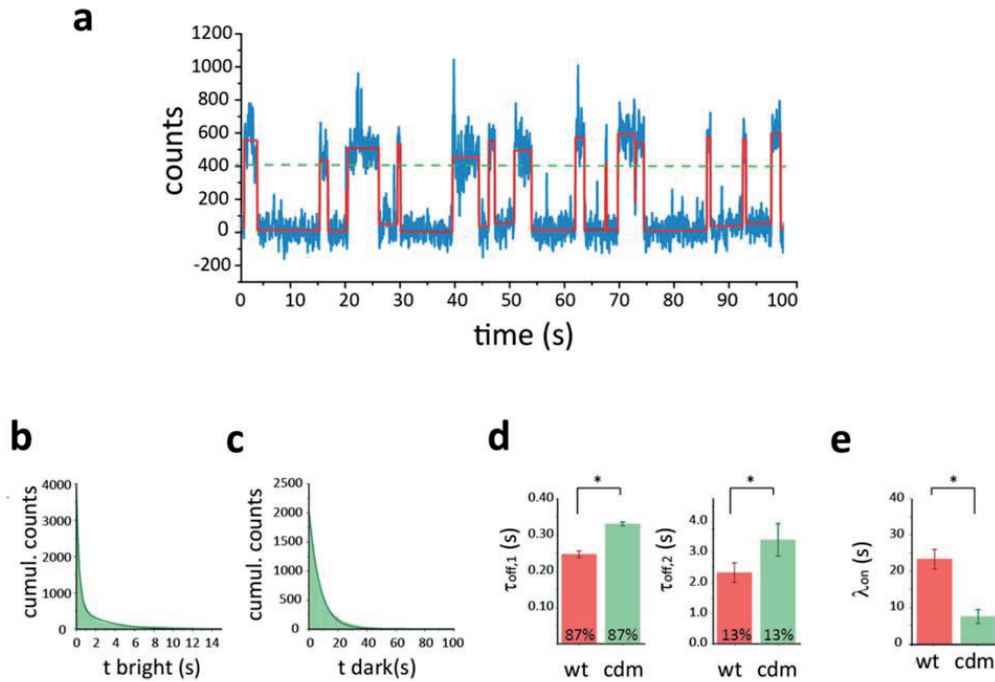


**Fig.31 Kinetics of HP1 $\alpha_{cdm}$**

**a)** Time trace (blue) fitted by a step function (red) using a threshold (green dashed line) to track HP1 $\alpha_{cdm}$  binding events on a single chromatin array (0.5 nM HP1 $\alpha_{cdm}$ ). **b)** HP1 $\alpha_{cdm}$  dissociation kinetics (100 chromatin arrays,  $10^5$  frames each) fitted by a double-exponential function (fit:  $\tau_{off,1} = 0.33 \text{ s} \pm 0.01 \text{ s}$  and  $\tau_{off,2} = 3.40 \text{ s} \pm 0.53 \text{ s}$ ). **c)** HP1 $\alpha_{cdm}$  association kinetics over 30 chromatin arrays, fitted by a single-exponential function (fit:  $\lambda_{on} = 7.45 \text{ s} \pm 1.87 \text{ s}$ ). **d)** Comparison of the average dissociation time constants  $\tau_{off,1}$  and  $\tau_{off,2}$  (fast and slow phase) between HP1 $\alpha$  and HP1 $\alpha_{cdm}$  (errors: SEM, 4-16 replicates, \* $P < 0.05$ , Student's t-test). **e)** Comparison of the apparent association time constant  $\lambda_{on}$  between HP1 $\alpha$  and HP1 $\alpha_{cdm}$  (errors: SEM, 4-16 replicates, \* $P < 0.05$ , Student's t-test). Figure was adapted from Kilic et al., 2015.

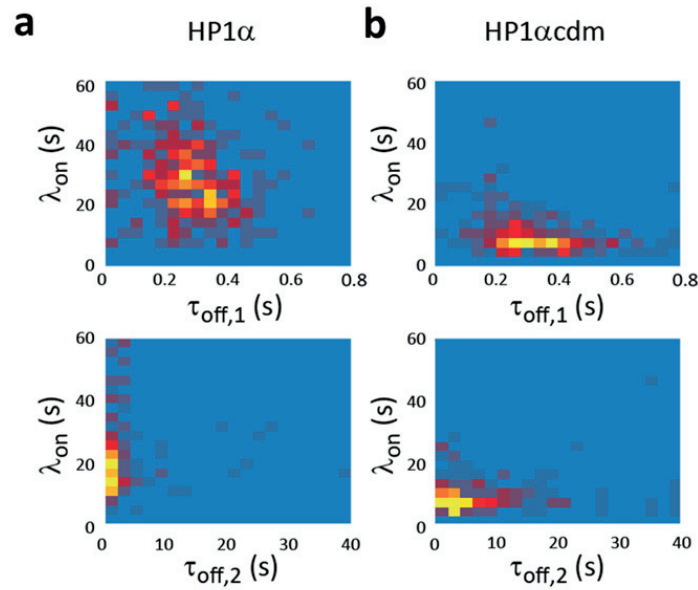


**Fig.32 Two-dimensional histogram to compare dissociation and association behaviour of HP1 $\alpha$  and HP1 $\alpha_{\text{cdm}}$**

**a)** Distribution of interaction kinetics from HP1 $\alpha$  with single chromatin arrays: Two dimensional histograms of single-array binding kinetics showing the correlation of residence times  $\tau_{\text{off},1}$  and  $\tau_{\text{off},2}$  with the apparent association time constant  $\lambda_{\text{on}}$ . **b)** Two dimensional histogram of single-array binding kinetics for HP1 $\alpha_{\text{cdm}}$ . Figure was adapted from Kilic et al., 2015.

## 1.6. Peptide-mediated dimerization of HP1 $\alpha$ prolongs binding on modified chromatin

Peptides containing a PxVxl/L motif, as utilized above as ligation peptide, have been shown to facilitate HP1 $\alpha$  dimerization through the CSD<sup>201</sup>. As a consequence, proteins interacting with the CSD have been found to stabilize interactions between chromatin and HP1<sup>58, 203</sup>. To verify these findings and use them in our *in vitro* system another HP1 $\alpha$  mutant was created. Unlike the I163E mutant, which is strictly monomeric, HP1 $\alpha$  (W174A) is unable to form interactions between the CSD and the PxVxl/L ligands and as such prevents ligand-driven HP1 $\alpha$  dimerization<sup>70</sup>. FRAP experiments, in mouse embryonic fibroblast cells (NIH 3T3), should give *in vivo* insight into this phenomenon, since the behaviour of labelled wild-type- and mutant HP1 $\alpha$  proteins upon photobleaching can be directly observed in living cells and this resembles a more native system than the *in vitro* TIRF assay. The wild-type- and the two mutant-HP1 $\alpha$  versions were fused to a monomeric fluorescent protein mEos3.2 for imaging purposes<sup>204</sup>. Upon transfection fluorescent HP1 $\alpha$  molecules formed heterochromatic foci, which was verified by DNA staining (Fig.33a)<sup>186</sup>. In FRAP experiments fluorophores of labelled proteins are bleached with a laser. The fluorescent signal of the bleached spot recovers over time, dependent on dissociation kinetics of bleached molecules and the binding kinetics of fluorescent molecules. Thus, if a protein, like HP1 $\alpha$ , can interact with structures within the bleached area, the recovery will be delayed. When we performed

FRAP experiments, we unveiled that the obligate monomeric I163E mutant resulted in highly impaired chromatin binding compared to wild-type HP1 $\alpha$ . Consistently, also the W174A mutant showed reduced affinity towards chromatin, faster dynamics and a comparatively larger mobile fraction than the wild-type HP1 $\alpha$ , indicating that the CSD domain is indeed essential for efficient recruitment to chromatin and stable association (Fig.33b) <sup>205</sup>. The photobleaching of wild-type HP1 $\alpha$  did not entirely recover, which suggests presence of an immobile HP1 $\alpha$  fraction that is tightly bound to chromatin (Fig.33b). The immobile HP1 $\alpha$  fraction is probably based on multivalent interactions with chromatin and protein-protein interactions, as it is not observed in the HP1 $\alpha$  mutants.

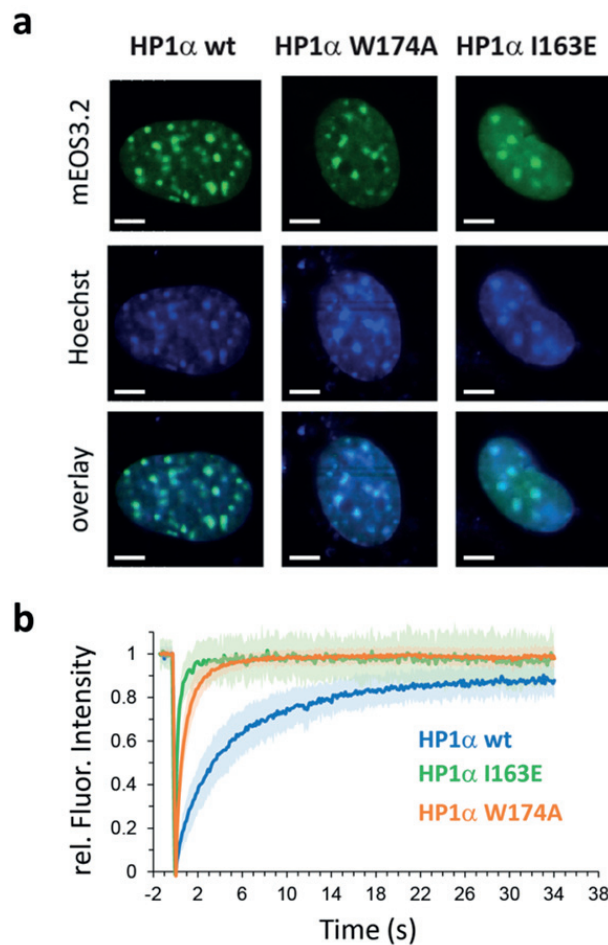


**Fig.33 Foci formation of mEOS3.2-HP1 $\alpha$  (wt, I163E and W174A) and enhanced FRAP of mEOS3.2-HP1 $\alpha$  mutants compared to wt mEOS3.2-HP1 $\alpha$**

**a)** Confocal fluorescence images of NIH 3T3 cells transfected with mEos3.2-HP1 $\alpha$ , mEos3.2-HP1 $\alpha$  (I163E) or mEos3.2-HP1 $\alpha$  (W174A) and overlay with Hoechst staining. Scale bar, 5  $\mu$ m. **b)** FRAP analysis of mEos3.2-HP1 $\alpha$  wt or W174A in heterochromatin foci ( $n = 15$  cells with two foci from each, the shaded area denotes the standard deviation at each time point). Analysis of the traces using a diffusion/binding model (Sprague, et al., 2004) results in the following values: HP1 $\alpha$ :  $\lambda_{on} = 1.2 \text{ s} \pm 0.4 \text{ s}$  and  $\tau_{off} = 2.8 \text{ s} \pm 1.2 \text{ s}$ , HP1 $\alpha$  (W174A):  $\lambda_{on} = 1.0 \text{ s} \pm 0.2 \text{ s}$  and  $\tau_{off} = 1.1 \text{ s} \pm 0.3 \text{ s}$ , HP1 $\alpha$  (I163E):  $\lambda_{on} = 1.8 \text{ s} \pm 0.3 \text{ s}$  and  $\tau_{off} = 0.8 \text{ s} \pm 0.1 \text{ s}$ . Figure was adapted from Kilic et al., 2015.

In order to test the ligand-mediated HP1 $\alpha$  dimerization in TIRF experiments, we synthesized another peptide variant (**P3**) of the PxVxl sequence of hSgoL1 (AA 488-457). Opposed to experiments including peptide **P2**, addition of **P3** was used to facilitate non-covalent dimerization of HP1 $\alpha$ .

Peptide **P3** (NH<sub>2</sub>-N<sub>1</sub>V<sub>2</sub>S<sub>3</sub>L<sub>4</sub>Y<sub>5</sub>P<sub>6</sub>V<sub>7</sub>V<sub>8</sub>K<sub>9</sub>I<sub>10</sub>R<sub>11</sub>R<sub>12</sub>L<sub>13</sub>S<sub>14</sub>-CONH<sub>2</sub>) was synthesized using the following protection groups: Asn(Trt), Lys(Boc), Arg(pbf), Tyr(tBu), Ser(tBu). After cleavage from the resin the peptide was purified using preparative RP-HPLC and analysed by RP-HPLC and ESI-MS (calculated MW = 1685.03 Da, observed MW= 1685.3 Da) (Fig.34a and 34b) <sup>186</sup>.

As a control peptide we synthesized a peptide **P4**, which is unable to dimerize HP1 $\alpha$  as the PxVxl motif was replaced by three alanines.

Peptide **P4** (NH<sub>2</sub>-N<sub>1</sub>V<sub>2</sub>S<sub>3</sub>L<sub>4</sub>Y<sub>5</sub>A<sub>6</sub>V<sub>7</sub>A<sub>8</sub>K<sub>9</sub>A<sub>10</sub>R<sub>11</sub>R<sub>12</sub>L<sub>13</sub>S<sub>14</sub>-CONH<sub>2</sub>) was synthesized using the following protection groups: Asn(Trt), Lys(Boc), Arg(pbf), Tyr(tBu), Ser(tBu). After cleavage from the resin the peptide was purified using preparative RP-HPLC and analysed by RP-HPLC and ESI-MS (Calculated MW = 1589.03 Da, observed MW= 1588.6 Da) (Fig.34c and 34d).

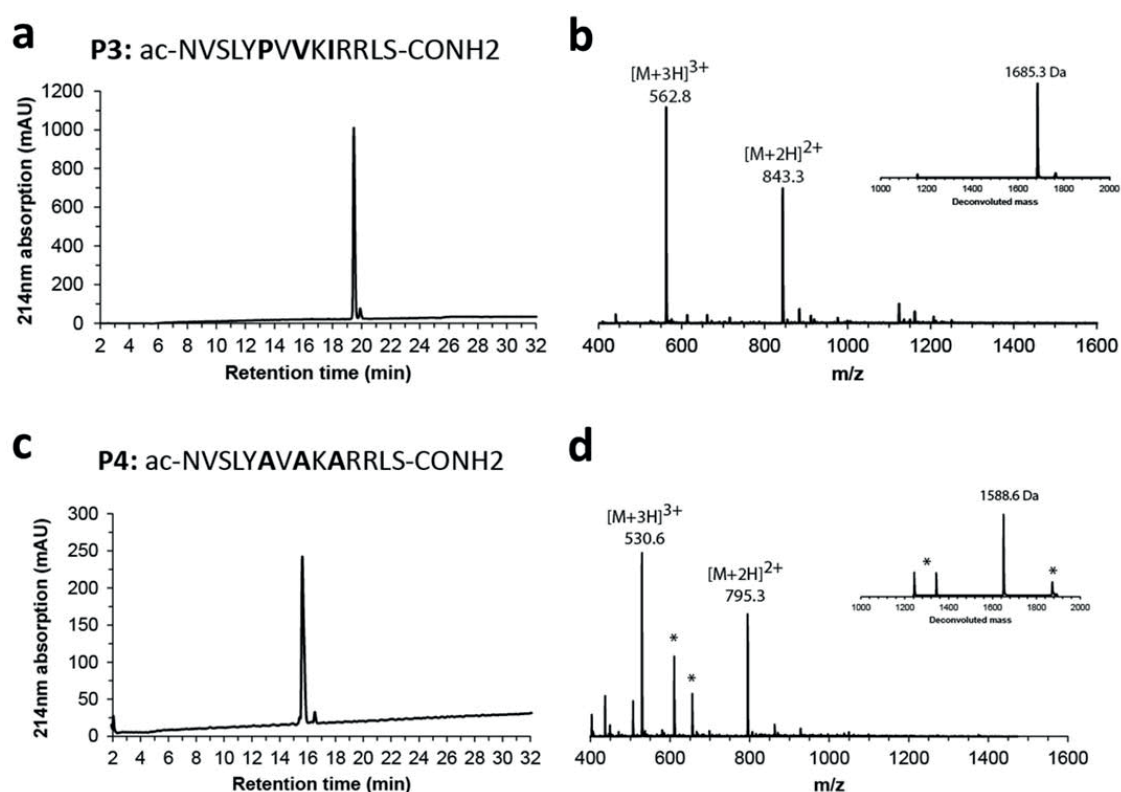


**Fig.34 Analysis of peptide P3 and P4 after synthesis**

**a)** Sequence of **P3**, HPLC and **b)** ESI-MS analysis of purified **P3**, (calculated mass: 1685.03Da, observed mass 1685.3Da). **c)** Sequence of **P4**, HPLC and **d)** ESI-MS analysis of purified **P4**, (calculated mass 1589.03Da, observed mass 1588.6Da). Figure was adapted from Kilic et al., 2015.

To evaluate interactions between HP1 $\alpha$  and the synthesized peptides, the binding constants were determined using microscale thermophoresis. Measurements were performed with hydrophilic capillaries. The HP1 $\alpha$ -Atto532 protein was provided by Sinan Kilic and I provided the interacting peptides **P3** and **P4**. The HP1 $\alpha$  concentration during measurements was at 50 nM, while peptide concentrations were altered from 1 nM to 40  $\mu$ M. The microscale thermophoresis analysis verified tight interactions of the synthesized peptide **P3** and HP1 $\alpha$  rendering a  $K_D$  of 110 nM (Fig.35)<sup>186</sup>. In contrast, no binding curve could be determined in thermophoresis experiments using peptide **P4** and HP1 $\alpha$ . This verified the requirement of the PxVxl motif in peptide **P3** for HP1 $\alpha$  binding.

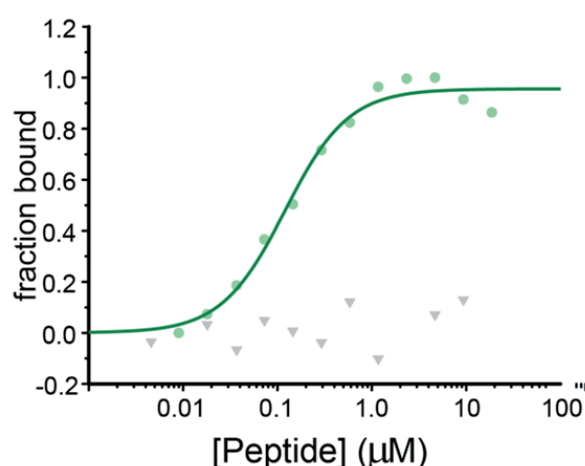


**Fig.35 Thermophoresis unveils interactions between P3 and HP1 $\alpha$**

Microscale thermophoresis analysis of binding **P3** (green) and **P4** (grey) to HP1 $\alpha$ , labelled with Atto532. The solid line is a fit to a one-site equilibrium binding model and results in a  $K_D = 0.11$   $\mu$ M. Figure was adapted from Kilic et al., 2015.

Encouraged by the **P3**-specific binding in thermophoresis assays, we included 1  $\mu$ M peptide **P3** in our TIRF binding measurements with wt HP1 $\alpha$ . Strikingly, an increase in residence times and significantly accelerated association dynamics were observed (Fig.36a, 36b)<sup>186</sup>. Moreover, the fluorescence intensity distribution of individual trace observation led to a 2.5-fold increase in dimerization of HP1 $\alpha$  (42 % dimeric HP1 $\alpha$ ), when **P3** was present<sup>186</sup>. As expected, the apparent association time constant increased in measurements containing the de-functionalized peptide **P4** (Fig.36c and 36d). A significant difference of  $\tau_{off,2}$  in measurements comparing the two peptides was not observed due to a strong variability between individual experiments (Fig.36c). We attribute a remaining non-specific effect of the peptides to direct peptide-DNA interactions, due to their poly-cationic nature.



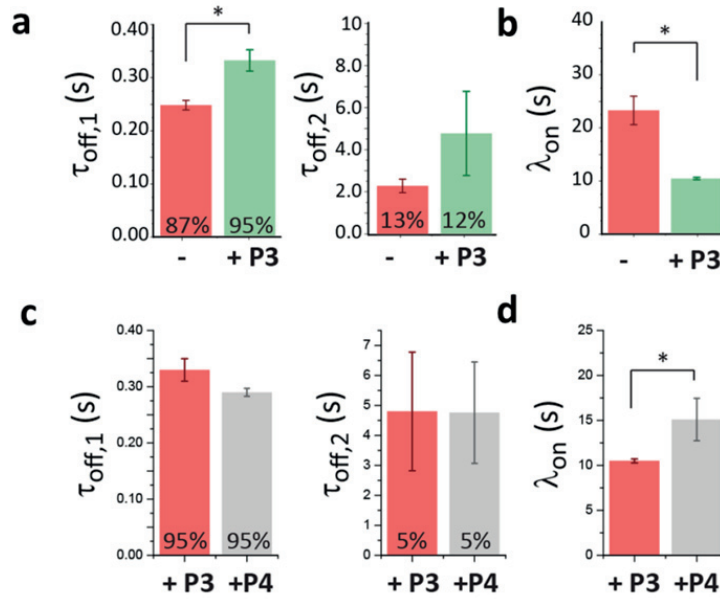


**Fig.36 Dissociation- and association kinetics of HP1 $\alpha$  without and with peptides P3 and P4**

**a)** Comparison of the average dissociation time constants  $\tau_{off,1}$  and  $\tau_{off,2}$  (fast and slow phase) between HP1 $\alpha$  in the absence and presence of **P3** (error bars: SEM, n = 4-16 replicates, \*P<0.05, Student's t-test). **b)** Comparison of the apparent association time constant  $\lambda_{on}$  between HP1 $\alpha$  in the absence and presence of **P3** (error bars: SEM, n = 4-16 replicates, \*P<0.05, Student's t-test). **c)** Comparison of the average dissociation time constants  $\tau_{off,1}$  and  $\tau_{off,2}$  (fast and slow phase) between HP1 $\alpha$  in the presence of **P3** and **P4** (error bars: SEM, n = 4, 2 replicates, \*P<0.05, Student's t-test). **d)** Comparison of the apparent association time constant  $\lambda_{on}$  between HP1 $\alpha$  in the presence of **P3** and **P4** (error bars: SEM, n = 4 replicates, \*P<0.05, Student's t-test). Figure was adapted from Kilic et al., 2015.

Together, all these experiments confirm that HP1 $\alpha$  dimerization, which in cells is supported by ligand polypeptides, leads to prolonged binding of HP1 $\alpha$  to H3K9me3-modified chromatin and association happens in an accelerated manner. The HP1 $\alpha$  single molecule measurements are summarized in Table 1<sup>186</sup>.



Experimental system		Dissociation kinetics				Association kinetics		Equilibrium	Replicates
Chromatin	Effector	$\tau_{off,1}(s)$	%A1	$\tau_{off,2}(s)$	%A2	$\lambda_{on}(s)$	$k_{on}(M^{-1}s^{-1}) \times 10^6$	$K_D (\mu M)$ *	n (n') **
H3K9me3 (100%)	HP1 $\alpha$	0.25 $\pm$ 0.03	87 $\pm$ 7	2.26 $\pm$ 1.22	13 $\pm$ 7	22.9 $\pm$ 9.8	3.64 $\pm$ 1.56	1.16 $\pm$ 0.54	16 (8)
H3K9me0	HP1 $\alpha$	0.08 $\pm$ 0.03	83 $\pm$ 10	(3.70 $\pm$ 4.90)‡	17 $\pm$ 10	N/A §	N/A §	N/A §	3 (2)
H3K9me3 (75%)	HP1 $\alpha$	0.19 $\pm$ 0.01	95 $\pm$ 3	4.03 $\pm$ 4.09	5 $\pm$ 3	51.0 $\pm$ 25.8	1.63 $\pm$ 0.82	3.23 $\pm$ 1.63	5 (3)
H3K9me3 (50%)	HP1 $\alpha$	0.17 $\pm$ 0.03	94 $\pm$ 6	4.09 $\pm$ 3.62	6 $\pm$ 6	48.2 $\pm$ 15.2	1.73 $\pm$ 0.55	3.40 $\pm$ 1.24	6 (4)
H3K9me3 (25%)	HP1 $\alpha$	0.15 $\pm$ 0.02	95 $\pm$ 2	4.57 $\pm$ 3.13	5 $\pm$ 2	75.8 $\pm$ 23.0	1.10 $\pm$ 0.33	6.06 $\pm$ 1.99	6 (3)
H3K9me3 (MN)	HP1 $\alpha$	0.13 $\pm$ 0.01	78 $\pm$ 11	(1.18 $\pm$ 0.62)‡	22 $\pm$ 11	N/A §	N/A §	N/A §	3 (3)
H3K9me3 (100%)	HP1 $\alpha$ +50nM comp.	0.19 $\pm$ 0.05	94 $\pm$ 3	3.97 $\pm$ 1.31	6 $\pm$ 3	23.8 $\pm$ 2.84	3.55 $\pm$ 0.42	1.48 $\pm$ 0.43	5 (3)
H3K9me3 (100%)	HP1 $\alpha$ +250nM comp.	0.13 $\pm$ 0.02	93 $\pm$ 2	3.93 $\pm$ 1.73	7 $\pm$ 2	43.3 $\pm$ 15.8	2.07 $\pm$ 0.62	3.72 $\pm$ 1.25	3 (2)
H3K9me3 (100%)	HP1 $\alpha$ +1000nM comp.	0.11 $\pm$ 0.01	93 $\pm$ 4	2.75 $\pm$ 0.72	7 $\pm$ 4	29.3 $\pm$ 5.51	2.92 $\pm$ 0.57	3.11 $\pm$ 0.67	4 (2)
H3K9me3 (100%)	HP1 $\alpha_{cmd}$	0.33 $\pm$ 0.01	87 $\pm$ 1	3.40 $\pm$ 0.53	13 $\pm$ 1	7.45 $\pm$ 1.87	22.4 $\pm$ 0.6 #	0.13 $\pm$ 0.01	4 (2)
H3K9me3 (100%)	HP1 $\alpha$ (I163E)	0.23 $\pm$ 0.10	85 $\pm$ 7	(4.11 $\pm$ 2.83)‡	15 $\pm$ 7	N/A §	N/A §	N/A §	4 (2)
H3K9me3 (100%)	HP1 $\alpha$ (W40A)	0.10 $\pm$ 0.02	85 $\pm$ 21	(0.56 $\pm$ 0.49)‡	15 $\pm$ 21	N/A §	N/A §	N/A §	2 (2)
H3K9me3 (100%)	HP1 $\alpha$ +P3	0.33 $\pm$ 0.04	95 $\pm$ 4	4.80 $\pm$ 3.96	5 $\pm$ 4	10.5 $\pm$ 0.59	7.94 $\pm$ 0.45	7.94 $\pm$ 0.45	4 (2)
H3K9me3 (100%)	HP1 $\alpha$ +P4	0.28 $\pm$ 0.01	93 $\pm$ 4	4.45 $\pm$ 2.10	7 $\pm$ 4	19.6 $\pm$ 6.52	4.25 $\pm$ 1.41	4.25 $\pm$ 1.41	4 (3)

**Table 1 Kinetic parameters of HP1 $\alpha$  – chromatin interaction dynamics**

The percentage numbers in the brackets denote the H3K9me3 modification density. MN denotes mononucleosomes, n is the number of replicates.

\* The  $K_D$ s are calculated based on the fast kinetic phase of the dissociation process.

\*\* n indicates the number of independent HP1 $\alpha$  injections. n' indicates the number of flow cells used.

‡ Due to insufficient statistics,  $\tau_{off,2}$  is poorly defined.

§ Due to insufficient statistics we cannot accurately determine association kinetics with  $\lambda_{on} > 100$  s.

#  $k_{on}$  is calculated per molecule of HP1 $\alpha_{cmd}$

Table 1 was adapted from Kilic et al., 2015.

## 1.7. Conclusion

We developed and tested a system with surface-immobilized designer chromatin using TIRFM for detection of fluorescently labelled proteins. This enabled us to measure HP1 $\alpha$  dynamics at the seconds to milliseconds timescale. Of note, our method allows to modify all the components of the system individually, a condition rarely achieved in *in vivo* measurements.

Here, we applied the TIRF-method to test different binding models of HP1 $\alpha$  (Fig.15). We directly observed a significant impact of the H3K9me3 in HP1 $\alpha$  recruitment to chromatin. In unmodified chromatin arrays, when the histone PTM was absent, the number of binding events were heavily reduced, and so were residency times ( $\tau_{off,1}$ ). We proposed a binding model of microdissociation and rapid rebinding upon presence of multiple H3K9me3 marks in close vicinity. We gradually reduced the amount of H3K9me3-modified histones in chromatin arrays and consistently observed a decrease in residency times and an increase in association times. In measurements employing mononucleosomes reduced binding times were detected, as well. These results, together with an HP1 $\alpha$  CD mutant (W40A) showed a strong effect of the reader domain to engage HP1 $\alpha$  on chromatin and that microdissociation events with rapid rebinding heavily contribute to efficient chromatin recruitment. We

expected oligomerization of HP1 $\alpha$  at high concentrations, which would supposedly lead to a stabilized complex. We tested this hypothesis by titrating different amounts of unlabelled HP1 $\alpha$  molecules. Strikingly, we observed increased, rather than decreased, binding dynamics the more competitor HP1 $\alpha$  we added. Thus, the proposed oligomerization model, based on Swi6, was rejected<sup>45</sup>. We explain these findings, as we did not employ the previously studied yeast homolog Swi6, but the human HP1 $\alpha$  protein. As Swi6 contains an extended  $\alpha$ -helix in the CD and a lysine containing loop, which were proposed to represent an additional site of interaction, we reasoned that the structural difference between the yeast and human homolog attributes to the different binding modes<sup>45, 206</sup>. To elucidate how multivalent binding of HP1 $\alpha$  affects chromatin binding we developed an EPL-based approach to covalently link HP1 $\alpha$  as a dimer. As expected we measured increased association and dissociation kinetics, when comparing wt HP1 $\alpha$  with the covalent dimer. This underlines the importance of HP1 $\alpha$  as a multivalent chromatin reader. We further planned to test HP1 $\alpha$  dynamics in the dimeric state without covalent-linkage and synthesized a peptide **P3**, which facilitates HP1 $\alpha$ -dimerization<sup>59</sup>. Based on results from thermophoresis assays, which indicated interaction of HP1 $\alpha$  and peptide **P3**, we performed TIRF measurements using **P3** and a non-interacting peptide **P4**. In these experiments we observed dissociation kinetics comparable to HP1 $\alpha_{\text{cdm}}$  in the presence of peptide **P3**.

In summary, we successfully developed and employed TIRFM on designer chromatin to study different binding models of HP1 $\alpha$ . We showed contribution of H3K9me3 and to mediate HP1 $\alpha$ -chromatin interactions, in dependence of the available binding sites and we showed a mechanism of facilitated dissociation at high HP1 $\alpha$  concentrations. Further, using a chemical approach to covalently link HP1 $\alpha$ , we unveiled enhanced association and increased dissociation times when HP1 $\alpha$  was present as a dimer, underlining its capability to act as multivalent reader. In cells, HP1 $\alpha$  dimerization is facilitated by PxVxl/L-motif containing peptides as hSgoL1, which we tested in FRAP experiments and TIRF measurements<sup>59</sup>. Consistently, we observed increased motility in monomeric HP1 $\alpha$  states and in TIRF measurements we obtained residency times ( $\tau_{\text{off},1}$ ) that were comparable to the covalently linked HP1 $\alpha$  dimer. Together, we unveiled a highly dynamic behaviour of HP1 $\alpha$  in heterochromatin formation.

Overall, our method shed light on different binding modes of HP1 $\alpha$  and can be employed to study different protein systems on designer chromatin.

## 2. Dynamics of the chromatin silencer complex PRC2

Essential content (figures, paragraphs) of this chapter has been published in Jeongyoon Choi, Andreas L. Bachmann, Katharina Tauscher, Christian Benda, Beat Fierz and Jürg Müller, *Nature Structural and Molecular Biology*, **2017**<sup>207</sup>.

I have performed the PRC2 single molecule measurements. Other experiments including protein expression, purification and labelling, electromobility shift assays, crystal structure analysis, polarization assays and HMTase assays were done by Jeongyoon Choi, who also assisted in initial establishment of the single-molecule assay.

### 2.1. Introduction

As shown in the previous chapter, single-molecule measurements have been successfully measured using the reader protein HP1 $\alpha$ . In order to study chromatin dynamics of a protein complex involved in heterochromatin formation, we established collaboration with the laboratory of Jürg Müller (Max Planck Institute of Biochemistry). Their expertise on the biology and biochemistry of the chromatin silencer and repressive histone mark writer PRC2 and our capabilities to create designer chromatin, including H3K27me3-modified nucleosomes, enabled us to combine our skills to a powerful application of studying PRC2 on the single molecule level<sup>208</sup>. Importantly, PRC2 is a histone mark writer complex, which renders it an interesting model system for further investigations.

The core of the human protein complex PRC2 consists of a conserved set of proteins including the catalytic subunit EZH2, the H3K27me3-specific reader EED, and the additional proteins SUZ12 and RBBP4. As this assembly represents simply the core complex of PRC2, we were interested how additional subunits would influence chromatin binding of the complex. Polycomblike proteins as the human PHF1, MTF2 and PHF19 have been shown by ChIP to be important for PRC2 targeting to chromatin and stimulating its catalytic activity<sup>87-90, 209</sup>. However, the structural and mechanistic details of these processes were still unknown. Thus, we set up to shed light onto the mechanism how PHF1 assists PRC2 in chromatin binding. Preliminary results from our collaborators using EMSA indicated that PHF1 might anchor PRC2 to chromatin and render its binding mode more stable (Fig.37).

Additionally, we aimed to study PRC2-chromatin interactions using modified chromatin arrays.

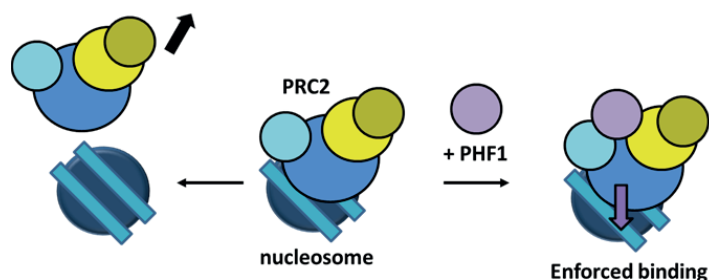


**Fig.37 Possible binding modes for PRC2 in dependence of PHF1**

PRC2 binds transiently to nucleosomes. Addition of PHF1 should intensify PRC2-binding to nucleosomes through interactions with DNA.

## 2.2. PHF1 prolongs binding of PRC2 to chromatin and DNA

### 2.2.1. Expression, purification and labelling of PRC2

To elucidate the chromatin binding mechanism of PRC2 to chromatin as a function of PHF1 we decided to employ our established single-molecule chromatin binding assay. This enables to directly observe interactions of individual PRC2 molecules with immobilized chromatin fibres and to determine if PHF1 or PHF1 mutants contribute to altered binding dynamics, which in turn might allow more efficient H3K27 methylation by PRC2.

In order to perform TIRF measurements and test chromatin binding of PRC2 and PRC2-PHF1, we required the purified and labelled PRC2 complex consisting of different subunits.

The protein complex (EZH2, EED, SUZ12 and RBBP4) was expressed by Jeongyoon Choi and purified with or without PHF1 as published in Choi et al., 2017<sup>207</sup>. To further identify the active region of PHF1, a PRC2-PHF1 mutant was created, containing only the last 5 kDa of PHF1 (AA 515-567, PHF1<sub>C</sub>), that was still stably associated with PRC2.

To detect the PRC2 complexes in single-molecule experiments, specific fluorescence labelling with a high-performance dye is required.

During our previous studies we applied EPL as a general labelling strategy for several proteins. However, EPL only works efficiently at room temperature (RT) and requires long incubation (~20h). These conditions are not suitable for all our proteins, including PRC2, which shows signs of aggregation if kept at RT for > 1 h, as we observed while handling the protein. Therefore we introduced a novel labelling method to our lab, which utilizes the *B. subtilis* Sfp phosphopantetheinyl transferase (Sfp synthase) to couple a Coenzyme A-molecule (CoA) to a short peptide tag (ybbr-tag; Fig.38)<sup>210</sup>. The ybbr-labelling system is highly similar to the ACP-tag labelling system, but compared to the ACP-tag (77 AA) the ybbr-tag consists of only 11 AA<sup>211</sup>.

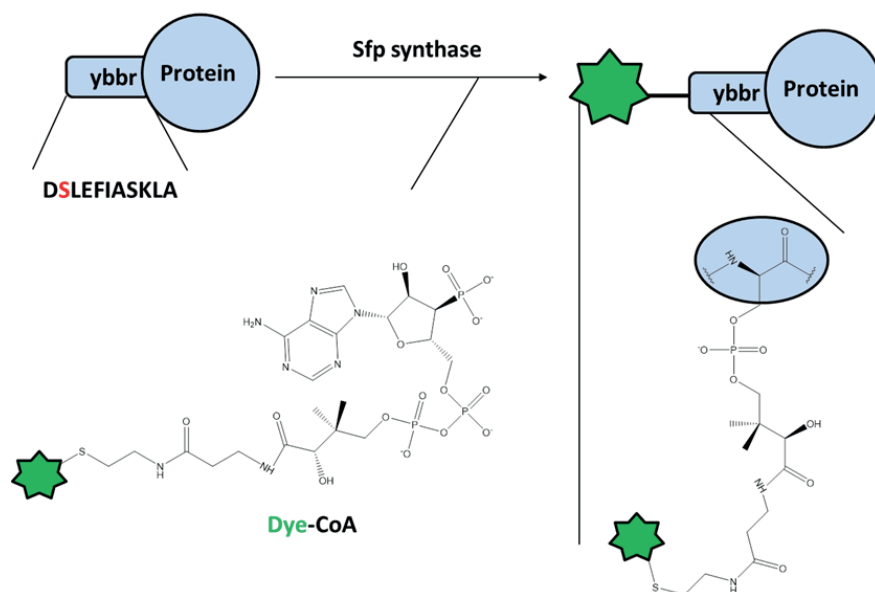


**Fig.38 Ybbr-labelling of a protein**

The protein of interest is fused to a ybbr-tag (DSLEFIASKLA). Sfp synthase is added to the protein with the fluorescently labelled substrate (Dye-CoA) and incubated for 2 h (4 °C). During this process the phosphopantetheine group of Dye-CoA is transferred to the serine of the ybbr-tag. The serine at the attachment site of the Dye-CoA is denoted with a blue oval. The green star indicates the fluorescent dye.

We selected the N-terminus of the catalytic subunit EZH2 to be subjected to ybbr-labelling using the fluorophore DY-547. All the complexes were thus expressed and purified with EZH2 containing an N-terminal ybbr-tag.

The labelling was performed at 4 °C for 2 h. We obtained the tetrameric- or pentameric, labelled PRC2 complex with a typical labelling efficiency of 53-69 % (Fig.39) <sup>207</sup>.

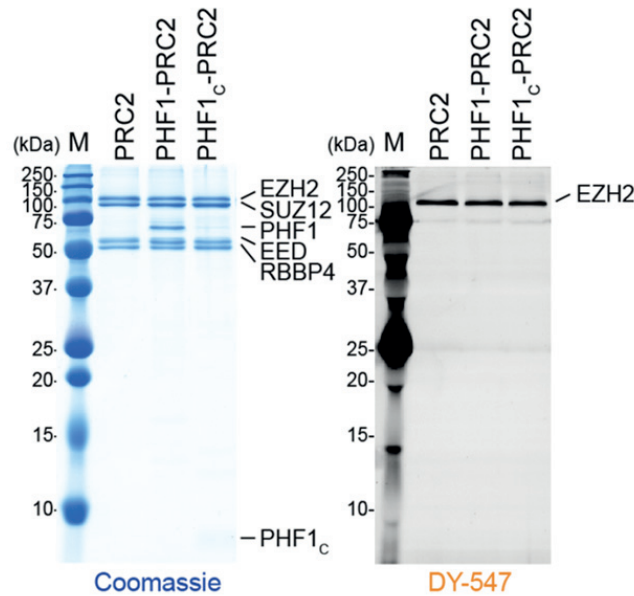


**Fig.39 Purified and fluorescently labelled PRC2 (SDS-PAGE, 13 %)**

DY-547-labelled PRC2, PHF1-PRC2 and PHF1<sub>c</sub>-PRC2 visualized using Coomassie staining (left) and 547 nm illumination to detect DY-547 emission (right). M = molecular weight marker. (PHF1<sub>c</sub> is hardly visible.) Figure was adapted from Choi et al., 2017 and was based on the work of Jeongyoon Choi.

## 2.2.2. Determining PRC2-chromatin interactions on the single-molecule scale

We performed single molecule experiments using the PRC2 complex and probed its behaviour towards unmodified chromatin (Fig.40a)<sup>207</sup>. For PRC2 imaging experiments, the flow channel was washed with low salt T50 buffer (50 mM NaCl), using an automated pump. The background level of fluorescence was recorded with both 532 nm and 640 nm excitation. Neutravidin was added to functionalize the biotin-PEG chains on the channel surface and this was followed by extensive washing with T50 buffer. Subsequently, biotinylated and Atto647N labelled chromatin arrays were flowed into the channel at a concentration of 500 pM and incubated for several minutes. The immobilization step was monitored by Atto647N emission, aiming for a coverage level of 100-200 arrays in a 25 x 50 um imaging area. Excess chromatin in solution as well as MMTV DNA and associated nucleosomes were removed by a washing step and the buffer exchanged to imaging buffer 5 (IB5, see “IV, 2.15. TIRF imaging”) engineered to maintain PRC2 and the fluorophores stable during measurements. PRC2 dilutions in imaging buffer 5 were freshly prepared from a 100 nM stock and injected into the channel. Imaging of PRC2 binding dynamics was performed using 532 nm excitation for 10'000 frames. Every 200 frames, the excitation was switched to 640 nm for one frame to record the positions of the chromatin arrays. These frames were used in data analysis to localize array positions and correct for stage drift (Fig.40b). Once

immobilized, chromatin arrays were used for measurements for maximal one hour, to avoid disintegration of the chromatin. During measurements a flow rate of 80  $\mu\text{l}/\text{min}$  was applied.

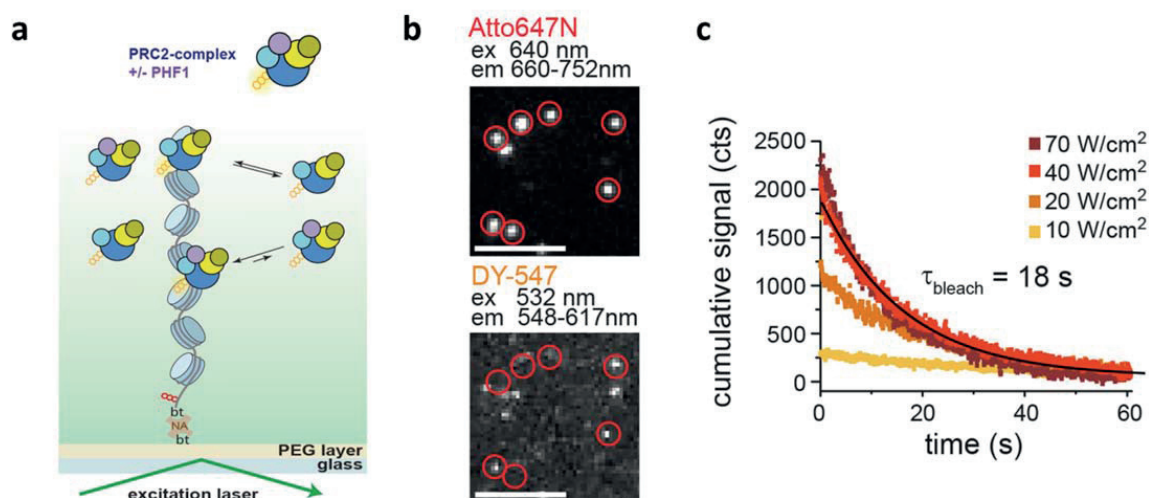


**Fig.40 Monitoring PRC2 binding towards chromatin on the single molecule level**

**a)** Scheme of the experiment: DY-547-labelled (yellow) PRC2 interacts with immobilized chromatin arrays (containing a red fluorophore), while the dynamic interactions are detected by TIRFM. Addition of PHF1 prolongs binding of PRC2. **b)** TIRF images showing chromatin positions detected in the far-red channel (top) and detecting PRC2 interaction dynamics in the green-orange channel (bottom). **c)** Photobleaching kinetics of DY-547-labelled PRC2 during laser irradiation at different intensities (10  $\text{W}/\text{cm}^2$ , 20  $\text{W}/\text{cm}^2$ , 40  $\text{W}/\text{cm}^2$  and 70  $\text{W}/\text{cm}^2$ ). At 40  $\text{W}/\text{cm}^2$  (experimental conditions) the fluorophore bleaching time constant ( $\tau_{\text{bleach}}$ ) is 18 s. Figure was adapted from Choi et al., 2017.

From binding experiments using 1-2 nM PRC2 and unmodified chromatin we generated cumulative histograms (movies were analysed as described in “IV Material and Methods, 2.15.3. TIRF data analysis” using formulas (4), (5), (6) on page 51 and formula (10)<sup>195</sup>, as annotated in Table 2) and dissociation times were fitted using a double-exponential decay function to obtain two residence times ( $\tau_{\text{off},1}$  and  $\tau_{\text{off},2}$ ). Association times were fitted using a single exponential decay function, which rendered an apparent association time constant ( $\lambda_{\text{on}}$ ).

For all measurements, light intensities of 40  $\text{W}/\text{cm}^2$  were employed for 532 nm and 20  $\text{mW}/\text{cm}^2$  for 640 nm. Photobleaching of DY-547 was compensated by applying bleaching correction: The labelled protein was immobilized on flow channels in imaging buffer 5 and bleaching rates at different laser intensities were measured. To correct for photobleaching, obtained histograms for dissociation times were divided by the bleaching histogram to obtain the final values (Fig.40c):



*Bleaching correction:*

$$C_{corr}(t) = \frac{C_{exp}(t)}{C_{bleach}(t)} \quad (9)$$

$C_{corr}(t)$  = bleaching corrected cumulative histogram from the experiment

$C_{exp}(t)$  = Cumulative histogram of individual experiment

$C_{bleach}(t)$  = Cumulative histogram of bleaching experiment

Since the cumulative bleaching histogram determines the bleaching rate under measuring conditions, formula (9) can be used to correct the experimental data: Longer events, which are more prone to bleaching over time, are corrected to a stronger extent than short events, based on the experimentally determined values from  $C_{bleach}(t)$ . Consistently, in measurements containing only extremely short events, the residency times upon bleaching correction are marginally affected. For further background information see also Teves et al., 2016<sup>212</sup>.

Measurements of PRC2 towards unmodified chromatin arrays revealed residence times in the multisecond time-scale ( $\tau_{off,1} = 0.29 \text{ s} \pm 0.03 \text{ s}$  and  $\tau_{off,2} = 2.28 \text{ s} \pm 0.44 \text{ s}$ ). When we added the pentameric complex, including full-length PHF1, binding events of PHF1-PRC2 temporally increased ( $\tau_{off,1} = 0.12 \text{ s} \pm 0.08 \text{ s}$  and  $\tau_{off,2} = 6.48 \text{ s} \pm 0.52 \text{ s}$ ) (Fig.41a)<sup>207</sup>. The double exponential fit yielded two residency times. The short phase was attributed to non-specific interactions with chromatin and therefore was not altered upon addition of PHF1<sup>213</sup>. The long phase however increased significantly and represents specific interactions with chromatin (Fig.41b). We next wondered whether C-terminal domains, including the last 5 kDa, of PHF1 were responsible for the observed effect. Thus, we repeated the measurements using pentameric PHF1<sub>C</sub>-PRC2 and received residency times that compared to the PRC2 condition ( $\tau_{off,1} = 0.22 \text{ s} \pm 0.05 \text{ s}$  and  $\tau_{off,2} = 2.86 \text{ s} \pm 0.07 \text{ s}$ ) (Fig.41c). Interestingly, the apparent association time constants were not significantly different, which attributes the effect of PHF1 to more efficient anchoring of PRC2 to chromatin. As interactions of PRC2 to chromatin are expected linked to histone and DNA interactions, we performed binding experiments using naked 177 bp-long double-stranded (ds) 601 DNA fragments. On the 601-DNA, all the three complexes again showed biexponential dissociation kinetics with a contribution of 30-56 % of long lasting binding events (Fig.41d). Interestingly, the long-lasting residence times of all three complexes on 601-DNA were increased almost two-fold compared to those observed on 12-mer nucleosome arrays, and, again, PHF1-PRC2 showed a significantly longer residency time than PRC2 and PHF1<sub>C</sub>-PRC2 (PRC2:  $\tau_{off,2} = 4.45 \text{ s} \pm 1.90 \text{ s}$ ; PHF1-PRC2:  $\tau_{off,2} = 10.38 \text{ s} \pm 2.46 \text{ s}$ ; PHF1<sub>C</sub>-PRC2:  $\tau_{off,2} = 6.83 \text{ s} \pm 1.63 \text{ s}$ ) (Fig.41e).



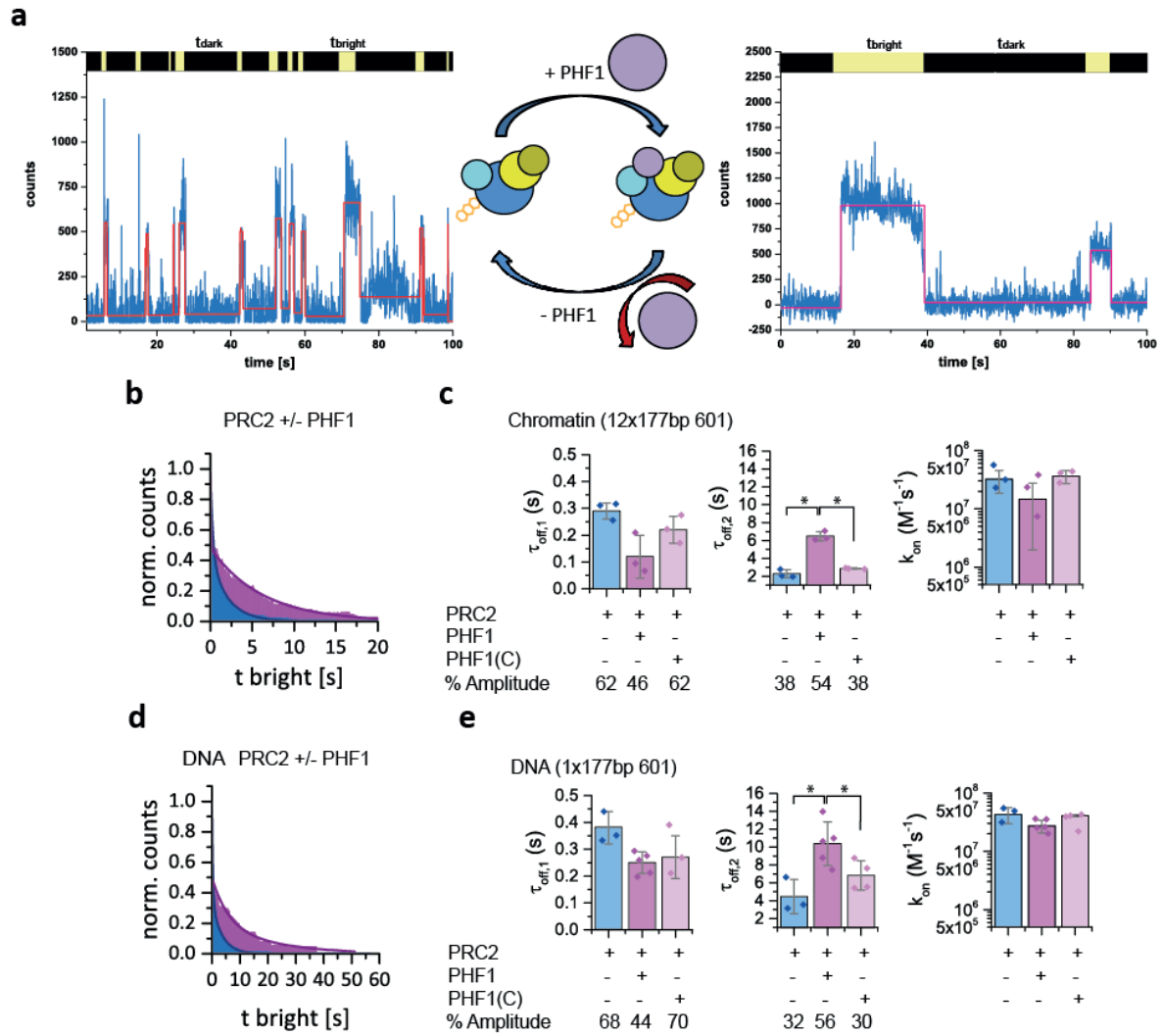


**Fig.41 Chromatin and DNA TIRF measurements unveil binding of PRC2 or prolonged binding of PHF1-PRC2**

**a)** Typical time trace of fluorescence intensity of PRC2 (left) and PHF1-PRC2 (right) binding events on a single chromatin array detected by DY-547 emission. The trace is fitted by a step function (red), and  $t_{\text{dark}}$  and  $t_{\text{bright}}$  were determined by a thresholding algorithm. **b)** Cumulative histograms of PRC2 (blue) and PHF1-PRC2 (violet) binding intervals on chromatin arrays for 5'000 frames, 50 ms per frame, fitted by biexponential functions (solid line). **c)** Time constants of the fast ( $\tau_{\text{off},1}$ ) and slow ( $\tau_{\text{off},2}$ ) dissociation process of indicated PRC2 complexes from chromatin arrays. Symbols show individual experimental results ( $n = 3$  independent experiments for all PRC2 complexes); error bars: standard deviation;  $*P < 0.05$ , two-tailed Student's t-test). **d)** Cumulative histograms of PRC2 (blue) and PHF1-PRC2 (violet) binding intervals on 601-DNA template for 5'000 frames, 50 ms per frame, fitted by biexponential functions (solid line). **e)** Time constants of the fast ( $\tau_{\text{off},1}$ ) and slow ( $\tau_{\text{off},2}$ ) dissociation process of indicated PRC2 complexes on 601-DNA templates. Symbols show individual experimental results ( $n = 3$  independent experiments for PRC2,  $n = 5$  independent experiments for PHF1-PRC2,  $n = 4$  independent experiments for PHF1<sub>C</sub>-PRC2); error bars: standard deviation;  $*P < 0.05$ , two-tailed Student's t-test). Figure was adapted from Choi et al., 2017.

Together, these experiments show that PRC2-chromatin interactions are mediated to a large extent by PRC2-DNA interactions. Additionally, single molecule analysis of the

different complexes unveiled a specific contribution to extended dwell times of PRC2 on DNA by the N-terminal portion of PHF1.

Although TIRF imaging analysis yielded exact residence time information, uncertainties in the on rate-constants precluded an exact determination of equilibrium affinities. Complementary ensemble measurements were performed by Jeongyoon Choi to quantify the binding affinities of the different PRC2 complexes to nucleosomes and dsDNA. In a first set of experiments, the binding of unlabelled PRC2, PHF1-PRC2 and PHF1<sub>C</sub>-PRC2 to reconstituted recombinant mononucleosomes was determined using EMSA.

EMSA shows an upward shift of the labelled DNA/nucleosome band on an agarose gel in dependence of the concentration of the added protein, if the protein of interest binds to DNA/nucleosomes. At high protein concentrations the DNA/nucleosome is tightly interacting with the protein of interest and thus the DNA/nucleosome moves more slowly through the agarose gel.

Densitometry analysis of the fluorescein (Flc; attached to the 215 bp DNA piece) signal in the EMSA, allowing quantification of the observed band, showed that the three complexes bound to mononucleosomes with midnanomolar affinities (PRC2,  $K_d = 163 \text{ nM} \pm 13 \text{ nM}$ ; PHF1-PRC2,  $K_d = 66 \text{ nM} \pm 4 \text{ nM}$ ; PHF1<sub>C</sub>-PRC2,  $K_d = 211 \text{ nM} \pm 9 \text{ nM}$ ) (Fig.42a)<sup>207</sup>. Of note, PHF1-PRC2 bound to the mononucleosomes with two- to three-fold higher affinity compared to PRC2 and PHF1<sub>C</sub>-PRC2.

Next, EMSA was carried out to analyse the binding of PRC2, PHF1-PRC2 and PHF1<sub>C</sub>-PRC2 to 30 bp-long dsDNA (PRE 11L; performed as published in Choi et al., 2017<sup>207</sup>). The quantification by densitometry showed that each of the three complexes bound to this DNA probe with midnanomolar affinity (PRC2,  $K_d = 64 \text{ nM} \pm 4 \text{ nM}$ ; PHF1-PRC2,  $K_d = 30 \text{ nM} \pm 3 \text{ nM}$ ; PHF1<sub>C</sub>-PRC2,  $K_d = 49 \text{ nM} \pm 4 \text{ nM}$ ) (Fig.42b). Consistent with the previous TIRF experiments, PRC2 complexes bound to DNA with about two- to three-fold higher affinity than to mononucleosomes. Importantly, comparison of binding by the three complexes unveiled that PHF1-PRC2 also bound dsDNA with two- to three-fold higher affinity than did PRC2 and PHF1<sub>C</sub>-PRC2.

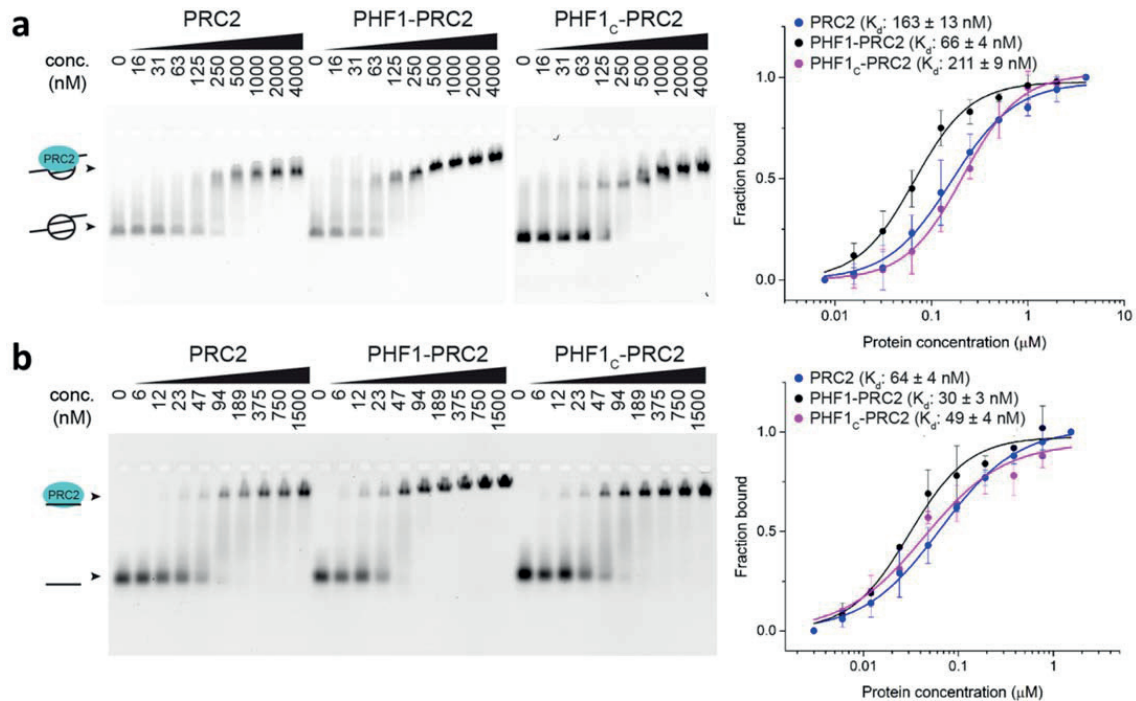


**Fig.42 High-affinity binding of PRC2 to mononucleosomes and DNA is enhanced by PHF1**

**a)** Left, binding reactions with the indicated concentrations of PRC2, PHF1-PRC2 or PHF1<sub>c</sub>-PRC2 and 45 nM Flc-labelled mononucleosomes, analysed by EMSA on 1.2 % agarose gels. Right, quantitative analysis of EMSA data by densitometry of Flc signals from independent experiments ( $n = 3$ ); error bars, standard deviation. **b)** Left, binding reactions as in **a)** but with 45 nM Flc-labelled PRE 11L dsDNA as probe. Right, quantitative analysis of EMSA results, like in **a)**. Note that because the measured  $K_d$  is rather similar to the probe concentration, it is possible that the reported apparent  $K_d$  values may underestimate the actual affinities. Figure was adapted from Choi et al., 2017 and was based on the work of Jeongyoon Choi.

We concluded that PRC2 complexes bind to dsDNA with midnanomolar affinity and we support the hypothesis that the N-terminal part of PHF1 directly contributes to DNA binding by PHF1-PRC2.

### 2.3. A winged-helix domain of PHF1 is essential for PRC2-chromatin interactions

The result that PHF1 assists binding of PRC2 to DNA and chromatin directly supported findings from solving the X-ray crystal structure of a Pcl fragment, performed by Jeongyoon Choi in the Müller laboratory. Interestingly, PHF1 and its paralogs MTF2 and PHF19, as well as *Drosophila* Pcl, all share a common domain organization (Fig.43a)<sup>207</sup>. Previous studies reported the tudor domains of Pcl, PHF1 and PHF19<sup>214-217</sup>. Based on the hypothesis that the DNA-interacting region of PHF1 might be located in the previously uncharacterized region C-terminal to the tudor domain, and through structure prediction (HHpred<sup>218</sup>), the conserved sequence downstream of the second PHD finger domain (PHD2) was identified as a potential

WH domain (Fig.43a). For further investigations a fragment of *Drosophila* Pcl (AA 419-694) was crystallized and the structure solved by our collaborators (Fig.43b) <sup>207</sup>. In the crystal structure of Pcl<sub>PHD2-WH</sub>, the PHD2-WH arrangement forms a single compact domain where the two folds tightly pack against each other through an interface that is formed by conserved residues in the PHD2 and WH domains (Fig.43c).

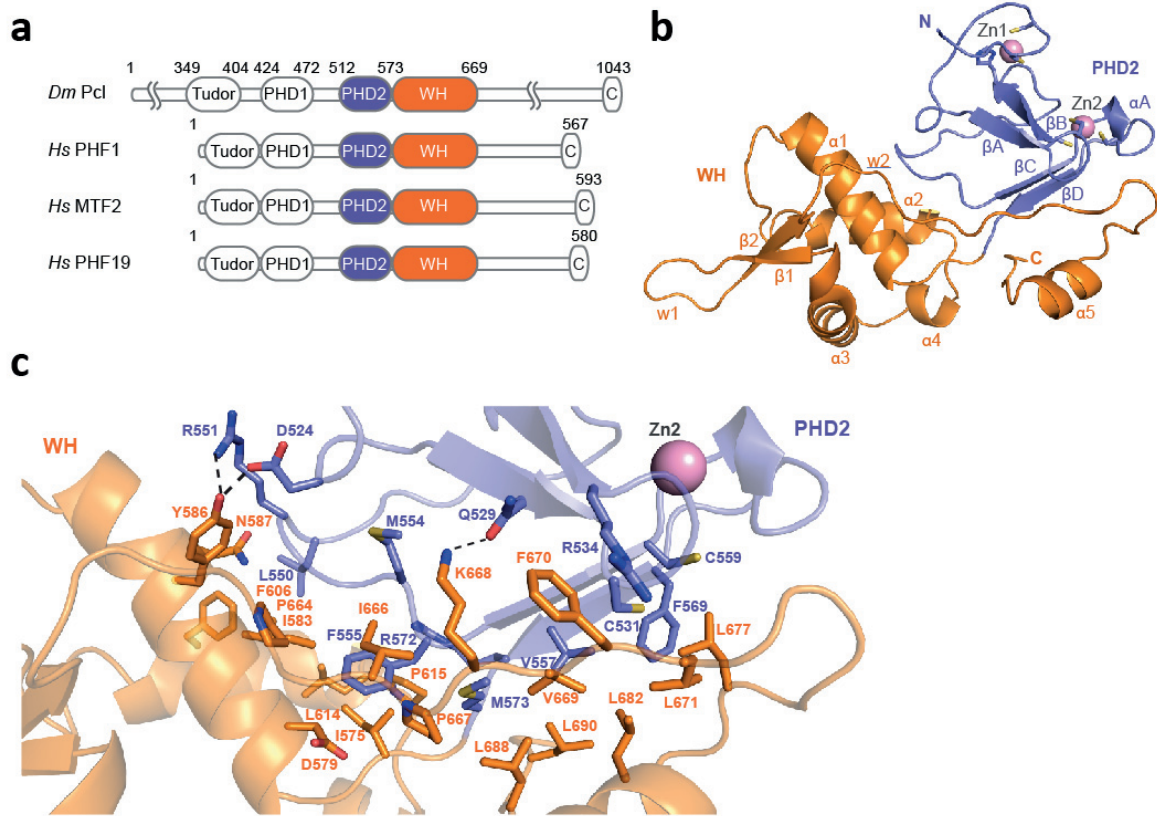


**Fig.43 Crystal structure of Pcl<sub>PHD2-WH</sub>**

**a)** Domain architecture of *Drosophila* (Dm) Pcl and the three human (Hs) orthologs PHF1, MTF2 and PHF19 with conserved tudor, plant homeodomain (PHD1 and PHD2), winged-helix (WH) and C-terminal (C) domains. **b)** Overall structure of Pcl<sub>PHD2-WH</sub>, colored as in **a**. Zn atoms (Zn1 and Zn2) in the PHD2 fold are shown as spheres. Secondary structure elements ( $\alpha$ ,  $\alpha$ -helix and  $\beta$ ,  $\beta$ -strand) are indicated; w1 and w2 refer to the typical loops of WH domains. **c)** Zoom-in view of the interface between PHD2 and WH domain; residues involved in the interaction are shown in stick representation; salt bridges are shown as dotted lines. Figure was adapted from Choi et al., 2017 and was based on the work of Jeongyoon Choi.

Superposition of the Pcl<sub>PHD2-WH</sub> structure onto the structure of the DNA-binding domain of the transcription factor forkhead box protein O1 (FOXO1), bound to its cognate DBE1 DNA element, yields a model of Pcl-DNA binding. In this model, the Pcl WH domain contacts DNA through interaction of the  $\alpha$ 3 helix with the major groove and wing 1 with the phosphate backbone (Fig.44a) <sup>207, 219</sup>. To test this model, DNA-binding activity was tested between wt Pcl<sub>PHD2-WH</sub> and mutants in the helix  $\alpha$ 3 (R631A, Q634A, K637A; Pcl<sub>PHD2-WH</sub><sup>H>A</sup>) or in

wing 1 (R650A, K651A; Pcl<sub>PHD2-WH</sub><sup>W>A</sup>) and the combination of both mutants (Pcl<sub>PHD2-WH</sub><sup>WH>A</sup>) (Fig.44a and 44b) .

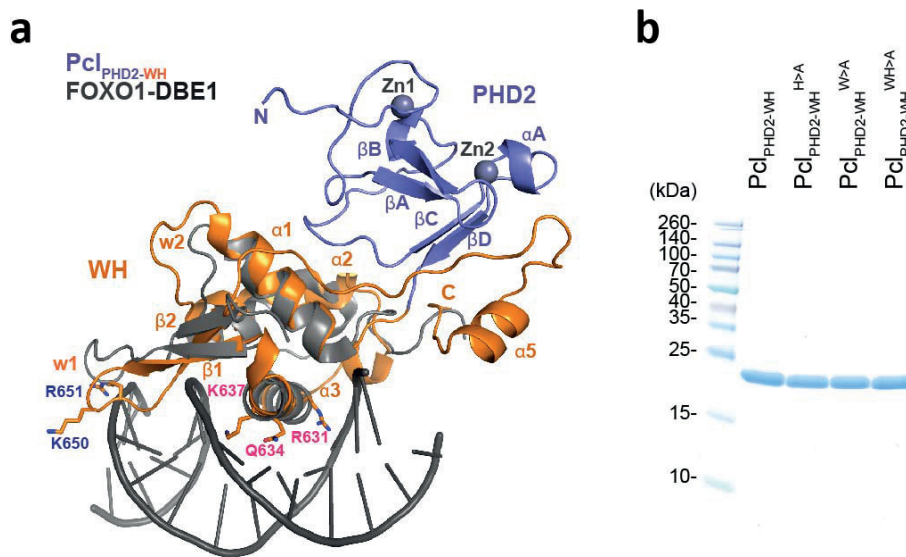


**Fig.44 Testing mutants of Pcl<sub>PHD2-WH</sub>**

**a)** Superposition of the Pcl<sub>PHD2-WH</sub> structure (violet-blue and orange) onto the FOXO1 structure in complex with the DBE1 DNA element (Brent et al., 2008) (dark gray, PDB: 3CO6). The amino acid residues that were mutated in Pcl<sub>PHD2-WH</sub><sup>H>A</sup> and Pcl<sub>PHD2-WH</sub><sup>W>A</sup> are shown in stick representation and labelled in magenta and violet-blue, respectively; in Pcl<sub>PHD2-WH</sub><sup>WH>A</sup>, all five residues were mutated. **b)** Purified wild-type and mutant Pcl<sub>PHD2-WH</sub> proteins used for DNA-binding assays, analysed on a 15 % SDS-PAGE gel and visualized using Coomassie staining. Figure was adapted from Choi et al., 2017 and was based on the work of Jeongyoon Choi.

In fluorescence polarisation assays (performed as published<sup>207</sup>) with the 30 bp PRE 11L DNA probe used previously, wt Pcl<sub>PHD2-WH</sub> bound to this probe with a K<sub>d</sub> value of 9.7 uM ± 0.2 uM, whereas all three mutant proteins showed greatly reduced DNA-binding activity (Fig.45a)<sup>207</sup>. We concluded that Pcl binds to its DNA via its WH domain. Moreover, the mutational analysis suggests that this binding occurs through interaction of the Pcl WH α3-helix with the major groove and of wing 1 with the phosphate backbone, as in the case of other WH domains<sup>219, 220</sup>.

To compare these results to the human model, DNA-binding activity of human PHF1 was tested. PHF1<sub>165-363</sub>, called PHF1<sub>PHD2-WH</sub>, also bound to DNA with midnanomolar affinity (Fig.45b). Another mutant (PHF1<sub>PHD2-WH</sub><sup>W>A</sup>) was generated by substituting the residues K323 and K324 in wing 1 with alanine (Fig.43a). Like Pcl<sub>PHD2-WH</sub><sup>W>A</sup>, the PHF1<sub>PHD2-WH</sub><sup>W>A</sup> protein showed drastically reduced DNA-binding activity (Fig.45b). PHF1 therefore also binds to DNA via its WH domain.



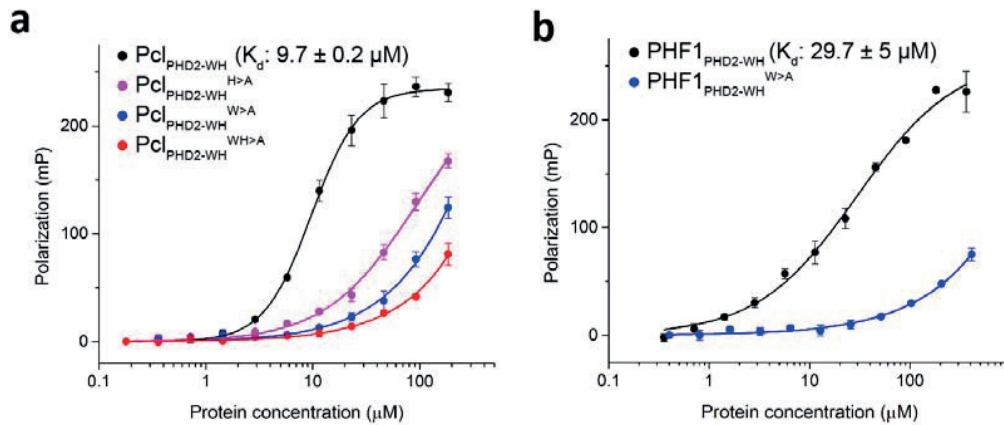


**Fig.45 The Pcl and PHF1 domains bind dsDNA**

**a)** Binding of wt and mutant Pcl<sub>PHD2-WH</sub> proteins to Flc-labelled PRE 11L DNA (45 nM), measured by fluorescence polarisation assays.  $n = 3$ , error bars: standard deviation; curve fitting was performed using the Hill function;  $K_d$  of interactions is indicated for wt Pcl<sub>PHD2-WH</sub>. **b)** Binding of wt and mutant PHF1<sub>PHD2-WH</sub> proteins to Flc-labelled PRE 11L DNA (45 nM), measured by fluorescence polarisation assays.  $n = 3$ , error bars: standard deviation; curve fitting was performed using the Hill function;  $K_d$  of interactions is indicated for wt PHF1<sub>PHD2-WH</sub>. Figure was adapted from Choi et al., 2017 and was based on the work of Jeongyoon Choi.

To characterize PHF1-PRC2 binding, mediated by the WH domain, in single molecule measurements, DY-547 labelled PHF1<sup>WH>E</sup>-PRC2 was generated, in which residues R304, S307, N310, K323 and K324 had been mutated to glutamate (Fig.46)<sup>207</sup>.

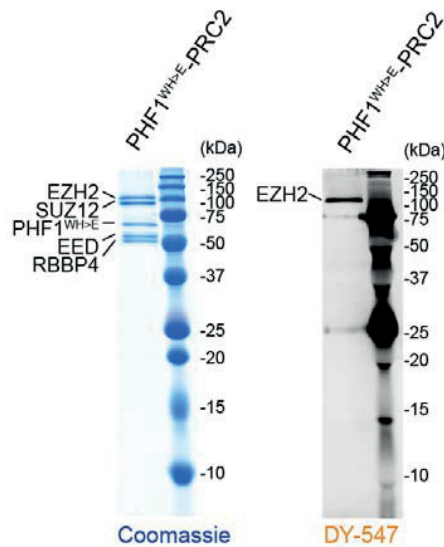


**Fig.46 Generation of DY-547 labelled PHF1<sup>WH>E</sup>-PRC2**

Analysis of the DY-547 labelled PHF1<sup>WH>E</sup>-PRC2, like in Figure 39. Figure was adapted from Choi et al., 2017 and was based on the work of Jeongyoon Choi.

We subjected the PHF1<sup>WH>E</sup>-PRC2 mutant protein to single molecule measurements, as described previously for other PRC2-complexes, and compared its binding behaviour to those of wt PHF1-PRC2 using the 12x601 nucleosome chromatin arrays. Supporting our hypothesis we observed reduced residence times ( $\tau_{\text{off},2}$ ) for PHF1<sup>WH>E</sup>-PRC2 compared to PHF1-PRC2 in measurements using chromatin arrays (Fig.47a) <sup>207</sup>. Consistently, measurements using naked DNA also showed a reduction of residency time for PHF1<sup>WH>E</sup>-PRC2 (Fig.47b). Additionally, we reconstituted mononucleosomes using the 1x177 bp 601 DNA template and measured binding kinetics for all the four complexes. Despite trends appearing similarly, we did not reach statistical significance in these measurements, due to high variation in the PHF1-PRC2 measurements (Table 2).

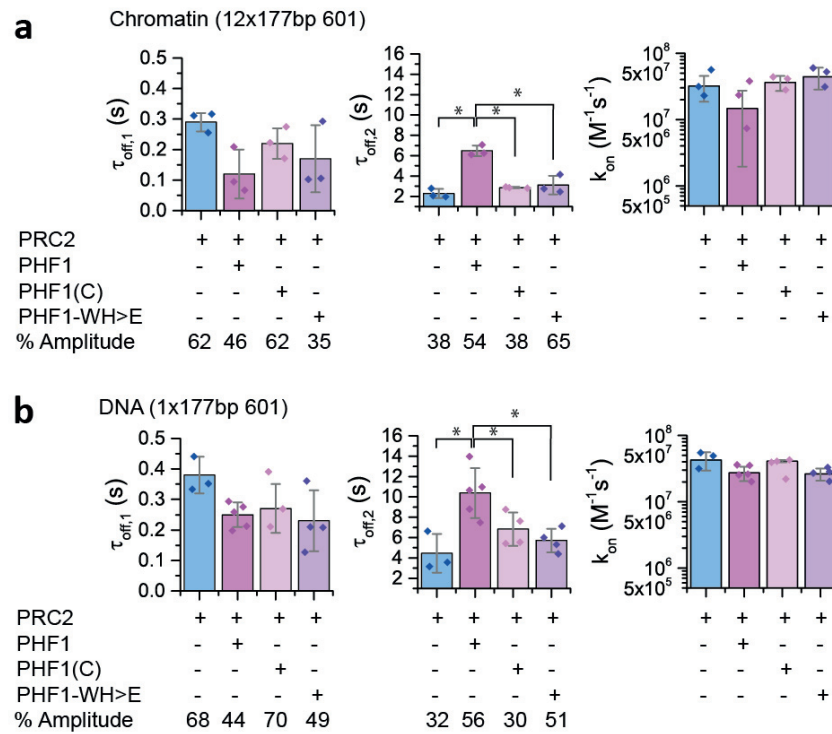


**Fig.47 Dissociation and association kinetics of PRC2, PHF1-PRC2, PHF1<sub>c</sub>-PRC2 and PHF1<sup>WH>E</sup>-PRC2 towards chromatin and naked DNA**

**a)** Time constants of the fast ( $\tau_{\text{off},1}$ ) and slow ( $\tau_{\text{off},2}$ ) dissociation process of indicated PRC2 complexes on chromatin arrays. Symbols show individual experimental results ( $n = 3$  independent experiments for all four PRC2 complexes); error bars: standard deviation; \* $P < 0.05$ , two-tailed Student's t-test). **b)** Time constants of the fast ( $\tau_{\text{off},1}$ ) and slow ( $\tau_{\text{off},2}$ ) dissociation process of indicated PRC2 complexes on 601-DNA templates. Symbols show individual experimental results ( $n = 3$  independent experiments for PRC2,  $n = 5$  independent experiments for PHF1-PRC2,  $n = 4$  independent experiments for PHF1<sub>c</sub>-PRC2 and PHF1<sup>WH>E</sup>-PRC2); error bars: standard deviation; \* $P < 0.05$ , two-tailed Student's t-test). Figure was adapted from Choi et al., 2017.

Together, these results in all three binding substrates have shown comparable residence times ( $\tau_{\text{off},2}$ ) for PRC2, PHF1<sub>c</sub>-PRC2 and PHF1<sup>WH>E</sup>-PRC2, when the WH motif was absent or disrupted, while intact PHF1-PRC2 showed prolonged residence times of the long-

phase. This suggests a crucial role for the WH motif of PHF1 in prolongation of PRC2 binding to a DNA substrate.

Next, we wanted to elucidate whether DNA binding by PHF1 might also account for the enhanced HMTase activity of PHF1-PRC2 as compared to PRC2<sup>88, 89</sup>. HMTase assays were performed on recombinant mononucleosomes assembled on a 215 bp-long 601-DNA fragment with purified PRC2, PHF1-PRC2, PHF1<sup>WH>A</sup>-PRC2 and PHF1<sup>WH>E</sup>-PRC2 (method as published in Choi et al., 2017<sup>207</sup>). In PHF1<sup>WH>A</sup>-PRC2, the PHF1 residues R304, S307, N310, K323, K324 were all mutated to alanine, and in PHF1<sup>WH>E</sup>-PRC2 the same residues were mutated to glutamate. In all cases, the HMTase reactions were evaluated by western blot analysis using antibodies against H3K27me1, H3K27me2 and H3K27me3. Experiments monitoring enzyme-concentration dependency (Fig.48a) and reaction progression over time (Fig.48b) showed that the wt PHF1-PRC2 complex possesses nearly three-fold higher HMTase activity compared to PRC2 (Fig.48a and 48b, compare lanes 5-7 to lanes 2-4), consistent with earlier reports<sup>88, 89, 207</sup>. In contrast, PHF1<sup>WH>E</sup>-PRC2 showed the same reduced level of HMTase activity, like PRC2 (Fig.48a and 48b, compare lanes 11-13 to lanes 5-7). PHF1<sup>WH>A</sup>-PRC2, containing the less-severe alanine mutations, showed a less drastic reduction of HMTase activity than did PHF1<sup>WH>E</sup>-PRC2 (Fig.48a and 48b, compare lanes 8-10 to lanes 5-7).



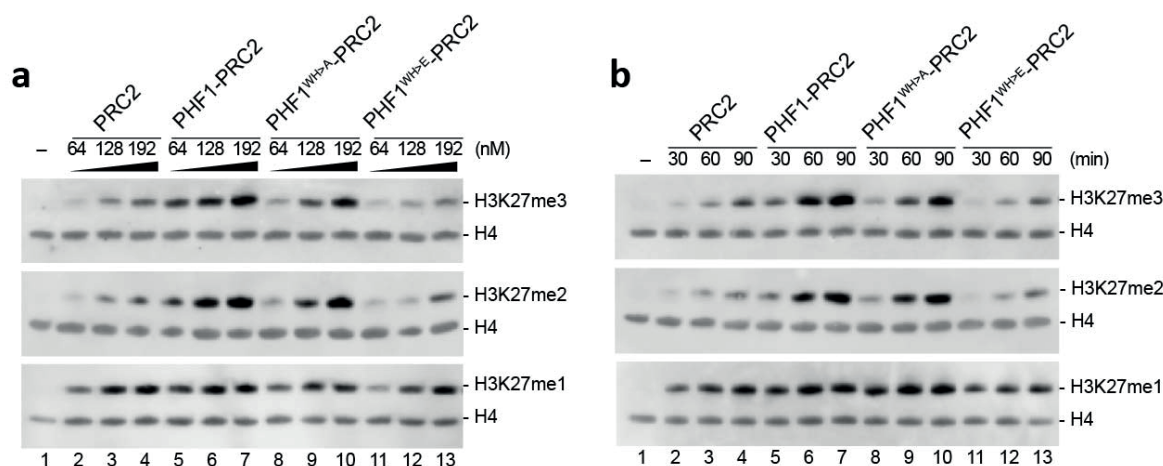


**Fig.48 DNA binding of PRC2 by PHF1 permits more efficient H3K27 methylation**

**a)** Western blot analysis of H3K27me1, H3K27me2 and H3K27me3 formation in HMTase reactions with the indicated concentrations of the different PRC2 complexes on mononucleosomes (446nM); reaction time was 90min in all cases. Histone H4 signal served as a loading control. **b)** Western blot analysis of HMTase reactions as in **a)**, with a fixed amount of the indicated PRC2 complexes (192nM) on mononucleosomes (446nM), but analysed after the indicated reaction times. Figure was adapted from Choi et al., 2017 and was based on the work of Jeongyoon Choi.

These indications led us to conclude that PHF1 enables PRC2 to methylate H3K27 more efficiently by prolonging the residence time of PRC2 on chromatin.

## 2.4. Defined chromatin modifications prolong PRC2 binding events

To understand the contribution of different histone marks towards PRC2 binding, we extended our PRC2 binding studies towards chromatin containing the H3K27me3, H3K36me3 or the oncogenic mutation mark H3K27M<sup>221</sup>. The H3K36me3 mark has been associated with an antagonizing effect to the repressive H3K27me3 mark, which is installed by PRC2, and has been shown to be tightly bound by PHF1<sup>216, 222</sup>. Histone octamers containing H3K27me3, H3K27M and H3K36me3 were used to assemble chromatin arrays, which we subjected to TIRF measurements.

We hypothesized that the H3K27me3 enhances residency times of bound PRC2 molecules, based on the reader activity of EED<sup>81</sup>. We expected the oncogenic H3K27M mark to anchor PRC2 to chromatin, and thus drastically prolong residency times<sup>80, 221</sup>. In contrast, the H3K36me3 mark was expected to show a decrease in PRC2 residency times, as it represents a mark of euchromatin<sup>216</sup>.

In this experiment, although lowered signal intensity, caused by low laser light, we observed significant prolongation of PRC2-chromatin binding with all three of the tested modifications (Fig.49). The non-modified condition of PRC2 binding to chromatin was comparable to the previous experiment ( $\tau_{\text{off},2} = 2.28 \text{ s} \pm 0.44 \text{ s}$ , here:  $2.67 \text{ s} \pm 0.34 \text{ s}$ ; Fig.47). The difference between the residency time  $\tau_{\text{off},2}$  for H3K27M and H3K27me3 was not

significant. We realized that this was not surprising, as the cofactor SAM would be required to effectively tighten PRC2 binding to H3K27M<sup>80</sup>. The observed prolonged binding towards the H3K36me3 mark was unexpected. Strikingly, also the microscopic association rate constant ( $k_{on}$ ) was increased ( $\lambda_{on}$  was decreased), which renders a 10-fold difference in the  $K_D$  value ( $K_D$  non-modified: 20 nM,  $K_D$  H3K36me3: 1.8nM). However, despite the contradictory role of the H3K36me3 mark, this makes sense knowing that H3K27me1, which can be installed by PRC2 and marks actively transcribed genes, positively correlates with H3K36me3<sup>223</sup>. We note that H3K36me3 has been associated with lowered activity of PRC2, but this might directly reflect the requirement to establish monomethylation of H3K27, which subsequently leads to gene activation<sup>216, 223</sup>. In summary, we observed prolonged binding of PRC2 on all the tested histone modification marks.

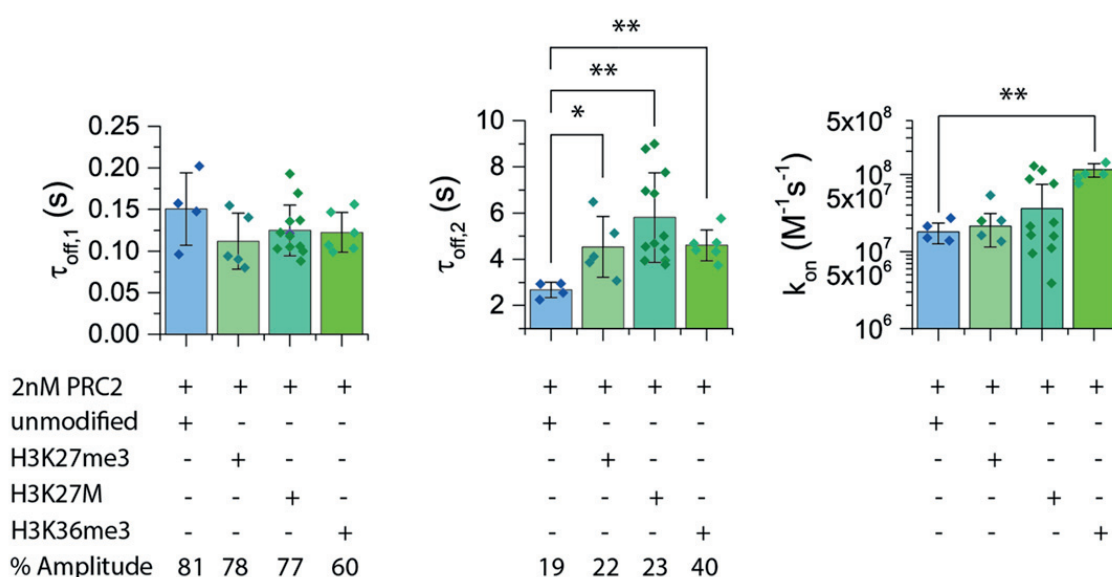


**Fig.49 H3K27me3-, H3K27M- and H3K36me3-modified chromatin fibres prolong PRC2 residency time**

Time constants of the fast ( $\tau_{off,1}$ ) and slow ( $\tau_{off,2}$ ) dissociation process of the core PRC2 complex on modified chromatin arrays. Symbols show individual experimental results ( $n = 4$  independent experiments for all four unmodified chromatin,  $n = 5$  for H3K27me3,  $n = 12$  for H3K27M,  $n = 6$  for H3K36me3); error bars: standard deviation; \* $P < 0.05$ , two-tailed Student's t-test).

A summary of all the measured kinetic values based on TIRF measurements can be found in Table 2<sup>195, 207</sup>.

Experimental system		Dissociation kinetics*				Association kinetics		Replicate
Binding substrates	Protein	$\tau_{off,1}(s)$	%A1	$\tau_{off,2}(s)$	%A2	$\lambda_{on}(s)$	$k_{on}^{**}$ ( $M^{-1}s^{-1}$ ) $\times 10^6$	n
Chromatin arrays unmodified	PRC2	0.29±0.03	62±6	2.28±0.44	38±6	15.53±6.48	32.05±13.44	3
Chromatin arrays unmodified	PHF1-PRC2	0.12±0.08	46±4	6.48±0.52	54±4	34.21±29.66	14.62±12.67	3
Chromatin arrays unmodified	PHF1 <sub>C</sub> -PRC2	0.22±0.05	62±4	2.86±0.07	38±4	13.82±3.55	36.19±9.29	3
Chromatin arrays unmodified	PHF1 <sup>WHSE</sup> -PRC2	0.17±0.11	35±11	3.11±0.91	65±11	22.59±8.22	44.27±16.0	3
Chromatin arrays unmodified (#2)	PRC2	0.15±0.04	81±5	2.67±0.34	19±5	27.78±8.27	18.00±5.36	4
Chromatin arrays H3K27me3	PRC2	0.11±0.03	78±7	4.54±1.31	22±7	23.37±10.78	21.39±9.87	5
Chromatin arrays H3K27M	PRC2	0.12±0.03	77±10	5.81±1.95	23±10	31.98±34.33	35.95±38.60	12
Chromatin arrays H3K36me3	PRC2	0.12±0.02	60±8	4.6±0.67	40±8	5.05±1.01	115.98±23.21	6
Mononucleosomes unmodified	PRC2	0.30±0.10	75±10	3.53±0.90	25±10	17.68±7.42	28.28±11.87	4
Mononucleosomes unmodified	PHF1-PRC2	0.16±0.11	46±15	9.25±4.87	54±15	37.03±10.77	13.5±3.93	5
Mononucleosomes unmodified	PHF1 <sub>C</sub> -PRC2	0.22±0.31	72±7	4.17±1.46	28±7	25.28±21.08	19.78±16.49	3
Mononucleosomes unmodified	PHF1 <sup>WHSE</sup> -PRC2	0.15±0.11	50±19	5.34±0.13	50±19	20.48±5.30	24.41±6.31	4
601-DNA	PRC2	0.38±0.06	68±5	4.45±1.90	32±5	11.72±3.63	42.67±13.24	3
601-DNA	PHF1-PRC2	0.25±0.04	44±8	10.38±2.46	56±8	18.39±4.55	27.19±6.72	5
601-DNA	PHF1 <sub>C</sub> -PRC2	0.27±0.08	70±5	6.83±1.63	30±5	12.21±0.51	40.95±1.71	5
601-DNA	PHF1 <sup>WHSE</sup> -PRC2	0.23±0.10	49±11	5.71±1.15	51±11	19.02±4.01	26.30±5.55	5

**Table 2 Kinetic parameters of PRC2 from TIRF measurements**

\* Obtained from a biexponential fit to the experimental data:  $y(t) = A1 * \exp(-t/\tau_{off,1}) + A2 * \exp(-t/\tau_{off,2})$

\*\* here we used an adapted version of formula (7):  $k_{on} = \frac{1}{\lambda_{on} \times [protein]} \quad (10)$

#2 indicates a second set of measurements on unmodified chromatin to investigate altered chromatin states.

Table 2 was partially adapted from Choi et al., 2017.

## 2.5. Conclusion

PRC2 is important for chromatin silencing through its function as chromatin writer of the H3K27me3 mark<sup>81</sup>. Misregulation of PRC2 often leads to cancer<sup>74</sup>. Therefore it is crucial to study and dissect the process of PRC2 recruitment to chromatin. Presence of PHF1 has been shown to stabilize PRC2 binding towards chromatin<sup>90</sup>. Here, we aimed to understand the mechanism how this happens in detail. Based on structure predictions we identified a conserved WH domain between four homologs of PHF1 (including Plc, MTF2 and PHF19) and the corresponding crystal structure of Plc was solved. Mutation analysis using polarization assays unveiled an essential contribution of residues mutated within the WH domain in Plc and PHF1. We performed EMSA and TIRF measurements using PRC2 and unveiled enforced binding to DNA, nucleosomes and chromatin fibres in the presence of full-length PHF1, compared to PRC2. Employing these types of experiments on PHF1-mutants containing either the C-terminal tail of PHF1 did not unveil a contribution of the C-terminal fragment. However, when we performed similar experiments using PHF1 with mutations in the WH

domain, we abolished the enhanced DNA binding effect of PHF1. HMTase assays further supported this finding, as PHF1-WH mutants showed lowered H3K27 methylase activity. Together these findings strongly indicate that PHF1 anchors PRC2 towards chromatin, a mechanism, which is strongly driven by PHF1-DNA interactions. Thus, PHF1 enables PRC2 to exert its function as chromatin writer in a more efficient manner, than PRC2 alone.

Further, we tested binding of PRC2 towards chromatin arrays containing the H3K27me3, the H3K27M or the H3K36me3 mark. Interestingly, all the different modifications led to enhanced PRC2 binding, and in the presence of H3K36me3 even association times ( $\lambda_{on}$ ) were decreased significantly. While prolonged binding on the H3K27me3 mark was expected, we expected even longer binding events in presence of the H3K27M mark. This was not the case, because to observe a strong effect of H3K27M, the PRC2 cofactor SAM is required<sup>80</sup>. The prolonged binding effect of H3K36me3 was rather unexpected and was attributed to PRC2-mediated establishment of H3K27me1, instead of H3K27me3, as the H3K36me3 mark lowers PRC2 activity upon binding<sup>216, 223</sup>. It remains unclear how and if PHF1 affects PRC2 binding dynamics in modified chromatin arrays.

Overall the PRC2-project has proven that we were able to transfer the TIRF system, which was established with HP1 $\alpha$ , to a complicated system, where we followed the single molecule dynamics of a protein complex and we found an explanation for recruitment and enhanced activity towards modification of chromatin by the PRC2-complex dependent on the WH domain of PHF1.

### 3. RNF168 in the DNA damage response

#### 3.1. Introduction

Single-molecule measurements have been successfully measured using the reader protein HP1 $\alpha$  and the protein complex PRC2. Next, we were interested to extend the established method to track a chromatin mark writer on the single molecule level performing its catalytic activity.

We previously performed single molecule measurements in a system with abruptly ending DNA strands. We reasoned that this might reflect a suitable model system for DSBs. Moreover, as our laboratory provides expertise in semi-synthesis of ubiquitin-modifications on chromatin, this prompted us to extend our studies to an ubiquitin mark writer protein of the DNA damage response, which is also a reader itself: RNF168<sup>224</sup>.

For the enzyme RNF168 we assumed a different binding mode than simple effector protein binding. RNF168 would associate with an ubiquitinated component (e.g. H2AK15). If it was recruited in a stable manner, it would perform writing of another ubiquitin mark on its substrate (e.g. another H2AK15) or it would fall off of the recruitment site before being able to act as a chromatin writer (Fig.50).

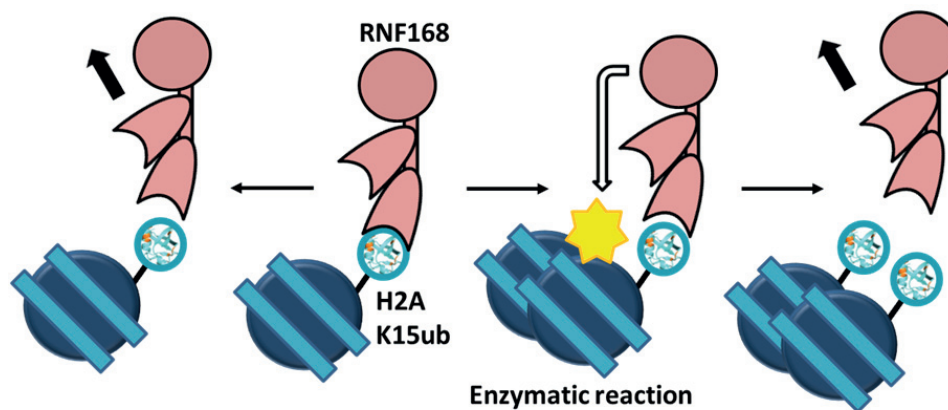


**Fig.50 Possible binding modes for RNF168**

RNF168 has been shown to bind ubiquitinated molecules. We expected the protein to probe onto nucleosomes and eventually perform an enzymatic reaction (indicated as yellow star placed through the white arrow) to install ubiquitin on a substrate.

Enzymatic chromatin ubiquitination has not yet been established in our lab. To study chromatin ubiquitination on the single molecule level, we first had to produce the different components of a chromatin-related ubiquitination system to characterize them and to analyse their behaviour towards different chromatin substrates. In order to develop a model system to elucidate mechanisms of chromatin ubiquitination, we defined a set of E1, E2 and E3, which we used during our studies and they will be described in the following.

### 3.2. Generation of the ubiquitination machinery

In order to investigate reading and writing of the E3 ubiquitin ligase in dependence of the chromatin state, we needed to express and purify the functional components of the ubiquitination cascade, which is driven upon primary DNA damage signals.

To initiate the ubiquitination machinery, we were required to express and purify the primary enzyme of the cascade: UBE1. The canonical E1 in human hUBA1/UBE1, which initiates ubiquitination, is a 120 kD and 1058 AA large protein encoded from a single open reading frame. Although the crystal structure of UBA1 has been assessed in *S. pombe*, *S. cerevisiae* and *M. musculus* up to now it remained challenging to determine the crystal structure of human UBA1 beyond AA 439 (Fig.51a)<sup>225-228</sup>. UBE1 is structured into two adenylation blocks (inactive adenylation domain (IAD, AA 1-439) and active adenylation domain (AAD, AA 439-950)) of which the latter is responsible for ubiquitin and ATP binding. These blocks are interspersed with conserved catalytic cysteine domains (first catalytic cysteine half-domain (FCCH, AA 204-295) and second catalytic cysteine half-domain (SCCH, AA 626-891)), the latter containing the active cysteine site (AA 632). A C-terminal ubiquitin-fold domain (UFD, AA 950-1058) is able to recognize the E2 enzyme. The second human E1, UBE1L2 is highly expressed in testis and likely organ-specific<sup>105</sup>. Thus, in this study we used UBE1 to initiate ubiquitination of substrates and formation of ubiquitination chains by its lysine residues.

The plasmid of the human ubiquitin-activating enzyme E1 (hUBE1) was purchased from Addgene and expressed in bacteria at 16 °C overnight. Notably, successful expression was only obtained in Rosetta™ 2 *E.coli* cells (Fig.51b). The bacterial lysate was complemented with BME, ATP and MgCl<sub>2</sub>, and lysed by sonication. As a primary purification step we employed Ni-affinity purification, as the protein contains an N-terminal 6xHis-tag. Elutions were pooled, concentrated and a buffer exchange was performed. The sample was flash frozen and stored at -80 °C until use (Fig.51c). We note that the final fraction contains significant impurities, as published previously<sup>229</sup>. As we co-purified the contaminants at every step of the purification, we attribute the additional bands to degradation products or deletion products of UBE1 (Fig.51c). The enzyme UBE1 was essential to activate E2 and subsequently E3 ubiquitin enzymes.



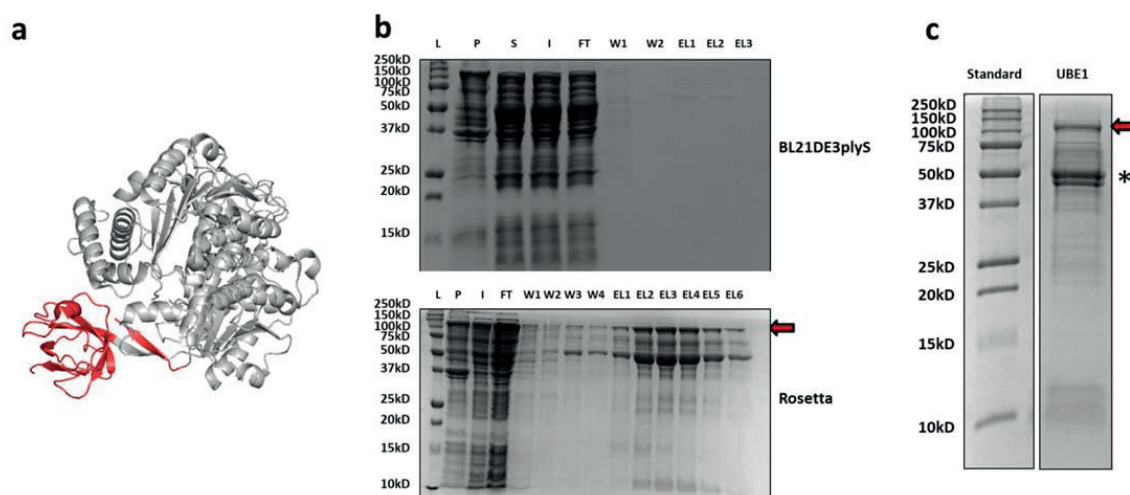


**Fig.51 UBE1 purification relies on protein expression in Rosetta cells (15 % SDS-PAGE gels)**

**a)** Crystal structure of UBE1 AA 50-431 (grey), FCCH (red). PDB: 4P22 (Xie, 2014). **b)** Nickel-affinity purification when the protein was expressed in BL21 DE3PlyS cells shows that no protein was retained in the elutions, while it was eluted (red arrow, expected size: 119 kD) in a similar experiment after expression in Rosetta cells. L = protein standard, P = Pellet after sonication, S = Supernatant after sonication, I = Input (filtered supernatant), FT = flow through, W1-4 = Wash1-4, EL1-6 = Elution1-6. Shown is the Coomassie staining. **c)** Analysis of the final fraction of UBE1 (red arrow) after expression in Rosetta cells and purification on SDS-PAGE. Asterisk denotes contaminants, which co-purify with UBE1. Shown is the Coomassie staining.

Next in line was the ubiquitin transferring enzyme UBE2D3/UbcH5C. The E2 ubiquitin-conjugating enzyme Ubch5 (now Ubch5A) was discovered as a human ortholog to ScUBC4/5 from *S. cerevisiae* and orthologs were also found in *C. elegans*, *D. melanogaster* and *A. thaliana*<sup>230-235</sup>. Later, two human paralogs were identified, which essentially founded the Ubch5 protein family<sup>232</sup>. The E2 enzyme UBE2D3/UbcH5C is known for its role in the nuclear factor kappa enhancer binding protein (NF-κB) pathway. Ubch5C is critical for cellular inhibitor of apoptosis protein 1 (c-IAP1) stability, which ultimately leads to liberation of NF-κB from its inhibitor (IκB) allowing transcription of inflammatory and immune responses<sup>236-238</sup>. In 2017 the crystal structure of UBE2D3 was solved up to 1.76 Å resolution<sup>238</sup>. This allowed identification of a polar groove surrounding the active site at C85 and unveiled a relatively stable tertiary structure of the 147 AA protein (Fig.52a)<sup>238</sup>.

Of note, during the early DDR mainly two different E2 enzyme types are involved. UBE2D3, in general, has been shown to be able to catalyse ubiquitin chain formation on K11-, K48- and K63<sup>239</sup>. The heteromeric E2 complex UBC13/MMS2, has been implicated in ubiquitin chain formation with RNF8 and RNF168 and forms K63-linked ubiquitin chains, a process which is dependent on MMS2<sup>48, 128, 240</sup>. RNF8 is the E3 ligase mainly interacting with UBC13/MMS2, but it requires RNF168/UBE2D3 in the nucleosomal context to prime H2A/H2A.X for RNF8-mediated chain elongation<sup>126, 128</sup>. As mono-ubiquitination of H2A/H2A.X by RNF168 represents a simple model of ubiquitination, we decided to focus

initially on the E2 enzyme UBE2D3. Further, we decided to use UBE2D3 because it has been used with a variety of E3 enzymes and showed high activity and low selectivity<sup>128, 241, 242</sup>.

The plasmid of the human ubiquitin-conjugating enzyme E2 (UBE2D3) was purchased from Addgene and expressed in Rosetta cells at 16 °C overnight. Expression and purification of the protein worked well, but initial activity tests unveiled completely abolished activity, compared to a commercially available hUBE2D3 version from Boston Biochem. In order to obtain comparable activity we had to reduce an N-terminal tag in the plasmid construct and further to reverse a point mutation (P18L) to obtain the native proline at position AA 18 (Fig.52b).

The bacterial lysate was sonicated. As a primary purification step we employed Ni-affinity purification, as the protein contains an N-terminal 6xHis-tag. Elutions were pooled, concentrated and a buffer exchange was performed to TEV cleavage buffer.

TEV protease was applied to remove the N-terminal 6xHis-tag. After completion, a reverse Ni-NTA purification was done. Thus, the TEV-protease (which contained a His-tag) and uncleaved UBE2D3 were bound to the resin. Eluted fractions containing UBE2D3 were pooled, concentrated and another buffer exchange was performed. The sample was complemented with 1 mM DL-dithiothreitol (DTT) and 10 % (v/v) glycerol, then flash frozen and stored at -80 °C until use (Fig.52c, 52d and 52e).



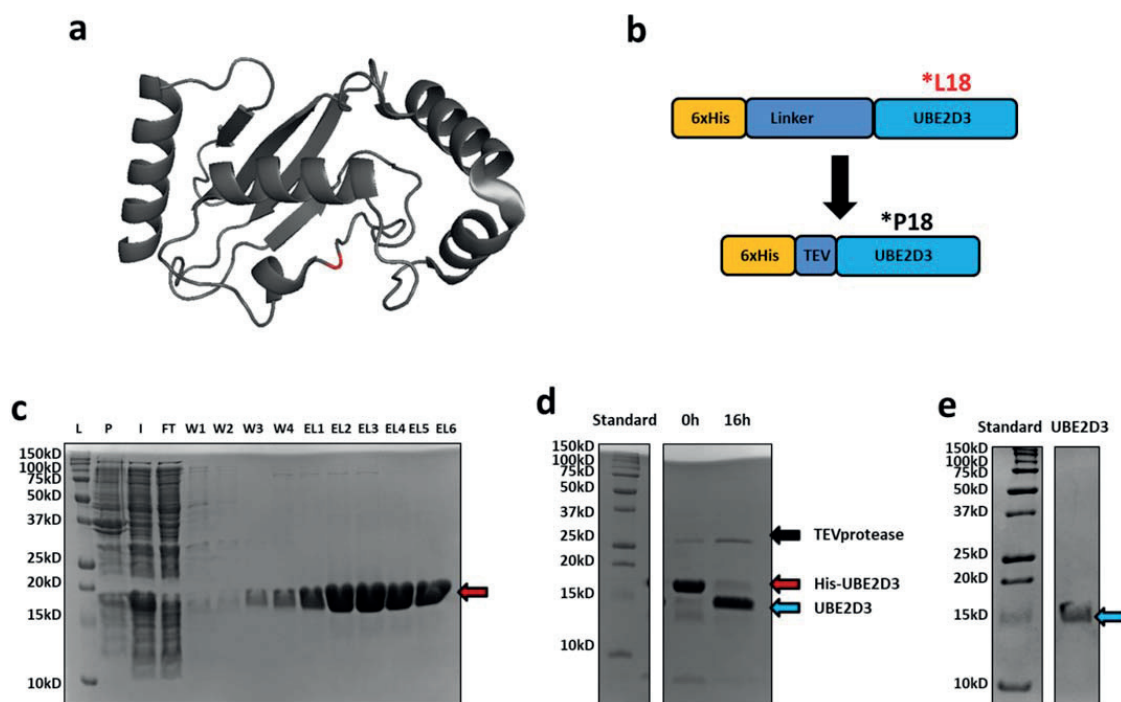


**Fig.52 UBE2D3 re-cloning, expression and purification (15 % SDS-PAGE gels)**

**a)** Crystal structure of hUBE2D3 AA 1-147 (dark grey), C85 active site (red). PDB: 5EGG (Wu et al., 2017). **b)** UBE2D3 protein engineering to render it functional with high activity (\* denotes a leucine mutation of the native proline, TEV = TEV protease cleavage site). **c)** Nickel-affinity purification when the protein was expressed in Rosetta cells shows a strong single band for the eluted 6xHis-UBE2D3 (red arrow, expected size: 19.1 kD). L = protein standard, P = Pellet after sonication, I = Input (filtered supernatant), FT = flow through, W1-4 = Wash1-4, EL1-6 = Elution1-6. Shown is the Coomassie staining. **d)** Monitoring TEV cleavage to remove the His-tag from the UBE2D3 N-terminus over 16 h (4 °C). After 16 h cleavage was almost complete (blue arrow). Shown is the Coomassie staining. **e)** SDS-PAGE analysis of the final fraction of UBE2D3 (blue arrow) after expression in Rosetta cells and purification. Shown is the Coomassie staining.

Activity was tested in an ubiquitination assay (for details see chapter “II, 3.3.1. Activity of RNF168 towards chromatin arrays”, ubiquitination assay), which leads to ubiquitination of fluorescently labelled histone H2A as observed through a band shift on SDS-PAGE. Shift of the H2A band was observed over time relative to a reaction containing commercially available UBE2D3 enzyme (Boston Biochem) to evaluate quality of the purified protein (Fig.53).

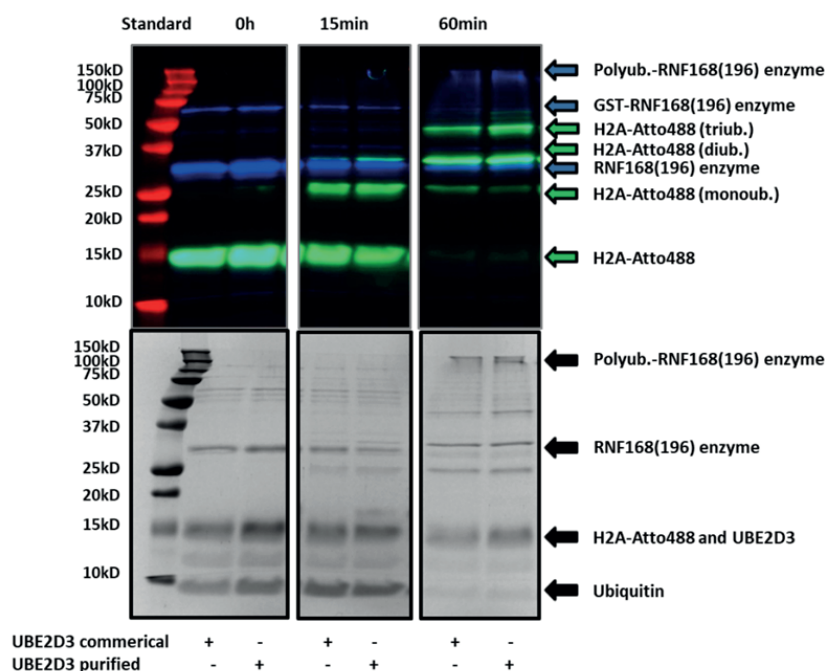


**Fig.53 Activity assay to monitor ubiquitination of H2A in histone octamers dependent on UBE2D3 (15 % SDS-PAGE gel)**

The top picture shows the fluorescence channels: red = 640 nm illumination (protein ladder), blue = 532 nm illumination (labelled RNF168(196)), green = 488 nm illumination (labelled H2A in histone octamers). The bottom picture shows colloidal Coomassie staining. The 488 nm channel shows an upwards shift of the labelled H2A protein over time (60 min). This unveils different ubiquitination states of H2A, as indicated with green arrows. The re-cloned version of UBE2D3 shows comparable activity compared to the commercially available UBE2D3 (Boston Biochem).

High activity of UBE2D3 was required to enable the E3 ubiquitin ligases to transfer the ubiquitin-moiety to the substrate.

The histone modification and the small protein ubiquitin (human ubiquitin variant C) was expressed in BL21 DE3 bacteria (37 °C, 4 h). To increase the yield drastically we decided to use a tag-less purification strategy, which precipitates all non-ubiquitin proteins at pH 5<sup>107</sup>. The bacterial lysate was sonicated and dialysed towards acetic acid (pH 5.0). After dialysis aggregates were removed by centrifugation. A cation exchange column (HiTrap™ SP HP) was employed as a second purification step. Fractions were analysed by SDS-PAGE and ubiquitin-containing fractions were desalted using RP-HPLC (semi- or preparative C18 column) (Fig.54a). Quality of the purified ubiquitin was analysed on RP-HPLC (analytical C18 column) and ESI-MS (Fig.54b and 54c). The collected protein was lyophilized, kept at -20 °C and dissolved in water (1 mg/ml) prior to usage.

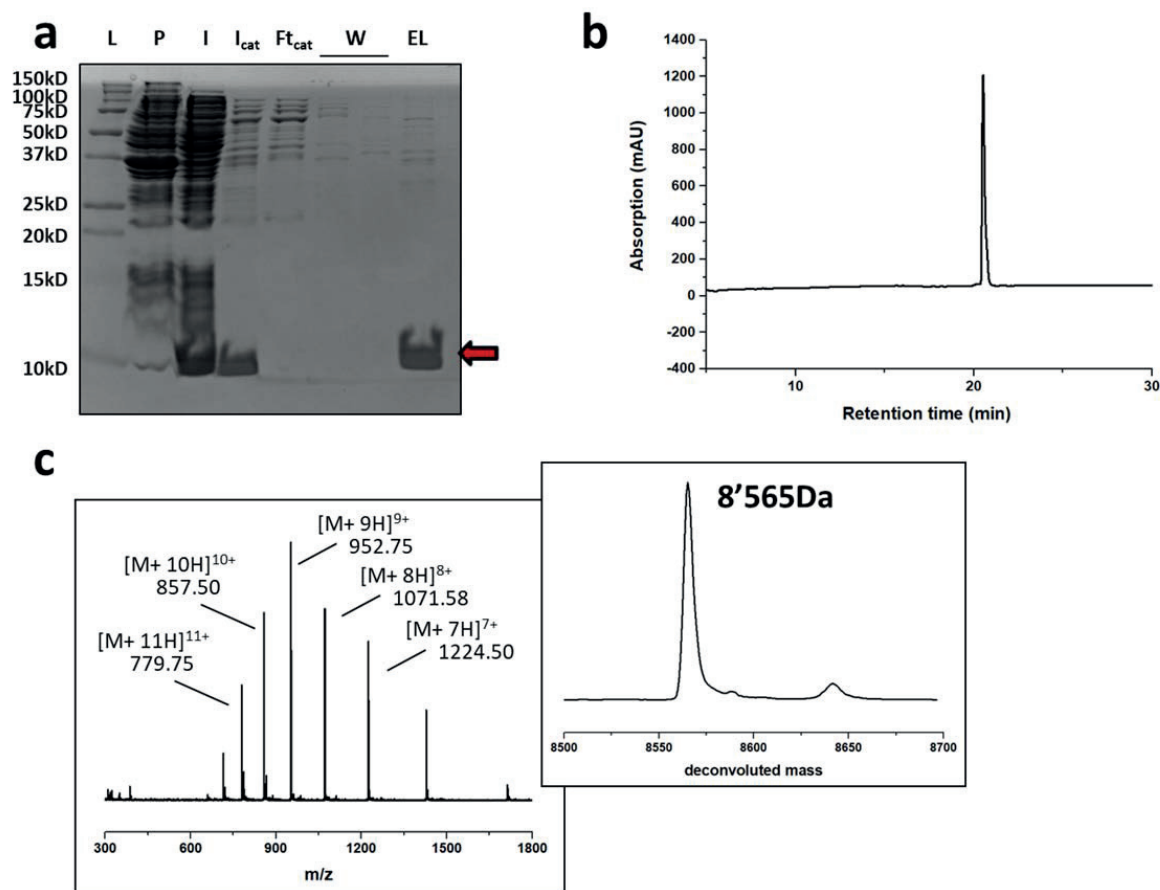


**Fig.54 Tag-less ubiquitin purification and analysis by RP-HPLC and ESI-MS**

**a)** Ubiquitin (red arrow) purification through dialysis at pH 5 monitored by SDS-PAGE (200 V, 50 min) and Coomassie staining. L = protein standard, P = Pellet after sonication, I = Input (dialysis),  $I_{cat}$  = Input (cation exchange),  $Ft_{cat}$  = flow through (cation exchange), W = Wash fractions, EL = Elution (collected sample from cation exchange). **b)** RP-HPLC and **c)** MS analysis of the final product, human ubiquitin (calculated mass: 8565 Da, observed mass: 8565 Da).

Having purified human ubiquitin available would render our ubiquitination system more native, as it consists of human protein versions, only.

In order to track ubiquitinated products more easily we aimed to fluorescently label ubiquitin using cysteine chemistry, because ubiquitin does not contain (multiple) native cysteines<sup>243-245</sup>. Noteworthy, purification of the tag-less ubiquitin version containing a cysteine mutation led to losses of protein yield. Thus, we used a construct containing a His-tag for protein purification (Construct: His-Thrombin-C-hUBIQUITIN (variant C), short: C-ubiquitin). C-ubiquitin was expressed in BL21 DE3PlyS cells (37 °C, 4 h). The protein was purified using Ni-NTA resin (see HP1 $\alpha$  purification protocol) and preparative RP-HPLC (as ubiquitin) by Caroline Lechner (LCBM, EPFL, CH).

For protein labelling, the lyophilized protein was dissolved in guanidine labelling buffer. A 10x excess of fluorescein-5-maleimide, dissolved in DMSO, was added to the protein. The reaction was kept covered in aluminium foil (4 °C) for 20 h. Then the reaction

product was purified using RP-HPLC (semi-preparative C18 column). The collected fractions were analysed by SDS-PAGE, analytical RP-HPLC and ESI-MS (Fig.55a, 55b and 55c). Based on the mass of the C-ubiquitin and the product, Fluorescein-ubiquitin, the initiator methionine was missing. Although removal of the initiator methionine (M1) is a completely natural process for some proteins, the M1 residue can be important for ubiquitin chain formation, known as the linear ubiquitin chain, and has been shown to be involved in different processes as degradation by the proteasome, regulation of innate immunity and inflammation<sup>246, 247</sup>. Thus, in experiments using the Fluorescein-ubiquitin, we lack the possibility to observe potential effects caused by linear ubiquitin chains. However, to our knowledge a direct link between RNF168 and linear ubiquitin chains has not been described. Based on this, we decided that the obtained Fluorescein-ubiquitin can be used in our *in vitro* experiments without having a major bias of the experimental outcome.

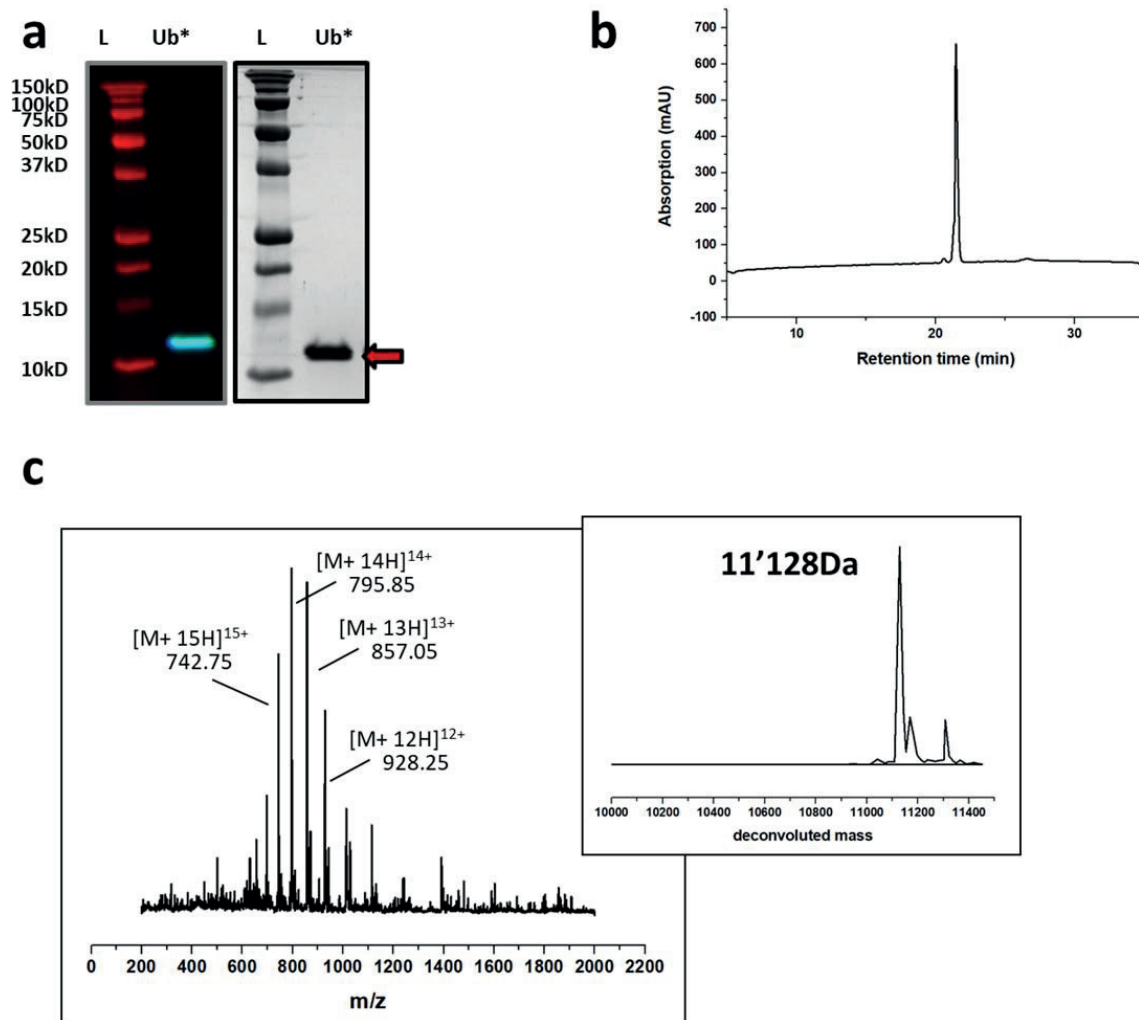


**Fig.55 C-ubiquitin labelling and analysis by SDS-PAGE, RP-HPLC and ESI-MS**

**a)** Fluorescein-ubiquitin (Ub\*, red arrow) final fraction analysed by SDS-PAGE and Coomassie staining (grey). The blue band shows the fluorescein signal. L = protein standard. **b)** RP-HPLC and **c)** MS analysis of the final product, human ubiquitin (calculated mass: 11'127 Da, observed mass: 11'128 Da). Based on the mass the initiator methionine is missing.

To complete a set of ubiquitination proteins in the DNA damage response cascade, we set our focus to the E3 ubiquitin-ligase proteins. The essential E3 ubiquitin ligases in the early DDR are RNF8 and RNF168, both of them being RING-type ubiquitin ligases. The canonical RING domain was described in 1991 by Freemont et al. with the sequence C-X<sub>2</sub>-C-X<sub>(9-39)</sub>-C-X<sub>(1-3)</sub>-H-X<sub>(2-3)</sub>-C-X<sub>2</sub>-C-X<sub>(4-48)</sub>-C-X<sub>2</sub>-C (X being any amino acid) and fits both, RNF8 and RNF168<sup>128, 248</sup>. The cysteine- and histidine-residues form a buried core and stabilize two zinc ions, which are essential for catalytic activity<sup>110, 249</sup>.

The mutational phenotypes of RNF168 have been observed and described in the year 2007 as the RIDDLE immunodeficiency syndrome in patients lacking sufficient DNA repair mechanism, which led to radiosensitivity, immunodeficiency, dysmorphic features and learning difficulties<sup>185</sup>. Two years later, a gene implicated in the RIDDLE syndrome, named RIDDLEIN, was identified as the previously discovered RNF168, using an RNA interference screen using foci formation of the DDR protein 53BP1 as readout<sup>171, 125</sup>. RNF168 is a 571 AA protein containing a catalytic RING domain (AA 16-55) and two ubiquitin-dependent DSB recruitment modules (UDM1 and UDM2; Fig.56)<sup>250, 251</sup>. UDM1 is separated into three functional motifs LR motif 1 (LRM1, AA 110-128), ubiquitin-interacting motif (UMI, AA 141-156) and motif interacting with ubiquitin 1 (MIU1, AA 171-188), as well as UDM2, namely ubiquitin-associated domain (UAD, AA 419-439), MIU2 (AA 439-462) and LRM2 (AA 466-478)<sup>250</sup>. While UDM1 has been shown to interact with RNF8-ubiquitination products, UDM2 was implicated in auto-recognition of RNF168 monoubiquitinated targets<sup>48, 134</sup>. At the C-terminus a PALB2-interacting domain (PID) was identified<sup>250</sup>. The PID was only found recently, and couples RNF168 to HR during the S/G2-phases of the cell cycle<sup>252</sup>. This was unexpected, as RNF168 was rather associated with the DNA repair mechanism of NHEJ and was thought to antagonize HR (at least during cell cycle phase G1). Interestingly, also HP1α was implicated in this regulation mechanism and was important for BRCA1 recruitment to DSB, which generally promotes HR, and HP1α affected arrest of the cell cycle at the G2/M checkpoint<sup>253</sup>. This highlights the importance of DDR regulation across the cell cycle, as NHEJ during replication could lead to catastrophic genome rearrangements<sup>254</sup>.

As we aimed to observe the activity of an ubiquitin-writer towards chromatin, we reasoned that RNF168 would be a good target of investigation. Not only would RNF168 be able to modify histone H2A/H2A.X in chromatin fibres, it was also known to contain two ubiquitin binding modules, which supposedly bind to ubiquitinated H1.2 and ubiquitinated H2A/H2A.X<sup>48, 49</sup>. Related to the HP1α project, this would put us in the position to create an anchor point on chromatin for RNF168 in single molecule measurements and potentially stimulate its activity.

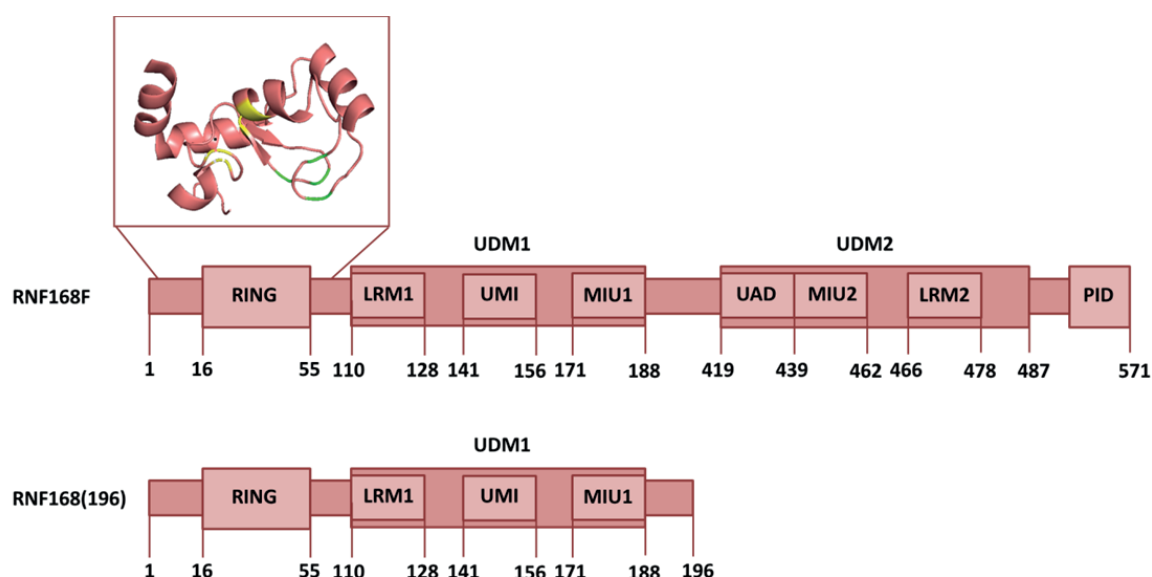


**Fig.56 Maps of RNF168 constructs indicate ubiquitin binding modules (UDM1 and UDM2) and the catalytic RING domain**

Illustrated are domain maps of the full length RNF168 protein (RNF168F) and a truncated construct, which was used for bacterial expression (RNF168(196)). Numbers below the maps denote the amino acid residues. Crystal structure of the RING domain: hRNF168 RING AA 3-93 (red), RING Cys1, 2, 4 and 5 (yellow), RING Cys3, 6, 7 and His (green). PDB: 4GB0 (Zhang et al., 2013). Figure was adapted from Takahashi et al., 2018.

The E3 human ubiquitin-ligase (hRNF168) was cloned from human cDNA library. RNF168 was expressed in Rosetta cells (16 °C, 16 h) harbouring an N-terminal glutathione S-transferase tag (GST-tag) and a C-terminal streptactin binding tag (STREP-tag) to perform a two-sided purification, as the protein stability at temperatures higher than 4 °C was very low and a lot of degradation products can appear. Initial purification via Ni-NTA resin (as published in Zhang et al., 2013) using a His-tag failed multiple times, as protein activity was lowered drastically <sup>251</sup>. Further the protein (truncated or full-length) is very sensitive to agitation and temperatures higher than 4 °C should be avoided rigorously during purification. Hence, attaching a fluorescent label onto the protein through EPL, which requires incubation at RT, was not successful. As protein labelling is a vital step to monitor single molecules, we switched to the ybbr-tag labelling method, which was applied for PRC2 <sup>210</sup>.

In the following, we will focus only on the strategies, which allowed us to produce highly enzymatically active versions of RNF168.

Expression of a full-length RNF168 protein construct (and subsequent small scale GST-tag purification) did not retain any protein (Fig.57a). As RNF168 expression in bacteria has not been achieved to this point, we decided to focus on a truncated version, which had been expressed successfully before <sup>128</sup>. We decided to express a construct containing AA 1-196, which contains the catalytic RING domain and the UDM1 (Construct: GST-Thrombin-

TEV-hRNF168(AA 1-196)-ybbr-Thrombin-STREP, short: RNF168(196); Fig.56). We further included an N-terminal GST-tag and a C-terminal STREP-tag, as we had observed degraded fragments of the protein on SDS-PAGE in earlier constructs. This enables to perform a double-affinity purification approach, which renders the non-truncated protein in the final elution.

After expression the lysate was sonicated. As initial purification step we performed glutathione-resin purification based on the N-terminal GST-tag of the protein (Fig.57b). Elutions were pooled, concentrated and a buffer exchange to ybbr labelling buffer was performed. TEV cleavage was applied to remove the N-terminal GST-tag (Fig.57c). After successful TEV cleavage, RNF168 was subjected to a Streptactin XT superflow column to ensure enrichment of the non-truncated protein by its C-terminal STREP-tag (Fig.57d). Elution fractions were pooled, concentrated and again a buffer exchange was performed. We added 20 % (v/v) glycerol, flash froze the protein in liquid nitrogen and kept the protein at -80 °C until use. Following this strategy, one liter bacterial culture rendered 190 ug RNF168(196).



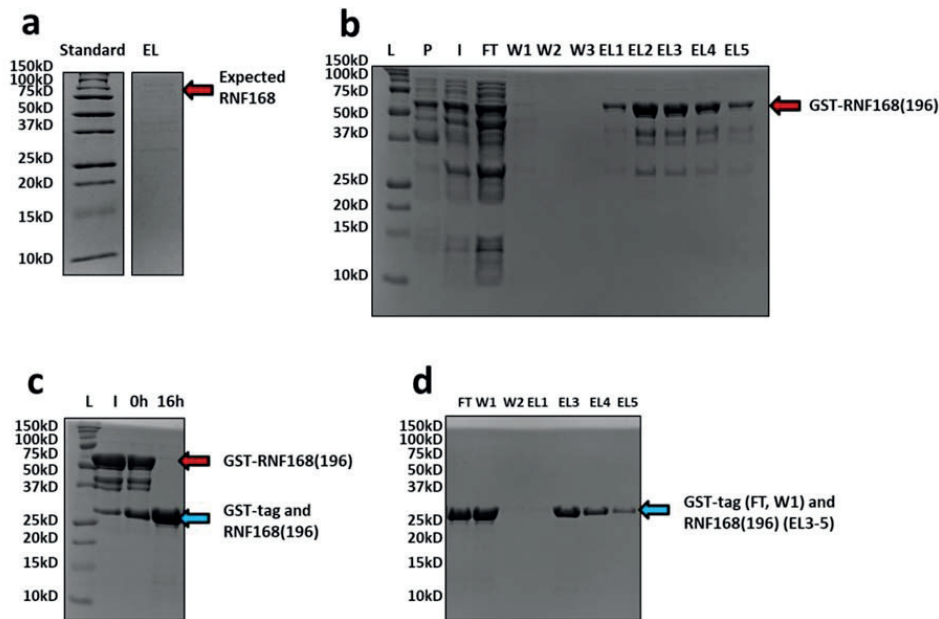


**Fig.57 RNF168 expression and purification**

**a)** RNF168 (full-length) purification using glutathione resin monitored by SDS-PAGE (200 V, 50 min) and Coomassie staining. EL = Elution of glutathione beads. Expected size: 96.3 kDa. **b)** RNF168(196) purification using glutathione resin monitored by SDS-PAGE (200 V, 50 min) and Coomassie staining. Red arrow: GST-RNF168(196), expected size: 54 kD. L = protein standard, P = Pellet after sonication, I = Input (filtered supernatant), FT = flow through, W1-3= Wash1-3, EL1-5 = Elution1-5. **c)** RNF168(196) TEV cleavage monitored by SDS-PAGE (200 V, 50 min) and Coomassie staining. TEV cleavage was completed after 16 h. RNF168 and the free GST-tag run at the same molecular weight of 25 kD (blue arrow, expected size: GST-tag: 28 kDa, RNF169(196): 26 kDa). L = protein standard, I = Input (TEV cleavage). **d)** Streptactin purification of RNF168 monitored by SDS-PAGE (200 V, 50 min) and Coomassie staining. Flow through and wash1 fractions show the free GST-tag (blue arrow), which disappears in wash2. Eluted is the pure RNF168(196) (blue arrow). FT = flow through, W1-2= Wash1-2, EL1-5 = Elution1-5.

Activity was tested in an ubiquitination assay (for details see chapter “II, 3.3.1. Activity of RNF168 towards chromatin arrays”, ubiquitination assay), which leads to ubiquitination of fluorescently labelled histone H2A as observed through a band shift on SDS-PAGE. Shift of the H2A band was observed over time relative to a reaction containing versions of RNF168(196) from two different purifications. The optimized purification scheme as described above led to high ubiquitination activity and comparatively high yields of RNF168(196) (Fig.58).



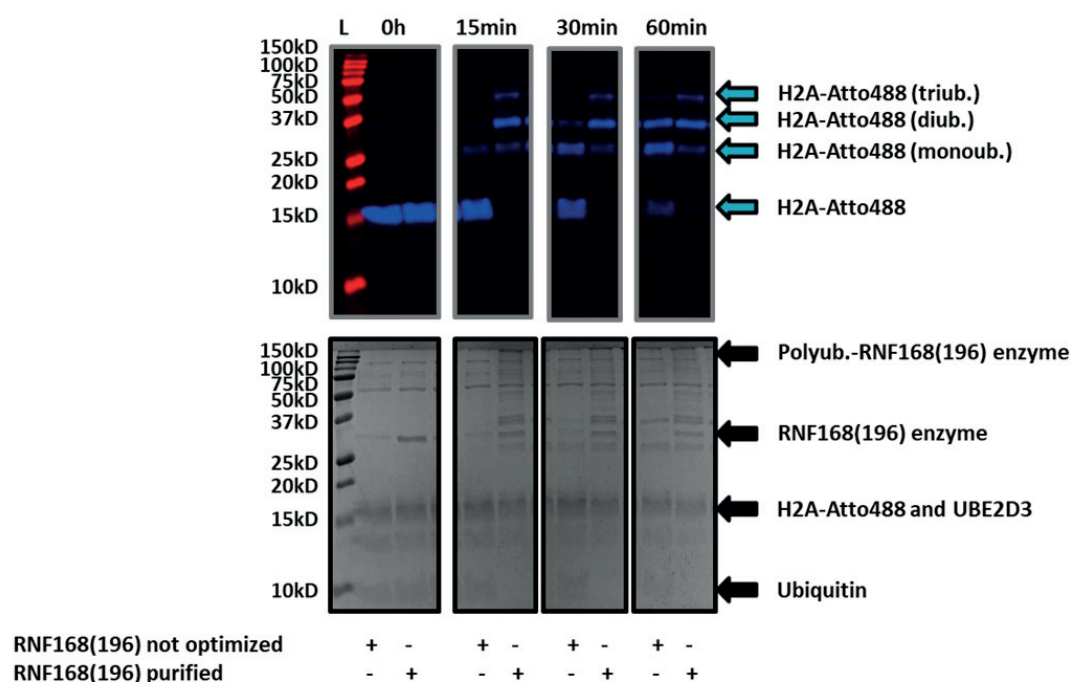


**Fig.58 Activity assay to monitor ubiquitination of H2A in histone octamers based on RNF168(196) (15 % SDS-PAGE gel)**

The top picture shows the fluorescence channels: red = 640 nm illumination (protein ladder), blue = 488 nm illumination (labelled H2A in histone octamers). The bottom picture shows colloidal Coomassie staining. The 488 nm channel shows an upwards shift of the labelled H2A protein over time (60 min). This unveils different ubiquitination states of H2A, as indicated with blue arrows. The optimized RNF168(196) purification strategy renders an E3 enzyme with high ubiquitination activity towards H2A. L = protein standard.

In order to use RNF168(196) under single molecule conditions, we needed to attach a fluorescent label onto the protein. As discussed above, EPL is not a suitable labelling approach for RNF168. Thus, we introduced a ybbr-tag at the C-terminus of the protein, upstream of the STREP-tag, which enables labelling with Sfp synthase.

Ybbr-labelling was performed. The reaction was kept for 1-2h with soft nutation and monitored by SDS-PAGE (Fig.59). Labelling efficiency was usually determined between 30-70 %.

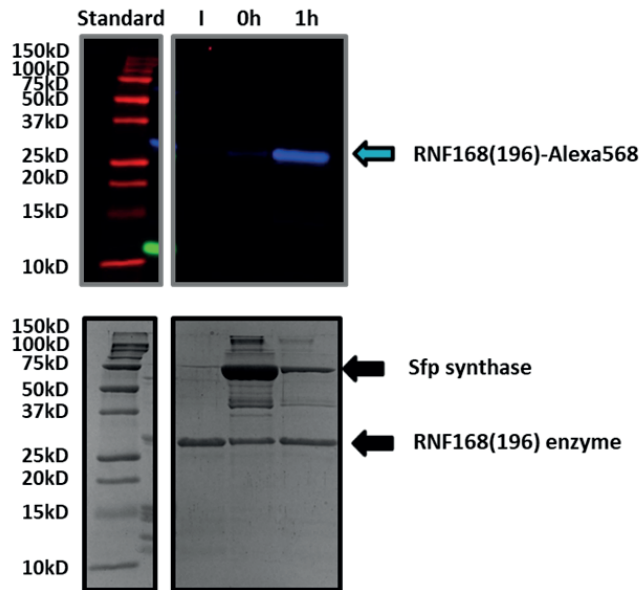


**Fig.59 Sfp labelling of RNF168(196)**

The top picture shows the fluorescence channels: red = 640 nm illumination (protein ladder), blue = 532 nm illumination (labelled RNF168 protein). The bottom picture shows colloidal Coomassie staining. Sfp synthase and contaminating bands disappeared to a large extent after 1h, probably due to aggregation, while the RNF168(196) band was not diminished. The fluorescence channel shows labelled RNF168(196) after 1 h. I = Input

To remove the excess of Alexa568-CoA a S200 10/300 GL gel filtration column was used for purification with buffer W containing 5 mM BME (Fig.60).

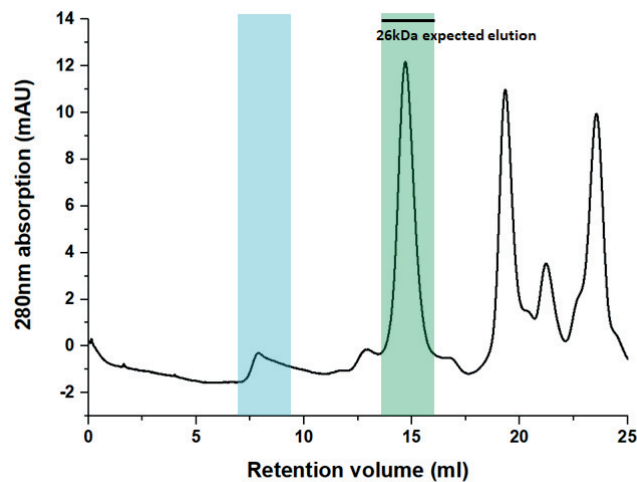


**Fig.60 S200 10/300 GL size exclusion of RNF168(196)-Alexa568 using buffer W (5 mM BME)**

Size exclusion chromatography leads to a peak (green) in the expected elution volume of 13-16 ml for the 26 kDa protein, which contains the labelled RNF168 protein. Addition of 5 mM BME is essential as otherwise the protein peak appears in the void volume (blue).

Labelled protein fractions were collected and checked for E3 ubiquitin ligase activity (Fig.61). Notably, RNF168 labelling did not affect the activity of the E3 ligase, when we compared unlabelled RNF168 and Alexa-568-RNF168 (Fig.61: R168 vs R168\*). The size exclusion purified, labelled RNF168 (Fig.61: R168\*\*) was catalytically active, as mono-, di- and tri-ubiquitinated H2A was observed.

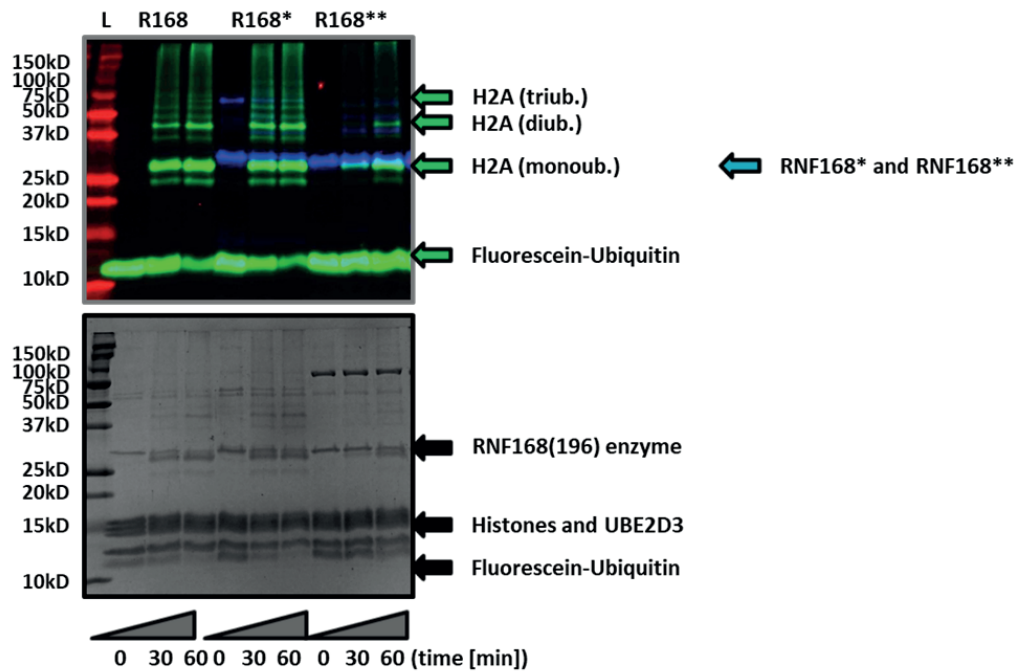


**Fig.61 Activity assay to monitor ubiquitination of H2A in histone octamers based on RNF168(196) labelling (15 % SDS-PAGE gel)**

The top picture shows the fluorescence channels: red = 640 nm illumination (protein ladder), blue = 532 nm illumination (labelled RNF168 versions: R168 (unlabelled), R168\* (labelled, no size exclusion), R168\*\* (size exclusion purified)), green: 488 nm illumination (labelled ubiquitin). The bottom picture shows colloidal Coomassie staining. The 488 nm channel shows 2-3 distinct upwards shifted bands reflecting H2A-mono-, di- and triubiquitin over a time span of 60 min. This unveils different ubiquitination states of H2A, as indicated with green arrows. Comparison of R168 and R168\* shows that the labelling did not affect activity. R168\*\* was still active after size exclusion. L = protein standard.

We note, when we used a different construct (GST-Thrombin-TEV-ybbr-hRNF168(AA 1-196)-Thrombin-STREP, short: ybbr-RNF168(196), Fig.61: RNF168\*) ybbr-labelling was employed between TEV cleavage and STREP-tag purification. This rendered high E3 ubiquitin ligase activity, but the size exclusion step was omitted, as we needed the E3 enzyme in highly concentrated aliquots for ubiquitination assays.

Together, UBE1, UBE2D3 and RNF168 are the minimal enzymes, which we selected and purified for our study of DDR-dependent ubiquitination mechanisms of chromatin.

Having the different components for RNF168-based ubiquitination in hands, we decided to characterize the newly purified proteins using ubiquitination assays towards histone octamers and chromatin fibres.

During the RNF168-project much more cloning work has been done and a summary of the important constructs for this project can be found in Table A5 (see chapter “VI Appendix”) <sup>35, 171</sup>.

### 3.3. Ubiquitination kinetics of chromatin fibres by RNF168

#### 3.3.1. Activity of RNF168 towards chromatin arrays

To compare ubiquitination of chromatin under different conditions, we first aimed to establish ubiquitination assays with the individual components to further characterize those components. Before the purified proteins would perform as expected in ubiquitination assays, we would not be able to study their dependence on the chromatin state.

Generally, in ubiquitination assays we test the capability of RNF168 to ubiquitinate its target H2A/H2A.X. Thus, the E1 enzyme UBE1 utilizes ATP and ubiquitin to charge the E2 enzyme UBE2D3. Charged UBE2D3 enables RNF168 to transfer ubiquitin to histone H2A (or H2A.X) if at least a H2A/H2B dimer is present <sup>35</sup>.

Ubiquitination assays were performed using UB buffer, which contains ATP and an ATP-regeneration system to ensure high activity of the E1 enzyme. UBE1 was always added last to the reaction mix, in order to start the reaction in a tightly timed manner. To quench the reaction we added sodium dodecyl sulfate (SDS) loading dye to the reaction mix and boiled the tube at 100 °C for 5 min. Assays were analysed using SDS-PAGE with fluorescence imaging and/or western blots.

To ensure a controlled ubiquitination procedure, we performed ubiquitination assays while excluding single components (Fig.62). The labelled H2A band only moved to higher molecular weight, when UBE1, UBE2D3, ubiquitin and RNF168 were present. Interestingly, the lack of histone octamers still enabled auto-ubiquitination of RNF168. In summary, this experiment verified that every component of the ubiquitination assay is vital to H2A-ubiquitination and solidifies our claim of having an RNF168-mediated ubiquitination system for histone H2A.

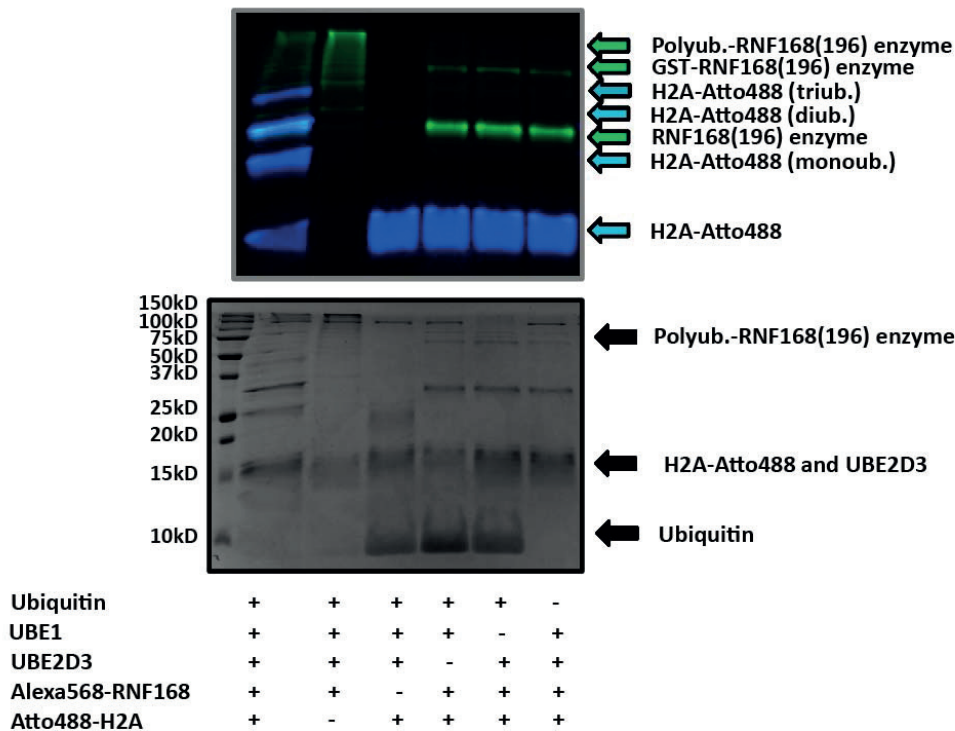


**Fig.62 Ubiquitination assay to monitor ubiquitination of H2A in histone octamers at 60 min by excluding different components (15 % SDS-PAGE gel)**

The top picture shows the fluorescence channels: blue = 532 nm illumination (labelled RNF168(196)), green = 488 nm illumination (labelled H2A in histone octamers). The bottom picture shows colloidal Coomassie staining. Ubiquitination assays lacking ubiquitin, UBE1, UBE2 or RNF168(196) did not show ubiquitinated H2A. When no histones were present, RNF168 got still auto-ubiquitinated.

To elucidate whether RNF168(196) is able to ubiquitinate chromatin arrays, we assembled chromatin arrays containing H3K9me3 and either Atto488-H2A or H4K16ac (provided by Louise Bryan)<sup>192</sup>. H4K16ac is a histone mark, which sterically opens chromatin and thus we were wondering whether ubiquitination would be facilitated in these arrays. The H3K9me3 mark was included, because our octamers only contained H4K16ac-H3K9me3 and not H4K16ac alone. We subjected 200-400 nM chromatin arrays to ubiquitination assays for 1 h. Then, some of the reaction sample was subjected to Scal digestion (37 °C, 20 h) in order to obtain mononucleosomes, which can be easily analysed on a 5 % TBE gel. Fluorescence detection unveiled mononucleosome ubiquitination (Fig.63a). To confirm ubiquitination of chromatin arrays, as mononucleosomes could have been ubiquitinated during the Scal digestion, we analysed them using SDS-PAGE after boiling the chromatin arrays. Indeed, the fluorescently labelled histone H2A showed mono-, di- and triubiquitination (Fig.63b). Further we monitored ubiquitination of Atto488-H2A by analysing different time points, which confirms stepwise ubiquitination of chromatin fibres (Fig.64).

Thus we verified activity of RNF168(196) towards chromatin arrays containing 12 nucleosomes.

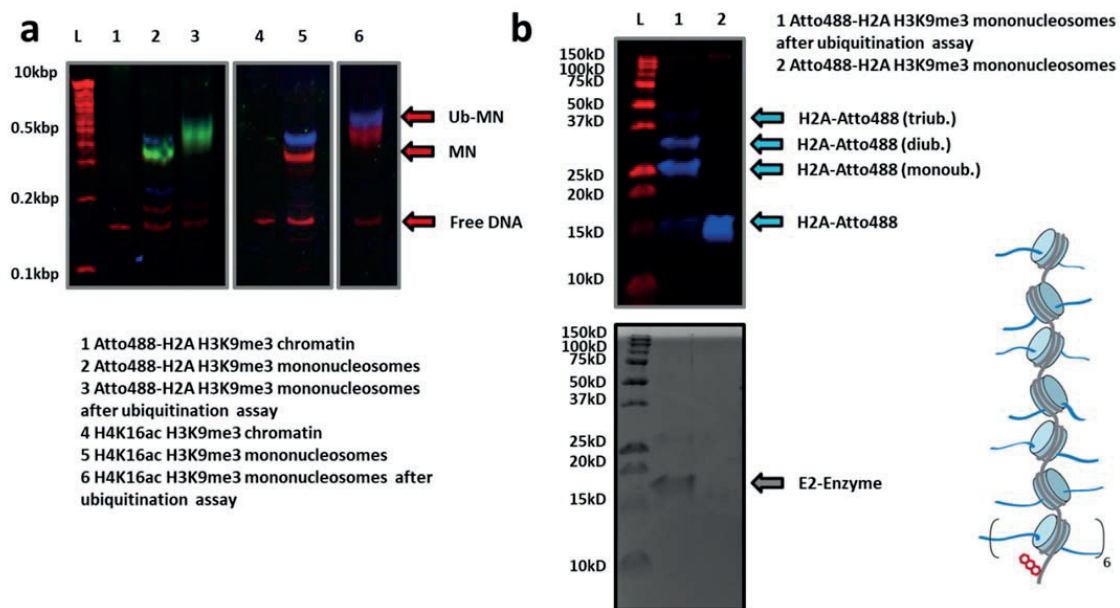


**Fig.63 Ubiquitination assay towards chromatin**

**a)** 5 % TBE gel to analyse *Scal*-digested chromatin arrays. After the ubiquitination reaction, mononucleosomes were shifted, which indicates ubiquitination of chromatin arrays. Red: Gelred (DNA), Green: 488 nm (Atto488-H2A), Blue: 640 nm (labelled DNA). L = 2-log DNA ladder. **b)** 15 % SDS-PAGE gel to analyse H2A from chromatin arrays. Red: 640 nm (ladder), Blue: 488 nm (Atto488-H2A). Grey: Coomassie staining. Ubiquitination of H2A is already present in (boiled) chromatin arrays, which indicates that ubiquitination did not happen with mononucleosomes during *Scal*-digestion. The band in lane 1 at 16kD in the Coomassie staining shows the E2 enzyme (grey arrow). L = protein ladder.

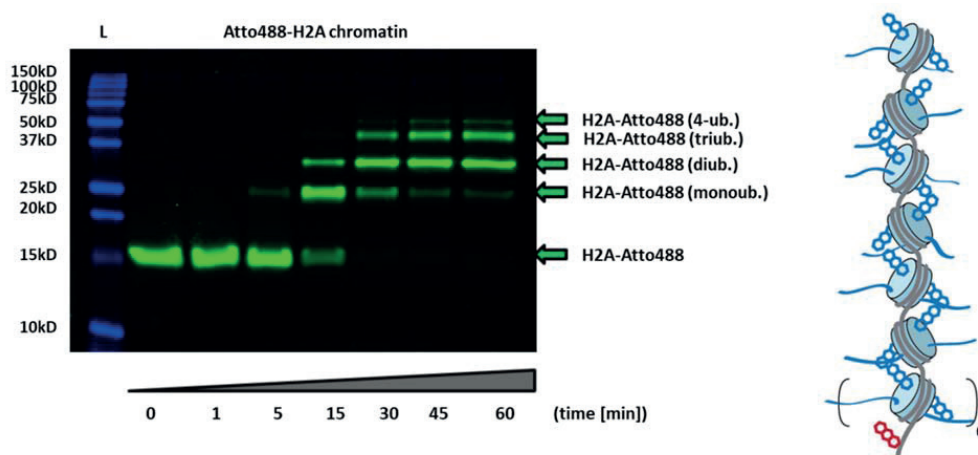


**Fig.64 Ubiquitination kinetics towards chromatin**

15 % SDS-PAGE gel to analyse H2A from chromatin arrays. Blue: 640 nm (ladder), Green: 488 nm (Atto488-H2A). From 1 min to 60 min a defined ubiquitination pattern arises on H2A. L = protein standard.



### 3.3.2. RNF168-mediated ubiquitination depends on accessibility of the nucleosome acidic patch

The nucleosome acidic patch is an important feature of the nucleosome for several proteins, including RNF168<sup>35, 133</sup>. Inaccessibility of the acidic patch can negatively influence activity of RNF168<sup>35</sup>. Recently, efforts were made to synthesize selective anti-cancer drugs using ruthenium compounds<sup>255</sup>. An impact was shown for the compound RAPTA-C to inhibit spreading and growth of tumor metastases and RAPTA-C has anti-angiogenic properties<sup>256, 257</sup>. Interestingly, RAPTA-C binds directly to the nucleosome acidic patch, while RAED-C, which also exerted anti-tumorigenic properties, rather interacted with the DNA sites of nucleosomes (Fig.65, as published in Adhireksan et al., 2014)<sup>255</sup>. Anti-cancer activity for cells had been found at 250  $\mu$ M for RAPTA-C ( $IC_{50}$ ), while it was determined at 4.5  $\mu$ M for RAED-C. As the mode of action for RAPTA-C has not been elucidated yet, we sought to investigate whether RAPTA-C (but not RAED-C) can inhibit ubiquitination activity of RNF168 by occluding the nucleosome acidic patch. To antagonize a potential effect by occluding the nucleosome acidic patch, we also employed our studies on chromatin containing the modification H4K16ac, which renders the nucleosome acidic patch accessible, as the normally interacting H4 tails is acetylated<sup>34, 258</sup>. Further, employing ubiquitination assays using unmodified or H4K16ac chromatin arrays, directly allowed us to evaluate the effect of H4K16ac-mediated decompaction on chromatin ubiquitination.

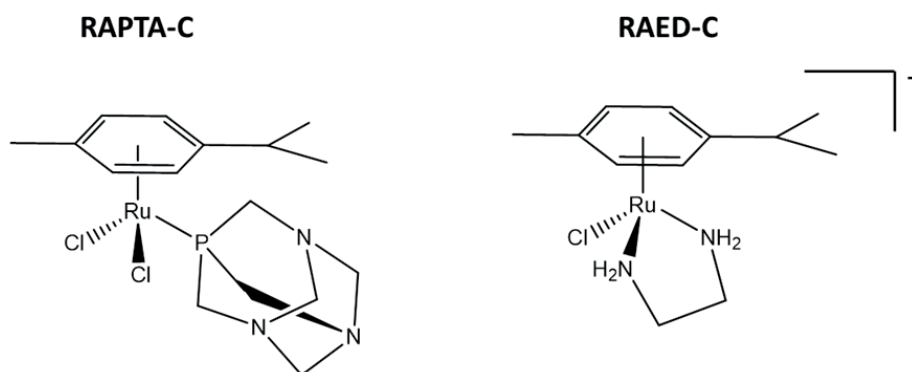


**Fig.65 Structure of RAPTA-C and the non-specific compound RAED-C**

Shown are the structural differences between RAPTA-C, which interacts with the nucleosome acidic patch and the non-interacting compound RAED-C.

We performed ubiquitination assays on 150-250 nM chromatin arrays containing unmodified (wt) histones, H4K16ac and including 250  $\mu$ M RAPTA-C or RAED-C (in wt chromatin) using RNF168(196). We compared the ubiquitination levels of H2A (based on Fluorescein-ubiquitin) over 60 min under the different conditions in 3-4 replicates of experiments. As the differences of ubiquitination in any condition were rather small, we analysed the SDS-PAGE gels using the band quantification tool of the software *Image Lab 4.1* (densitometry).

We quantified bands of mono-ubiquitinated- and di-ubiquitinated H2A. Indeed, H4K16ac chromatin fibres exerted faster ubiquitination kinetics than wt fibres, while RAPTA-C treated chromatin was ubiquitinated more slowly (Fig.66). The control compound RAED-C displayed ubiquitination kinetics of wt chromatin arrays. As the different replicates of experiments showed slightly different absolute values, which depends e.g. on pipetting or polymerization of the gels, we normalized the data to the first replicate. These values were analysed for ubiquitination of H2A under different conditions and statistically solidified our findings (Fig.67). Conclusively, we found that activity of RNF168 was compromised, when the nucleosome acidic patch was occluded by RAPTA-C, while activity was enhanced, when the acidic patch was openly accessible as mediated by H4K16 acetylation.

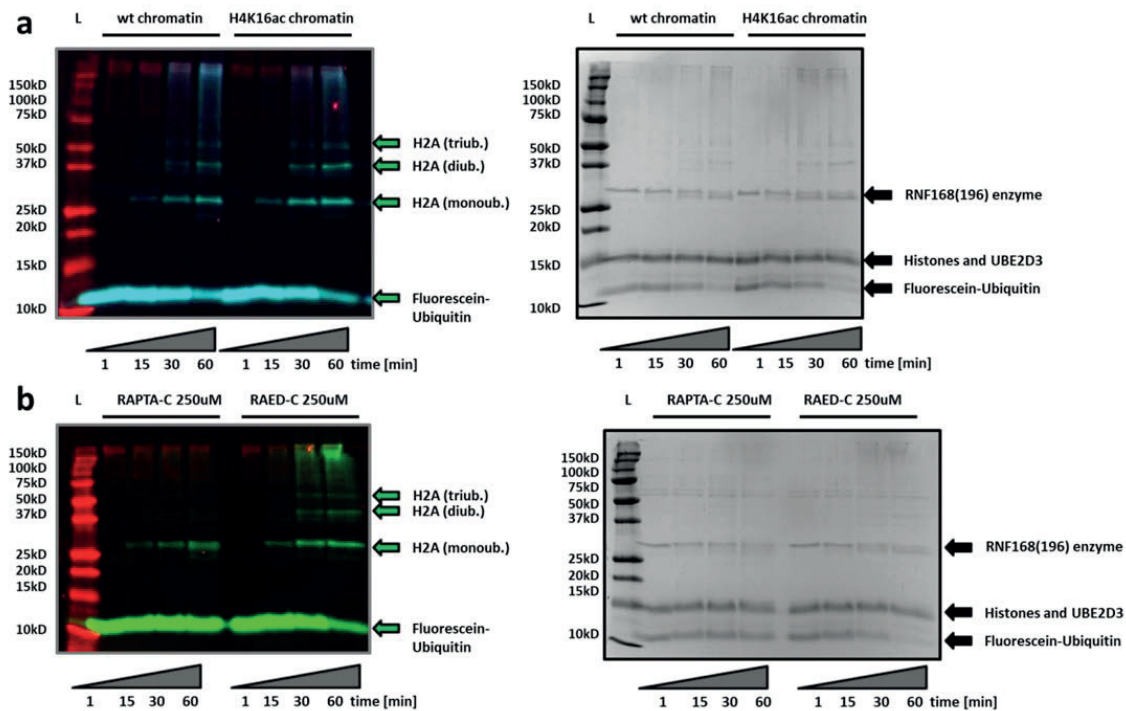


**Fig.66 Ubiquitination kinetics towards chromatin (wt and H4K16ac) and impact of RAPTA-C (wt chromatin)**

15 % SDS-PAGE gels to analyse H2A from chromatin arrays. Red: 640 nm (ladder), Green-Turquoise: 488 nm (Atto488-H2A). From 1 min to 60 min a defined ubiquitination pattern arises on H2A. L = protein standard. Ubiquitination speed was increased in chromatin arrays containing H4K16ac (**a**), while it was reduced in unmodified chromatin arrays containing 250 uM RAPTA-C (**b**). The control compound RAED-C did not alter ubiquitination kinetics. (n = 3).



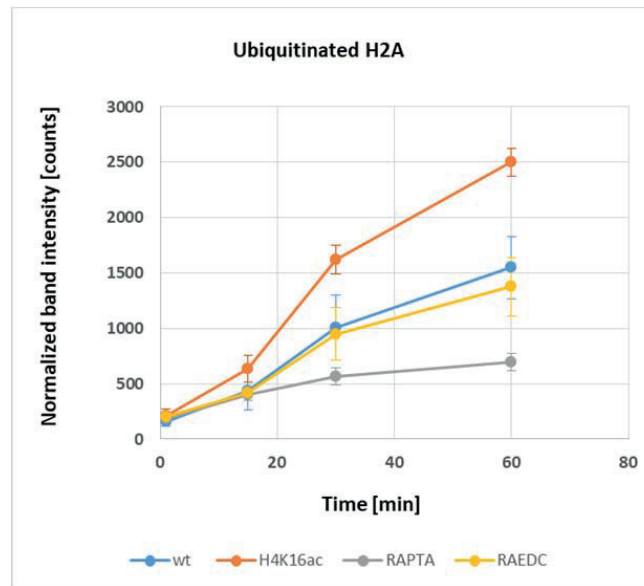


**Fig.67 Quantification of ubiquitination kinetics (unmodified and H4K16ac chromatin, RAPTA-C)**

Normalized ubiquitination of the 3-4 replicates using a band quantification tool summarizes faster kinetics of ubiquitination of H2A in chromatin fibres containing H4K16ac and reduced kinetics in unmodified fibres containing 250  $\mu$ M RAPTA-C. The control compound RAED-C reflected conditions of unmodified chromatin.

### 3.3.3. Testing UDM2 of RNF168 with semi-synthetic H2A.XK15ub

As for the H4K16ac mark, ubiquitination of H2B has been shown to sterically open up chromatin conformation<sup>23</sup>. As RNF168 possesses ubiquitin binding modules, we were wondering whether a chemically placed ubiquitin-moiety on histone H2A/H2A.X would enable facilitated ubiquitination and stimulate RNF168 activity. We planned to perform ubiquitination assays using RNF168 on chromatin arrays containing H2A.X or H2A.X with a pre-installed ubiquitin on the RNF168 target site lysine 15 (H2A.XK15ub). We reasoned that the second binding module of RNF168 has been shown to interact with H2A/H2A.X ubiquitination products (UDM2) and thus we concluded that we would need the full-length protein to perform these studies.

We decided to express the full-length RNF168 protein in a baculovirus-insect cell expression system. We designed a construct with an *in vivo* auto-cleavable N-terminal His-SUMO-tag, which enhances soluble expression, a downstream FLAG-tag for detection and purification, a C-terminal ybbr-tag for labelling, and a downstream STREP-tag for purification (His-SUMO-Flag-Thrombin-hRNF168(AA 1-571)-ybbr-TEV-STREP, short: RNF168F, Table A5). The human RNF168 gene was cloned into an acceptor plasmid (Pacebac1, gentamycin resistance) using Gibson cloning. The bacmid was created by transforming the Pacebac1-vector into DH10MB cells, followed by blue-white screening. Once the bacmid was obtained, we transfected Sf9 insect cells for baculovirus production. Protein expression was monitored by co-expression of YFP from the same baculoviral construct, driven under an alternative,

weaker promoter. RNF168 was expressed in Sf9 insect cells using Sf900 II medium for 4 days (multiplicity of infection (MOI) 5-7) (Fig.68).

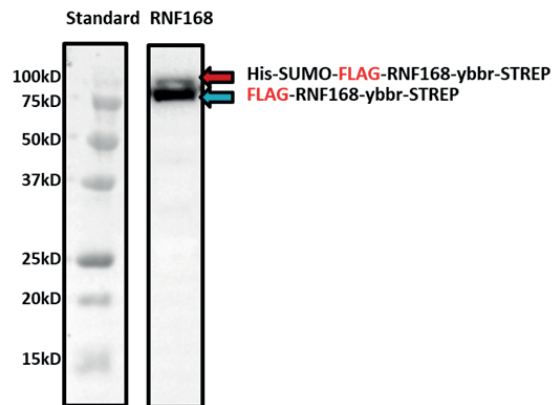


**Fig.68 Insect cell expression of full-length RNF168 for 4 days in Sf900 II medium**

Illustrated is an anti-FLAG western blot to show protein expression in cell lysates. The protein is expressed with the His-SUMO tag (red arrow), which is cleaved inside the cell and renders the target protein without His-SUMO (blue arrow).

Expected size: SUMO-HIS-FLAG-RNF168-ybbr-STREP: 83 kD, SUMO-HIS-FLAG-RNF168-ybbr-STREP: 70 kD (the protein typically runs at higher MW than expected).

Upon expression, the lysate was sonicated and a STREP-tag purification was done on Streptactin XT Superflow columns as a primary purification step (Fig.69a). TEV protease cleavage was performed to cleave off the C-terminal STREP-tag during 16 h at 4 °C. After cleavage, the sample was subjected to ybbr-labelling for 3.5 h using Alexa568-CoA (Fig.69b). To remove the remaining Alexa568-CoA, we performed a FLAG-affinity purification on magnetic FLAG-beads. (Fig.69c). Elutions were pooled and concentrated. The sample was flash frozen and stored at -80 °C until use (Fig.69d).

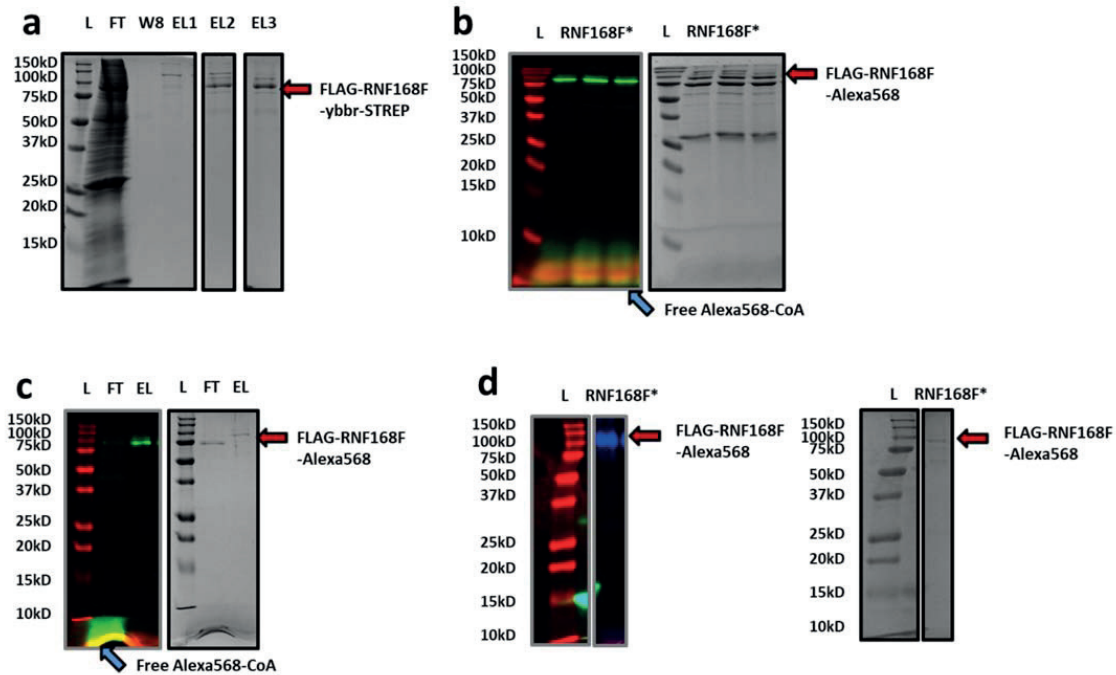


**Fig.69 Purification of full-length RNF168 (RNF168F)**

**a)** SDS-PAGE (Coomassie staining) of streptactin purification of RNF168F. The protein is eluted as a double band (83 kDa and 70 kDa) from EL3. L = protein standard, FT= flow through, W8 = Wash8, EL1-3 = elution 1-3. **b)** SDS-PAGE (Coomassie staining and fluorescence illumination (red: protein ladder, green: Alexa568)) of the ybbr-labelling of RNF168F after TEV cleavage. The protein is clearly labelled in all three lanes. L = protein standard. **c)** SDS-PAGE (Coomassie staining and fluorescence illumination (red: protein ladder, green: Alexa568)) of the FLAG purification. A single labelled band is obtained in the elution. L = protein standard, FT= flow through, EL = elution. **d)** SDS-PAGE (Coomassie staining and fluorescence illumination (red: protein ladder, blue: Alexa568)) of the final fraction of Alexa568-RNF168F (RNF168F\*). L = protein standard.

Ubiquitination assays were done to confirm activity of the labelled protein (Fig.70). More protein was purified without labelling. To do so, the procedure was stopped after the Streptactin purification.

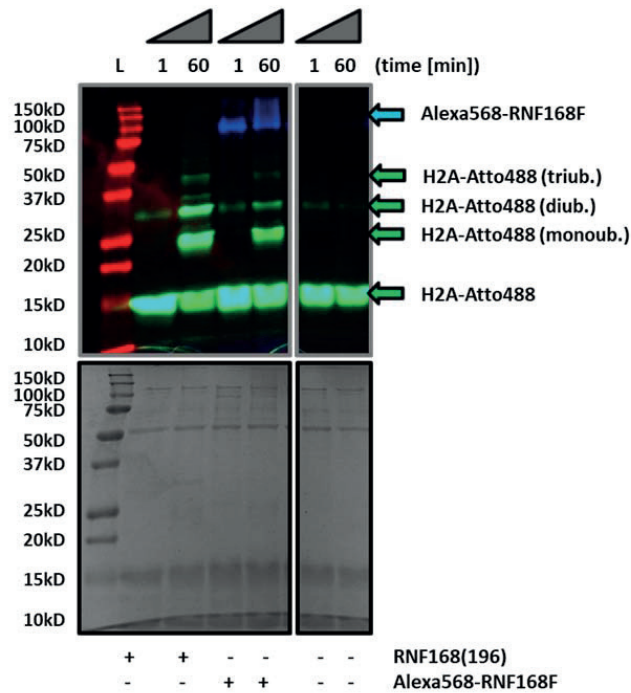


**Fig.70 Activity assay of RNF168F**

SDS-PAGE (Coomassie staining) and fluorescence illumination (red: protein ladder, blue: Alexa568, green: Atto488) of ubiquitination assay. The labelled RNF168F from insect cells shows activity. Activity was also seen in the control using RNF168(196). The Atto-488 labelled band at 25-37kD after 1min reaction time occurs based on an unexpected behaviour of old histone octamers. The Coomassie bands show the histone octamers (~15kD) and the bands of the UBE1 sample (100kD and 50kD). RNF168 was highly dilute and hardly visible without fluorescent label. L = protein standard.

Having the full-length RNF168 (RNF168F) version with high activity available enabled us to further analyse the ubiquitination kinetics of chromatin arrays bearing H2A.X and H2A.XK15ub. The chemical ubiquitin modification of H2A.X was done by Sinan Kilic<sup>259</sup>. We performed ubiquitination assays employing RNF168F on 100nM chromatin fibres of each histone type (12x nucleosome positioning sequences) (Fig.71a). Quantification of addition of a single ubiquitin molecule to each respective “chromatin ground state” (chromatin state at time point  $t = 0$  min) led to a significant increase at 13 min for the original H2A.X-chromatin array (Fig.71b). This indicates that the primary ubiquitin on H2A.X is not stimulating chain elongation in an accelerated manner, but rather decreases ubiquitination speed, compared to installation of the primary ubiquitin.

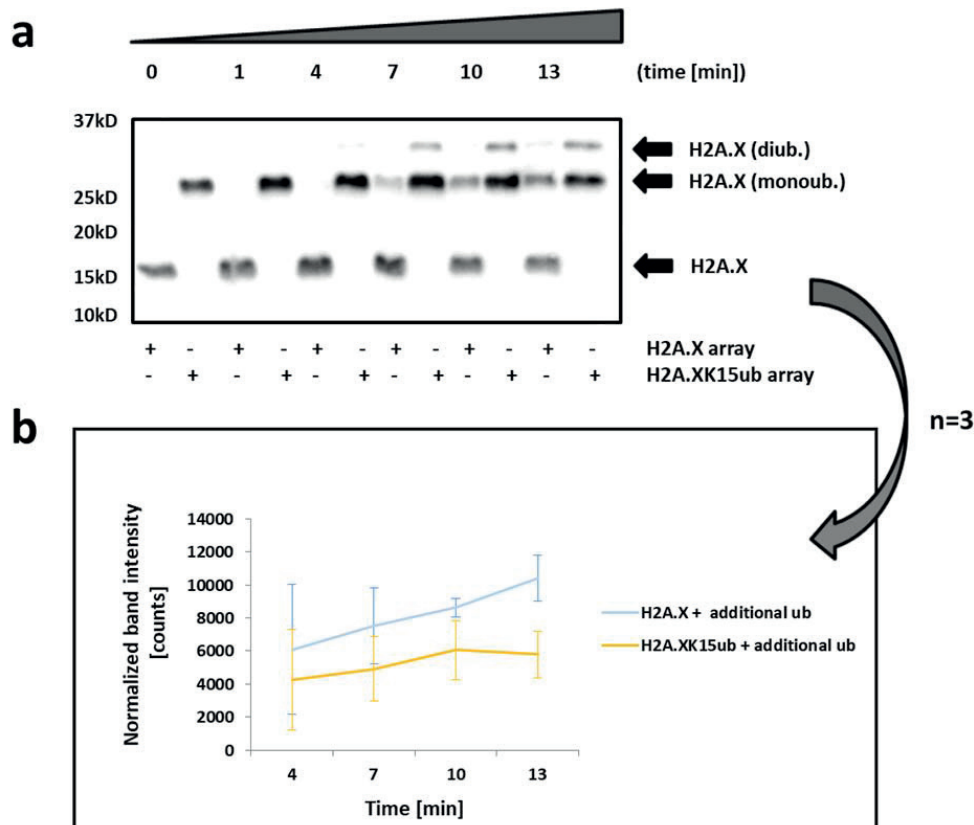


**Fig.71 Ubiquitination kinetics towards chromatin (100nM) containing H2A.X and H2A.XK15ub**

**a)** Anti-H2A.X western blot shows ubiquitination pattern by RNF168F on free H2A.X and pre-ubiquitinated H2A.X on lysine 15. (Shown is  $n = 1$  out of  $n = 3$ ). **b)** Quantification of single ubiquitin addition indicates small differences in ubiquitination speed for H2A.X and pre-modified arrays. At time point  $t = 13$  min single ubiquitin addition of the originally H2A.X array happened significantly faster compared to the originally H2A.XK15ub. (error bars: standard deviation,  $n = 3$  replicates,  $*P < 0.05$ , Student's t-test).

In summary, we successfully developed ubiquitination assays towards designer chromatin and characterized ubiquitination kinetics in dependence of the nucleosome acidic patch. Indeed, RNF168 activity was lowered, when the acidic patch was occluded by the anti-cancer compound RAPTA-C. In contrast, using H4K16ac chromatin arrays led to increased RNF168 ubiquitination activity over time, as the nucleosome acidic patch was rendered accessible, and chromatin conformation was decompacted<sup>34, 258</sup>. We further investigated ubiquitination kinetics in dependence of the H2AK15ub mark. Opposed to the hypothesis of increased RNF168-dependent ubiquitination velocity upon a primary ubiquitin mark on H2A.X, we did not observe a stimulating effect of a semi-synthetically installed ubiquitin mark.

In single molecule measurements, contributions of an additional binding domain can significantly influence protein binding to chromatin. In order to further understand the contribution of UDM1 and UDM2, we decided to investigate the behaviour of RNF168 towards K63-linked di-ubiquitin chains.

### 3.4. UDM1 of RNF168 is able to bind K63-linked ubiquitin chains

As we were not able to see a stimulating effect of H2A.XK15ub on RNF168 ubiquitination activity, mediated through UDM2, we sought to further investigate UDM1, which has been shown to interact with K63-linked ubiquitin chains on the linker histone H1.2<sup>48</sup>. Thus, we aimed to measure interactions between K63-di-ubiquitin and the UDM1 of RNF168 using pull-down experiments. Our strategy started with immobilization of GST-RNF168(AA 1-196) on the glutathione resin. We used the protein from bacterial lysates in order to obtain large amounts of a continuously covered RNF168 resin. 350-500 µl RNF168-resin were transferred to a Micro Bio-Spin™ Column per employed experimental condition and we applied 290 pmol di-ubiquitin (K48- or K63-linked, Boston Biochem) to the RNF168-resin. The resin was washed and elution fractions were collected. An anti-ubiquitin western blot was done for analysis (Fig.72a). Strikingly, GST-RNF168(196) was able to pull-down specifically K63-linked di-ubiquitin chains but not K48-linked chains (Fig.72b).

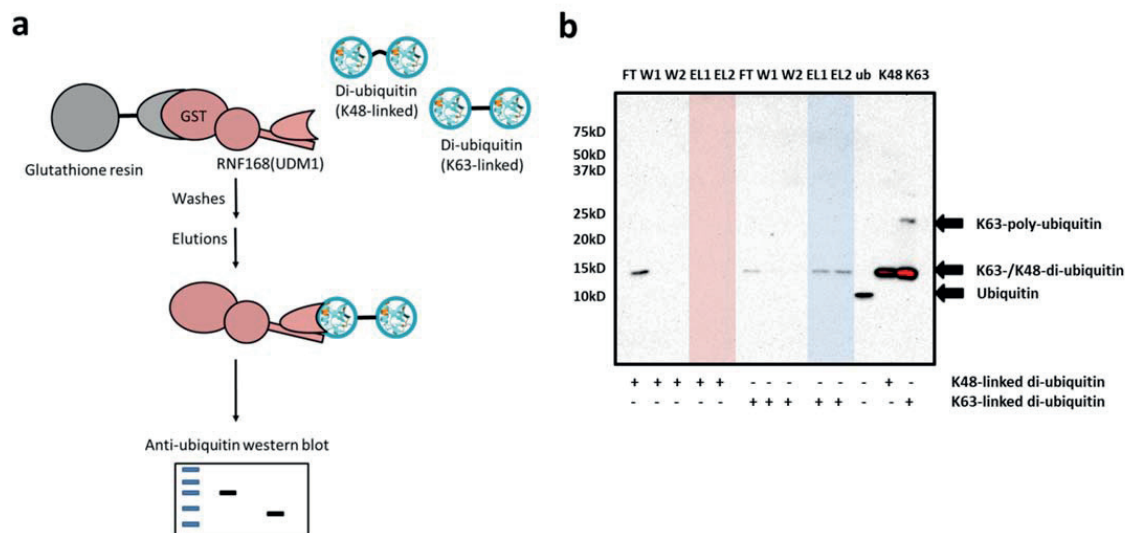


**Fig.72 Specific K63-linked-ubiquitin chain pull-down by GST-RNF168(196)**

**a)** Experimental strategy to test, if the UDM1 of RNF168 is able to pull-down K63-linked- or K48-linked di-ubiquitin. GST-RNF168(196) is immobilized on glutathione beads and di-ubiquitin variants are added in individual tubes. After wash steps, the GST-RNF168(196) is eluted together with interaction partners. **b)** Anti-ubiquitin western blot shows a specific enrichment of native K63-linked di-ubiquitin (blue), but not K48-linked di-ubiquitin (red). FT = flow through, W1-2 = Wash1-2, EL1-2 = Elution 1-2, ub = ubiquitin band, K48 = K48-di-ubiquitin band, K63 = K63-di-ubiquitin band. (n = 3).

As native ubiquitin chains are costly, we tested, in collaboration with the Marx laboratory (Joachim Lutz, University of Konstanz, Germany), whether GST-RNF168(196) was able to also recognize their synthetically modified ubiquitin chains (Fig.73a)<sup>260</sup>. We repeated the pull-down experiment for the native- and synthetic ubiquitin chains of both linkage types and observed specific pull-down for the K63-linked di-ubiquitin (Fig.73b). This was an interesting finding, as we could proof compatibility of the chemically linked ubiquitin chains



with a biologically relevant protein system. We note that the synthetic di-ubiquitin chains were not separated from chain formation products containing 3 or more ubiquitin moieties to perform this experiment.

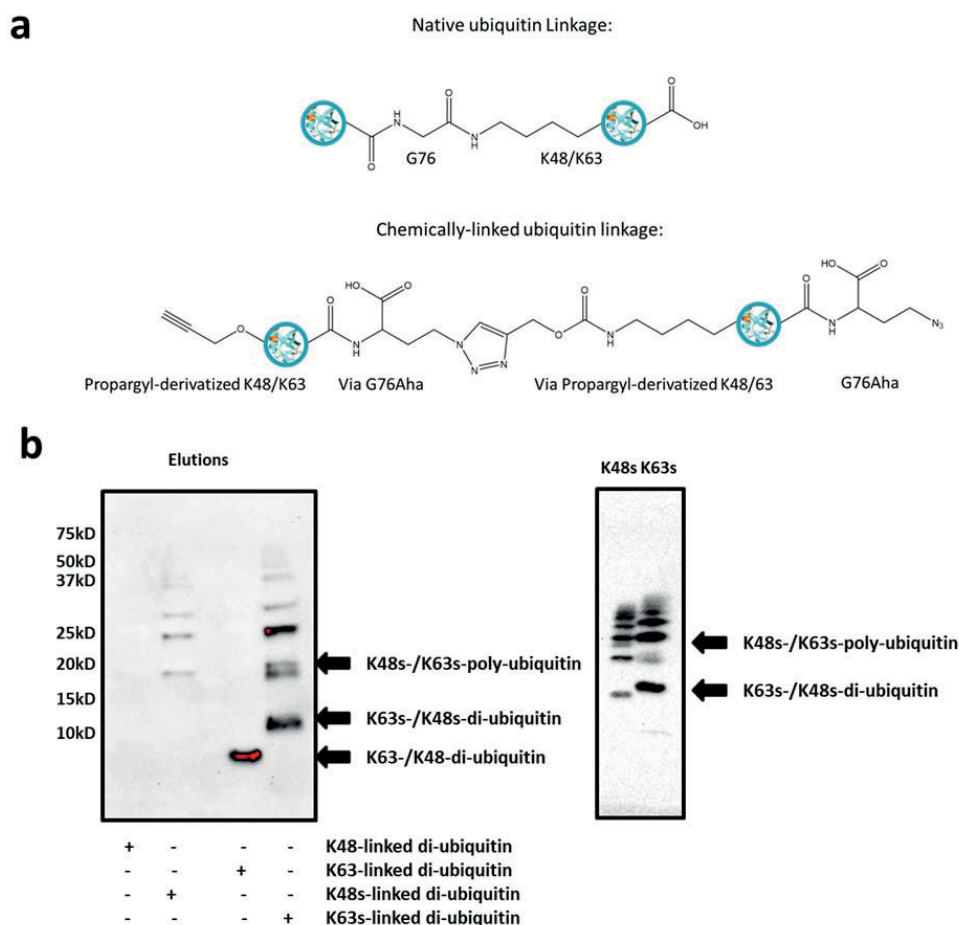


**Fig.73 Specific K63-linked-ubiquitin chain (native and synthetic) pull-down by GST-RNF168(196)**

**a)** Shown is the difference between native ubiquitin bonds and chemically linked ubiquitin bonds.

**b)** Anti-ubiquitin western blot shows a specific enrichment of native (K63) and synthetic (K63s) K63-linked di-ubiquitin, but not native (K48) or synthetic (K48s) K48-linked di-ubiquitin. , K48s = synthetic K48-ubiquitin chains, K63s = synthetic K63-ubiquitin chains. Synthetic di-ubiquitin was produced by Joachim Lutz. (n = 3)

It remains interesting to investigate, whether H1.2-K63-linked-di-ubiquitin can increase RNF168 ubiquitination activity and if it is possible to measure the behaviour of RNF168 in single molecule experiments containing the K63-linked ubiquitin in mononucleosomes or chromatin arrays. However, this is quite challenging as H1.2-monomonucleosomes are barely stable for 1 day at 4 °C.

### 3.5. Conclusion

We established an RNF168-dependend ubiquitination system to ubiquitinate chromatin fibres.

We report several findings concerning RNF168-mediated ubiquitination. First, activity of RNF168 was dependent on the steric availability of the nucleosome acidic patch. When the acidic patch was occluded (RAPTA-C) or rendered accessible (H4K16ac), the ubiquitination kinetics, based on mono- and di-ubiquitination, were altered. This was consistent with studies employing a LANA-peptide to occlude the nucleosome acidic patch<sup>35, 261</sup>. Second, it was unclear whether primary ubiquitination of H2A.X would prime RNF168 or RNF8 for ubiquitin chain elongation. We reject the hypothesis of accelerated ubiquitination of H2A.X by RNF168 upon installation of a primary ubiquitin-moiety on the lysine 15 residue. Third, we were able to reproduce binding of RNF168(196) to K63-linked di-ubiquitin, but not K48-linked di-ubiquitin, and we showed that RNF168(196) is also able to specifically bind chemically linked K63-di-ubiquitin, but neither chemically modified K48-linked di-ubiquitin<sup>48</sup>. This underlines the importance of chromatin recognition by the UDM1 and shows that chemically modified ubiquitin chains are useful for meaningful studies in combination with native proteins, although they cannot be hydrolysed by DUBs<sup>260</sup>. Conclusively, we shed light onto different aspects of RNF168-mediated ubiquitination in bulk measurements, which forms the basis to study RNF168 on the single molecule level.



### III Conclusions and Discussion

Understanding the recruitment- and regulation mechanisms of proteins by chromatin PTMs and the chromatin compaction state in healthy cells is an essential step to elucidate the mechanisms abrogated in neurodegenerative diseases and cancer. In the cell, accessibility and availability of chromatin by effector proteins is often mediated through networks of proteins and multiple histone PTMs, which leads to fine-tuned signalling cascades, rather than a stringent “on-and-off” state. An example is shown by the distinction between HR and NHEJ during the DDR, which contains numerous regulators and allows directing towards either an error-prone or error-sensitive DNA repair mechanism. Regulation of this process is most likely dependent on the cell cycle, as error-prone DNA repair during replication could induce deleterious effects<sup>142</sup>.

Here, we aimed to dissect and study chromatin-protein interactions in different model systems using a bottom-up approach, where we built designer chromatin fibres and a defined protein system employing TIRFM. We have shown ability to immobilized single chromatin fibres in flow channels on a microscopy glass slide, which can be visualized as distinct fluorescence spots, without disintegration of the chromatin fibres. Addition of fluorescently labelled effector proteins under suitable imaging conditions allowed us to monitor dynamics of the protein of interest towards defined sets of chromatin fibres bearing histone modifications. Opposed to bulk measurements, here we were able to completely control our imaging system by chemically modifying chromatin or mutating interacting proteins and we obtained dynamic information.



# 1. HP1 $\alpha$ is a highly dynamic, multivalent chromatin reader

Establishment and maintenance of heterochromatin is essential to maintain proper cell function. An important factor involved in heterochromatin regulation is the HP1 $\alpha$  protein. In order to gain insight how HP1 $\alpha$  mechanistically interacts with chromatin, we applied TIRFM to investigate proposed binding models and dissect the different binding modes of HP1 $\alpha$  by altering available binding sites on chromatin, the amount of reader domains within one protein unit or the protein concentration in solution.

In a first set of measurements, we tested a simple binding model of HP1 $\alpha$  association/dissociation, which recognizes H3K9me3 during heterochromatin formation and we obtained kinetic values in the second to millisecond timescale. Residence times on chromatin were characterized by two exponential processes, the short phase reflecting simple HP1-H3K9me3 interactions, while the long phase events were attributed to multimeric interactions<sup>186, 192</sup>. By altering the number of available H3K9me3-binding sites, either using mononucleosomes or chromatin arrays with reduced H3K9me3 sites, we learned that indeed availability of multiple binding sites in close vicinity allowed microdissociation and rapid rebinding events. Consistently, when the CD was mutated in HP1 $\alpha$ , protein dynamics resembled the conditions without H3K9me3 marks. We reasoned that in the presence of multiple H3K9me3 marks and a high concentration of HP1 $\alpha$  molecules, the proteins would be able to form an oligomeric complex<sup>45, 70</sup>. However, when we increased the concentration of HP1 $\alpha$  by adding unlabelled competitor protein, we observed a decrease in residence times and thus accelerated dynamics, known as facilitated dissociation. Importantly, we performed our experiments using human HP1 $\alpha$  and not the yeast homolog Swi6, which had been implicated in the oligomerization model<sup>45</sup>. We explain these contradictory results by a distinct difference in sequence homology, as Swi6 contains an extended  $\alpha$ -helix in its CD as well as a lysine containing loop, which both were proposed to represent an additional site of interaction<sup>206</sup>.

The estimated HP1 $\alpha$  concentration in cells is 0.5-1  $\mu$ M, dependent on the chromatin compartment<sup>69</sup>. Based on the  $K_D$  of the CSD (0.5-5  $\mu$ M), we expect a large fraction of cellular HP1 $\alpha$  to be monomeric<sup>201, 262</sup>. Cells circumvent this problem by CSD-affinity ligands, as hSgol1, which interact with HP1 $\alpha$  proteins and lead to dimerization<sup>59</sup>. We tested a hSgol1-based interaction peptide (**P3**) towards the HP1 $\alpha$ -H3K9me3 chromatin system. Strikingly, we observed a specific increase in residence time, when the peptide was present. These results coincided with FRAP experiments including an HP1 $\alpha$  variant with a point mutation in the CSD, as a larger mobile fraction of HP1 $\alpha$  was observed, compared to the wt protein. To covalently link HP1 $\alpha$  as a dimer, we developed an EPL-based approach to link the two HP1 $\alpha$  moieties with another hSgol1-based peptide (**P2**). Single molecule dynamics of the obligatory dimeric HP1 $\alpha_{\text{cdm}}$  unveiled an increase in residency times, which was comparable to the experiment using the dimerization peptide **P3**.

Altogether, these experiments show how human HP1 $\alpha$  interacts dynamically and highly competitively with heterochromatin (H3K9me3), dependent on available binding sites, HP1 $\alpha$  protein concentration and the dimerization state of HP1 $\alpha$ . We verified the proposed binding models showing microdissociation with rapid rebinding, facilitated dissociation and dimeric protein binding. Further, our findings on the HP1 $\alpha$ -H3K9me3 model validated the functionality of our developed platform to measure single molecule protein-chromatin interaction dynamics.

We examined the impact of HP1 $\alpha$  multivalency towards H3K9me3- chromatin binding, we just started to understand the most essential binding mechanisms and thus it was highly interesting to further investigate other contributing factors for HP1 $\alpha$  binding. In a further leading project, we investigated different linker lengths between nucleosomes and different chromatin compaction states using H4K16ac-chromatin to study an open chromatin conformation and H1.1-chromatin to investigate compacted chromatin<sup>14, 18, 23, 192, 263, 264</sup>. As expected, binding experiments using H4K16ac-modified chromatin arrays led to a decrease in residency time, while H1.1-chromatin led to prolonged residency times<sup>192</sup>. Further, we found evidence that DNA interactions were essential to mediate efficient H3K9me3-chromatin binding, based on experiments including HP1 $\beta$ , HP1 $\gamma$ , which have been shown to exert significantly reduced binding to DNA compared to HP1 $\alpha$ <sup>265</sup>. Moreover, phosphorylation of HP1 also contributed to DNA-mediated H3K9me3-chromatin binding<sup>192</sup>. All these findings allowed to invoke a kinetic model with applied simulations, which revealed the predominant binding pathways of HP1 $\alpha$  being involved in DNA bound states<sup>192</sup>.

## 2. A winged-helix motif of PHF1 facilitates prolonged residence time of PRC2 on chromatin and DNA

Ability to measure single-molecule dynamics in the HP1 $\alpha$  model system prompted us to employ an alternative system using a protein complex involved in heterochromatin formation. As the Müller laboratory was experienced in purification, labelling and characterization of PRC2, we sought to apply their protein system onto our single molecule platform. The goal was to study the effect of the polycomb accessor protein PHF1 towards chromatin binding of PRC2.

By comparing single molecule binding experiments applying PRC2 with- or without PHF1 using chromatin, mononucleosomes or DNA as a substrate, we detected an increase in residence time, when PHF1 was present. Similar results were obtained in EMSA, which enabled us to determine the  $K_D$ -values of chromatin interactions. To mechanistically explain the anchoring effect of PHF1, we repeated these experiments with a small C-terminal fragment of PHF1 only and we obtained results comparable to PRC2 experiments without PHF1. Our colleagues were able to crystallize Pcl1 and identified a previously predicted WH domain. When we tested a defined WH mutant, we confirmed importance of the mutated residues, as we obtained binding kinetics as for the PRC2-only condition. Finally, HMTase assays with reduced H3K27 methylation activity using the same WH mutant, led us to the conclusion that PHF1 is important to anchor PRC2 onto chromatin via the WH domain of PHF1 and thus allows efficient H3K27 methylation.

In a next step, we measured binding dynamics of PRC2 towards modified chromatin. This included the H3K27me3, which can be recognized by the reader domain of EED, the oncogenic mutation H3K27M and the H3K36me3 mark for actively transcribed chromatin<sup>72, 81, 216</sup>. Interestingly, we observed increased residency times for all the different chromatin modifications and an increased association rate in conditions including the H3K36me3 mark. Enhanced binding towards H3K27me3 was expected, as PRC2 is a writer and reader of this chromatin mark. However, we expected further prolonged binding of PRC2 towards the H3K27M mutation. This was not the case, most likely due to the fact that we did not add the cofactor SAM, which has been shown to be required for a strong effect of H3K27M on PRC2 binding<sup>80</sup>. Rejecting our initial hypothesis, the H3K36me3 mark increased residency times of PRC2 towards chromatin. Importantly, PRC2 is also responsible to drive catalysis of H3K27me1 and H3K27me2<sup>266, 267</sup>. We explain our results by the positive correlation of H3K36me3 and H3K27me1 at active transcription sites, as H3K27me1 is most likely driven upon H3K36me3-mediated reduction of PRC2 activity<sup>216, 223</sup>. The ambiguous role of H3K36me3 in PRC2-recruitment and -function, either to establish H3K27me1 or H3K27me3, raises the question how PHF1 affects PRC2 recruitment to H3K36me3 chromatin. Presence of PHF1, which has been able to bind H3K36me3 and subsequently leads to suppression of H3K27 methylation, might reflect a key regulatory mechanism to determine, if high or low activity of PRC2 is required, based on the surrounding histone landscape<sup>216</sup>.

In summary, we measured prolonged binding of PRC2 by PHF1 to chromatin. We showed that mainly DNA interactions were responsible for the anchoring effect of PHF1, as measurements using naked DNA unveiled even longer residency times than on chromatin. Moreover, we found that a WH domain in Polycomblike proteins, was essential to prolong PRC2 binding on chromatin or DNA and we observed increased residency times of PRC2 for H3K27me3-, H3K27M- and H3K36me3-modified chromatin arrays using TIRFM.

### 3. K63-linked ubiquitin chains recruit RNF168 to chromatin via UDM1 and allow ubiquitination of H2A/H2A.X dependent on the nucleosome acidic patch

We then extended our studies to a chromatin mark writer, by applying a third binding model employing RNF168, which ubiquitinates H2A/H2A.X in the DDR. We first needed to establish an ubiquitination system towards chromatin to study the mechanistic details. We established expression and purification of UBE1 and UBE2D3 at high activity. Further, we expressed and purified human ubiquitin at high levels and attached a cysteine site for ubiquitin labelling. Finally, we refined protocols to express, label and purify RNF168 at high activity. Expression of the truncated version (RNF168(196)) was possible in bacteria, while expression of the full-length protein (RNF168F) was only achieved in insect cells.

Production of these ubiquitination cascade components allowed us to perform ubiquitination assays on histone octamers and chromatin arrays containing distinct modifications.

We tested RNF168(196)-mediated ubiquitination of chromatin arrays in dependence of the H4K16ac mark, which sterically opens up chromatin and renders the nucleosome acidic patch accessible<sup>14, 34</sup>. Using a fluorescent readout, we showed that chromatin arrays containing H4K16ac were ubiquitinated faster than non-modified arrays. A recently published anti-cancer agent, RAPTA-C, has been shown to interact with the nucleosome acidic patch<sup>255</sup>. We thought that the anti-cancer activity of RAPTA-C might be mediated by competitive inhibition of the nucleosome acidic patch towards RNF168. Based on our findings in H4K16ac chromatin fibres, we tested the effect RAPTA-C (at 250  $\mu$ M) in RNF168-mediated ubiquitination assays. Consistently, we observed a reduction in ubiquitination when RAPTA-C, but not a control compound RAED-C was present. A concentration of 250  $\mu$ M RAPTA-C corresponded to the IC<sub>50</sub>-value in the A2780 cancer cell line<sup>255</sup>. However based on the relatively weak (2-fold) decrease in ubiquitination kinetics compared to control conditions (wt- or RAED-C), using a system without cellular barriers or compound degradation, we concluded that the anti-cancer activity of RAPTA-C might not solely result from inhibition of RNF168 activity.

As RNF168F is able to bind ubiquitinated H2A/H2A.X, we wondered whether pre-installed ubiquitin on H2A.XK15 would accelerate ubiquitination kinetics towards attachment of an additional ubiquitin moiety<sup>128</sup>. In our laboratory we recently established chemical ubiquitination of H2A.X at residue K15 as published in Kilic et al., 2018<sup>259</sup>. We performed ubiquitination assays towards chromatin containing either H2A.X or H2A.XK15ub and measured addition of the first ubiquitination moiety using anti-H2A.X western blots. After several minutes, this rendered a slight increase of ubiquitination, when no ubiquitin was installed on H2A.X at the beginning of the reaction. This supported the current

hypothesis that ubiquitin chain elongation might be driven by RNF8, as the initial ubiquitin mark on H2A.X did not stimulate activity of RNF168 towards ubiquitin chain formation<sup>128</sup>.

As we managed to ubiquitinate chromatin fibres *in vitro*, we started to transfer the ubiquitination system to the single molecule level. In comparison to the HP1 $\alpha$ - or PHF1-PRC2-system, DNA-mediated interactions are not the primary recruitment factor for RNF168, which would enhance its chromatin binding affinity<sup>35</sup>. Interestingly, when we performed pulldown experiments with RNF168(196) towards either native or chemically linked (in collaboration with the Marx laboratory) K63-di-ubiquitin, we detected a ubiquitin signal, which indicated interaction. A similar signal was not observed when K48-linked di-ubiquitin was employed. Based on these results we are convinced that K63-linked interactions might be relevant to recruit RNF168 to chromatin fibres. However, the DDR-relevant target protein to incorporate K63-linked ubiquitin chains on nucleosomes is histone H1.2<sup>48</sup>. This complicates our studies significantly, because it is challenging to incorporate K63-linked di-ubiquitin chains on H1.2. Work is ongoing to incorporate H1.2-di-ubiquitin (which was produced by Joachim Lutz, Marx laboratory, Konstanz, Germany) into nucleosomes. We are convinced that nucleosome particles containing H2A.XK15ub with H1.2-K63-linked-di-ubiquitin would enable recruitment of RNF168 in TIRFM, mediated through bivalent binding.



## 4. Concluding remarks

With regard to all three different protein systems, we established a method to join chemical biology and biophysics by chemically modifying chromatin and proteins to trace their dynamic interactions on the single molecule level. This method enabled us to validate different binding models of HP1 $\alpha$  and PRC2. Although, we were not yet able to study RNF168 on the single molecule level, we expressed and characterized the protein in bulk assays, which will help to understand how our experimental system can be optimized to study RNF168 or other E3 ubiquitin ligases.

For both, HP1 $\alpha$  and PRC2, we identified crucial protein-DNA interactions to ensure stable chromatin binding and this phenomenon has also been seen for other chromatin effectors as SUV39H1, PRC1 and BRDT, in addition to the PTM reader domains<sup>192, 268-271</sup>. These findings point towards essential regulatory mechanisms through multivalent chromatin binding via one or several specifically modified residues or non-specific properties of the nucleosome as e.g. DNA binding. We reasoned that this might also be true for RNF168, where an integrated action of K63-linked ubiquitin chains of a substrate X, ubiquitination of H2A/H2A.X and accessibility of the nucleosome acidic patch are required for stable localization of the protein towards chromatin and ubiquitination activity.



## IV Material and Methods

Some subchapters of “Material and Methods” were described as published (Kilic et al., 2015 and Choi et al., 2017)<sup>186, 207</sup>.

### 1. Materials

A list of the material used in the discussed projects can be found in “VI Appendix” for antibodies (Table A1), materials (Table A2) and equipment (Table A3). Information to the suppliers is given in Table A4.

DNA oligos were purchased from Integrated DNA technologies (IDT, Iowa, USA). Sequencing of plasmids was done by Fasteris (Geneva, Switzerland). Fluorescent dyes were purchased from ATTO-TEC GmbH (Siegen, Germany). Single-point mutations were done using a QuikChange II XL site-directed mutagenesis kit from Agilent (Basel, Switzerland). Bacterial cells for recombinant protein expression were grown in an HT infors AG incubator (Basel, Switzerland). Manual peptide synthesis and reactions on a solid-phase were carried out in reaction vessels from Peptide International Inc. (KY, USA) and automated peptide synthesis done on a Tribute instrument from Peptides International Inc. Amino acid derivatives and resins were purchased from Novabiochem, Merck (Hohenbrunn, Germany). Peptide synthesis (and EPL) solvents and reagents were from Acros Organics (Geel, Belgium) (dimethylformamide, dichloromethane, N,N-diisopropylethylamine and piperidine) or Protein Technologies Inc. (Tucson, AZ, USA) (HBTU). Cation- and anion exchange purification was done using HiTrap SP HP (5 ml) and HiTrap Q FF (1 ml) trap from GE Healthcare. Analytical RP-HPLC was performed on an Agilent Zorbax C18 column, employing 0.1 % TFA in water (RP-HPLC solvent A) and 90 % acetonitrile, 0.1 % TFA in water (RP-HPLC solvent B), as the mobile phases. Typical analytical gradients were 0-70 % solvent B over 30 min at flow rate 1 ml/min. Preparative scale purifications were conducted on an Agilent 1260 preparative HPLC system. A Zorbax C18 preparative column (7 µm, 21.2 x 250 mm) or a semi-preparative column (5 µm, 9.4 x 250 mm) was employed at a flow rate of 20 ml/min or 4 ml/min, respectively. Fluorescence spectra measurements were carried out with a Fluorolog®-3 Horiba Jobin Yvon spectrofluorometer (Kyoto Japan). Live-cell confocal microscopy was done on a LSM700 inverted microscope from Zeiss. For single-molecule TIRF microscopy a Nikon Ti-E inverted fluorescence microscope, controlled by NIS-elements, equipped with a CFI Apo TIRF 100x Oil immersion objective (NA1.49) was used.



## 2. Methods

Herein, we discuss the methods, which were applied during this study.

### 2.1. SDS-polyacrylamide gel electrophoresis

#### **Casting gels:**

Typically, a 15 % running gel using acrylamide / bis solution (30 %, 1:29) was poured. For polymerization with ammonium persulfate and TEMED the gel was covered with an isopropanol layer. Then, a 5 % stacking gel was poured onto the top of the running gel.

#### **Running conditions:**

Samples (5-10  $\mu$ l) for SDS-PAGE were combined with 12  $\mu$ l SDS-loading dye (62.5 mM Tris-HCl pH 6.8, 25 % (v/v) glycerol, 2 % (w/v) SDS, 0.01 % bromophenol blue) and boiled at 95 °C for 5 min. Gels were run in 1x Tris-glycine-SDS buffer (25 mM Tris-HCl pH 8.3, 192 mM glycine, 0.5 % (w/v) SDS) for 50-60 min, 200 V, RT. Fluorescence images were taken, if required, on a ChemiDoc™ MP imaging system.

#### **Coomassie staining:**

After electrophoresis, Brilliant blue R250 solution (0.05 % (w/v) brilliant blue R250, 45 % (v/v) methanol, 10 % (v/v) acetic acid) was added to the gel for 45 min, RT, agitating. The gel was destained using water or Coomassie destaining solution (47.5 % (v/v) methanol, 10 % (v/v) acetic acid) for 1 h, RT, agitating.

#### **Colloidal Coomassie staining:**

After running the SDS-PAGE gel, it was fixed for 1 h in fixing solution (40 % (v/v) ethanol, 10 % (v/v) acetic acid). Then 2x 10 min washes in MiliQ (MQ) water were performed. The gel was stained using QC Colloidal Coomassie staining solution (Cat#: 161-0803, Bio-Rad) at RT, 1 h or overnight, agitating. Destaining using 1 % (v/v) acetic acid was done for 1 h, RT, agitating. Images were taken on a ChemiDoc™ MP imaging system.

### 2.2. Western blotting

#### **Western transfer:**

A western transfer of an SDS-PAGE gel was done by assembling the “sandwich”: A PVDF membrane was activated for 30-60 s in methanol, rinsed with water and kept for 5 min in Western running buffer (25 mM Tris-HCl pH 8.3, 192 mM Glycine, 0.5 % (w/v) SDS), 10-20 % (v/v) methanol). The membrane was placed on the positive plate (red) and covered with the SDS-gel, which was placed on the negative plate (black). Transfer conditions were 200 mA, 2.-2.5 h, 4 °C in Western running buffer.

**Western blotting:**

The membrane was blocked for 1 h, RT, agitating, using 5 % milk in TTBS or 5 % BSA fraction V in TTBS buffer (50 mM Tris-HCL pH 7.6, 150 mM NaCl, 0.05 % (v/v) tween 20). After a TTBS wash, the primary antibody (1:1000-1:2000) was added in a solution of TTBS containing 1-2 % milk or 2 % BSA fraction V and the membrane was kept under agitation at RT for 1 h. After 3x6 min TTBS washes, the secondary antibody (anti-mouse 1:5000, anti-rabbit 1:10'000) HPR-linked antibody was added under agitation at RT for 50 min. After 3x5 min TTBS washes and a 1x5 min TBS (50 mM Tris-HCL pH 7.6, 150 mM NaCl) wash, the membrane was incubated for 1-5 min in the dark with a 1:1 solution of Clarity™ Western ECL Blotting Substrates. This was followed by subsequent imaging of the membrane using a ChemiDoc™ MP imaging system. If the membrane was subjected to a different set of antibodies, mild membrane stripping was performed: The membrane was washed 2x5 min in stripping buffer (200 mM glycine, 0.1 % SDS, 1 % tween 20, pH 2.2), then 2x10 min in TTBS and 2x5 min in TTBS.

## 2.3. Agarose gel electrophoresis

**Casting agarose gels:**

0.7-2 % agarose gels were poured by adding agarose to 1x TBE buffer (90 mM Tris-HCl, 89 mM boric acid, 2 mM EDTA (pH 8.0)) and dissolving it using microwave heating.

**Running conditions:**

Gels were pre-run for 10 min at 110 V (5-10 min, RT). Samples were completed with 6x DNA loading dye (30 % (v/v) glycerol, 0.25 % (w/v) bromophenol blue, pH 8.0) and after loading onto the gel, electrophoresis was done at 110 V (40 min, RT) in 1x TBE buffer. After the run, fluorescence images were taken, if required, on a ChemiDoc™ MP imaging system. Then gels were stained for 10-30 min in GelRed solution (15 ul GelRed per 50 ml MiliQ (MQ) water). GelRed images were taken on a ChemiDoc™ MP imaging system.

## 2.4. Cloning

### 2.4.1. CPEC

**Primer design and PCR protocols:**

Circular polymerase extension cloning (CPEC) is a scarless and largely sequence-independent cloning method<sup>272</sup>.

For CPEC, we designed 4 primers containing a ~20 bp overhang of the insert piece and the vector piece, respectively. Such primers were also used to insert start/stop codons

and small tags and protease cleavage sites. Melting temperatures for the part that anneals with the insert/vector were determined using the following website:

[http://www.bioinformatics.org/sms2/pcr\\_primer\\_stats.html](http://www.bioinformatics.org/sms2/pcr_primer_stats.html), 20.11.2014

Primers, which were used to find a target sequence from the lab-intern HeLa cDNA library were BLASTed in order to avoid off-target amplification using the following website:

<http://blast.ncbi.nlm.nih.gov/Blast.cgi>, 31.08.2017

For linearization of fragments the following PCR reactions were usually done:

<b>Table M1 PCR reaction for vector of interest (CPEC)</b>			
Component	stock	Vol used (ul)	Final conc.
Template DNA	1 ng/ul (plasmid)	11 ul	0.1 ng/ul
FWD primer	10 uM	5.5 ul	0.5 uM
REV primer	10 uM	5.5 ul	0.5 uM
dNTP	10 mM	2.2 ul	0.2 mM
DMSO	-	3.3 ul	-
water	-	59.4 ul	-
Phusion HF buffer	5 x	22 ul	1 x
Phusion Polymerase	2 U/ul	1.1 ul	-

<b>Table M2 PCR reaction for insert of interest (CPEC)</b>			
Component	stock	Vol used (ul)	Final conc.
Plasmid or cDNA library	Concentration of cDNA library was unknown	5 ul	???
FWD primer	10 uM	2.5 ul	0.5 uM
REV primer	10 uM	2.5 ul	0.5 uM
dNTP	10 mM	1 ul	0.2 mM
DMSO	-	1.5 ul	-
water	-	27 ul	-
Phusion HF buffer	5 x	10 ul	1 x
Phusion Polymerase	2 U/ul	0.5 ul	-

<b>Table M3 PCR program for vector/insert of interest (CPEC)</b>			
Step	T	time	cycle
denaturation	95 °C	30 s	1
denaturation	95 °C	10 s	30-31
Annealing	66 °C (depends on primer)	15 s	
Extension	72 °C (depends on polymerase)	30 s per kb	
Final extension	72 °C	5 min	1
Hold	4 °C	forever	-

The PCR product was usually analysed on an agarose gel (0.7 %) and then a DpnI enzyme digestion was done at 37 °C, 2 h to get rid of the starting plasmid. To obtain pure fragments a PCR purification kit (Qiagen) was used following the manufacturer's protocol if the reaction was pure. If one of the reactions was not rendering a single band, we excised the band of interest from an agarose gel and used a gel extraction kit (Qiagen) for purification.

<b>Table M4 CPEC PCR reaction: 2x25 ul (one reaction serves as control without the polymerase)</b>			
Component	stock	Vol used (ul)	Final conc.
Linear vector DNA	13.2 ng/ul	16 ul	4 ng/ul
Linear insert DNA	26.7 ng/ul	3 ul	1.6 ng/ul
dNTP	10 mM	2 ul	0.4 mM
DMSO	-	1.5 ul	-
water	-	17.5 ul	-
Phusion HF buffer	5 x	10 ul	1 x
Phusion Polymerase	2 U/ul	0.5 ul / -	-

<b>Table M5 CPEC PCR program</b>			
Step	T	time	cycle
denaturation	98 °C	3 min	1
denaturation	98 °C	30 s	3
Annealing	66 °C	30 s	
Extension	72 °C (depends on polymerase)	2 min	
Final extension	72 °C	10 min	1
Hold	4 °C	forever	-



### Transformation into bacteria:

5 µl product of the CPEC reaction were mixed with 50 µl DH5α competent cells and were incubated on ice for 15 min. In a waterbath (42 °C) a heat shock was performed for 40 s, then the sample was placed on ice for 2 min. 900 µl SOC medium (2 % (w/v) tryptone, 0.5 % (w/v) yeast extract, 2.5 mM KCl, 10 mM MgSO<sub>4</sub>, 20 mM glucose, in MQ water, pH 6.8-7.0) was added to the bacteria and they were grown at 37 °C for 1 h. Bacteria were centrifuged for 1 min, 15'000 rpm, RT and they were plated on LB agar plates containing the corresponding antibiotics (ampicillin: 100 µg/ml, kanamycin: 50 µg/ml, gentamycin: 10 µg/ml, tetracycline: 10 µg/ml).

Typically, the obtained colonies were expanded in 5 ml LB broth containing antibiotics and the cultures were subjected to a miniprep (Qiagen). The final plasmid was often sent for sequencing to verify successful cloning.

## 2.4.2. Gibson cloning

### Primer design and PCR protocols:

Gibson cloning is generally very similar to CPEC cloning. One disadvantage is the cost, as three different enzymes are required (T5 exonuclease, Phusion polymerase and Taq ligase), but it is advantageous over CPEC as less polymerase derived mutations are accumulated<sup>273</sup>.

Four primers were designed for the insert of interest and the vector of interest, as such that 25-35 bp will overlap after amplification. As for CPEC, such primers were also used to insert start/stop codons and small tags and protease cleavage sites. Melting temperatures for the part that anneals with the insert/vector were determined using the following website:

[http://www.bioinformatics.org/sms2/pcr\\_primer\\_stats.html](http://www.bioinformatics.org/sms2/pcr_primer_stats.html), 20.11.2014

For linearization of fragments the following PCR reaction was usually done:

<b>Table M6 PCR reaction for vector of interest (Gibson)</b>			
Component	stock	Vol used (ul)	Final conc.
Plasmid	2 ng/ul	1.1 ul	0.02 ng/ul
FWD primer	10 uM	2.75 ul	0.25 uM
REV primer	10 uM	2.75 ul	0.25 uM
dNTP	10 mM	2.2 ul	0.2 mM
MQ water	-	77.8 ul	-
5x Q5 buffer	5 x	22 ul	1 x
Q5 DNA Polymerase	2 U/ul	1.1 ul	-

<b>Table M7 PCR reaction for insert of interest (Gibson)</b>			
Component	stock	Vol used (ul)	Final conc.
Plasmid or cDNA library	Concentration of cDNA library was unknown	5 ul	??? ng/ul
FWD primer	10 uM	2.5 ul	0.23 uM
REV primer	10 uM	2.5 ul	0.23 uM
dNTP	10 mM	2.2 ul	0.2 mM
MQ water	-	77.8 ul	-
5x Q5 buffer	5 x	22 ul	1 x
Q5 DNA Polymerase	2 U/ul	1.1 ul	-

<b>Table M8 PCR program for vector/insert of interest (Gibson)</b>			
Step	Temperature	Time	Cycle
Initial denaturation	98 °C	30 s	1
Denaturation	98° C	10 s	30
Annealing	58 °C (H), 62 °C (E), 67 °C (C) , 69 °C (A) (Temperature gradient, as it depends on primers)	30 s	
Extension	72 °C (depends on polymerase)	(30 s per 1 kb)	
Final extension	72 °C	2 min	1
Hold	12 °C	-	1

The PCR product was usually analysed on an agarose gel (0.7 %) and then a DpnI enzyme digestion was done at 37 °C, 2 h to get rid of the starting plasmid. To obtain pure fragments, we excised the band of interest from an agarose gel and used a gel extraction kit (Qiagen) for purification. A Gibson assembly was performed using an equimolar amount (50-100 ng) of insert and vector in a 10 ul reaction. Half of this reaction was mixed with 15 ul water (control) and the other half with 15 ul of “Gibson final assembly mix (1.33x Iso buffer (133 mM Tris-HCl, 13.3 mM MgCl<sub>2</sub>, 266 uM dNTP, 13.3 mM DTT, 0.0065 % (w/v) PEG6000, 1.33 mM NAD), 0.08 U T5 exonuclease, 0.5 U Phusion polymerase, 80 U Taq DNA ligase”. The reactions were incubated at 50 °C (waterbath) for 60 min.

### Transformation into bacteria:

5 µl of the Gibson reaction were mixed with 50 µl DH5α competent cells and were incubated on ice for 15 min. In a waterbath (42 °C) a heat shock was performed for 40 s, then the sample was placed on ice for 2 min. 900 µl SOC was added to the bacteria and they were grown at 37 °C for 1 h. Bacteria were centrifuged for 1 min, 15'000 rpm, RT and they were plated on LB agar plates containing the corresponding antibiotics (ampicillin: 100 µg/ml, kanamycin: 50 µg/ml, gentamycin: 10 µg/ml, tetracycline: 10 µg/ml).

Typically, the obtained colonies were expanded in 5 ml LB broth containing antibiotics and the cultures were subjected to a miniprep (Qiagen). The final plasmid was often sent for sequencing to verify successful cloning.

### 2.4.3. Bacmid production

The gene of interest was cloned into a Pcebac1-vector by Gibson cloning. The vector was transformed into DH10MultiBac cells using 100 µl of chemically competent bacteria. They were grown at 37 °C for 4 h and plated on LB plates containing 10 µg/ml gentamycin (pacebac1), 10 µg/ml tetracycline (helper plasmid), 50 µg/ml, kanamycine (bacmid), 0.5 mM IPTG and 200 µg/ml X-Gal. Cells were grown for 1-5 days to make sure to only pick white colonies, as bacteria, which incorporate the gene of interest into the bacmid, disrupt the LacZ open reading frame and thus appear white. Selected colonies were expanded in 4 ml 2x TY medium containing all three antibiotics (20 h, 37 °C, agitating). Mini-cultures were centrifuged (8000 rpm, 5 min, 4 °C) and an alkaline lysis was performed as follows:

200 µl cold buffer P1 (Qiagen) was added to resuspend the pellet. Cells were lysed by adding 200 µl buffer P2 (Qiagen) for maximally 5 min, followed by addition of 280 µl buffer N3 (Qiagen). Samples were centrifuged (13'000 rpm, 10 min, 4 °C) to keep the supernatant. 550 µl isopropanol was added, samples were mixed and centrifuged (13'000 rpm, 30 min, 4 °C). The pellet was washed with 500 µl 70 % (v/v) ethanol, centrifuged (13'000 rpm, 15 min, 4 °C) and the pellet was kept. The wash step was repeated once and the sample was air dried under sterile conditions. The bacmid was resuspended in 40 µl sterile water. Bacmids were analysed using a PCR reaction for the insert: 100 ng bacmid were combined with the PCR solution (1x Q5 polymerase buffer, 0.2 mM dNTP, 1.5 mM MgCl<sub>2</sub>, 10 µM Forward primer "pUC-M13Forward", 10 µM Reverse primer "pUC-M13Reverse", 1 U Q5 high fidelity polymerase) in a final volume of 50 µl.

pUC-M13Forward: CCC AGT CAC GAC GTT GTA AAA CG

pUC-M13Reverse: AGC GGA TAA CAA TTT CAC ACA GG

The following PCR program was used:

<b>Table M9 PCR program for bacmid verification</b>			
Step	Temperature	Time	Cycle
Initial denaturation	94 °C	3 min	1
Denaturation	94 °C	45 s	25-35
Annealing	55 °C / 58 °C	45 s	
Extension	72 °C	5 min	
Final extension	72 °C	7 min	1
Hold	4 °C	-	1

5-10 ul of the PCR reaction were analysed on agarose gel electrophoresis (0.7 % gel). The pure bacmid without insert is expected at 350 bp. The successfully modified bacmid is expected at 2400-4200 bp.

## 2.5. Cell cultures and baculovirus production

### Cell maintenance:

Sf9 Cells originating from *Spodoptera frugiperda* pupal ovarian tissue were cultivated in SF900 II insect cell medium with 0.5x penicillin/streptomycin (P/S, 10'000 U/ml stock) at 28 °C, shaking at 90 rpm in a cell incubator (Ecotron, Infors HT).

### Splitting cells:

Cells were grown to  $2-4 \times 10^6$  cells/ml and counted using a Neubauer counting chamber and every 2-3 days until passage 25, cells were diluted in fresh Sf900 II medium to  $0.5-0.6 \times 10^6$  cells/ml.

### Freezing cells/Thawing cells:

For freezing, insect cells were centrifuged at 27 °C, 5 min, 1000 rpm. Freezing medium (10 % Fetal calf serum (FCS), 10 % DMSO (sterile) in SF-900 II medium (no P/S)) was used to resuspend the cell pellet.  $1 \times 10^7$  cells per freezing vial were frozen in a slow cooling gradient and stored in a liquid nitrogen preservation tank. To revive cells, the frozen cells were thawed at 37 °C rapidly and diluted in 25 ml SF900 II medium containing 0.5x P/S and 5 % FCS.

### Baculovirus production:

We followed tightly the Invitrogen guide “Bac-to-Bac® Baculovirus Expression System”:

To obtain a first viral stock “P1”, 8 x10<sup>5</sup> Sf9 cells were plated in each well of a six-well plate. Cells were allowed to attach for 15 min, RT. Grace insect medium containing 1.5 % FCS was combined with Cellfectin II reagent (Cellfectin II 2:25). 2 ug of the bacmid of interest was diluted in 100 ul Grace insect medium, then the bacmid solution was combined with the Cellfectin II 2:25 solution and incubated at RT for 15 min. Finally, the Cellfectin II bacmid solution was added dropwise to the cells and cells were incubated at 28 °C for 5 h. The Cellfectin II bacmid solution was withdrawn and baculovirus was propagated in Sf900 II medium with P/S for 96 h at 28 °C. As infected cells appeared enlarged and detached from the surface of the six-well plate, we centrifuged them for 5 min, 200 xg, RT, complemented the supernatant with 1 % FCS and stored the viral stock P1 at 4 °C, light protected.

To obtain a viral stock P2 T75 tissue culture flasks were seeded with 2 x10<sup>7</sup> cells and P1 was added using the following formula:

*Viral amplification:*

$$P1(required) = \frac{0.1MOI \times 2 \times 10^7 cells}{assumed\ P1\ viral\ titer: 5 \times 10^6 pfu/ml} \quad (M1)$$

After 3 days viral stock P2 was collected as and stored as described above for P1. To obtain viral stock P3 the procedure was repeated using P2 as inoculum and Nalgene™ Erlenmeyer culture flasks.

## Viral plaque assay

The viral titer of viral stock P3 was determined as follows:

10<sup>6</sup> cells per well were allowed to attach in 6-well plates. Serial dilutions of viral stock P3 were prepared reaching from 10<sup>-4</sup> to 10<sup>-8</sup> and added to the cells for exactly 1 h. Then 1 % agarose in 1x SF900 II medium was added to the six-well plate agarose was left to solidify for 1 h, RT. Then six-well plates were kept in a humid chamber at 28 °C for 10 days. Viral plaques were counted to determine the viral titer of viral stock P3.

## 2.6. Peptide synthesis

Peptide **P1** (Thz-G<sub>2</sub>-C<sub>3</sub>-CONH<sub>2</sub>, Thz: thiazolidine) was synthesized manually on a Rink amide resin using Boc-Thiazolidine and Fmoc-Cys(Trt)-OH, employing a Fmoc-protection strategy and standard HBTU coupling protocols. The peptide was cleaved from the resin using 95 % TFA, 2.5 % TIS, 2.5 % water and purified using preparative RP-HPLC (on a 20-50 % gradient). Subsequently, 1.5 mg peptide (5 umol) was dissolved in labelling buffer (200 mM

phosphate pH 7.3, 5 M guanidium hydrochloride) to a concentration of 10 mM. 1 mg of Atto532-iodoacetamide (1  $\mu$ mol) was subsequently added in 50  $\mu$ l DMSO, and the reaction was incubated until completed as judged by RP-HPLC. Residual unreacted dye was quenched by the addition of 2 mM BME. Then, 0.5 M methoxylamine was added and the pH was adjusted to 5 using 2 M NaOH. Opening of the thiazolidine was followed by RP-HPLC and ESI-MS. After completion the peptide was purified using semipreparative RP-HPLC and a gradient of 0-70 %B in 45 min. Final products were analysed by RP-HPLC and ESI-MS (calculated exact mass = 1009.26 Da, observed mass = 1008.25 Da).

Peptide **P2** (ac-K<sub>1</sub>S<sub>2</sub>L<sub>3</sub>Y<sub>4</sub>P<sub>5</sub>V<sub>6</sub>V<sub>7</sub>K<sub>8</sub>I<sub>9</sub>R<sub>10</sub>R<sub>11</sub>K<sub>12</sub>G<sub>13</sub>C<sub>14</sub>G<sub>15</sub>-CONH<sub>2</sub>) was synthesized on the Tribute automated peptide synthesizer (PTI) using standard HBTU coupling protocols, and the following protection groups: Cys(Trt), Lys(Boc), Arg(pbf), Tyr(tBu), Ser(tBu). In addition, K<sub>1</sub> and K<sub>12</sub> were included containing an Alloc-protecting group. After synthesis, the N-terminus was acetylated using 3x20 min incubation of peptidyl-resin with 10 % acetic anhydride, 10 % *N,N*-diisopropylethylamine (DIPEA) in dimethylformamide (DMF), followed by extensive washes. Then, the Alloc-groups on the two lysines were removed by 3x30 min treatment of the peptidyl-resin with 0.25 equivalents of tetrakis(triphenylphosphine) palladium(0) (Pd(PPh<sub>3</sub>)<sub>4</sub>) in dichloromethane (DCM) and containing 24 equivalents of phenylsilane (PhSiH<sub>3</sub>). The resin was subsequently washed with 0.5 % DIPEA in DMF, 0.5 % sodium diethylthio-carbamate in DMF, 0.5 % hydroxybenzotriazole in DMF and finally DMF. Then, Boc-Thz was coupled to both deprotected lysines in one step using standard HBTU activation and 10x excess to the peptide. Subsequently, the peptide was cleaved from the resin and labelled with Atto532-iodoacetamide as described for **P2**. The final product was analysed by RP-HPLC and ESI-MS (calculated MW = 2680.24 Da, observed MW= 2679.35 Da).

Peptide **P3** (NH<sub>2</sub>-N<sub>1</sub>V<sub>2</sub>S<sub>3</sub>L<sub>4</sub>Y<sub>5</sub>P<sub>6</sub>V<sub>7</sub>V<sub>8</sub>K<sub>9</sub>I<sub>10</sub>R<sub>11</sub>R<sub>12</sub>L<sub>13</sub>S<sub>14</sub>-CONH<sub>2</sub>) was synthesized on the Tribute automated peptide synthesizer (PTI) using standard HBTU coupling protocols, and the following protection groups: Asn(Trt), Lys(Boc), Arg(pbf), Tyr(tBu), Ser(tBu). After cleavage from the resin the peptide was purified using preparative RP-HPLC and analysed by RP-HPLC and ESI-MS (calculated MW = 1685.03 Da, observed MW= 1685.3 Da).

Peptide **P4** (NH<sub>2</sub>-N<sub>1</sub>V<sub>2</sub>S<sub>3</sub>L<sub>4</sub>Y<sub>5</sub>A<sub>6</sub>V<sub>7</sub>A<sub>8</sub>K<sub>9</sub>A<sub>10</sub>R<sub>11</sub>R<sub>12</sub>L<sub>13</sub>S<sub>14</sub>-CONH<sub>2</sub>) was synthesized on the Tribute automated peptide synthesizer (PTI) using standard HBTU coupling protocols, and the following protection groups: Asn(Trt), Lys(Boc), Arg(pbf), Tyr(tBu), Ser(tBu). After cleavage from the resin the peptide was purified using preparative RP-HPLC and analysed by RP-HPLC and ESI-MS (Calculated MW = 1589.03 Da, observed MW= 1588.6 Da).

## 2.7. HP1 $\alpha$ purification and labelling

HP1 $\alpha$  (CBX5) was cloned into a pET15b expression vector, which harbours an N-terminal hexahistidine-tag (6xHis) with a downstream thrombin cleavage site. Subsequently, the protein was expressed in *E.coli* BL21 DE3 cells, as follows: 3 liter LB media supplemented with 100  $\mu$ g/ml ampicillin were inoculated from starter cultures and incubated at 37 °C with

220 rpm rotation for 2 h. The temperature was then reduced to 18 °C and the cultures were allowed to grow until reaching an OD600 of 0.6. Expression was induced by addition of IPTG to a final concentration of 0.25 mM, followed by further incubation at 18 °C for 16-20 h. Cells were harvested, resuspended and lysed in Ni-NTA lysis buffer (25 mM phosphate, 50 mM NaCl, 5 mM imidazole, 1 mM protease inhibitor tablet/50 ml, pH 8.0) by sonication.

Lysed cells were centrifuged at 15'000 xg for 15 min and the soluble fraction was loaded onto 2 ml Ni-NTA resin per liter culture. The protein was bound to the resin by gentle nutating for 30 min before the flow through (FT) was collected. Then, the resin was washed with 2x5 column volumes (CVs) of Ni-NTA wash buffer (25 mM phosphate pH 8.0, 50 mM NaCl, 20 mM imidazole), and then the protein eluted with 2x1.5 CV of Ni-NTA elution buffer (25 mM phosphate pH 8.0, 50 mM NaCl, 400 mM imidazole). Elutions were pooled and purified using AIEX using 1 ml HiTrap Q FF: After loading the protein solution, the column was washed with 3 CV of AIEX buffer A (50 mM phosphate pH 7.5, 50 mM NaCl) and subsequently eluted using a 0-100% gradient from AIEX buffer A to AIEX buffer B (50 mM phosphate pH 7.5, 1000 mM NaCl) over 20 CV followed by 3 CV of AIEX buffer B. Fractions were analysed using SDS-PAGE and pooled accordingly. 10 U of thrombin were added to the pooled fractions from AIEX to remove the N-terminal 6xHis-tag. Cleavage was monitored by RP-HPLC and ESI-MS, and was typically complete after 2-3 h. The cleaved protein was then purified by gel filtration on a Superdex 200 10/300GL column, using HP1 gel filtration buffer (50 mM HEPES pH 7.5, 150 mM NaCl, 2.5 mM DTT). Fractions containing the protein were pooled and concentrated to 40-100 uM. Then the protein was either mixed with glycerol to a final concentration of 30 % glycerol, flash frozen and stored at -80 °C or kept on ice at 4 °C until use.

#### **HP1 $\alpha$ labelling using EPL:**

Lyophilized stocks of NpuC-peptide (prepared as described <sup>191</sup>) were dissolved in water to a concentration of 2 mM, as quantified by UV spectroscopy ( $\epsilon_{280\text{nm}}$ , NpuC-CysOMe = 2980 M<sup>-1</sup>cm<sup>-1</sup>). 125 ul stocks of this were flash frozen and stored at -80 °C for later use. For the preparation of NpuC-resin, 500 ul of SulfoLink resin slurry was put into a small fritted column and washed with water. A 125 ul stock of the NpuC-CysOMe peptide was mixed with 125 ul of 2x coupling buffer (100 mM Tris pH 8.5, 10 mM EDTA), TCEP was added to a final concentration of 25 mM and the pH was adjusted to 8.5. The peptide solution was added to the SulfoLink resin in the capped fritted column and incubated for 45 min (15 min included agitation by nutation), then the column was drained and washed with 2x1 CV of 1x coupling buffer. Residual unconjugated iodoacetamide groups on the resin were capped by treatment with cysteine methylester (CysOMe). 500 ul of HP1 $\alpha$ -GG-NpuN-6xHis at a concentration of 50 uM was added to 125 ul of the NpuC resin in a small fritted column and incubated on a nutator for 5 min. The flow through was collected and the resin washed with 4 CV of binding buffer (100 mM phosphate pH 7.2, 1 mM EDTA, 1 mM TCEP) with 500 mM NaCl, 4 CV of binding buffer with 300 mM NaCl and 4 CV of binding buffer with 150 mM



NaCl. Then 1 CV of *in situ* EPL buffer (50 mM MPAA, 200 mM MESNA, 100 mM phosphate, pH 7.7-7.9, 150 mM NaCl, 10 mM TCEP, 1 mM EDTA) containing 1 mM of peptide **P1** was added to the resin and the column was capped and incubated on a nutator for 16-18 h. The eluate was collected and the column further washed with 3x1 CV of intein column elution buffer (200 mM MESNA, 100 mM phosphate, pH 7.2, 150 mM NaCl, 10 mM TCEP, 1 mM EDTA). All fractions were analysed by SDS-PAGE. Elution fractions were pooled and purified by gel filtration using a Superdex S200 10/300GL column using HP1 gel filtration buffer. Fractions with the labelled/dimerized protein were analysed by SDS-PAGE, pooled and concentrated to 10-20  $\mu$ M. 20 % glycerol was added, the final concentration and labelling efficiency was determined by UV spectroscopy using the extinction coefficient for HP1 $\alpha$  at 280 nm of  $\epsilon_{280\text{nm}} = 29450 \text{ M}^{-1}\text{cm}^{-1}$  and for Atto532 at 532 nm of  $\epsilon_{532\text{nm}} = 115'000 \text{ M}^{-1}\text{cm}^{-1}$ . Further the fluorescence emission spectra were analysed by fluorometry. The labelled protein was mixed with glycerol and flash frozen in 5-10  $\mu$ l aliquots in liquid  $\text{N}_2$  and stored at  $-80^\circ\text{C}$  until use. Finally, the protein was further analysed by RP-HPLC and ESI-MS (HP1 $\alpha$  (Atto532): calculated molecular weight (MW) = 23'200.0 Da, observed MW = 23'204.0 Da).

## 2.8. TEV protease expression and purification

TEV protease was expressed in Rosetta cells (1 liter LB medium, 100  $\mu$ g/ml ampicillin, 35  $\mu$ g/ml chloramphenicol, 2 g/l glucose). Cells were allowed to grow until an OD600 of 0.6 and then they were induced using 1 mM IPTG (16  $^\circ\text{C}$ , 16-20 h). 25 ml Ni-NTA lysis buffer without protease inhibitors were used to dissolve the bacterial pellet from a 1 liter culture. The pellet was flash frozen and kept at  $-80^\circ\text{C}$  until further use.

After thawing, the lysate was sonicated, centrifuged (10 min, 15'000 rpm, 4  $^\circ\text{C}$ ) and the supernatant was filtered (0.2  $\mu$ m diameter filter). 2.5 ml Ni-NTA resin were equilibrated with 10 mM imidazole (1 h, 4  $^\circ\text{C}$ ). The lysate was incubated with the Ni-NTA resin for 1 h (4  $^\circ\text{C}$ , gentle agitation). Afterwards, the flow through was collected and 2x5.2 CV washes were performed with TEV-Ni-NTA wash buffer I (25 mM phosphate pH 8.0, 50 mM NaCl, 20 mM imidazole) and 2x5.2 CV TEV-Ni-NTA wash buffer II (25 mM phosphate pH 8.0, 50 mM NaCl, 50 mM imidazole). Elutions were performed using 5x0.8 CV TEV-Ni-NTA elution buffer (50 mM phosphate pH 8.0, 300 mM NaCl, 250 mM imidazole). Each elution fraction was complemented immediately with 1 mM DTT and 1 mM EDTA to prevent precipitation of the protease. The self-cleavable MBP-tag was removed operating a 2 ml MBPTrap HP (GE Healthcare) manually as follows: the pooled Ni-NTA elutions were diluted (1:1 volume) in MBP binding buffer (20 mM Tris-HCl pH 7.4, 200 mM NaCl, 1 mM EDTA, 1 mM DTT). The column was equilibrated with water and MBP-binding buffer, then the sample was applied and washed using 1x7 CV MBP-binding buffer. 1x5 CV MBP-elution buffer was applied for MBP protein elution (20 mM Tris-HCl pH 7.4, 200 mM NaCl, 1 mM EDTA, 1 mM DTT, 10 mM maltose), while the TEV protease was collected from the flow through and wash fractions.

TEV-containing fractions were concentrated using filter columns (10K, 4 ml, Amicon using centrifugation (4000 xg, 5-30 min, 4  $^\circ\text{C}$ )) and then the columns were used for a buffer



exchange (5x steps) with TEV protease buffer (20 mM Tris-HCl pH 8.0, 200 mM NaCl, 2 mM EDTA). Then, 10 mM DTT and 25 % (v/v) glycerol were gently added to the concentrated TEV protease sample. The TEV protease was kept at -20 °C until use.

## 2.9. Expression and purification of ubiquitin machinery proteins

### 2.9.1. UBE1 purification

The plasmid of the human ubiquitin-activating enzyme E1 (hUBE1) was purchased from Addgene (Plasmid #34965, Cynthia Wolberger <sup>274</sup>) and expressed in bacteria. Notably, successful expression was only obtained in Rosetta™ 2 ((DE3) Competent cells (71397-3) (F-ompT hsdSB(rB<sup>-</sup> mB<sup>-</sup>) gal dcm (DE3) pRARE (CAMR))) *E.coli* cells using 0.2 mM IPTG for induction in 1 liter LB medium (ampicillin 100 µg/ml) containing 1 µM zinc chloride at an OD<sub>600</sub> of 0.6 at 16 °C during 16 h. The pellet was dissolved in 25 ml Cell lysis buffer (50 mM Tris pH 8.0, 300 mM NaCl, 1 µM ZnCl<sub>2</sub>, 0.05 % (v/v) Nonidet P40, 5 mM BME, 5 mM trisodium citrate, 10 % (w/v) glycerol, 1 mM PMSF, 1 protease tablet (SigmaFAST, EDTA free) per 50 ml) and frozen at -80 °C. After thawing, the lysate was complemented with 1 mM BME, 0.1 mM ATP and 1 mM MgCl<sub>2</sub> and subsequently lysed by sonication.

Lysed cells were centrifuged at 15'000 xg for 10 min and the soluble fraction was filtered and then loaded onto 1.5 ml Ni-NTA resin per liter culture, as the protein contains an N-terminal 6xHis-tag. The protein was bound to the resin by gentle nutating for 1 h (4 °C) before the flow through was collected. Then, the resin was washed with 2x5.3 CVs of E1-Ni-NTA wash buffer I (50 mM phosphate pH 8.0, 300 mM NaCl, 20 mM imidazole, 1 mM BME, 0.1 mM ATP and 1 mM MgCl<sub>2</sub>), 2x5.3 CVs of E1-Ni-NTA wash buffer II (50 mM phosphate pH 8.0, 300 mM NaCl, 50 mM imidazole, 1 mM BME, 0.1 mM ATP and 1 mM MgCl<sub>2</sub>), and then the protein was eluted with 6x0.33 CV of E1-Ni-NTA elution buffer (50 mM phosphate pH 8.0, 300 mM NaCl, 250 mM imidazole, 1 mM BME, 0.1 mM ATP and 1 mM MgCl<sub>2</sub>). Elutions were pooled, concentrated using filter columns (3K, 0.5 ml, Amicon) and then the columns were used for a buffer exchange (6xsteps) with E1 buffer (50 mM HEPES pH 7.5, 150 mM NaCl, 0.1 mM DTT, 10 % (v/v) glycerol, 0.1 mM ATP, 1 mM MgCl<sub>2</sub>). The sample was flash frozen and stored at -80 °C until use. We note that the final fraction was not entirely pure, but it was as pure as published previously, which was sufficient for ubiquitination assays <sup>229</sup>.

### 2.9.2. UBE2D3 purification

The plasmid of the human ubiquitin-conjugating enzyme E2 (UBE2D3) was purchased from Addgene (Plasmid #15784, Wade Harper <sup>275</sup>) and expressed in bacteria (Rosetta, 16 °C, 16 h, 0.5 mM IPTG, 1 µM zinc chloride, 100 µg/ml ampicillin in 1 liter LB medium) at an OD<sub>600</sub> of 0.6. Expression and purification of the protein worked well, but initial activity tests showed no activity, compared to a commercially available hUBE2D3 version from Boston Biochem. In order to obtain comparable activity we had to reduce an N-terminal tag in the

plasmid construct and further to reverse a point mutation (P18L) to obtain the native proline at position AA 18.

After expression, the pellet was dissolved in 25 ml Cell lysis buffer and frozen at -80°C. After thawing, the lysate was sonicated. Lysed cells were centrifuged at 15'000 xg for 10 min and the soluble fraction was filtered and then loaded onto 1.5 ml Ni-NTA resin per liter culture, as the protein contains an N-terminal 6xHis-tag. The protein was bound to the resin by gentle nutating for 1 h (4 °C) before the flow through was collected. Then, the resin was washed with 2x5.3 CVs of E2-Ni-NTA wash buffer I (50 mM phosphate pH 8.0, 300 mM NaCl, 20 mM imidazole, 5 mM BME, 0.1 mM ATP, 1 uM ZnCl<sub>2</sub>, 1 mM MgCl<sub>2</sub>, 1 mM PMSF), 2x5.3 CVs of E2-Ni-NTA wash buffer II (50 mM phosphate pH 8.0, 300 mM NaCl, 50 mM imidazole, 5 mM BME, 0.1 mM ATP, 1 uM ZnCl<sub>2</sub>, 1 mM MgCl<sub>2</sub>, 1 mM PMSF), and then the protein eluted with 5x0.66 CV of E2-Ni-NTA elution buffer (50 mM phosphate pH 8.0, 300 mM NaCl, 250 mM imidazole, 5 mM BME, 0.1 mM ATP, 1 uM ZnCl<sub>2</sub>, 1 mM MgCl<sub>2</sub>, 1 mM PMSF). Elutions were pooled, concentrated using filter columns (3K, 0.5 ml, Amicon) and then the columns were used for a buffer exchange (6xsteps) with TEV cleavage buffer (20 mM Tris-HCl pH 7.4, 100 mM NaCl, 5 mM BME, 10 uM ZnCl<sub>2</sub>, 5 mM citrate). To remove potential aggregates the sample was centrifuged (5 min, 13'000 rpm, 4 °C) and the supernatant was kept.

TEV protease was applied to remove the N-terminal 6xHis-tag for 16 h (4 °C, gentle nutation, 1:20 weight ratio TEV protease). After completion, a reverse Ni-NTA purification was done on 2 ml resin. The TEV-protease and uncleaved UBE2D3 were bound to the resin by gentle nutating for 30 min (4 °C). 2x2 CV washes were done with TEV cleavage buffer to collect the UBE2D3. Then, 2x2 CV and 1x4 CV washes using E2-REV-Ni-NTA wash buffer I ((50 mM phosphate pH 8.0, 300 mM NaCl, 20mM imidazole) were performed and collected. 2x4 CV washes using E2-REV-Ni-NTA wash buffer II ((50 mM phosphate pH 8.0, 300 mM NaCl, 50 mM imidazole) were done to collect potentially residual protein. Fractions were pooled, concentrated using filter columns (3K, 0.5 ml, Amicon) and then the columns were used for a buffer exchange (6xsteps) with E2 buffer (50 mM HEPES pH 7.5, 150 mM NaCl, 1 uM ZnCl<sub>2</sub>, 1 mM MgCl<sub>2</sub>). Then the sample was complemented with 1 mM DTT and 10 % (v/v) glycerol. To remove potential aggregates the sample was centrifuged (5 min, 13'000 rpm, 4 °C) and the supernatant was flash frozen and stored at -80 °C until use.

### 2.9.3. Ubiquitin purification

#### **Tag-less ubiquitin purification:**

The histone modification and small protein ubiquitin (human ubiquitin variant C) was expressed in BL21 DE3 bacteria (37 °C, 4 h, 0.5 mM IPTG, 100 ug/ml ampicillin in 1 liter LB medium). To increase the yield drastically we decided to use a tag-less purification strategy, which precipitates all non-ubiquitin proteins at pH 5<sup>107</sup>.

After expression, the pellet was dissolved in 25ml ubiquitin lysis buffer (20 mM HEPES pH 7.5, 66 mM ZnCl<sub>2</sub>) and frozen at -80 °C. After thawing, the lysate was sonicated. Lysed cells were centrifuged at 15'000 xg for 10 min and the soluble fraction was filtered. The filtered lysate was dialysed (Spectra/por, 3'500 MWCO, 29 mm diameter) for 24 h (4 °C) towards 100 mM acetic acid (pH 5.0). Aggregates were removed by 2x centrifugation (12'000 rpm, 30 min, 4 °C). A cation exchange column (HiTrap™ SP HP, 5 ml) was used as ubiquitin has a pI = 6.56 and thus is positively charged at pH 5. After equilibration of the column in Cation buffer A (100 mM acetic acid pH 5, 10 mM NaCl) the ubiquitin sample was applied and the flow through was collected. A wash using 1x5 CV Cation buffer A was performed, then the ubiquitin was eluted using a salt gradient from 100 mM to 1000 mM NaCl with 250mM NaCl intervals (3 CV buffer volume for each step). Fractions were analysed by SDS-PAGE and ubiquitin-containing fractions were desalted using RP-HPLC (semi- or preparative C18 column, 2 ml/min flow). Quality of the purified ubiquitin was analysed on RP-HPLC (analytical C18 column) and ESI-MS. The collected protein was lyophilized, kept at -20 °C and dissolved in water (1 mg/ml) prior to usage.

#### **His-tagged Cys-ubiquitin purification:**

Purification of the tag-less ubiquitin version containing a cysteine mutation led to losses of protein yield. Thus, we used a construct containing a His-tag for protein purification (Construct: His-Thrombin-C-hUBIQUITIN (variant C), short: C-ubiquitin). C-ubiquitin was expressed in BL21 DE3PlyS cells (37 °C, 4 h, 0.2 mM IPTG, 100 ug/ml ampicillin in 1 liter LB medium). The protein was purified using Ni-NTA resin (see HP1α purification protocol) and preparative RP-HPLC (as ubiquitin) by Caroline Lechner (LCBM, EPFL, CH). The lyophilized protein was dissolved in guanidine labelling buffer (6 M guanidium hydrochloride, 200 mM sodium phosphate, pH 7.4) to a final concentration of 75 uM. A 10x excess of fluorescein-5-maleimide, dissolved in DMSO, was added to the protein. The reaction was kept covered in aluminium foil (4 °C) for 20 h. Then the reaction was purified using RP-HPLC on a semi-preparative C18 column. The collected fractions were analysed by SDS-PAGE, analytical RP-HPLC and ESI-MS.

#### **2.9.4. RNF168 purification from bacterial expression**

In the following, we will focus only on the strategy, which allowed us to produce highly enzymatically active versions of RNF168.

The E3 human ubiquitin-ligase (hRNF168) was cloned from a lab-internal human cDNA library. RNF168 was expressed in Rosetta cells (16 °C, 16h, 0.2 mM IPTG, 1 uM zinc chloride, 100 ug/ml ampicillin in 1 liter LB medium) harbouring an N-terminal GST-tag and a C-terminal STREP-tag to perform a two-sided purification, as the protein stability at temperatures higher than 4 °C was very low and a lot of degradation products can appear. Initial purification via Ni-NTA resin (as published in Zhang et al., 2013) using a His-tag failed multiple times, as protein activity was lowered drastically<sup>251</sup>. Further the protein (truncated

or full-length) is very sensitive to agitation and temperatures higher than 4 °C should be avoided rigorously during purification.

After expression, the pellet was dissolved in 25 ml Cell lysis buffer and frozen at -80 °C. Then, after thawing, the lysate was sonicated. Lysed cells were centrifuged at 15'000 xg for 10 min and the soluble fraction was filtered and then loaded onto 1.5ml glutathione resin per liter culture, as the protein contains an N-terminal GST-tag. The protein was bound to the resin after equilibration with PBS (pH 7.3) by gentle nutating for 1 h (4°C) before the flow through was collected. Then, the resin was washed with 3x10 CV of GST-binding buffer (PBS pH 7.3, 1 mM BME, 1 uM ZnCl<sub>2</sub>). RNF168 was eluted with 5x1.3 CV GST-elution buffer (PBS pH 7.3, 1 mM BME, 1 uM ZnCl<sub>2</sub>, 10 mM reduced L-glutathione). Elutions were pooled, concentrated using filter columns (3K, 0.5 ml, Amicon) and then the columns were used for a buffer exchange (6xsteps) with ybbr labelling buffer (50 mM HEPES pH 7.5, 1 mM BME, 1 uM ZnCl<sub>2</sub>). TEV protease was applied to remove the N-terminal GST-tag for 16 h (4 °C, gentle nutation, 1:20 weight ratio TEV protease). After successful TEV cleavage, RNF168 was subjected to a Streptactin XT superflow column to ensure enrichment of the non-truncated protein by its C-terminal STREP-tag. After equilibration of the column with buffer W (100 mM Tris-HCl pH 8.0, 150 mM NaCl, 1 uM ZnCl<sub>2</sub>, 1 mM PMSF, 1-5 mM BME) the protein was applied and the flow through was collected. We performed 7x1 CV buffer W washes. Elution was done using 6x0.5 CV buffer E (100 mM Tris-HCl pH 8.0, 150 mM NaCl, 1 uM ZnCl<sub>2</sub>, 1 mM PMSF, 1-5 mM BME, 50 mM biotin). Fractions were pooled, concentrated using filter columns (3K, 0.5 ml, Amicon) and then the columns were used for a buffer exchange (6xsteps) with buffer W. To remove potential aggregates the sample was centrifuged (5 min, 13'000 rpm, 4 °C). We added 20 % (v/v) glycerol to reduce freezing damage, flash froze the protein in liquid nitrogen and kept the protein at -80 °C until use. Following this strategy, one liter bacterial culture rendered 190 ug RNF168(196).

### 2.9.5. RNF168 purification from insect cell expression

Upon expression, 232 ml insect cell culture were centrifuged (200 xg, 6 min, 4 °C) and the pellet was flash frozen and stored at -80 °C. The pellet was dissolved in 56 ml Cell lysis buffer, sonicated and centrifuged (20'000 xg, 30 min, 4 °C). STREP purification was done by equilibrating 3x1 ml Streptactin XT Superflow columns with buffer W2 (100 mM Tris-HCl pH 8.0, 150 mM NaCl, 2uM ZnCl<sub>2</sub>, 1-5 mM BME). Then the protein solution was added to the three columns equally and flown through slowly for binding. Each column was washed with 8x1 CV buffer W2. Elutions were done with 6x1 CV buffer E12 (100 mM Tris-HCl pH 8.0, 150 mM NaCl, 2 uM ZnCl<sub>2</sub>, 1-5 mM BME, 50 mM biotin). We added TEV protease (1:1 weight ratio) to the sample to cleave off the C-terminal STREP-tag during 16 h at 4 °C (gently agitating). The sample was centrifuged (13'000rpm, 5 min, 4°C) to remove aggregates and subjected to ybbr-labelling in 15x1.1 ml volumes using 0.7 uM Sfp synthase (NEB), 9 uM Alexa568-CoA, 10 mM MgCl<sub>2</sub>, 1 mM BME (was already in the sample) and 1-2 uM protein-ybbr. Reactions were incubated for 3.5 h (4 °C, gently agitating). To remove the remaining Alexa568-CoA, we performed a FLAG-affinity purification on magnetic FLAG-beads. 15x200 ul

packed beads were equilibrated with 2 ml TBS buffer (50 mM Tris-HCl pH 7.4, 150 mM NaCl), then the labelled RNF168 solution was added to the beads (16 h, 4 °C, gently agitating). The supernatant was removed (FT) beads were washed with 24x5 CV FLAG-Wash buffer (50 mM Tris-HCl pH 8.0, 150 mM NaCl, 0.4 mM BME, 10 % (v/v) glycerol, 2 uM ZnCl<sub>2</sub>) and eluted 4x1 CV using FLAG-Elution buffer (50 mM Tris-HCl pH 8.0, 150 mM NaCl, 0.4 mM BME, 10 % (v/v) glycerol, 2 uM ZnCl<sub>2</sub>, 100 ug/ml FLAG-peptide (produced by Caroline Lechner). During the first elution step the buffer was incubated with the beads for 2 h (4 °C, gently agitating) and for the subsequent 3 elution steps incubation was done for 30 min each. Elutions were pooled and concentrated using filter columns (3K, 0.5 ml, Amicon). Potential aggregations were removed by centrifugation (13'000 rpm, 5 min, 4 °C. The sample was flash frozen and stored at -80 °C until use. Ubiquitination assays were done to confirm activity of the labelled protein. Sometimes the protein was purified without labelling. To do so, the procedure was stopped after the streptactin purification.

## 2.10. CoA labelling

8 mM Alexa Fluor 568 C5 maleimide (dissolved in anhydrous DMSO) was combined with 16.8 mM CoA trilithium salt, which had been dissolved in sodium phosphate buffer (100 mM sodium phosphate pH 7) previously. The reaction was kept gently agitating at RT for 1 h. The reaction mixture was purified using semi-preparative C18 column (0-70 % gradient B) and the two enantiomers of Alexa568-CoA were collected, as both can be used for labelling of ybbr-proteins. The pure fractions were lyophilized and kept at -20 °C until use.

## 2.11. Ybbr labelling

### **For PRC2:**

Ybbr-labelling for EZH2 was done in 250 ul volumes using 50 mM HEPES, 150 mM NaCl, 1 uM Sfp synthase (NEB), 10 uM DY547-CoA (NEB), 10 mM MgCl<sub>2</sub> and 5 uM ybbr-protein. The reaction was kept for 2h with soft nutation (4 °C, wrapped in aluminium foil) and analysed by SDS-PAGE. This was done by Jeongyoon Choi.

### **For RNF168:**

Ybbr-labelling was done in 100 ul volumes after STREP-tag purification for RNF168(196) using 0.4 uM Sfp synthase (NEB), 10 uM Alexa568-CoA, 10 mM MgCl<sub>2</sub>, 1 mM BME and 10 uM protein-ybbr. The reaction was kept for 1-2h with soft nutation (4 °C, wrapped in aluminium foil) and monitored by SDS-PAGE.

## 2.12. Nucleosome core particle assembly

### 2.12.1. 177bp 601 DNA recovery

#### **12x177 bp 601 DNA gigaprep:**

The plasmid harbouring the desired sequence “BFD14\_pWM530 (4181 bp)” was heat-shock-transformed into a competent DH5 $\alpha$  bacterial strain. The bacteria containing the plasmid were cultured in 6 liter 2x TY (1.6 % (w/v) tryptone, 1 % (w/v) yeast extract, 0.5 % (w/v) NaCl, pH 7.0) complemented with 100 ug/ml ampicillin (20 h, 37 °C, 200 rpm) and 2 drops per liter of antifoam. The cultures were centrifuged (4000 xg, 10 min, 15 °C), and an alkaline lysis was done at 4 °C: 6 x 1 liter bacterial pellets were dissolved in 80 ml lysis buffer 1 (50 mM glucose, 25 mM Tris, 10 mM EDTA, pH 8.0), then 240 ml lysis buffer 2 (0.2 M NaOH, 1 % SDS, RT) was added for maximally 5 min and next 240 ml lysis buffer 3 (4 M potassium acetate, 2 M acetic acid) were added until precipitation formed. The mixture was incubated on ice for 15 min and then centrifuged for 15 min, 11'000 xg, 4 °C.

#### **12x177 bp 601 DNA isopropanol precipitation and purification:**

The supernatant was filtered through two layers of miracloth and 0.52 volumes of isopropanol were added. The mixture was incubated at RT for 30 min, then centrifuged at 11'000 xg, RT, 20 min. The pellet was dried and 25 ml TE 10/50 buffer (TE 10/50 (10 mM Tris, 50 mM EDTA) was added. 1 mg RNase A was added and the reaction was kept at 37 °C, 2 h. Afterwards, the reaction was complemented with 2 M KCl and TE 10/50 buffer was added to a total volume of 35 ml. The sample was centrifuged at 20'000 xg, 10 min, 10 °C. The plasmid was purified using FPLC (ÄKTA™ pure, unicorn6.3; Column: Sepharose 6 XK 30/50 (560 ml column volume), 50 ml superloop) and collected in the void volume of the column. The fractions containing the desired plasmid were subjected to another isopropanol precipitation and dissolved in TE 10/50 buffer.

#### **12x177 bp 601 DNA labelling and biotinylation via oligo ligation for chromatin arrays:**

##### **a) Preparation of the 12x601 sequence (unlabelled array DNA)**

The DNA, which was isolated with an isopropanol precipitation was ethanol precipitated (1:10 volumes of 24 M NaAc pH 5.2 and 2.5 volumes of cold ethanol, precipitated for 30 min at -20°C and pellet wash with 70% ethanol) for resuspension in MQ water. An HF-EcoRV restriction digestion was performed and the restriction enzyme was heat inactivated afterwards. The 12x177 bp 601 piece was PEG precipitated and dephosphorylated using Antarctic phosphatase. After heat inactivation, another ethanol precipitation was done, followed by an HF-BsaI restriction digestion (3 h, 37 °C) with subsequent heat inactivation. A 7 % (w/v) PEG precipitation was performed twice by adding 1:10 volumes of 5 M NaCl and PEG from a 40 % stock solution. Each precipitation was done



at 4 °C for 1 h. The final pellet was dissolved in 1x TE buffer (10 mM Tris-HCl pH 8.0, 1 mM EDTA). To remove NaCl another ethanol precipitation was done.

#### **b) Preparation of the biotin/Atto647N oligo**

A TIRF adaptor DNA oligo (5'-/5Phos/CAG CTA GTC TGC/iAmMC6T/CA GAT ATC GTC G/3Bio/-3') from IDT was ethanol precipitated. 5nmol of the oligo was diluted in labelling buffer (189 mM disodium tetraborate, pH 8.5) containing 89 ug Atto647N NHS-ester dissolved in DMSO (anhydrous). Thus, the reaction is performed using a 20x molar dye excess. The reaction was kept in the dark, overnight (o/n), with soft agitation. The labelled oligo was annealed to its complementary DNA stand without biotin or fluorescent dyes using a temperature gradient reaching from 95 °C to 25 °C. Each step was performed for 2 min.

#### **c) Ligation of the unlabelled array DNA with the labelled DNA oligo**

The unlabelled array DNA and the small biotin/Atto647N oligo were ligated in a reaction, having 3x molar excess of the small oligo, using T4 DNA ligase. The reaction was done o/n, RT, in the dark, with soft agitation. To remove the labelled oligo a PCR purification (Qiagen) following the manufacturer's protocol was done, followed by two PEG precipitation steps (8 % PEG). A final ethanol precipitation was done and the DNA was resuspended in 1x TE buffer. A typical labelling efficiency was 90 % labelling.

#### **1x177 bp 601 DNA with biotin and Atto647N for mononucleosomes via PCR**

A PCR reaction using the following primers was used to amplify the 1x177 bp 601 DNA:

5' /5ATTO647NN/CGCACACTGTGCCAAGTACTTAC

3' /5Biosg/GCTAGCGGTTTGAGACCAAGTACTCCATGGATCTAGAGATCTCTGC

Sequence (green: nucleosome positioning sequence), which was amplified from a Lab-internal plasmid:

CGCACACTGTGCCAAGTACTTACGCGGCCGCCCTGGAGAATCCCGGTGCCGAGGCCGCTCAATTGGT  
CGTAGACAGCTCTAGCACCGCTTAAACGCACGTACGCGCTGTCCCCGCGTTTTAACC GCCAAGGGG  
ATTACTCCCTAGTCTCCAGGCACGTGTCAGATACTGCAGAGATCTCTAGATCCATGGAGTACTTGGTC  
TCAAACCGCTAGC

<b>Table M10 PCR reaction to create 1x177 bp 601 DNA</b>		
Component	Stock	50x50 ul reactions
Template DNA plasmid	2 ng/ul	50 ul
5' primer	100 uM	6.25 ul
3' primer	100 uM	5 ul
dNTP	10 mM	50 ul
Thermopol buffer	10 x	250 ul
water	-	2073.75 ul
Taq polymerase	5 u/ul	15 ul

<b>Table M11 PCR program to create 1x177bp 601 DNA</b>			
Step	Temp	time	Cycles
Denaturation	94 °C	20 s	1
Denaturation	94 °C	20 s	29
Annealing	60 °C	20 s	
Extension	72 °C	20 s	
Final Extension	72 °C	20 s	1
Hold	12 °C	forever	1

Reactions were pooled and a PEG precipitation (11 %) was done twice. The re-dissolved pellets were subjected to an ethanol precipitation and dissolved in MQ water.

### 2.12.2. Histone octamer assembly

Lyophilized human core histones (H2A, H2B, H4, H3 C110A) were dissolved to ~2 mg/ml in histone unfolding buffer (20 mM Tris-HCl pH 7.5, 6 M guanidium-HCl, 5 mM DTT), they were incubated for 10 min, 4 °C and then centrifuged (1 min, 15'000 rpm, 4 °C). Non-aggregated histones were mixed: 53 nmol H3 C110A, 53 nmol H4, 58.3 nmol H2A and 58.3 nmol H2B. The histone mixture was dialyzed using a Slide-A-Lyzer dialysis cassette (7000 MWCO, Thermo Scientific) against histone octamer refolding buffer (10 mM Tris-HCl pH 7.5, 2 M NaCl, 1 mM EDTA, 1 mM DTT) o/n. Dialyzed octamers were centrifuged 10 min, 15'000 rpm, 4 °C to remove aggregates. The sample was concentrated using vivaspin 500 (MWCO 10'000) spin columns at 8000 xg, 10 min, 4 °C. Concentrated octamers were centrifuged 10 min, 15'000rpm, 4 °C to remove aggregates once more. Octamers were separated using the size exclusion chromatography column (FPLC, S200 10/300 GL). Octamers elute at 13 ml, tetramers (H4-H3) at 14 ml and dimers (H2A/H2B) at 16 ml elution volume. Octamer-containing fractions were pooled and concentrated using vivaspin 500 columns. Then the octamers were centrifuged for 10 min, 15'000 rpm, 4 °C to remove aggregates. Octamers are stored at -20 °C in 50 % glycerol.



H3K27me3 octamers were supplied by Caroline Lechner, H3K36me3 were supplied Caroline Lechner and Nora Guidotti (LCBM, EPFL, CH), and *X. leavis* histones containing the H3K27M mutation were provided by Jeongyoon Choi.

### 2.12.3. Mononucleosome assembly

Mononucleosomes were either refolded using the dialysis method in “IV, 2.12.4. Chromatin assembly” or by following the protocol described in Dyer et al., 2004<sup>164</sup>.

#### **Luger microscale mononucleosome assembly:**

Labelled, biotinylated 1x177 bp 601 DNA was combined with 2 M NaCl and different ratios of modified or unmodified octamers at RT. Samples were centrifuged for 15 min, 15'000 rpm, 4 °C. The mononucleosome solution (2 M NaCl) was diluted after 30 min using 10 mM Tris-HCl buffer pH 7.6 and then every hour to lower the salt concentration as follows: 1 M, 800 mM, 670 mM, 400 mM, 200 mM. Then, samples were left for another hour, centrifuged again 15 min, 15'000 rpm, 4 °C and quality was assessed on a self-made 5 % TBE gel (using acrylamide/bisacrylamide (19:1), 40 %) or a 5 % TBE Criterion gel (200 V, 60 min, 4 °C).

### 2.12.4. Chromatin assembly

Opposed to mononucleosome assemblies, it is important to ensure occupancy of all the 12 nucleosome positioning sequences with individual histone octamers. Thus, we add MMTV DNA to the nucleosome formation solution, which has lower affinity for histone octamers than the 601 DNA. Typically, we assemble 0.8 uM chromatin arrays in 30 ul as follows: labelled, biotinylated 12x177 bp 601 DNA was combined with different ratios of modified or unmodified octamers (e.g. 1.5, 1.8 equivalent) and 0.5 equivalent of MMTV in dialysis end buffer (10 mM Tris-HCl pH 7.5 (4 °C), 10 mM KCl, 0.1 mM EDTA), which was complemented with 2 M NaCl. The samples were placed in Slide-A-lyzer MINI dialysis units (10'000 MWCO) in dialysis start buffer (10 mM Tris-HCl pH 7.5 (4 °C), 1.4 M KCl, 0.1 mM EDTA). The dialysis was driven by a peristaltic pump to dilute the dialysis start buffer (200 ml) with dialysis end buffer (2 liter) in ~16 h, 4 °C. The next day, chromatin arrays were kept in the end buffer and a small sample was subjected to a HF-ScaI restriction digestion (37 °C, 6 h) as the enzyme cleaves the DNA between the nucleosome positioning sequences and renders mononucleosomes. Quality of chromatin arrays and ScaI-mediated mononucleosomes was assessed on a self-made 5 % TBE gel (using acrylamide/bisacrylamide (19:1), 40 %) or a 5 % TBE Criterion gel (in 0.5x TBE buffer, 200 V, 60 min, 4 °C).

MMTV DNA sequence:

```
ACTTGCAACAGTCCTAACATTCACCTCTTGTGTGTTTGTGTCTGTTCCGCGATCCCGTCTCCGCTCGTCA  
CTTATCCTTCACTTCCAGAGGGTCCCCCGCAGACCCCGCGACCCTGGTCGGCCGACTGCGGCAC  
AGTTTTTTG
```

## 2.13. Agarose polyacrylamide composite gel electrophoresis

### **Casting gels:**

For analysis of chromatin arrays, a 1 % agarose and 1.5 % acrylamide/bisacrylamide (40 %, 1:19) was prepared by adding acrylamide to the hot 1 % agarose solution. Gel-polymerization was induced with ammonium persulfate and TEMED. The gel was poured into assembled 20 x 20 cm glass plates and polymerized for 1 h.

### **Running conditions:**

Samples (1-2 ug) for APAGE were combined with D-sucrose (5 % (w/v)) for loading. Gels were run in 0.25x TAE buffer (10 mM Tris-HCl, 0.03 % (v/v) glacial acetic acid, 0.25 mM EDTA (pH 8.0)) for 2.5 h, 200 V, 4 °C.

### **Analysis:**

The gel was stained for 10-30 min in GelRed solution (15 ul GelRed per 50 ml MQ water). GelRed images and fluorescence images were taken on a ChemiDoc™ MP imaging system.

## 2.14. Preparation of flow channels for TIRF microscopy

### **Glassware cleaning and silanization:**

In our laboratory, typically, we applied piranha cleaning of glassware, which employs a solution of hydrogen peroxide and sulfuric acid. After rigorous cleaning we functionalized the glass with 3-aminopropyltriethoxysilane (APTES) in order to attach PEG chains to the glass surface. This was important to avoid non-specific sticking of proteins to the glass surface, which would be illuminated by TIRF. To investigate single molecules engaging on chromatin, we envisioned a system, where we could attach chemically modified chromatin chains to the surface of the glass slide. In order to do so, some of the utilized PEG-chains were functionalized with biotin. By attaching biotin to DNA, which we use for chromatin/nucleosome assembly, we were able to immobilize the nucleosome particles on the glass surface using neutravidin-biotin interactions. Selective excitation of fluorophores on the glass surface using TIRF microscopy would be possible to identify nucleosome particles, if the fluorophore was attached to the DNA, which we engaged for nucleosome/chromatin formation. After APTES-treatment, we assembled glass slides and coverslips with two-sided sticky tape to create a maximum of flow channels (in our case four) per slide, which can be employed for TIRF microscopy. In the following we describe this procedure in detail:

A Dremel Europe workstation 4000 drill machine was used to drill 4x2 holes (1 mm diameter) into a glass slide (26 mm x 76 mm). Glass slides and coverslips (24 mm x 40 mm) were placed in glass staining jars and sonicated (Sonicator Elmasonic P, Frequency: 37, Power:

100, Temperature 23 °C) for 20 min in 10 % (w/v) Alcanox. Alcanox was disposed and glassware was washed extensively with MQ water. Then, glassware was sonicated for 20min in acetone, washed with MQ water and sonicated for 20 min in ethanol with a subsequent wash step. Dry glassware was incubated with fresh piranha solution (3:1 sulfuric acid and hydrogen peroxide) for 1 h, RT, in the fumehood. Glassware wash rinsed extensively with MQ water until the pH was neutral. Glassware was prepared for silanization during a 10 min sonication step in acetone. 2 % (v/v) APTES in acetone was added to the glassware for 5 min, RT, the glassware was sonicated in APTES solution for 1 min and incubated for another 5 min, RT. The silanization reaction was quenched with MQ water. Glassware was dried with N<sub>2</sub> (g) and assembled to flow channels containing 4 channels per glass slide using double-sticky tape (0.12 mm) as channel walls and epoxy glue to seal the channel ends. Assembled flow channels were evacuated and stored at -20 °C.

#### **Flow channel assembly and PEGylation:**

On the day of measurement flow channels were thawed for 1 h, RT. Evacuated flow channels were filled with air and pipette tips were glued into the drill holes using epoxy glue as injection reservoirs. PEGylation was done for 3 h as follows: 10 mg BIOTIN-PEG-SC (MW: 5000) and 40 mg mPEG-SC (MW: 5000) were dissolved in 350 ul sodium tetraborate buffer (189 mM sodium tetraborate, pH 8.5) within 8 s via centrifugation (4 °C) and injected into the flow channels.

### **2.15. TIRF imaging**

For (objective-type) TIRF imaging, a fully automated Nikon Ti-E inverted fluorescence microscope, controlled by NIS-elements, equipped with a CFI Apo TIRF 100x Oil immersion objective (NA 1.49) and equipped with a manually controlled TIRF illuminator arm was employed. Data was acquired using an iXon EMCCD camera (Andor), with one pixel corresponding to 160nm. Excitation light was provided from a home-built laser bench. Employed lasers were: A coherent OBIS 640 LX (640 nm, 40 mW), coherent OBIS 488 LX (488 nm, 50 mW) and a TECGL Series WS 532 (532 nm, 30 mW). Wavelength selection and switching of the excitation light was performed using an AOTF controlled by NIS-elements.

Imaging buffer conditions:

IB1: 50 mM HEPES pH 7.5, 130 mM KCl, 10% (v/v) glycerol, 0.005 % (v/v) tween 20, 2 mM trolox, 3.2 % (w/v) glucose, 1x glucose oxidase/catalase enzymatic oxygen depleting system.

IB2: 50 mM HEPES pH 7.5, 130 mM KCl, 10 % (v/v) glycerol, 0.005 % (v/v) tween 20, 2 mM trolox, 3.2 % (w/v) glucose, 50 mM MgCl<sub>2</sub>, 1 uM ZnCl<sub>2</sub>, 1x glucose oxidase/catalase enzymatic oxygen depleting system.

IB3: 30 mM HEPES pH 7.5, 20 mM NaCl, 2 mM trolox, 3.2 % (w/v) glucose, 10 mM Imidazole, 5 mM MgCl<sub>2</sub>, 1.1 uM ZnCl<sub>2</sub>, 1 mM BME, 2 mM ATP, 5 mg/ml BSA, 10mM creatine phosphate, 0.2 ug/ml creatine kinase, 1x glucose oxidase/catalase enzymatic oxygen depleting system.

IB4: 30 mM HEPES pH 7.5, 20 mM NaCl, 2 mM trolox, 3.2 % (w/v) glucose, 10 mM Imidazole, 1  $\mu$ M ZnCl<sub>2</sub>, 1 mM BME, 2 mM ATP, 10 % (v/v) glycerol, 0.1 mg/ml BSA, 1x glucose oxidase/catalase enzymatic oxygen depleting system.

IB5: 30 mM HEPES pH 7.5, 50 mM NaCl, 2 mM trolox, 3.2 % (w/v) glucose, 0.005 % (v/v) tween 20, , 0.1  $\mu$ M ZnCl<sub>2</sub>, 10 % (v/v) glycerol, 5 mg/ml BSA, 1x glucose oxidase/catalase enzymatic oxygen depleting system.

### 2.15.1. HP1 $\alpha$ TIRF imaging

For chromatin imaging experiments with HP1 $\alpha$ , the flow channel was washed with 50  $\mu$ l T50 buffer (10 mM Tris pH 8.0, 50 mM NaCl), using an automated pump (WPI SP210IWZ syringe pump). The background level of fluorescence was recorded with both 532 nm and 640 nm excitation. 50  $\mu$ l of 0.2 mg/ml neutravidin solution was then injected into the channel and incubated 5 min, followed by washing with 500  $\mu$ l T50. Subsequently, biotinylated and Atto647N labelled chromatin arrays were flowed into the channel at a concentration of 500 pM, followed by 2 min incubation. The immobilization step was monitored by Atto647N emission, aiming for a coverage level of 100-200 arrays in a 25 x 50  $\mu$ m imaging area. Excess chromatin in solution as well as MMTV DNA and associated nucleosomes were removed by a washing step and the buffer exchanged to imaging buffer (50 mM HEPES pH 7.5, 130 mM KCl, 10 % (v/v) glycerol, 0.005 % (v/v) tween 20, 2 mM trolox, 3.2 % (w/v) glucose, 1x glucose oxidase/catalase enzymatic oxygen depleting system). HP1 $\alpha$  dilutions in imaging buffer were freshly prepared from a 100 nM stock and injected into the channel. Imaging of HP1 $\alpha$  binding dynamics was performed at a framerate of 20 frames/s (50 ms integration time) using 532 nm excitation for 10'000 frames. Every 200 frames, the excitation was switched to 640 nm for one frame to record the positions of the chromatin arrays. These frames were used in data analysis to localize array positions and correct for stage drift. Once immobilized, chromatin arrays were used for measurements for maximal one hour, to avoid disintegration of the chromatin. For all measurements, light intensities of 20 W/cm<sup>2</sup> were employed for 532 nm and 40 mW/cm<sup>2</sup> for 640 nm.

### 2.15.2. PRC2 TIRF imaging

For PRC2 imaging experiments, the flow channel was washed with 50  $\mu$ l T50 buffer (10 mM Tris pH 8.0, 50 mM NaCl), using an automated pump (WPI SP210IWZ syringe pump). The background level of fluorescence was recorded with both 532 nm and 640 nm excitation. 50  $\mu$ l of 0.2 mg/ml neutravidin solution was then injected into the channel and incubated 5 min, followed by washing with 500  $\mu$ l T50. Subsequently, biotinylated and Atto647N labelled chromatin arrays were flowed into the channel at a concentration of 500 pM, followed by 2 min incubation. The immobilization step was monitored by Atto647N emission, aiming for a coverage level of 100-200 arrays in a 25 x 50  $\mu$ m imaging area. Excess chromatin in solution as well as MMTV DNA and associated nucleosomes were removed by a washing step and the buffer exchanged to imaging buffer 5 (30 mM HEPES pH 7.5, 50 mM

NaCl, 2 mM trolox, 3.2 % (w/v) glucose, 0.005 % (v/v) tween 20, 0.1  $\mu$ M ZnCl<sub>2</sub>, 10 % (v/v) glycerol, 5 mg/ml BSA, 1x glucose oxidase/catalase enzymatic oxygen depleting system). PRC2 dilutions in imaging buffer 5 were freshly prepared from a 100 nM stock and injected into the channel. Imaging of PRC2 binding dynamics was performed at a framerate of 20 frames/s (50 ms integration time) using 532 nm excitation for 10'000 frames. Every 200 frames, the excitation was switched to 640 nm for one frame to record the positions of the chromatin arrays. These frames were used in data analysis to localize array positions and correct for stage drift. Once immobilized, chromatin arrays were used for measurements for maximal one hour, to avoid disintegration of the chromatin. During measurements a flow rate of 80  $\mu$ l/min was applied.

### 2.15.3. TIRF data analysis

Movies of HP1 $\alpha$ /PRC2 binding dynamics were processed with a custom-built Matlab (Mathworks) program suite. First, a background correction was applied by fitting a two dimensional Gaussian profile to the image (overwhelming background) and subtracted from each frame. Subsequently, chromatin array positions were determined by a thresholding/local maxima approach. Then, all images were aligned using the chromatin array images (every 200<sup>th</sup> frame) to correct for stage drift. In a semiautomatic program, well isolated chromatin peaks were selected in the frames recorded with 640 nm excitation. The fluorescence intensity within a 2 pixel radius around the peak was integrated over the whole stack of images and extracted as a fluorescence intensity vs time trace, showing HP1 $\alpha$  binding events. Every detected peak (532 nm excitation, corresponding to bound HP1 $\alpha$  molecules) was automatically fitted to a two-dimensional Gaussian profile, and the peak width as well as x, y positions were recorded. Peaks with a width exceeding the experimentally determined point spread function (PSF) for a single Atto532 dye molecule, as well as peaks whose maxima were offset from the determined chromatin position were excluded from further analysis. Traces were then filtered using a forward-backward non-linear filter to reduce noise, while preserving sharp transitions<sup>276</sup>. Steps (binding events) were detected using a thresholding algorithm in a semi-automatic procedure, and on- and off-times were determined. All the fitted traces were further checked manually.

Cumulative histograms were generated from traces corresponding to individual chromatin arrays or from cumulative histograms from 100 traces and fitted to either single- or double exponential kinetics.

For PRC2 dissociation kinetics bleaching correction was applied.

#### **Bleaching correction:**

500 nM EZ-link maleimide-PEG<sub>2</sub>-biotin was incubated with 100 nM labelled PRC2 for 1 h in bleaching buffer (50 mM HEPES pH 7.5, 50 mM NaCl, 0.001 % (v/v) tween 20, 10 % (v/v) glycerol to biotinylate the labelled PRC2. Then the reaction was dialysed against fresh bleaching buffer for 3 h (4 °C). The sample was centrifuged for 10 min (15'000 rpm, 4 °C).

The labelled protein was immobilized on flow channels in imaging buffer 5 and bleaching rates at different laser intensities were measured. To correct for photobleaching, obtained cumulative histograms for dissociation times were divided by the bleaching histogram to obtain the final values (see formula (9), page 72).

## 2.16. Thermophoresis assays

To evaluate interactions between HP1 $\alpha$  and the synthesized peptides, a microscale thermophoresis was done on a Monolith NT.115 (NanoTemper Technologies GmbH, Munich, Germany) using hydrophilic capillaries employing NT.control- and NT.analysis software. The HP1 $\alpha$ -Atto532 protein was provided by Sinan Kilic and the interacting peptides **P3** and **P4** by me. Measurements were done in Thermophoresis buffer (50 mM HEPES pH 7.5, 150 mM NaCl, 1 mM DTT, 0.05 % (v/v) tween 20). The HP1 $\alpha$  concentration was at 50 nM, while peptide concentrations were altered from 1 nM to 40  $\mu$ M.

## 2.17. Ubiquitination assays

Ubiquitination assays were performed in volumes of 30-40  $\mu$ l using 1xUB buffer (30 mM HEPES pH 7.5, 5 mM MgCl<sub>2</sub>, 0.2 mM DTT, 10 mM sodium citrate, 20 mM ATP, 10 mM creatine phosphate tetrahydrate, 0.2  $\mu$ g/ml creatine phosphokinase). Creatine phosphokinase was included to ensure regeneration of ADP to ATP using its substrate creatine phosphate. We typically added 3-31  $\mu$ M ubiquitin, 42-600 nM UBE1, 400 nM -3.65  $\mu$ M UBE2D3, 0.1-1  $\mu$ M RNF168 and 400-900nM Atto488-H2A octamers. UBE1 was always added last to the reaction mix, then the reaction was started at 37 °C for 1-2 h. To quench the reaction we added 12  $\mu$ l SDS-loading dye to 5-10  $\mu$ l of the corresponding reaction mix and boiled the tube at 100 °C for 5 min. Assays were analysed using SDS-PAGE with fluorescence imaging and/or western blots.

### Ubiquitination assay quantification by densitometry:

Bands were initially normalized to comparable starting levels of the reaction (based on labelled ubiquitin or H2A). As usually the different replicates of experiments showed slightly different absolute values, which depends e.g. on pipetting, we normalized the data to the first replicate. The ubiquitination-band intensity at time point 1 min ( $I_{1min}$ ) was divided by the ubiquitination-band intensity at the last time point ( $I_{end}$ ). This rendered a value of ubiquitination success ( $U_s$ ) for each replicate.  $U_s$  of the first replicate ( $U_{s1}$ ) was divided by  $U_s$  of each replicate ( $U_{sn}$ ) to obtain a normalization value for each replicate towards replicate 1. The absolute intensity values ( $I_n$ ) were multiplied by the individual normalization factor ( $U_{norm}$ ) and rendered levels of relative ubiquitination activity, named normalized band intensity ( $I_{norm}$ ):



*Ubiquitination success:*

$$U_S = \frac{I_{1min}}{I_{end}} \quad (M2)$$

*Ubiquitination normalization factor:*

$$U_{norm} = \frac{U_{S1}}{U_{Sn}} \quad (M3)$$

*Normalized band intensity:*

$$I_{norm} = U_{norm} \times I_n \quad (M4)$$

When we calculated total ubiquitination using quantification of the sum of mono- and di-ubiquitin bands, we doubled values of di-ubiquitin bands, based on the two ubiquitin-moieties present on H2A.

In cases when H2A was used as read-out,  $U_S$  could not be assessed, as the H2A band was always non-existent at the last time point. In these cases starting levels of H2A ( $H_{start}$ ) of individual replicates ( $n_1, n_2$ ) were simply normalized to each other:

*Histone H2A normalization factor:*

$$H_{norm} = \frac{H_{start,n1}}{H_{start,n2}} \quad (M5)$$

Normalized band intensity (H2A):

$$I_{norm (H2A)} = H_{norm} \times I_n \quad (M6)$$

## 2.18. Pull-down of ubiquitin chains by RNF168

The glutathione resin was “charged” with RNF168 as described:

After expression, the pellet was dissolved in 25 ml Cell lysis buffer and frozen at -80 °C. Then, after thawing, the lysate was sonicated. Lysed cells were centrifuged at 15'000 xg for 10 min and the soluble fraction was filtered and then loaded onto 1.5ml glutathione resin per liter culture, as the protein contains an N-terminal GST-tag. The protein was bound to the resin after equilibration with PBS (pH 7.3) by gentle nutating for 1 h (4°C) before the flow through was collected. Then, the resin was washed with 3x10 CV of GST-binding buffer (PBS pH 7.3, 1 mM BME, 1 uM ZnCl<sub>2</sub>).

350-500 ul RNF168-resin were transferred to a Micro Bio-Spin™ Column per experimental condition. We applied 290 pmol di-ubiquitin (K48- or K63-linked, Boston Biochem; synthetic K48-, synthetic K63-linked, Joachim Lutz, University of Konstanz, Germany) in 205 ul PBS (pH 7.3) and tubes were incubated for 30-60 min (4 °C, gentle agitation). Then the resin was washed with 3x750 ul PBS (pH 7.3, 1 mM BME, 1 uM ZnCl<sub>2</sub>).

Elution was done using 2x150-300 ul GST-elution buffer. An anti-ubiquitin western blot was done for analysis.

## 2.19. FRAP measurements

Microscopy was performed 24-32 h post-transfection using an inverted LSM 700 confocal microscope and a Plan apochromat x 63/1.4NA objective. The solid-state lasers at 405 nm and 488 nm were used for excitation. A short pass filter below 490 nm and a long pass filter beyond 490 nm were used for DAPI and mEos3.2 fluorescence, respectively. Images were acquired in 512 x 512 pixels with a 0.07 um pixel size, 12-bit grey-scale depth, line averaging of 4 and a pixel dwell time of 6.30 us. The laser power was set at 1.5 – 3.0 %, the master gain at 750 – 800 and the digital gain at 1.5 using a pinhole size of 60.5 um. FRAP bleaching and time-series images were acquired in 128 x 128 pixels with 0.07 um pixel size, 12-bit grey-scale depth and a pixel dwell time of 1.58 us (scan time: 121 ms). Master gain and digital gain were 750 – 800 and 1.5, respectively, with the pinhole set at 201 um. A circular spot of 14 pixels (1.04 um) in diameter was used for bleaching. Twenty pre-bleach images were acquired before 10 iterations of a bleaching pulse at 80 % laser power used and images were acquired for the subsequent 34 s. Photobleaching during the time-series was corrected using the intensity in the bleach region relative to the entire acquisition region. The time-intensity acquisitions were normalized to the pre-bleach intensity and the first image after the bleach pulse. Results are averaged over 30-40 individual FRAP curves for the wild-type and the mutants.



## V Abbreviations

AA	Amino acids
AAD	Active adenylation domain
AIEX	Anion exchange chromatography
AOTF	Acousto-optical tunable filter
APAGE	Agarose polyacrylamide composite gel electrophoresis
APH	Affinity purification handle
APTES	3-Aminopropyltriethoxysilane
ATM	Ataxia telangiectasia mutated
ATR	Ataxia telangiectasia mutated and Rad3-related
BME	$\beta$ -mercaptoethanol
BRD4	Bromodomain-containing protein 4
c-IAP1	cellular inhibitor of apoptosis protein 1
CBX	Chromobox
CD	Chromo domain
ChIP	Chromatin immunoprecipitation
CoA	Coenzyme A
CPEC	Circular polymerase extension cloning
CSD	Chromoshadow domain
CV	Column volume
DCM	Dichloromethane
DDR	DNA damage response
DIPEA	<i>N,N</i> -diisopropylethylamine
DMF	Dimethylformamide
DNA	Deoxyribonucleic acid
ds	double-stranded

DSB	DNA double-strand break
DTT	DL-Dithiothreitol
DUB	Deubiquitinating enzyme
EBD	EED-binding domain
EED	Embryonic ectoderm development
EMSA	Electromobility shift assay
EM	Electron microscopy
EMT	Electron microscopy tomography
EPL	Expressed protein ligation
ESI-MS	Electrospray mass spectrometry
E(Z)	Enhancer of zeste
EZH2	Enhancer of zeste homolog 2
E1	Ubiquitin-activating enzyme
E2	Ubiquitin-conjugating enzyme
E3	Ubiquitin ligase
FCCH	First catalytic cysteine half-domain
FCS	Fetal calf serum
FHA	Forkhead-associated domain
Flc	Fluorescein
FOXO1	Forkhead box protein O1
FRAP	Fluorescence recovery after photobleaching
smFRET	single-molecule Förster resonance energy transfer
FT	Flow through
GST-tag	Glutathione S-transferase tag
h	<i>Homo Sapiens</i>
HDAC	Histone deacetylase

HF-enzyme	High-fidelity enzyme
HP1	Heterochromatin protein 1
HP1 $\alpha_{\text{cdm}}$	covalently linked dimeric HP1 alpha protein
HR	Homologous recombination
hSgoL1	human shugoshin 1 protein
IAD	Inactive adenylation domain
IDT	Integrated DNA technologies
ITC	Isothermal calorimetry
kDa	kilo Dalton
LRM1/2	LR motif 1/2
L3MBTL2	Lethal(3)malignant brain tumour-like protein 2
RT	Room Temperature
MDC1	Mediator of DNA damage checkpoint 1
meDIP	methyated DNA immunoprecipitation
MIU1/2	Motif interacting with ubiquitin 1
MOI	Multiplicity of infection
MQ water	MiliQ water = ddH <sub>2</sub> O
MW	Molecular weight
NCL	Native chemical ligation
NF- $\kappa$ B	Nuclear factor kappa enhancer binding protein
NHEJ	Non-homologous end joining
NPS	Nucleosome positioning sequences
NpuN/NpuC	<i>N. punctiforme</i> split-intein (N-terminal or C-terminal part)
o/n	overnight
P/S	Penicillin/Streptomycin
PcG	Polycomb group

Pcl	Polycomblike
PCR	Polymerase chain reaction
Pd(PPh <sub>3</sub> ) <sub>4</sub>	Tetrakis(triphenylphosphine) palladium(0)
PEG	Poly(ethylene glycol)
PHD	Plant homeodomain
PhSiH <sub>3</sub>	Phenylsilane
PID	PALB2-interacting domain
PIKK	Phosphatidyl inositol 3' kinase-related kinase
PRC1/2	Polycomb repressive complex 1/2
PSF	Point spread function
PTM	post-translational modification
RBBP4	Retinoblastoma-binding protein 4
RING	Really Interesting New Gene
RNA	Ribonucleic acid
RNF168	RING finger protein 168
RP-HPLC	Reversed-phase HPLC
SCCH	Second catalytic cysteine half-domain
SDS	Sodium dodecyl sulfate
SDS-PAGE	SDS-polyacrylamide gel electrophoresis
SEM	Standard error of the mean
SFP synthase	Sfp phosphopantetheinyl transferase
SPPS	Solid-phase peptide synthesis
STREP-tag	Streptactin binding tag
SUZ12	Suppressor of zeste 12 protein homolog
TIRFM	Total internal reflection fluorescence microscopy
Thz	Thiazolidine

UAA	Unnatural amino acid
UAD	Ubiquitin-associated domain
UDM1/2	Ubiquitin-dependent DSB recruitment module 1/2
UFD	Ubiquitin-fold domain
UMI	Ubiquitin-interacting motif
WH	Winged-helix
wt	wild-type
6xHis	Hexahistidine-tag



## VI Appendix

Table A1	
Antibodies	Supplier
Antibody: Anti-H1.2 (# GTX122561, polyclonal, rabbit, Wb use 1:5000)	Gene Tex
Antibody: Anti-H2A (#39209, polyclonal, rabbit, Wb use 1:1000)	Active Motif
Antibody: Anti-H2A acidic patch (#07-146, polyclonal, rabbit, Wb use 1:1000)	Millipore
Antibody: Anti-H2A.X (#07-627, polyclonal, rabbit, Wb use 1:2000)	Millipore
Antibody: Anti-FLAG M2 (#F1804-50UG, monoclonal, mouse)	Sigma
Antibody: Anti-H3K9me3 (#61013, monoclonal, mouse, Wb use 1:250)	Active Motif
Antibody: anti-ubiquitin (#P4D1 sc-8017, mouse)	Santa Cruz
Antibody: secondary HPR-linked anti-mouse antibody (goat)	Sigma
Antibody: secondary HPR-linked anti-rabbit antibody IgG (#711-035-152, donkey)	Immunoresearch laboratories Inc.

Table A2

Materials	Supplier
Acetic acid (glacial)	Merck
Acetone	Sigma
Acetonitrile	Lab Scan
Acrylamide/bisacrylamide (19:1), 40%	Bio-Rad
Acrylamide/bisacrylamide (29:1), 30%	Bio-Rad
Alconox	Sigma and Alconoc Inc.
Adenosine 5'-triphosphoric acid disodium salt (C <sub>10</sub> H <sub>14</sub> N <sub>5</sub> Na <sub>2</sub> O <sub>13</sub> P <sub>3</sub> , ATP)	Applichem
Agarose	Bio-Rad
Agarose: 4% agarose gel (for cell culture) 18300-012 40ml	Gibco - Life Technologies, Thermo Scientific
Alexa Fluor 568 C5 Maleimide	Thermo Fisher Scientific, life technologies
Ammonium persulfate	Bio-Rad
Ampicillin sodium salt	Applichem
Antarctic phosphatase (5U/ul)	NEB
Antarctic phosphatase buffer 10x	NEB
Antibiotics (Penicillin/Streptomycin, 10'000U/ml)	Life Technologies, Thermo Scientific
Antifoam 204 (A6426-100g)	Sigma
Biotin (B4501-1G)	Sigma
BIOTIN-PEG-SC (MW: 5000)	Laysan Bio Inc.
Biotin-16-dCTP (1mM)	Jena Bioscience
Boric acid	Merck and Fluka
Bovine Serum Albumin, protease free (BSA)	Sigma
Bovine Serum Albumin for TIRF (fraction V)	Carl Roth
Bradford dye reagent	Bio-Rad
Bromophenol blue	Applichem
HF-Bam enzyme (20U/ul)	NEB
HF-BsaI enzyme (20U/ul)	NEB
HF-EcoRV enzyme (20U/ul)	NEB
Calcium chloride dihydrate (CaCl <sub>2</sub> *2H <sub>2</sub> O)	Applichem
Catalase (from Bovine liver)	Sigma
Cellfectin II reagent	Life Technologies, Thermo Scientific
Chloramphenicol	Applichem
Clarity™ Western ECL Blotting Substrates	Bio-Rad
Clicked K48 di-ubiquitin	Marx Lab, Konstanz, Germany
Clicked K63 di-ubiquitin	Marx Lab, Konstanz, Germany
CoA tritium salt dihydrate	Applichem, BioChemica
Coomassie (brilliant blue R250)	Fisher BioReagents
QC Colloidal Coomassie stain (1l, Cat#: 161-0803)	Bio-Rad
Creatine phosphate tetrahydrate (327.14g/mol)	Sigma
Creatine (phospho-)kinase (Rabbit muscle, MW: 81'000D)	Sigma
Criterion gel 5% TBE	Bio-Rad
Cut smart buffer	NEB
D-desthiobiotin	Sigma
D-sucrose	Fisher Scientific
Diethylether	Merck
Dimethyl sulfoxide (DMSO) anhydrous	Sigma
Dimethyl sulfoxide (DMSO)	Sigma
Disodiumtetraborate decahydrate	Applichem
DL-Dithiothreitol (DTT)	Sigma
DNAseI (A3778,0100)	Applichem
dNTP	NEB
DpnI restriction enzyme	NEB
Dulbecco's PBS for cell culture (without Ca <sup>++</sup> /Mg <sup>++</sup> , 3-05F29-I)	BioConcept
EcoRV-HF restriction enzyme	NEB
Ethylenediamintetraaceticacid (EDTA)	Applichem
Ethanol	Sigma
EZ-link maleimide-PEG <sub>2</sub> -biotin (#21901)	Thermo Scientific
Fetal Calf Serum (FCS)	Gibco - Life Technologies, Thermo Scientific



Table A2 (continued)

Fluorescein-5-maleimide	Thermo Fisher Scientific
Gelred	Biotium
Gentamycin (BP918-1, C21H43SO7*H2SO4, CAS: 1405-41-0)	Fisher BioReagents
Glucose	Fisher BioReagents
Glucose oxydase (from Aspergillus Niger)	Sigma
Glycerol	Fisher Scientific
Glycine	Sigma
Grace insect medium (1x)	Life technologies, Thermo Scientific
Guanidium hydrochloride	MP biomedical
HEPES	Sigma
His-Ube1 (E1, 121kD)	Boston Biochem
Hydrochloric acid (HCl)	Merck
Hydrogen peroxide (H2O2)	Merck
Hydrogen peroxide (H2O2 30% stock)	Rectolab S.A.
Imidazole	Fisher Scientific
Insect cells Sf-9 in Sf-900 II medium	Life technologies, Thermo Scientific
Isopropyl β-D-1-thiogalactopyranoside (IPTG)	Applichem
Kanamycin sulphate	Carls roth
K48 linked di-ubiquitin (UC-200B, 1mg/ml, 58uM)	Boston Biochem
K63 linked di-ubiquitin (UC-300B, 1mg/ml, 58uM)	Boston Biochem
L-glutathione reduced	Sigma
LB agar, Miller	Fisher BioReagents
LB broth	Fisher BioReagents
Lysozyme	Applichem
Magnesium chloride hexahydrate (MgCl2*6H2O)	Fluka
Magnesium sulfate heptahydrate (MgSO4*7H2O)	Fluka
D-(+)-Maltose monohydrate, BP684-500)	Fisher BioReagents
Manganese (II) chloride tetrahydrate (MnCl2*4H2O)	Applichem
Medium: Sf-900™ II SFM (1x) serum-free (10902-096 500ml)	Gibco - Life Technologies, Thermo Scientific
Medium for viral plaque assay: Sf-900™ (1.3x, 10967-032 100ml)	Gibco - Life Technologies, Thermo Scientific
Methanol	Sigma
Methanol	Thommen-Furler AG
MiliQ water	Thermo scientific GenPure
MiliQ water	Thermo Electron LED GmbH
mPEG-SC (MW: 5000)	Laysan Bio Inc.
NAD	Applichem
NEB 2 buffer	NEB
NEB 4 buffer	NEB
Neutravidin	Thermo Scientific
Nickel(II) sulfate (NiSO4)	Fisher Scientific
Nonfat dried milk powder	Applichem
Nonidet P40 (NP-40, IPEGAL® CA-630)	Sigma
PfuUltra HF DNA pol. (2U/ul)	Agilent
Phenylmethanesulfonylfluoride (PMSF)	Applichem
Phusion high-fidelity DNA polymerase (2U/ul)	NEB
Phusion buffer 5x	NEB
Pipes (piperazine-N,N'-bis (2-ethane sulfonic acid)	Applichem
Poly(ethylene glycol) 6000 (PEG 6000, 81255-1kg)	Sigma
Potassium acetate	Applichem
Potassium chloride	Sigma and Acros
Potassium dihydrogen phosphate (KH2PO4)	Applichem
Potassium hydroxide (KOH,)	Sigma
Precision Plus Protein™ All Blue Prestained Protein Standards #1610373	Bio-Rad
Precision Plus Protein™ Dual Color Standards, 500 µl #1610374	Bio-Rad
Protease inhibitor cocktail tablet EDTA free (SigmaFAST™, S8830)	SigmaFAST™
Protease tablets (Complete, EDTA free protease inhibitor cocktail)	Roche
Proteinase K from Tritirachium album (P2308-25mg)	Sigma
proTEV plus 5U/ul	Promega

**Table A2 (continued)**

PVDF membrane	Bio-Rad
Quik reaction buffer 10x	Agilent
Quik solution	Agilent
Q5 buffer 5x	NEB
Q5 high-fidelity DNA polymerase (2U/ul)	NEB
Rnase A (10mg/ml)	Qiagen
Scal-HF restriction enzyme	NEB
Sfp synthase (40uM, 25nmol)	NEB
Sodium acetate trihydrate	Applichem
Sodium azide	Applichem
Sodium chloride	Applichem
Sodium dodecyl sulfate (SDS)	Applichem
Sodium hydroxide (NaOH)	Fluka
Sodium phosphate monobasic	Fisher BioReagents
Spectinomycin dihydrochlorid pentahydrate	Applichem
Sulfuric acid (H2SO4)	Merck
Taq DNA ligase (40U/ul)	NEB
Taq polymerase (5U/ml, M0267L)	NEB
TEMED	Bio-Rad
Tetracycline	Alfa Aesar
TEV protease (1mg/ml)	Caroline Lechner, EPFL, Switzerland
Thermopol buffer 10x	NEB
Thrombin Bovine (604980-100U)	Merck
Tris(2-carboxyethyl)phosphine (TCEP)	Sigma
Trisodium citric acid, anhydrous	Alfa Aesar
Triisopropylsilane (TIS)	Sigma
Trifluoroacetic acid, HPLC grade (TFA)	Fisher Bioreagents
Trifluoroacetic acid (TFA)	Sigma
Tris ultrapure	Applichem
Triton-X100	Sigma
Tryptone	Sigma
Tween 20	Applichem
T4 DNA ligase	NEB
T4 ligase buffer (10x)	NEB
T5 Exonuclease (10U/ul)	NEB
Ubch5c/UBE2D3 (17kD)	Boston Biochem
Ubiquitin (from bovine erythrocytes, 8.5kD)	Sigma
water extrapure (water plus, CAS N. 7732-18-5)	Carlo Erna Reagents
X-gal	Fisher BioReagents
Yeast Extract	Applichem
Zinc chloride	Merck
100bp DNA ladder	NEB
1kb DNA ladder	NEB
2-log DNA ladder	NEB
2-log DNA ladder (Quick-load®)	NEB
2-mercaptoethanol (BME)	Sigma
2-propanol / isopropanol	Merck
2-(4'-Hydroxybenzeneazo)benzoic acid	Sigma
= 4'-Hydroxyazobenzene-2-carboxylic acid (HABA)	
3-Aminopropyltriethoxysilane 99% (APTES)	Sigma and Acros
(+/-) 6-Hydroxy-2,5,7,8-tetramethylchroman-2-carboxylic acid	Sigma

Table A3

Equipment	Supplier
Acryl Cuvette 10x10x45mm REF:67.738	Sarstedt
Anti-FLAG® M2 magnetic beads (M8823-1ml)	Sigma
APAGE glass plates 20cmx20cm	Biorad
BD syringe	Becton Dickinson and company
Cation exchange: HiTrap™ SP HP 5ml column	GE healthcare
Cell culture sterile bench / hood	Heracus instruments GmbH
Cell shaker/incubator	Ecotron, Infors HT
Centrifuge (small) 5424 R	Eppendorf
Centrifuge (big), Allegra® x-15R centrifuge	Beckman coulter
Centrifuge (very big), Avanti™ J-20 xp1 centrifuge ( Rotor: JA-12, JLA 8.1000)	Beckman coulter
ChemiDoc™ MP imaging system	Bio-Rad
Chitin resin	NEB
Coverslips (24mmx40mm)	Menzel, Thermo Scientific
Dialysis membrane tubes = Slide-A-lyzer MINI dialysis units (10'000 MWCO)	Thermo Scientific
DH5alpha, BL21DE3, BL21DE3plyS competent E.coli cells	Novagen
DH10MultiBac cells	Schalch Lab, Geneva, CH
Double sticky tape (0.12mm)	GRACE Bio-labs
Drill machine, Dremel Europe workstation 4000	-
Epoxy glue	ITV Devcon Inc.
ESI-MS (LCQFleet Ion trap Thermo Fisher Mass spectrometer)	Thermo Fisher
Filter column, 3K, 0.5ml	Amicon, Merck
Filter column, 10K, 4ml	Amicon, Merck
Filter column, 10K, 0.5ml (Vivaspin)	Sartorius
Food vacuumizer and plastic foil (V2860)	Foodsaver
FPLC: ÄKTA™ pure, unicorn6.3; Column: Superdex S200 10/300GL (24ml column volume)	GE healthcare
FPLC: ÄKTA™ pure, unicorn6.3; Column: Sepharose 6 XK 30/50 (560ml column volume)	GE healthcare
Freezer (-80°C), Platilab 500V 4-STD, 4/11/2013, L503438 2013	Angelantoni Lifesciences
Glass slides with drillholes (26mmx76mm)	Menzel, Thermo Scientific
Gloves for piranha solution (Camatril 730, size 09)	KCI
Glutathione sepharose 4B	GE healthcare
High precision cell cuvette (3x3mm light path, Quarz (suprasil®), Art no.: 105-251-15-40)	Hellma Analytics
His Trap FF 5ml	GE Healthcare
RP-HPLC (Agilent 1260 series instrument with an Agilent Zorbax C18 column (5µm, 4.6 x 150 mm))	Agilent
MBPTrap HP 2x1ml	GE healthcare
Magnet (Dynal bead separations)	Invitrogen
Membrane Spectra/por 3,500 MWCO 29mm diameter	Spectrumlabs
Micro Bio-Spin(TM) Column Cat# 732.6204 0.8ml bed volume	Bio-Rad
Miracloth	Millipore, Merck
Nalgene™ Single-Use PETG Erlenmeyer Flasks with Plain Bottom: Sterile, 125ml, 250ml, 500ml, 1000ml	Thermo Scientific
NanoDrop2000 Spectrophotometer	Thermo Scientific
Neubauer chamber (for cell counting)	Celeromics
Ni-NTA agarose beads	Qiagen
Orange nitrile gloves	SHIELD scientific
Oven, Thermocenter, TC-100B	Salvis AG
Parafilm (W154956)	Neenah
PCR thermocycler	Bio-Rad
PD-10 G25 desalting column ( 17-0851-01)	GE Healthcare
Peristaltic pump (serial No. A16005123)	IDEX corporation, Ismatec
Peristaltic pump, (Minipuls3, Serial No.: 610A7061)	Gilson Inc.
Preparative HPLC (Agilent 1260 preparative HPLC system)	Agilent
A Zorbax C18 preparative column (7 µm, 21.2 x 250 mm)	Agilent
A Zorbax C18 semi-preparative column (5µm, 9.4 x 250 mm))	Agilent
QIAquick PCR purification kit	Qiagen
Rosetta™ 2 (DE3) Competent cells (71397-3)	Novagen, Merck
(F- ompT hsdSB(rB- mB-) gal dcm (DE3) pRARE (CAMR))	
SDS-gel electrophoresis chamber, holder and power pack	Bio-Rad
Slide-A-Lyzer dialysis cassette (7000 MWCO, 0.5-3ml capacity, #66370)	Thermo Scientific
Sonicator (tip) vibra cell 75041	Bioblock Scientific
Sonicator (bath) Elmasonic P, Frequency: 37, Power: 100, Temp. 23°C	Elma Schmidbauer GmbH
SpectrQ, Fluorolog®-3 Spectrofluorometer S.O. 265029	Horiba Scientific
Streptactin superflow column (0.2ml bed vol, cat: 2-1207-51)	iBA
StreptactinXT superflow column, gravity column (1ml bed.vol, cat: 2-4012-001)	iBA
SulfoLink resin	Thermo Scientific

Table A3 (continued)	
TPP® tissue culture flask (T75)	Sigma
Vacuum pump	Thermo Scientific
Vivaspin 500 (MWCO 10'000, PES membrane)	Sartorius
Waterbath, SUB Aqua 25 plus	Grant
Waterbath	Thermo Scientific
Western blot: sponges	Bio-Rad
Western blot: gel holder	Bio-Rad
Western blot: gel holder cell	Bio-Rad
Western blot: Trans-blot cell	Bio-Rad
845x UV-visible system, 8453 spectrophotometer	Agilent
0.2um filter, PES-20/25 0.2um Chromafil® xtra	Macherey
0.2um filter filtropur pyrogenfree	Sarstedt
0.2um cellulose acetate filter	Sartorius
0.22um disposable sterile filter Express™ plus	Millipore
125ml filter-erlenmeyer flask (plain bottom)	Fisher Scientific
6-well plates	VWR international

Table A4

Supplier Informations	
Abnova	Taipei city, Taiwan
Acros Organics	Geel, Belgium
Active Motif	CA, USA
Alconox Inc.	NY, USA
Agilent Technologies	CA, USA
Alfa Aesar	MA, USA
Amicon (Merck)	Hohenbrunn, Germany
Angelantoni Lifesciences	Massa Martana, Italy
Applchem	Darmstadt, Germany
ATTO-TEC GmbH	Siegen, Germany
Beckman coulter International S.A.	Nyon, Switzerland
Becton Dickinson and company	NJ, USA
Bio-rad Laboratories Inc.	CA, USA
Bioconcept AG	Allschwil, CH
Biotium	CA, USA
Boston Biochem	MA, USA
Calbiochem	(see Millipore, Merck)
Carl Roth	Karlsruhe, DE
Carlo Erba Reagents	MI, Italy
Celeromics Technologies	Valencia, Spain
Devcon Inc.	AB, Canada
Eppendorf	Hamburg, Germany
Fasteris	Geneva, Switzerland
Fisher BioReagents	PA, USA
Fisher Scientific	Fair lawn, NJ, US/Loughborough, UK
Fluka, Biochemika	Buchs, AG, Switzerland
Foodsaver	-
Gene Tex Inc.	CA, USA
GE Healthcare life sciences	(Buckinghamshire, UK)
Gilson Inc.	Villiers le Bel, France
GRACE Bio labs	OR, USA
Grant Instruments	Cambridgeshire, UK
Hellma Analytics	Müllheim, Germany
Heraeus instruments GmbH	Hanau, Germany
Horiba Scientific	Kyoto, Japan
iBA lifesciences	Goettingen, Germany
Infors HT	Basel, Switzerland
Integrated DNA technologies Inc. (IDT)	IA USA
Jackson immunoResearch Laboratories Inc.	PA, USA
Jena Bioscience	Jena, DE
KCl, Inc.	-
Lab Scan Analytical Sciences	Gliwice, Poland
Laysan Bio Inc.	AL, USA
Macherey Nagel AG	Oensingen, Switzerland
Millipore Corporation, Merck	Darmstadt, Germany
MP Biomedicals	Illkirch, France
Neenah	WI, USA
New England Biolabs	Ipswich, MA, USA
Novabiochem, Merck	Hohenbrunn, Germany
Promega	Madison, WI, USA
Qiagen	Limburg, Netherlands
Rectolab	Servion, CH
Roche	Basel, Switzerland
Salvis AG	Oftringen, Switzerland
Santa Cruz Biotechnology	Texas, USA
Sarstedt AG and Co.	Nümbrecht, Germany
Sartorius stedim biotech	Göttingen, Germany
SHIELD scientific	Bennekom, Netherlands
Sigma-Aldrich Chemical Company	Steinheim, Germany
Spectrumlabs	CA, USA
Thermo Electron LED GmbH	MA, USA
Thermo Scientific	MA USA
Thommen-Furler AG	Büren, Switzerland
VWR international S.à.r.l.	Nyon, France

Table A5

<b>Important plasmids for protein expression in the RNF168-project</b>		
<b>Construct</b>	<b>Vector/Resistances</b>	<b>Purpose and Notes</b>
<b>E1 ubiquitin-activating enzymes</b>		
His-hUBE1	PET21b / Ampicillin	To charge E2 enzymes with ubiquitin
<b>E2 ubiquitin-conjugating enzymes</b>		
His-45AA-hUBE2D3(mutated)	pDEST17 / Ampicillin	Was not functional
His-TEV-hUBE2D3	PET15b / Ampicillin	To trigger E3 enzymes
His-Thrombin-hUBE2A	PET15b / Ampicillin	To trigger E3 enzymes
hUBE2N-His	PET21 / Ampicillin	To trigger E3 enzymes
GST-hUBE2V1	Unkown / Ampicillin	To trigger E3 enzymes
<b>E3 ubiquitin ligase enzymes</b>		
GST-Thrombin-TEV-hRNF2-ybbr	pGEX / Ampicillin	For protein expression in bacteria, ybbr-tag for labelling
hBMI1 (no tag)	PET15b / Ampicillin	For protein expression in bacteria, purification only with RNF2
GST-Thrombin-TEV-hRNF8(AA 351-485)-ybbr-Thrombin-STREP	pGEX / Ampicillin	Truncated version of RNF8 for bacterial expression
GST- Thrombin-TEV-hRNF168(AA 1-196)	pGEX / Ampicillin	To create a tag-less version of RNF168 by removing the GST-tag
hRNF168(AA 1-196)-NpuN-His	PET15b / Ampicillin	Truncated RNF168 version for bacterial expression, split intein (NpuN) for labelling using EPL, but His-tag purification lowered activity and the protein aggregates during EPL.
GST-Thrombin-TEV-hRNF168(AA 1-196)-ybbr-Thrombin-STREP	pGEX / Ampicillin	Truncated RNF168 version for bacterial expression, ybbr-tag for labelling (C-ter), based on Stewart et al., 2009
GST-Thrombin-TEV-ybbr-hRNF168(AA 1-196)-Thrombin-STREP	pGEX / Ampicillin	Truncated RNF168 version for bacterial expression, ybbr-tag for labelling (N-ter), based on Stewart et al., 2009
GST-Thrombin-3C-hRNF168(AA 1-189)-ybbr-Thrombin-STREP	pGEX / Ampicillin	Truncated RNF168 version for bacterial expression, 3C cleavage site for easier handling than TEV cleavage site, shortened version for better stability
GST-Thrombin-3C-hRNF168(AA 1-113)-ybbr	pGEX / Ampicillin	RNF168 RING domain, to have a construct without any binding motif, based on Mattioli et al., 2014
GST-Thrombin-TEV-hRNF168(AA 1-571)-ybbr-Thrombin-STREP	pGEX / Ampicillin	Full-length protein, we were not able to express it in bacteria
GST-Thrombin-3C-hRNF168(AA 1-189)-10xGS(linker)-hRNF168(AA439-477,MIU2)-ybbr-TEV-STREP	pGEX / Ampicillin	To express a stable version of RNF168 containing the two ubiquitin binding motifs, based on Stewart et al., 2009
His-SUMO-Flag-Thrombin-hRNF168(AA 1-571)-ybbr-TEV-STREP	Pacebac1 / Gentamycin	For full-length protein expression in insect cells through a bacmid
His-SUMO-Flag-Thrombin-hRNF168(AA 1-571)-ybbr-TEV-STREP	Bacmid / Gentamycin, Kanamycin and Tetracyclin	For full-length protein expression in insect cells incorporated via DH10MB cells

Table A5 (continued)		
<b>ubiquitin</b>		
hUBIQUITIN variant C (no tag)	PET15b / Ampicillin	Conjugation to substrate
hUBIQUITIN variant C (no tag) all lysines mutated to arginine	PET15b / Ampicillin	Conjugation to substrate, to avoid chain formation
hUBIQUITIN variant C (no tag) cysteine insertion after methionine	PET15b / Ampicillin	For ubiquitin labelling (mutation leads to yield losses during purification)
His-Thrombin-C-hUBIQUITIN (variant C)	PET15b / Ampicillin	For ubiquitin labelling
<b>TEV protease</b>		
His-TEV(Protease)-TEV-MBP OR MBP-TEV-TEV(Protease)-His	Unknown / Ampicillin	TEV cleavage site, we don't know the exact sequence
<b>General notes</b>		
His, GST, SUMO, FLAG, STREP, MBP denote purification tags and ybbr denotes a tag for protein labelling FLAG-tag: DYKDDDDK STREP-tag: WSHPPQFEK Thrombin, TEV, 3C denote corresponding cleavage sites		

Constructs in Table A5 were designed based on: Mattioli et al., 2014<sup>35</sup> and Stewart et al., 2009<sup>171</sup>.





## VII References

1. Avery, O.T., et al., *Studies on the chemical nature of the substance inducing transformation of Pneumococcal types* J Exp Med, 1943. **79**(2): p. 137-158.
2. Watson, J.D. and F.H.C. Crick, *Molecular structure of nucleic acids*. Nature, 1953. **171**(4356): p. 737-738.
3. Reeves, R., *High mobility group (HMG) proteins: Modulators of chromatin structure and DNA repair in mammalian cells*. DNA Repair (Amst), 2015. **36**: p. 122-36.
4. Kornberg, R.D., *Structure of chromatin*. Annu Rev Biochem, 1977. **46**: p. 931-54.
5. Luger, K., et al., *Crystal structure of the nucleosome core particle at 2.8 Å resolution*. Nature, 1997. **389**(6648): p. 251-60.
6. McGinty, R.K. and S. Tan, *Nucleosome structure and function*. Chem Rev, 2015. **115**(6): p. 2255-73.
7. Blank, T.A. and P.B. Becker, *The effect of nucleosome phasing sequences and DNA topology on nucleosome spacing*. J Mol Biol, 1996. **260**(1): p. 1-8.
8. Le, J.V., et al., *Probing Nucleosome Stability with a DNA Origami Nanocaliper*. ACS Nano, 2016. **10**(7): p. 7073-84.
9. Tachiwana, H., et al., *Structural basis of instability of the nucleosome containing a testis-specific histone variant, human H3T*. Proc Natl Acad Sci U S A, 2010. **107**(23): p. 10454-9.
10. Simpson, R.T., *Structure of the chromatosome, a chromatin particle containing 160 base pairs of DNA and all the histones*. Biochemistry, 1978. **17**(25): p. 5524-31.
11. Felsenfeld, G. and M. Groudine, *Controlling the double helix*. Nature, 2003. **421**(6921): p. 448-53.
12. Jenuwein, T. and C.D. Allis, *Translating the histone code*. Science, 2001. **293**(5532): p. 1074-80.
13. McGinty, R.K., R.C. Henrici, and S. Tan, *Crystal structure of the PRC1 ubiquitylation module bound to the nucleosome*. Nature, 2014. **514**(7524): p. 591-6.
14. Shogren-Knaak, M., et al., *Histone H4-K16 acetylation controls chromatin structure and protein interactions*. Science, 2006. **311**(5762): p. 844-847.
15. Robinson, P.J., et al., *EM measurements define the dimensions of the "30-nm" chromatin fiber: evidence for a compact, interdigitated structure*. Proc Natl Acad Sci U S A, 2006. **103**(17): p. 6506-11.
16. Ekundayo, B., T.J. Richmond, and T. Schalch, *Capturing Structural Heterogeneity in Chromatin Fibers*. J Mol Biol, 2017. **429**(20): p. 3031-3042.
17. Schalch, T., et al., *X-ray structure of a tetranucleosome and its implications for the chromatin fibre*. Nature, 2005. **436**(7047): p. 138-41.
18. Song, F., et al., *Cryo-EM study of the chromatin fiber reveals a double helix twisted by tetranucleosomal units*. Science, 2014. **344**(6182): p. 376-80.
19. Kilic, S., et al., *Single-molecule FRET reveals multiscale chromatin dynamics modulated by HP1alpha*. Nat Commun, 2018. **9**(1): p. 235.
20. Ou, H.D., et al., *ChromEMT: Visualizing 3D chromatin structure and compaction in interphase and mitotic cells*. Science, 2017. **357**(6349).
21. Grigoryev, S.A., et al., *Evidence for heteromorphic chromatin fibers from analysis of nucleosome interactions*. Proc Natl Acad Sci U S A, 2009. **106**(32): p. 13317-22.
22. Gardner, K.E., C.D. Allis, and B.D. Strahl, *Operating on chromatin, a colorful language where context matters*. J Mol Biol, 2011. **409**(1): p. 36-46.
23. Fierz, B., et al., *Histone H2B ubiquitylation disrupts local and higher-order chromatin compaction*. Nat Chem Biol, 2011. **7**(2): p. 113-9.
24. Vermeulen, M. and H.T. Timmers, *Grasping trimethylation of histone H3 at lysine 4*. Epigenomics, 2010. **2**(3): p. 395-406.

25. Peters, A.H., et al., *Histone H3 lysine 9 methylation is an epigenetic imprint of facultative heterochromatin*. Nat Genet, 2002. **30**(1): p. 77-80.
26. Rougeulle, C., et al., *Differential histone H3 Lys-9 and Lys-27 methylation profiles on the X chromosome*. Mol Cell Biol, 2004. **24**(12): p. 5475-84.
27. Black, J.C., C. Van Rechem, and J.R. Whetstine, *Histone lysine methylation dynamics: establishment, regulation, and biological impact*. Mol Cell, 2012. **48**(4): p. 491-507.
28. Di Cerbo, V., et al., *Acetylation of histone H3 at lysine 64 regulates nucleosome dynamics and facilitates transcription*. Elife, 2014. **3**: p. e01632.
29. Zhang, T.Y., S. Cooper, and N. Brockdorff, *The interplay of histone modifications - writers that read*. EMBO Rep, 2015. **16**(11): p. 1467-1481.
30. Jack, A.P., et al., *H3K56me3 is a novel, conserved heterochromatic mark that largely but not completely overlaps with H3K9me3 in both regulation and localization*. PLoS One, 2013. **8**(2): p. e51765.
31. Tan, M.J., et al., *Identification of 67 Histone Marks and Histone Lysine Crotonylation as a New Type of Histone Modification*. Cell, 2011. **146**(6): p. 1015-1027.
32. Robinson, P.J.J., et al., *30 nm chromatin fibre decompaction requires both H4-K16 acetylation and linker histone eviction*. J Mol Biol, 2008. **381**(4): p. 816-825.
33. Hilfiker, A., et al., *mof, a putative acetyl transferase gene related to the Tip60 and MOZ human genes and to the SAS genes of yeast, is required for dosage compensation in Drosophila*. Embo Journal, 1997. **16**(8): p. 2054-2060.
34. Dorigo, B., et al., *Chromatin fiber folding: requirement for the histone H4 N-terminal tail*. J Mol Biol, 2003. **327**(1): p. 85-96.
35. Mattioli, F., et al., *The nucleosome acidic patch plays a critical role in RNF168-dependent ubiquitination of histone H2A*. Nat Commun, 2014. **5**: p. 3291.
36. Chernikova, S.B., et al., *Deficiency in Mammalian Histone H2B Ubiquitin Ligase Bre1 (Rnf20/Rnf40) Leads to Replication Stress and Chromosomal Instability*. Cancer Res, 2012. **72**(8): p. 2111-2119.
37. Tang, L., E. Nogales, and C. Ciferri, *Structure and function of SWI/SNF chromatin remodeling complexes and mechanistic implications for transcription*. Prog Biophys Mol Biol, 2010. **102**(2-3): p. 122-8.
38. Lieleg, C., et al., *Nucleosome spacing generated by ISWI and CHD1 remodelers is constant regardless of nucleosome density*. Mol Cell Biol, 2015. **35**(9): p. 1588-605.
39. Nielsen, P.R., et al., *Structure of the HP1 chromodomain bound to histone H3 methylated at lysine 9*. Nature, 2002. **416**(6876): p. 103-107.
40. Ntranos, A. and P. Casaccia, *Bromodomains: Translating the words of lysine acetylation into myelin injury and repair*. Neurosci Lett, 2016. **625**: p. 4-10.
41. Dey, A., et al., *The double bromodomain protein Brd4 binds to acetylated chromatin during interphase and mitosis*. Proc Natl Acad Sci U S A, 2003. **100**(15): p. 8758-8763.
42. Young, L.C., D.W. McDonald, and M.J. Hendzel, *Kdm4b histone demethylase is a DNA damage response protein and confers a survival advantage following gamma-irradiation*. J Biol Chem, 2013. **288**(29): p. 21376-88.
43. Wu, R., et al., *H3K9me3 demethylase Kdm4d facilitates the formation of pre-initiative complex and regulates DNA replication*. Nucleic Acids Res, 2017. **45**(1): p. 169-180.
44. Leipe, D.D. and D. Landsman, *Histone deacetylases, acetoin utilization proteins and acetyl polyamine amidohydrolases are members of an ancient protein superfamily*. Nucleic Acids Res, 1997. **25**(18): p. 3693-3697.
45. Canzio, D., et al., *Chromodomain-mediated oligomerization of HP1 suggests a nucleosome-bridging mechanism for heterochromatin assembly*. Mol Cell, 2011. **41**(1): p. 67-81.
46. Boyer, L.A., et al., *Polycomb complexes repress developmental regulators in murine embryonic stem cells*. Nature, 2006. **441**(7091): p. 349-53.
47. Lund, A.H. and M. van Lohuizen, *Polycomb complexes and silencing mechanisms*. Curr Opin Cell Biol, 2004. **16**(3): p. 239-46.

48. Thorslund, T., et al., *Histone H1 couples initiation and amplification of ubiquitin signalling after DNA damage*. *Nature*, 2015. **527**(7578): p. 389-93.
49. Pinato, S., et al., *UMI, a novel RNF168 ubiquitin binding domain involved in the DNA damage signaling pathway*. *Mol Cell Biol*, 2011. **31**(1): p. 118-26.
50. James, T.C. and S.C. Elgin, *Identification of a nonhistone chromosomal protein associated with heterochromatin in Drosophila melanogaster and its gene*. *Mol Cell Biol*, 1986. **6**(11): p. 3862-72.
51. Eissenberg, J.C., et al., *Mutation in a heterochromatin-specific chromosomal protein is associated with suppression of position-effect variegation in Drosophila melanogaster*. *Proc Natl Acad Sci U S A*, 1990. **87**(24): p. 9923-7.
52. Lomberg, G., L. Wallrath, and R. Urrutia, *The Heterochromatin Protein 1 family*. *Genome Biol*, 2006. **7**(7): p. 228.
53. Norwood, L.E., et al., *Conserved properties of HP1(Hsalpha)*. *Gene*, 2004. **336**(1): p. 37-46.
54. Aasland, R. and A.F. Stewart, *The chromo shadow domain, a second chromo domain in heterochromatin-binding protein 1, HP1*. *Nucleic Acids Res*, 1995. **23**(16): p. 3168-73.
55. Jones, D.O., I.G. Cowell, and P.B. Singh, *Mammalian chromodomain proteins: their role in genome organisation and expression*. *Bioessays*, 2000. **22**(2): p. 124-37.
56. Bannister, A.J., et al., *Selective recognition of methylated lysine 9 on histone H3 by the HP1 chromo domain*. *Nature*, 2001. **410**(6824): p. 120-4.
57. Lachner, M., et al., *Methylation of histone H3 lysine 9 creates a binding site for HP1 proteins*. *Nature*, 2001. **410**(6824): p. 116-20.
58. Thiru, A., et al., *Structural basis of HP1/PXVXL motif peptide interactions and HP1 localisation to heterochromatin*. *EMBO J*, 2004. **23**(3): p. 489-99.
59. Kang, J., et al., *Mitotic centromeric targeting of HP1 and its binding to Sgo1 are dispensable for sister-chromatid cohesion in human cells*. *Mol Biol Cell*, 2011. **22**(8): p. 1181-90.
60. Cowieson, N.P., et al., *Dimerisation of a chromo shadow domain and distinctions from the chromodomain as revealed by structural analysis*. *Curr Biol*, 2000. **10**(9): p. 517-25.
61. Muchardt, C., et al., *Coordinated methyl and RNA binding is required for heterochromatin localization of mammalian HP1alpha*. *EMBO Rep*, 2002. **3**(10): p. 975-81.
62. Keller, C., et al., *HP1(Swi6) mediates the recognition and destruction of heterochromatic RNA transcripts*. *Mol Cell*, 2012. **47**(2): p. 215-27.
63. Shimojo, H., et al., *Extended string-like binding of the phosphorylated HP1alpha N-terminal tail to the lysine 9-methylated histone H3 tail*. *Sci Rep*, 2016. **6**: p. 22527.
64. James, T.C., et al., *Distribution patterns of HP1, a heterochromatin-associated nonhistone chromosomal protein of Drosophila*. *Eur J Cell Biol*, 1989. **50**(1): p. 170-80.
65. Azzaz, A.M., et al., *Human heterochromatin protein 1alpha promotes nucleosome associations that drive chromatin condensation*. *J Biol Chem*, 2014. **289**(10): p. 6850-61.
66. du Chene, I., et al., *Suv39H1 and HP1gamma are responsible for chromatin-mediated HIV-1 transcriptional silencing and post-integration latency*. *EMBO J*, 2007. **26**(2): p. 424-35.
67. Freitag, M., et al., *HP1 is essential for DNA methylation in neurospora*. *Mol Cell*, 2004. **13**(3): p. 427-34.
68. Cheutin, T., et al., *Maintenance of stable heterochromatin domains by dynamic HP1 binding*. *Science*, 2003. **299**(5607): p. 721-5.
69. Muller, K.P., et al., *Multiscale analysis of dynamics and interactions of heterochromatin protein 1 by fluorescence fluctuation microscopy*. *Biophys J*, 2009. **97**(11): p. 2876-85.
70. Brasher, S.V., et al., *The structure of mouse HP1 suggests a unique mode of single peptide recognition by the shadow chromo domain dimer*. *EMBO J*, 2000. **19**(7): p. 1587-97.
71. Hansen, K.H., et al., *A model for transmission of the H3K27me3 epigenetic mark*. *Nat Cell Biol*, 2008. **10**(11): p. 1291-U89.
72. Lewis, E.B., *A gene complex controlling segmentation in Drosophila*. *Nature*, 1978. **276**(5688): p. 565-70.

73. Jiang, D., Y. Wang, and Y. He, *Repression of FLOWERING LOCUS C and FLOWERING LOCUS T by the Arabidopsis Polycomb repressive complex 2 components*. PLoS One, 2008. **3**(10): p. e3404.
74. Simon, J.A. and C.A. Lange, *Roles of the EZH2 histone methyltransferase in cancer epigenetics*. Mutat Res, 2008. **647**(1-2): p. 21-9.
75. Plath, K., et al., *Role of histone H3 lysine 27 methylation in X inactivation*. Science, 2003. **300**(5616): p. 131-5.
76. Shao, Z., et al., *Stabilization of chromatin structure by PRC1, a Polycomb complex*. Cell, 1999. **98**(1): p. 37-46.
77. Kuzmichev, A., et al., *Histone methyltransferase activity associated with a human multiprotein complex containing the Enhancer of Zeste protein*. Genes Dev, 2002. **16**(22): p. 2893-905.
78. Kaneko, S., et al., *PRC2 binds active promoters and contacts nascent RNAs in embryonic stem cells*. Nat Struct Mol Biol, 2013. **20**(11): p. 1258-64.
79. Jiao, L. and X. Liu, *Structural basis of histone H3K27 trimethylation by an active polycomb repressive complex 2*. Science, 2015. **350**(6258): p. aac4383.
80. Justin, N., et al., *Structural basis of oncogenic histone H3K27M inhibition of human polycomb repressive complex 2*. Nat Commun, 2016. **7**: p. 11316.
81. Margueron, R., et al., *Role of the polycomb protein EED in the propagation of repressive histone marks*. Nature, 2009. **461**(7265): p. 762-7.
82. Pasini, D., et al., *Suz12 is essential for mouse development and for EZH2 histone methyltransferase activity*. EMBO J, 2004. **23**(20): p. 4061-71.
83. Murzina, N.V., et al., *Structural basis for the recognition of histone H4 by the histone-chaperone RbAp46*. Structure, 2008. **16**(7): p. 1077-85.
84. Cao, R., Y. Tsukada, and Y. Zhang, *Role of Bmi-1 and Ring1A in H2A ubiquitylation and Hox gene silencing*. Mol Cell, 2005. **20**(6): p. 845-54.
85. Simon, J.A. and R.E. Kingston, *Mechanisms of polycomb gene silencing: knowns and unknowns*. Nat Rev Mol Cell Biol, 2009. **10**(10): p. 697-708.
86. Duncan, I.M., *Polycomblike: a gene that appears to be required for the normal expression of the bithorax and antennapedia gene complexes of Drosophila melanogaster*. Genetics, 1982. **102**(1): p. 49-70.
87. Nekrasov, M., et al., *Pcl-PRC2 is needed to generate high levels of H3-K27 trimethylation at Polycomb target genes*. EMBO J, 2007. **26**(18): p. 4078-88.
88. Sarma, K., et al., *Ezh2 requires PHF1 to efficiently catalyze H3 lysine 27 trimethylation in vivo*. Mol Cell Biol, 2008. **28**(8): p. 2718-31.
89. Cao, R., et al., *Role of hPHF1 in H3K27 methylation and Hox gene silencing*. Mol Cell Biol, 2008. **28**(5): p. 1862-72.
90. Savla, U., et al., *Recruitment of Drosophila Polycomb-group proteins by Polycomblike, a component of a novel protein complex in larvae*. Development, 2008. **135**(5): p. 813-7.
91. O'Connell, S., et al., *Polycomblike PHD fingers mediate conserved interaction with enhancer of zeste protein*. J Biol Chem, 2001. **276**(46): p. 43065-73.
92. Smeenk, G. and N. Mailand, *Writers, Readers, and Erasers of Histone Ubiquitylation in DNA Double-Strand Break Repair*. Front Genet, 2016. **7**: p. 122.
93. Kleiger, G. and T. Mayor, *Perilous journey: a tour of the ubiquitin-proteasome system*. Trends Cell Biol, 2014. **24**(6): p. 352-9.
94. Xu, P., et al., *Quantitative proteomics reveals the function of unconventional ubiquitin chains in proteasomal degradation*. Cell, 2009. **137**(1): p. 133-45.
95. Tokunaga, F., et al., *Involvement of linear polyubiquitylation of NEMO in NF-kappaB activation*. Nat Cell Biol, 2009. **11**(2): p. 123-32.
96. Vijay-Kumar, S., C.E. Bugg, and W.J. Cook, *Structure of ubiquitin refined at 1.8 A resolution*. J Mol Biol, 1987. **194**(3): p. 531-44.



97. Bremm, A., S.M. Freund, and D. Komander, *Lys11-linked ubiquitin chains adopt compact conformations and are preferentially hydrolyzed by the deubiquitinase Cezanne*. Nat Struct Mol Biol, 2010. **17**(8): p. 939-47.
98. Matsumoto, M.L., et al., *K11-linked polyubiquitination in cell cycle control revealed by a K11 linkage-specific antibody*. Mol Cell, 2010. **39**(3): p. 477-84.
99. Virdee, S., et al., *Engineered diubiquitin synthesis reveals Lys29-isopeptide specificity of an OTU deubiquitinase*. Nat Chem Biol, 2010. **6**(10): p. 750-7.
100. Komander, D. and M. Rape, *The ubiquitin code*. Annu Rev Biochem, 2012. **81**: p. 203-29.
101. Tenno, T., et al., *Structural basis for distinct roles of Lys63- and Lys48-linked polyubiquitin chains*. Genes Cells, 2004. **9**(10): p. 865-75.
102. Varadan, R., et al., *Solution conformation of Lys63-linked di-ubiquitin chain provides clues to functional diversity of polyubiquitin signaling*. J Biol Chem, 2004. **279**(8): p. 7055-63.
103. Thrower, J.S., et al., *Recognition of the polyubiquitin proteolytic signal*. EMBO J, 2000. **19**(1): p. 94-102.
104. Jacobson, A.D., et al., *The lysine 48 and lysine 63 ubiquitin conjugates are processed differently by the 26 S proteasome*. J Biol Chem, 2009. **284**(51): p. 35485-94.
105. Pelzer, C., et al., *UBE1L2, a novel E1 enzyme specific for ubiquitin*. J Biol Chem, 2007. **282**(32): p. 23010-4.
106. Haglund, K. and I. Dikic, *Ubiquitylation and cell signaling*. EMBO J, 2005. **24**(19): p. 3353-9.
107. David, Y., et al., *The E2 ubiquitin-conjugating enzymes direct polyubiquitination to preferred lysines*. J Biol Chem, 2010. **285**(12): p. 8595-604.
108. Ye, Y. and M. Rape, *Building ubiquitin chains: E2 enzymes at work*. Nat Rev Mol Cell Biol, 2009. **10**(11): p. 755-64.
109. Haas, A.L., et al., *Ubiquitin-activating enzyme. Mechanism and role in protein-ubiquitin conjugation*. J Biol Chem, 1982. **257**(5): p. 2543-8.
110. Deshaies, R.J. and C.A. Joazeiro, *RING domain E3 ubiquitin ligases*. Annu Rev Biochem, 2009. **78**: p. 399-434.
111. Schulman, B.A. and J.W. Harper, *Ubiquitin-like protein activation by E1 enzymes: the apex for downstream signalling pathways*. Nat Rev Mol Cell Biol, 2009. **10**(5): p. 319-31.
112. Harper, J.W. and S.J. Elledge, *The DNA damage response: ten years after*. Mol Cell, 2007. **28**(5): p. 739-45.
113. Hu, H. and R.A. Gatti, *MicroRNAs: new players in the DNA damage response*. J Mol Cell Biol, 2011. **3**(3): p. 151-8.
114. Bartek, J., J. Bartkova, and J. Lukas, *DNA damage signalling guards against activated oncogenes and tumour progression*. Oncogene, 2007. **26**(56): p. 7773-9.
115. Jackson, S.P. and J. Bartek, *The DNA-damage response in human biology and disease*. Nature, 2009. **461**(7267): p. 1071-8.
116. Rogakou, E.P., et al., *DNA double-stranded breaks induce histone H2AX phosphorylation on serine 139*. J Biol Chem, 1998. **273**(10): p. 5858-68.
117. Friesner, J.D., et al., *Ionizing radiation-dependent gamma-H2AX focus formation requires ataxia telangiectasia mutated and ataxia telangiectasia mutated and Rad3-related*. Mol Biol Cell, 2005. **16**(5): p. 2566-76.
118. Zhao, H., et al., *BCL10 regulates RNF8/RNF168-mediated ubiquitination in the DNA damage response*. Cell Cycle, 2014. **13**(11): p. 1777-87.
119. Celeste, A., et al., *Histone H2AX phosphorylation is dispensable for the initial recognition of DNA breaks*. Nature Cell Biology, 2003. **5**: p. 675-679.
120. Stucki, M., et al., *MDC1 directly binds phosphorylated histone H2AX to regulate cellular responses to DNA double-strand breaks*. Cell, 2005. **123**(7): p. 1213-26.
121. Chapman, J.R. and S.P. Jackson, *Phospho-dependent interactions between NBS1 and MDC1 mediate chromatin retention of the MRN complex at sites of DNA damage*. EMBO Rep, 2008. **9**(8): p. 795-801.

122. Liu, J., et al., *Structural mechanism of the phosphorylation-dependent dimerization of the MDC1 forkhead-associated domain*. Nucleic Acids Res, 2012. **40**(9): p. 3898-912.
123. Jungmichel, S., et al., *The molecular basis of ATM-dependent dimerization of the Mdc1 DNA damage checkpoint mediator*. Nucleic Acids Res, 2012. **40**(9): p. 3913-28.
124. Huen, M.S., et al., *RNF8 transduces the DNA-damage signal via histone ubiquitylation and checkpoint protein assembly*. Cell, 2007. **131**(5): p. 901-14.
125. Doil, C., et al., *RNF168 binds and amplifies ubiquitin conjugates on damaged chromosomes to allow accumulation of repair proteins*. Cell, 2009. **136**(3): p. 435-46.
126. Mailand, N., et al., *RNF8 ubiquitylates histones at DNA double-strand breaks and promotes assembly of repair proteins*. Cell, 2007. **131**(5): p. 887-900.
127. Pinato, S., et al., *RNF168, a new RING finger, MIU-containing protein that modifies chromatin by ubiquitination of histones H2A and H2AX*. BMC Mol Biol, 2009. **10**: p. 55.
128. Mattioli, F., et al., *RNF168 ubiquitinates K13-15 on H2A/H2AX to drive DNA damage signaling*. Cell, 2012. **150**(6): p. 1182-95.
129. Nowsheen, S., et al., *L3MBTL2 orchestrates ubiquitin signalling by dictating the sequential recruitment of RNF8 and RNF168 after DNA damage*. Nat Cell Biol, 2018. **20**(4): p. 455-464.
130. Liu, C., et al., *RNF168 forms a functional complex with RAD6 during the DNA damage response*. J Cell Sci, 2013. **126**(Pt 9): p. 2042-51.
131. Cao, J. and Q. Yan, *Histone ubiquitination and deubiquitination in transcription, DNA damage response, and cancer*. Front Oncol, 2012. **2**: p. 26.
132. Gatti, M., et al., *A novel ubiquitin mark at the N-terminal tail of histone H2As targeted by RNF168 ubiquitin ligase*. Cell Cycle, 2012. **11**(13): p. 2538-44.
133. Leung, J.W., et al., *Nucleosome acidic patch promotes RNF168- and RING1B/BMI1-dependent H2AX and H2A ubiquitination and DNA damage signaling*. PLoS Genet, 2014. **10**(3): p. e1004178.
134. Panier, S., et al., *Tandem protein interaction modules organize the ubiquitin-dependent response to DNA double-strand breaks*. Mol Cell, 2012. **47**(3): p. 383-95.
135. Kim, H., J. Chen, and X. Yu, *Ubiquitin-binding protein RAP80 mediates BRCA1-dependent DNA damage response*. Science, 2007. **316**(5828): p. 1202-5.
136. Sobhian, B., et al., *RAP80 targets BRCA1 to specific ubiquitin structures at DNA damage sites*. Science, 2007. **316**(5828): p. 1198-202.
137. Botuyan, M.V., et al., *Structural basis for the methylation state-specific recognition of histone H4-K20 by 53BP1 and Crb2 in DNA repair*. Cell, 2006. **127**(7): p. 1361-73.
138. Wilson, M.D., et al., *The structural basis of modified nucleosome recognition by 53BP1*. Nature, 2016. **536**(7614): p. 100-3.
139. Fradet-Turcotte, A., et al., *53BP1 is a reader of the DNA-damage-induced H2A Lys 15 ubiquitin mark*. Nature, 2013. **499**(7456): p. 50-4.
140. Min, J., et al., *L3MBTL1 recognition of mono- and dimethylated histones*. Nat Struct Mol Biol, 2007. **14**(12): p. 1229-30.
141. Acs, K., et al., *The AAA-ATPase VCP/p97 promotes 53BP1 recruitment by removing L3MBTL1 from DNA double-strand breaks*. Nat Struct Mol Biol, 2011. **18**(12): p. 1345-50.
142. Lee, B.L., et al., *Molecular Basis for K63-Linked Ubiquitination Processes in Double-Strand DNA Break Repair: A Focus on Kinetics and Dynamics*. J Mol Biol, 2017. **429**(22): p. 3409-3429.
143. Kolas, N.K., et al., *Orchestration of the DNA-damage response by the RNF8 ubiquitin ligase*. Science, 2007. **318**(5856): p. 1637-40.
144. Hu, Y., et al., *Regulation of 53BP1 protein stability by RNF8 and RNF168 is important for efficient DNA double-strand break repair*. PLoS One, 2014. **9**(10): p. e110522.
145. Kalb, R., et al., *BRCA1 is a histone-H2A-specific ubiquitin ligase*. Cell Rep, 2014. **8**(4): p. 999-1005.
146. Muller, J. and P. Verrijzer, *Biochemical mechanisms of gene regulation by polycomb group protein complexes*. Curr Opin Genet Dev, 2009. **19**(2): p. 150-8.

147. Simon, J.A. and R.E. Kingston, *Occupying chromatin: Polycomb mechanisms for getting to genomic targets, stopping transcriptional traffic, and staying put*. Mol Cell, 2013. **49**(5): p. 808-24.
148. Morey, L. and K. Helin, *Polycomb group protein-mediated repression of transcription*. Trends Biochem Sci, 2010. **35**(6): p. 323-32.
149. Facchino, S., et al., *BMI1 confers radioresistance to normal and cancerous neural stem cells through recruitment of the DNA damage response machinery*. J Neurosci, 2010. **30**(30): p. 10096-111.
150. Ismail, I.H., et al., *BMI1-mediated histone ubiquitylation promotes DNA double-strand break repair*. J Cell Biol, 2010. **191**(1): p. 45-60.
151. Gieni, R.S., et al., *Polycomb group proteins in the DNA damage response: a link between radiation resistance and "stemness"*. Cell Cycle, 2011. **10**(6): p. 883-94.
152. Maity, S.K., et al., *Total chemical synthesis of histones and their analogs, assisted by native chemical ligation and palladium complexes*. Nat Protoc, 2017. **12**(11): p. 2293-2322.
153. Kumar, K.S., et al., *Total chemical synthesis of di-ubiquitin chains*. Angew Chem Int Ed Engl, 2010. **49**(48): p. 9126-31.
154. Dawson, P.E., et al., *Synthesis of proteins by native chemical ligation*. Science, 1994. **266**(5186): p. 776-9.
155. Muir, T.W., *Semisynthesis of proteins by expressed protein ligation*. Annu Rev Biochem, 2003. **72**: p. 249-89.
156. Schnolzer, M., et al., *In situ neutralization in Boc-chemistry solid phase peptide synthesis. Rapid, high yield assembly of difficult sequences*. Int J Pept Protein Res, 1992. **40**(3-4): p. 180-93.
157. Perler, F.B., M.Q. Xu, and H. Paulus, *Protein splicing and autoproteolysis mechanisms*. Curr Opin Chem Biol, 1997. **1**(3): p. 292-9.
158. Southworth, M.W., et al., *Control of protein splicing by intein fragment reassembly*. EMBO J, 1998. **17**(4): p. 918-26.
159. Mills, K.V., et al., *Protein splicing in trans by purified N- and C-terminal fragments of the Mycobacterium tuberculosis RecA intein*. Proc Natl Acad Sci U S A, 1998. **95**(7): p. 3543-8.
160. Muir, T.W., D. Sondhi, and P.A. Cole, *Expressed protein ligation: a general method for protein engineering*. Proc Natl Acad Sci U S A, 1998. **95**(12): p. 6705-10.
161. Severinov, K. and T.W. Muir, *Expressed protein ligation, a novel method for studying protein-protein interactions in transcription*. J Biol Chem, 1998. **273**(26): p. 16205-9.
162. Evans, T.C., Jr., J. Benner, and M.Q. Xu, *Semisynthesis of cytotoxic proteins using a modified protein splicing element*. Protein Sci, 1998. **7**(11): p. 2256-64.
163. Noren, C.J., et al., *A general method for site-specific incorporation of unnatural amino acids into proteins*. Science, 1989. **244**(4901): p. 182-8.
164. P.N.Dyer, et al., *Reconstitution of Nucleosome Core Particles from Recombinant Histones and DNA*. Methods in enzymology, 2004. **375**: p. 23-44.
165. Zhu, B., et al., *Monoubiquitination of human histone H2B: the factors involved and their roles in HOX gene regulation*. Mol Cell, 2005. **20**(4): p. 601-11.
166. McGinty, R.K., et al., *Chemically ubiquitylated histone H2B stimulates hDot1L-mediated intranucleosomal methylation*. Nature, 2008. **453**(7196): p. 812-6.
167. Simon, M.D., et al., *The site-specific installation of methyl-lysine analogs into recombinant histones*. Cell, 2007. **128**(5): p. 1003-12.
168. Yan, L.Z. and P.E. Dawson, *Synthesis of peptides and proteins without cysteine residues by native chemical ligation combined with desulfurization*. J Am Chem Soc, 2001. **123**(4): p. 526-33.
169. Neumann, H., et al., *A method for genetically installing site-specific acetylation in recombinant histones defines the effects of H3 K56 acetylation*. Mol Cell, 2009. **36**(1): p. 153-63.

170. Lowary, P.T. and J. Widom, *New DNA sequence rules for high affinity binding to histone octamer and sequence-directed nucleosome positioning*. J Mol Biol, 1998. **276**(1): p. 19-42.
171. Stewart, G.S., et al., *The RIDDLE syndrome protein mediates a ubiquitin-dependent signaling cascade at sites of DNA damage*. Cell, 2009. **136**(3): p. 420-34.
172. Joo, H.Y., et al., *In vitro and in vivo assays for studying histone ubiquitination and deubiquitination*. Methods Mol Biol, 2015. **1288**: p. 213-30.
173. Mueller, A.M., et al., *MicroScale Thermophoresis: A Rapid and Precise Method to Quantify Protein-Nucleic Acid Interactions in Solution*. Methods Mol Biol, 2017. **1654**: p. 151-164.
174. Kim, S., et al., *Mechanism of Histone H3K4me3 Recognition by the Plant Homeodomain of Inhibitor of Growth 3*. J Biol Chem, 2016. **291**(35): p. 18326-41.
175. Hirotsu, Y., et al., *Nrf2-MafG heterodimers contribute globally to antioxidant and metabolic networks*. Nucleic Acids Res, 2012. **40**(20): p. 10228-39.
176. Truax, A.D. and S.F. Greer, *ChIP and Re-ChIP assays: investigating interactions between regulatory proteins, histone modifications, and the DNA sequences to which they bind*. Methods Mol Biol, 2012. **809**: p. 175-88.
177. Mattheyses, A.L., S.M. Simon, and J.Z. Rappoport, *Imaging with total internal reflection fluorescence microscopy for the cell biologist*. J Cell Sci, 2010. **123**(Pt 21): p. 3621-8.
178. Cerf, A., H.C. Tian, and H.G. Craighead, *Ordered arrays of native chromatin molecules for high-resolution imaging and analysis*. ACS Nano, 2012. **6**(9): p. 7928-34.
179. Bennink, M.L., et al., *Unfolding individual nucleosomes by stretching single chromatin fibers with optical tweezers*. Nat Struct Biol, 2001. **8**(7): p. 606-10.
180. Neuman, K.C. and A. Nagy, *Single-molecule force spectroscopy: optical tweezers, magnetic tweezers and atomic force microscopy*. Nat Methods, 2008. **5**(6): p. 491-505.
181. Ha, T., et al., *Probing the interaction between two single molecules: fluorescence resonance energy transfer between a single donor and a single acceptor*. Proc Natl Acad Sci U S A, 1996. **93**(13): p. 6264-8.
182. Funke, J.J., et al., *Uncovering the forces between nucleosomes using DNA origami*. Sci Adv, 2016. **2**(11): p. e1600974.
183. Martin-Fernandez, M.L., C.J. Tynan, and S.E. Webb, *A 'pocket guide' to total internal reflection fluorescence*. J Microsc, 2013. **252**(1): p. 16-22.
184. Mohammad, F., et al., *EZH2 is a potential therapeutic target for H3K27M-mutant pediatric gliomas*. Nat Med, 2017. **23**(4): p. 483-492.
185. Stewart, G.S., et al., *RIDDLE immunodeficiency syndrome is linked to defects in 53BP1-mediated DNA damage signaling*. Proc Natl Acad Sci U S A, 2007. **104**(43): p. 16910-5.
186. Kilic, S., et al., *Multivalency governs HP1alpha association dynamics with the silent chromatin state*. Nat Commun, 2015. **6**: p. 7313.
187. Hinde, E., F. Cardarelli, and E. Gratton, *Spatiotemporal regulation of Heterochromatin Protein 1-alpha oligomerization and dynamics in live cells*. Sci Rep, 2015. **5**: p. 12001.
188. Eisert, R.J. and M.L. Waters, *Tuning HP1alpha chromodomain selectivity for di- and trimethyllysine*. ChemBiochem, 2011. **12**(18): p. 2786-90.
189. Kaustov, L., et al., *Recognition and specificity determinants of the human cbx chromodomains*. J Biol Chem, 2011. **286**(1): p. 521-9.
190. Clegg, R.M., *Fluorescence resonance energy transfer and nucleic acids*. Methods Enzymol, 1992. **211**: p. 353-88.
191. Vila-Perello, M., et al., *Streamlined expressed protein ligation using split inteins*. J Am Chem Soc, 2013. **135**(1): p. 286-92.
192. Bryan, L.C., et al., *Single-molecule kinetic analysis of HP1-chromatin binding reveals a dynamic network of histone modification and DNA interactions*. Nucleic Acids Res, 2017. **45**(18): p. 10504-10517.
193. Fish, K.N., *Total internal reflection fluorescence (TIRF) microscopy*, 2009, Curr Protoc Cytom



194. Keyel, P.A., S.C. Watkins, and L.M. Traub, *Endocytic adaptor molecules reveal an endosomal population of clathrin by total internal reflection fluorescence microscopy*. J Biol Chem, 2004. **279**(13): p. 13190-204.
195. Peterson, E.M., M.W. Manhart, and J.M. Harris, *Single-Molecule Fluorescence Imaging of Interfacial DNA Hybridization Kinetics at Selective Capture Surfaces*. Anal Chem, 2016. **88**(2): p. 1345-54.
196. Steffen, P.A., J.P. Fonseca, and L. Ringrose, *Epigenetics meets mathematics: towards a quantitative understanding of chromatin biology*. Bioessays, 2012. **34**(10): p. 901-13.
197. Ha, T., *Single-molecule approaches embrace molecular cohorts*. Cell, 2013. **154**(4): p. 723-6.
198. Sing, C.E., M. Olvera de la Cruz, and J.F. Marko, *Multiple-binding-site mechanism explains concentration-dependent unbinding rates of DNA-binding proteins*. Nucleic Acids Res, 2014. **42**(6): p. 3783-91.
199. Loparo, J.J., et al., *Simultaneous single-molecule measurements of phage T7 replisome composition and function reveal the mechanism of polymerase exchange*. Proc Natl Acad Sci U S A, 2011. **108**(9): p. 3584-9.
200. Graham, J.S., R.C. Johnson, and J.F. Marko, *Concentration-dependent exchange accelerates turnover of proteins bound to double-stranded DNA*. Nucleic Acids Res, 2011. **39**(6): p. 2249-59.
201. Mendez, D.L., et al., *The HP1a disordered C terminus and chromo shadow domain cooperate to select target peptide partners*. Chembiochem, 2011. **12**(7): p. 1084-96.
202. Yamagishi, Y., et al., *Heterochromatin links to centromeric protection by recruiting shugoshin*. Nature, 2008. **455**(7210): p. 251-5.
203. Eskeland, R., A. Eberharter, and A. Imhof, *HP1 binding to chromatin methylated at H3K9 is enhanced by auxiliary factors*. Mol Cell Biol, 2007. **27**(2): p. 453-65.
204. Zhang, M., et al., *Rational design of true monomeric and bright photoactivatable fluorescent proteins*. Nat Methods, 2012. **9**(7): p. 727-9.
205. Sprague, B.L., et al., *Analysis of binding reactions by fluorescence recovery after photobleaching*. Biophys J, 2004. **86**(6): p. 3473-95.
206. Canzio, D., et al., *A conformational switch in HP1 releases auto-inhibition to drive heterochromatin assembly*. Nature, 2013. **496**(7445): p. 377-81.
207. Choi, J., et al., *DNA binding by PHF1 prolongs PRC2 residence time on chromatin and thereby promotes H3K27 methylation*. Nat Struct Mol Biol, 2017. **24**(12): p. 1039-1047.
208. Lechner, C.C., N.D. Agashe, and B. Fierz, *Traceless Synthesis of Asymmetrically Modified Bivalent Nucleosomes*. Angew Chem Int Ed Engl, 2016. **55**(8): p. 2903-6.
209. Walker, E., et al., *Polycomb-like 2 associates with PRC2 and regulates transcriptional networks during mouse embryonic stem cell self-renewal and differentiation*. Cell Stem Cell, 2010. **6**(2): p. 153-66.
210. Yin, J., et al., *Genetically encoded short peptide tag for versatile protein labeling by Sfp phosphopantetheinyl transferase*. Proc Natl Acad Sci U S A, 2005. **102**(44): p. 15815-20.
211. George, N., et al., *Specific labeling of cell surface proteins with chemically diverse compounds*. J Am Chem Soc, 2004. **126**(29): p. 8896-7.
212. Teves, S.S., et al., *A dynamic mode of mitotic bookmarking by transcription factors*. Elife, 2016. **5**.
213. Morisaki, T., et al., *Single-molecule analysis of transcription factor binding at transcription sites in live cells*. Nat Commun, 2014. **5**: p. 4456.
214. Friberg, A., et al., *Structure of an atypical Tudor domain in the Drosophila Polycomblike protein*. Protein Sci, 2010. **19**(10): p. 1906-16.
215. Ballare, C., et al., *Phf19 links methylated Lys36 of histone H3 to regulation of Polycomb activity*. Nat Struct Mol Biol, 2012. **19**(12): p. 1257-65.
216. Musselman, C.A., et al., *Molecular basis for H3K36me3 recognition by the Tudor domain of PHF1*. Nat Struct Mol Biol, 2012. **19**(12): p. 1266-72.

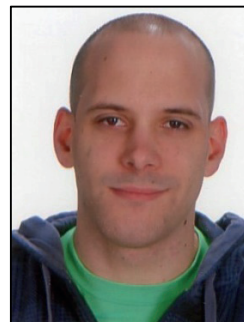
217. Cai, L., et al., *An H3K36 methylation-engaging Tudor motif of polycomb-like proteins mediates PRC2 complex targeting*. Mol Cell, 2013. **49**(3): p. 571-82.
218. Soding, J., A. Biegert, and A.N. Lupas, *The HHpred interactive server for protein homology detection and structure prediction*. Nucleic Acids Res, 2005. **33**(Web Server issue): p. W244-8.
219. Brent, M.M., R. Anand, and R. Marmorstein, *Structural basis for DNA recognition by FoxO1 and its regulation by posttranslational modification*. Structure, 2008. **16**(9): p. 1407-16.
220. Clark, K.L., et al., *Co-crystal structure of the HNF-3/fork head DNA-recognition motif resembles histone H5*. Nature, 1993. **364**(6436): p. 412-20.
221. Lewis, P.W., et al., *Inhibition of PRC2 activity by a gain-of-function H3 mutation found in pediatric glioblastoma*. Science, 2013. **340**(6134): p. 857-61.
222. Popovic, R., et al., *Histone methyltransferase MMSET/NSD2 alters EZH2 binding and reprograms the myeloma epigenome through global and focal changes in H3K36 and H3K27 methylation*. PLoS Genet, 2014. **10**(9): p. e1004566.
223. Ferrari, K.J., et al., *Polycomb-dependent H3K27me1 and H3K27me2 regulate active transcription and enhancer fidelity*. Mol Cell, 2014. **53**(1): p. 49-62.
224. Fierz, B., et al., *Stability of nucleosomes containing homogenously ubiquitylated H2A and H2B prepared using semisynthesis*. J Am Chem Soc, 2012. **134**(48): p. 19548-51.
225. Xie, S.T., *Expression, purification, and crystal structure of N-terminal domains of human ubiquitin-activating enzyme (E1)*. Biosci Biotechnol Biochem, 2014. **78**(9): p. 1542-9.
226. Olsen, S.K. and C.D. Lima, *Structure of a ubiquitin E1-E2 complex: insights to E1-E2 thioester transfer*. Mol Cell, 2013. **49**(5): p. 884-96.
227. Lee, I. and H. Schindelin, *Structural insights into E1-catalyzed ubiquitin activation and transfer to conjugating enzymes*. Cell, 2008. **134**(2): p. 268-78.
228. Szczepanowski, R.H., R. Filipek, and M. Bochtler, *Crystal structure of a fragment of mouse ubiquitin-activating enzyme*. J Biol Chem, 2005. **280**(23): p. 22006-11.
229. Wolberger, C., *A spectrophotometric assay for conjugation of ubiquitin and ubiquitin-like proteins*. Anal Biochem, 2011.
230. Seufert, W. and S. Jentsch, *Ubiquitin-conjugating enzymes UBC4 and UBC5 mediate selective degradation of short-lived and abnormal proteins*. EMBO J, 1990. **9**(2): p. 543-50.
231. Scheffner, M., J.M. Huibregtse, and P.M. Howley, *Identification of a human ubiquitin-conjugating enzyme that mediates the E6-AP-dependent ubiquitination of p53*. Proc Natl Acad Sci U S A, 1994. **91**(19): p. 8797-801.
232. Jensen, J.P., et al., *Identification of a family of closely related human ubiquitin conjugating enzymes*. J Biol Chem, 1995. **270**(51): p. 30408-14.
233. Treier, M., W. Seufert, and S. Jentsch, *Drosophila UbcD1 encodes a highly conserved ubiquitin-conjugating enzyme involved in selective protein degradation*. EMBO J, 1992. **11**(1): p. 367-72.
234. Zhen, M., et al., *The ubc-2 gene of Caenorhabditis elegans encodes a ubiquitin-conjugating enzyme involved in selective protein degradation*. Mol Cell Biol, 1993. **13**(3): p. 1371-7.
235. Girod, P.A., et al., *Homologs of the essential ubiquitin conjugating enzymes UBC1, 4, and 5 in yeast are encoded by a multigene family in Arabidopsis thaliana*. Plant J, 1993. **3**(4): p. 545-52.
236. Dynek, J.N., et al., *c-IAP1 and UbcH5 promote K11-linked polyubiquitination of RIP1 in TNF signalling*. EMBO J, 2010. **29**(24): p. 4198-209.
237. Iwai, K., *Diverse roles of the ubiquitin system in NF-kappaB activation*. Biochim Biophys Acta, 2014. **1843**(1): p. 129-36.
238. Wu, F., et al., *Structural analysis of recombinant human ubiquitin-conjugating enzyme UbcH5c*. Acta Pharm Sin B, 2017. **7**(3): p. 390-394.
239. Jin, L., et al., *Mechanism of ubiquitin-chain formation by the human anaphase-promoting complex*. Cell, 2008. **133**(4): p. 653-65.

240. Hofmann, R.M. and C.M. Pickart, *Noncanonical MMS2-encoded ubiquitin-conjugating enzyme functions in assembly of novel polyubiquitin chains for DNA repair*. Cell, 1999. **96**(5): p. 645-53.
241. Bentley, M.L., et al., *Recognition of Ubch5c and the nucleosome by the Bmi1/Ring1b ubiquitin ligase complex*. EMBO J, 2011. **30**(16): p. 3285-97.
242. Polanowska, J., et al., *A conserved pathway to activate BRCA1-dependent ubiquitylation at DNA damage sites*. EMBO J, 2006. **25**(10): p. 2178-88.
243. Ratner, V., et al., *A general strategy for site-specific double labeling of globular proteins for kinetic FRET studies*. Bioconjug Chem, 2002. **13**(5): p. 1163-70.
244. Kao, M.W., et al., *Strategy for efficient site-specific FRET-dye labeling of ubiquitin*. Bioconjug Chem, 2008. **19**(6): p. 1124-6.
245. Smith, J.J., et al., *Orthogonal site-specific protein modification by engineering reversible thiol protection mechanisms*. Protein Sci, 2005. **14**(1): p. 64-73.
246. Liao, Y.D., et al., *Removal of N-terminal methionine from recombinant proteins by engineered E. coli methionine aminopeptidase*. Protein Sci, 2004. **13**(7): p. 1802-10.
247. Rieser, E., S.M. Cordier, and H. Walczak, *Linear ubiquitination: a newly discovered regulator of cell signalling*. Trends Biochem Sci, 2013. **38**(2): p. 94-102.
248. Freemont, P.S., I.M. Hanson, and J. Trowsdale, *A novel cysteine-rich sequence motif*. Cell, 1991. **64**(3): p. 483-4.
249. Itahana, K., et al., *Targeted inactivation of Mdm2 RING finger E3 ubiquitin ligase activity in the mouse reveals mechanistic insights into p53 regulation*. Cancer Cell, 2007. **12**(4): p. 355-66.
250. Takahashi, T.S., et al., *Structural insights into two distinct binding modules for Lys63-linked polyubiquitin chains in RNF168*. Nat Commun, 2018. **9**(1): p. 170.
251. Zhang, X., et al., *Structural basis for role of ring finger protein RNF168 RING domain*. Cell Cycle, 2013. **12**(2): p. 312-21.
252. Luijsterburg, M.S., et al., *A PALB2-interacting domain in RNF168 couples homologous recombination to DNA break-induced chromatin ubiquitylation*. Elife, 2017. **6**.
253. Lee, Y.H., et al., *HP1 promotes tumor suppressor BRCA1 functions during the DNA damage response*. Nucleic Acids Res, 2013. **41**(11): p. 5784-98.
254. Daley, J.M. and P. Sung, *53BP1, BRCA1, and the choice between recombination and end joining at DNA double-strand breaks*. Mol Cell Biol, 2014. **34**(8): p. 1380-8.
255. Adhireksan, Z., et al., *Ligand substitutions between ruthenium-cymene compounds can control protein versus DNA targeting and anticancer activity*. Nat Commun, 2014. **5**: p. 3462.
256. Scolaro, C., et al., *In vitro and in vivo evaluation of ruthenium(II)-arene PTA complexes*. J Med Chem, 2005. **48**(12): p. 4161-71.
257. Nowak-Sliwinska, P., et al., *Organometallic ruthenium(II) arene compounds with antiangiogenic activity*. J Med Chem, 2011. **54**(11): p. 3895-902.
258. Wang, X. and J.J. Hayes, *Acetylation mimics within individual core histone tail domains indicate distinct roles in regulating the stability of higher-order chromatin structure*. Mol Cell Biol, 2008. **28**(1): p. 227-36.
259. Kilic, S., et al., *A bi-terminal protein ligation strategy to probe chromatin structure during DNA damage*. Chem Sci, 2018. **9**(15): p. 3704-3709.
260. Rosner, D., et al., *Click chemistry for targeted protein ubiquitylation and ubiquitin chain formation*. Nat Protoc, 2015. **10**(10): p. 1594-611.
261. Barbera, A.J., et al., *The nucleosomal surface as a docking station for Kaposi's sarcoma herpesvirus LANA*. Science, 2006. **311**(5762): p. 856-61.
262. Muller-Ott, K., et al., *Specificity, propagation, and memory of pericentric heterochromatin*. Mol Syst Biol, 2014. **10**: p. 746.
263. Allahverdi, A., et al., *The effects of histone H4 tail acetylations on cation-induced chromatin folding and self-association*. Nucleic Acids Res, 2011. **39**(5): p. 1680-91.

264. Routh, A., S. Sandin, and D. Rhodes, *Nucleosome repeat length and linker histone stoichiometry determine chromatin fiber structure*. Proc Natl Acad Sci U S A, 2008. **105**(26): p. 8872-7.
265. Nishibuchi, G., et al., *N-terminal phosphorylation of HP1alpha increases its nucleosome-binding specificity*. Nucleic Acids Res, 2014. **42**(20): p. 12498-511.
266. McCabe, M.T., et al., *Mutation of A677 in histone methyltransferase EZH2 in human B-cell lymphoma promotes hypertrimethylation of histone H3 on lysine 27 (H3K27)*. Proc Natl Acad Sci U S A, 2012. **109**(8): p. 2989-94.
267. Cao, R., et al., *Role of histone H3 lysine 27 methylation in Polycomb-group silencing*. Science, 2002. **298**(5595): p. 1039-43.
268. Muller, M.M., et al., *A two-state activation mechanism controls the histone methyltransferase Suv39h1*. Nat Chem Biol, 2016. **12**(3): p. 188-93.
269. Francis, N.J., R.E. Kingston, and C.L. Woodcock, *Chromatin compaction by a polycomb group protein complex*. Science, 2004. **306**(5701): p. 1574-7.
270. Zhen, C.Y., et al., *Live-cell single-molecule tracking reveals co-recognition of H3K27me3 and DNA targets polycomb Cbx7-PRC1 to chromatin*. Elife, 2016. **5**.
271. Miller, T.C., et al., *A bromodomain-DNA interaction facilitates acetylation-dependent bivalent nucleosome recognition by the BET protein BRDT*. Nat Commun, 2016. **7**: p. 13855.
272. Quan, J. and J. Tian, *Circular polymerase extension cloning of complex gene libraries and pathways*. PLoS One, 2009. **4**(7): p. e6441.
273. Gibson, D.G., et al., *Enzymatic assembly of DNA molecules up to several hundred kilobases*. Nat Methods, 2009. **6**(5): p. 343-U41.
274. Berndsen, C.E. and C. Wolberger, *A spectrophotometric assay for conjugation of ubiquitin and ubiquitin-like proteins*. Anal Biochem, 2011. **418**(1): p. 102-10.
275. Jin, J., et al., *Dual E1 activation systems for ubiquitin differentially regulate E2 enzyme charging*. Nature, 2007. **447**(7148): p. 1135-8.
276. Chung, S.H. and R.A. Kennedy, *Forward-backward non-linear filtering technique for extracting small biological signals from noise*. J Neurosci Methods, 1991. **40**(1): p. 71-86.

*Ideas, methods and results for this manuscript were inspired from my own work (First year research plan, Andreas L. Bachmann, EPFL, 2015) and results were adapted from our publications (Kilic et al., 2015 and Choi, Bachmann et al., 2017).*

## VIII Curriculum Vitae



### **PARTICULARS**

Name	Andreas Bachmann
Adress	Breitenstrasse 34 CH 8108 Dällikon
Telephone	044 844 37 53
Cellphone	079 481 72 69
E-Mail	andre-bachmann@gmx.ch
Nationality	Swiss (CH)
Confession	Roman Catholic
Marital status	single
Date of birth	16. January 1989

### **EDUCATION AND DIPLOMA**

Date (from - until)	February 2014 – September 2018
Name and type of the job training- or educational institution	Ecole polytechnique fédérale de Lausanne (EPFL), Doctorand in Chemistry
Date (from - until)	September 2013 – January 2014
Name and type of the job training- or educational institution	Spanish course level B1 and work in the laboratory of Oncology at University Francisco de Vitoria, Madrid
Date (from - until)	May 2013 – August 2013
Name and type of the job training- or educational institution	Technical assistant at Institute of Molecular Health Sciences, ETH Zürich
Date (from - until)	September 2011 – May 2013
Name and type of the job training- or educational institution	ETH Zürich Master of Science in Biology

Date (from - until)	September 2008 – October 2011
Name and type of the job training- or educational institution	ETH Zürich Bachelor of Science in Biology

Date (from - until)	August 2004 – September 2008
Name and type of the job training- or educational institution	Grammar school, Kantonsschule Oerlikon

Date (from - until)	August 2002 – July 2004
Name and type of the job training- or educational institution	Secondary school A, Regensdorf

Date (from - until)	August 1995 – July 2002
Name and type of the job training- or educational institution	Primary school, Dällikon

## PERSONAL SKILLS AND ABILITIES

Mother tongue	German
Other languages	French, Spanish, English
People skills	Dancing activities, practical courses during studying
Computer literacy	„R“, Word, Excel, PowerPoint, Origin, ChemBioDraw, ImageJ, basic Matlab skills

<b>VOCATIONAL</b>	Laboratory – experiments:  Cell culture and transfection of eukaryotic cells RNA isolation from cell cultures and tissues Real-Time RT-PCR Standart cloning techniques Chromatin immunoprecipitation with lysate from cells and tissues Work with microRNAs Preparation of protein lysates and Western blot analysis Protein expression in bacteria and insect cells <i>In vitro</i> protein purification techniques Single-molecule TIRF microscopy Chemical modifications of proteins as protein labelling Peptide synthesis HPLC / Size exclusion chromatography Mass spectrometry Cleaning of glass with piranha solution
-------------------	-------------------------------------------------------------------------------------------------------------------------------------------------------------------------------------------------------------------------------------------------------------------------------------------------------------------------------------------------------------------------------------------------------------------------------------------------------------------------------------------------------------------------------------------------------------------------------------------------------------------------------------------------------------------------------



ubiquitination assays

Additional experience in:

Pyrosequencing

Fluorescence Microscopy

Tutoring in: mathematics, physics, biology and chemistry

Assistant in a laboratory for practical courses in biology and chemistry

Amag Buchs ZH – job in the factory

## OTHER SKILLS AND RESPONSIBILITIES

Project planning and accomplishment	Various projects and conceptual classes during studies at ETH and EPFL
Emergency relief	Completed in order to get driver licence
Driver licence	B1 (auto) Advanced driving class
Fire combat	How to combat fires efficiently, completed during studies at ETH Zürich
Irradiation safety	„Basic knowledge of radioprotection“, completed during studies at ETH Zürich
Laser hazard training	“Basic knowledge how to deal with lasers”, completed during studies at EPFL
How to avoid plagiarism	“Basic course for proper citation and to avoid plagiarism”, completed during studies at EPFL
Teaching toolkit	“Workshop to learn how to teach students”, completed during studies at EPFL
Basic skills	Independent problem solving skills, acquired during doctoral training Being able to work in a team, acquired during doctoral training

## HOBBIES

Reading

Painting

Jogging

Dancing (Standard and latin)

Human relationships

## SCIENTIFIC ARTICLES

**Engineered Multivalent Sensors to Detect Coexisting Histone Modifications in Living Stem Cells (Delachat et al., Nov 2017, Cell Chemical Biology)**

**DNA binding by PHF1 prolongs PRC2 residence time on chromatin and thereby promotes H3K27 methylation (Choi & Bachmann et al., Oct 2017, Nature Structural & Molecular Biology)**

**Single-molecule kinetic analysis of HP1-chromatin binding reveals a dynamic network of histone modification and DNA interactions (Bryan et al., Aug 2017, Nucleic Acids Research)**

Molecular and Chemical Mechanism in Epigenetics – Swiss Summer School 2015 July 12–17, 2015, Hotel Kurhaus, Arolla, Switzerland

**Multivalency governs HP1a association dynamics with the silent chromatin state (Kilic et al., Jun 2015, Nature Communications)**

Heterochromatin Assembly and Dynamics on the Single Molecule Level (Jan 2015, Biophysical Journal)

Conference Report: Molecular and Chemical Mechanism in Epigenetics (Jan 2015)

**A novel Nrf2-miR-29-desmocollin-2 axis regulates desmosome function in keratinocytes (Kurinna et al., Oct 2014, Nature Communications)**

SUPPLEMENT -



